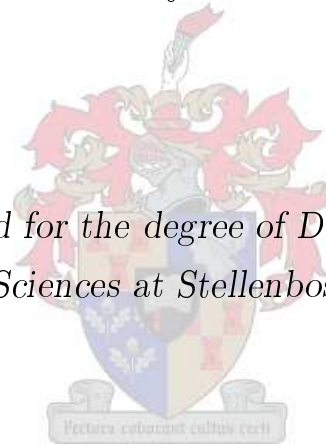# Modelling of the motion of a mixture of particles and a Newtonian fluid

by

Josefine Maryna Wilms

*Dissertation approved for the degree of Doctor of Philosophy*
*in the Natural Sciences at Stellenbosch University*

Promoters:

Dr G.J.F. Smit                Dr G.P.J. Diedericks

Faculty of Natural Sciences                CSIR

Department of Applied Mathematics                Stellenbosch

November 2011

# Declaration

By submitting this dissertation electronically, I declare that the entirety of the work contained therein is my own, original work, that I am the sole author thereof (save to the extent explicitly otherwise stated), that reproduction and publication thereof by Stellenbosch University will not infringe any third party rights and that I have not previously in its entirety or in part submitted it for obtaining any qualification.

Signature: ..............................

J.M. Wilms

2011/11/25

Date: ...................................

# Abstract

A theoretical model for the prediction of particle motion through a traversing Newtonian fluid is proposed. The model is derived by treating the fluid as a continuum and modelling its motion with the Navier-Stokes momentum- and mass conservation equations. Application of a Representative Elementary Volume (REV) yields expressions for the conservation equations in terms of averages. The particles are assumed rigid and momentum- and mass conservation equations are initially derived from Newtonian principles for a single solid, spherical particle. A summation-based averaging procedure is applied to obtain conservation expressions in terms of averaged variables for the particle phase.

Using the principle of momentum conservation, a collision-sphere model is applied to model the transfer of momentum between particles. The momentum transfer between the particles and the continuum is modelled using a modification of an existing representative unit cell model for two-phase motion, matched with an REV-averaged form of the Stokes drag law. In addition, an asymptotic matching procedure is applied between low- and high Reynolds number flows. The matching procedures render the model applicable to a wide range of particle volume fractions and Reynolds numbers.

The theoretical model is implemented into a numerical code and the numerical results, yielded from these simulations, are tested against results obtained through settling tube experiments done by the author at the Council for Scientific and Industrial Research (CSIR) in Stellenbosch as well as published experimental results from literature.

# Opsomming

'n Teoretiese model vir die voorspelling van partikelbeweging deur 'n omringende dinamiese Newtoniese vloeistof word voorgestel. Die vloeistof momentum- en massabehoud word met die Navier-Stokes momentum- en massabehoudsvergelykings gemodelleer. Hierdie vergelykings word in terme van gemiddelde vloeistof eienskappe voorgestel deur 'n verteenwoordigende eenheidsvolume toe te pas. Dit word aanvaar dat die deeltjies solied en bolvormig is. Momentum- en massabehoudsvergelykings vir die deeltjies word afgelei deur, aanvanklik, behoudsvergelykings vir 'n enkele partikel, op grond van Newton se wette, daar te stel. Volume gemiddeldes van bogenoemde deeltjievergelykings word verkry deur die toepassing van 'n sommasie tegniek.

Momentumoordrag tussen individuele deeltjies is gemodelleer deur die beginsel van momentumbehoud en 'n botsing-sfeer model te gebruik. 'n Bestaande verteenwoordigende eenheidssel model is gewysig om dit van toepassing op twee-fase vloei te maak. 'n Kombinasie van die laasgenoemde model en die Stokes vergelyking vir die wrywingskrag op 'n sfeer, is gebruik om momentumoordrag tussen die deeltjies en die vloeistof te modelleer. Daarbenewens is 'n asimptotiese passingstegniek gebruik om 'n passing tussen lae- en hoë Reynolds getal vloeie te bewerkstellig. Die passingsprosedures het tot die gevolg dat die model geskik is vir modellering oor 'n wye spektrum konsentrasie- en Reynoldsgetalwaardes.

Die vergelykings is geïmplementeer deur 'n rekenaar program in Fortran te ontwikkel. Die afvoer van hierdie simulasies is vergelyk met eksperimentele resultate, afkomstig van valbuis-eksperimente uitgevoer vir hierdie studie by die Wetenskaplike Navorsing en Nywerheidsraad (WNNR), asook eksperimentele resultate vanuit die literatuur.

# Acknowledgements

I wish to acknowledge the following for their contributions towards this study:

# Contents

# List of Figures

# List of Tables

# Nomenclature

**Symbols**

| | | |
|---|---|---|
| $C_D$ | Drag coefficient for a particulate phase . . . . . . . . . . . . . . . | $[\,-\,]$ |
| $C_{Ds}$ | Drag coefficient for single particle in suspension . . . . . . . . . . | $[\,-\,]$ |
| $D_p$ | Characteristic dimension of particulate phase . . . . . . . . . . . | $[\,\mathrm{m}\,]$ |
| $d_c$ | Distance between plates for Plane Poiseuille flow . . . . . . . . . | $[\,\mathrm{m}\,]$ |
| $d_p$ | Particle diameter . . . . . . . . . . . . . . . . . . . . . . . . . . | $[\,\mathrm{m}\,]$ |
| $D_S$ | Characteristic dimension of physical system . . . . . . . . . . . . | $[\,\mathrm{m}\,]$ |
| $D_V$ | Characteristic dimension of averaging volume . . . . . . . . . . . | $[\,\mathrm{m}\,]$ |
| $\underline{\mathcal{F}}$ | Total applied force . . . . . . . . . . . . . . . . . . . . . . . . . . | $[\,\mathrm{N}\,]$ |
| $\underline{F}_{AM}$ | Added mass force . . . . . . . . . . . . . . . . . . . . . . . . . . . | $[\,\mathrm{N}\,]$ |
| $\underline{F}_B$ | Basset force . . . . . . . . . . . . . . . . . . . . . . . . . . . . . | $[\,\mathrm{N}\,]$ |
| $\underline{F}_{Buoy}$ | Buoyancy force . . . . . . . . . . . . . . . . . . . . . . . . . . . | $[\,\mathrm{N}\,]$ |
| $\underline{F}_c$ | Stress gradient force . . . . . . . . . . . . . . . . . . . . . . . . | $[\,\mathrm{N}\,]$ |
| $\underline{F}_D$ | Drag force . . . . . . . . . . . . . . . . . . . . . . . . . . . . . . | $[\,\mathrm{N}\,]$ |
| $\underline{F}_{HI}$ | History force . . . . . . . . . . . . . . . . . . . . . . . . . . . . | $[\,\mathrm{N}\,]$ |
| $\underline{F}_M$ | Magnus force . . . . . . . . . . . . . . . . . . . . . . . . . . . . | $[\,\mathrm{N}\,]$ |
| $\underline{F}_P$ | Pressure force . . . . . . . . . . . . . . . . . . . . . . . . . . . . | $[\,\mathrm{N}\,]$ |

$\underline{\mathcal{F}}_{pc}$ Coupling force or particle-continuum interaction force . . . . . . . [N]

$\underline{F}_{pp}$ Particle-particle collision force . . . . . . . . . . . . . . . . . . . [N]

$\underline{F}_S$ Saffman force . . . . . . . . . . . . . . . . . . . . . . . . . . . . [N]

$\underline{F}_{Surf}$ Surface force . . . . . . . . . . . . . . . . . . . . . . . . . . . [N]

$\underline{F}_{TR}$ Transverse or lift force . . . . . . . . . . . . . . . . . . . . . . [N]

$\underline{F}_{Vol}$ Volume force . . . . . . . . . . . . . . . . . . . . . . . . . . . [N]

$\underline{F}_{VM}$ Virtual mass force . . . . . . . . . . . . . . . . . . . . . . . . . [N]

$\underline{F}_W$ Weight force . . . . . . . . . . . . . . . . . . . . . . . . . . . . [N]

$G_{p(i)}$ Centre of mass of $i^{th}$ particle . . . . . . . . . . . . . . . . . . [−]

$g_0$ Radial distribution function . . . . . . . . . . . . . . . . . . . . . [−]

$\underline{\underline{I}}$ Unit tensor, $\underline{\underline{I}} = \underline{i}\,\underline{i} + \underline{j}\,\underline{j} + \underline{k}\,\underline{k}$ . . . . . . . . . . . . . . . . . . . [−]

$\underline{I}$ Momentum transfer integral for single-phase flow . . . . . . . . . $[\text{kg}\cdot\text{m}^{-2}\cdot\text{s}^{-2}]$

$\underline{I}^{pc}$ Momentum transfer integral for two-phase flow . . . . . . . . . . $[\text{kg}\cdot\text{m}^{-2}\cdot\text{s}^{-2}]$

$\underline{I}_o$ Viscous contribution to $\underline{I}$ . . . . . . . . . . . . . . . . . . . . . $[\text{kg}\cdot\text{m}^{-2}\cdot\text{s}^{-2}]$

$\underline{I}_o^{pc}$ Viscous contribution to $\underline{I}^{pc}$ . . . . . . . . . . . . . . . . . . . $[\text{kg}\cdot\text{m}^{-2}\cdot\text{s}^{-2}]$

$\underline{I}_\infty^{pc}$ Inertial contribution to $\underline{I}^{pc}$ . . . . . . . . . . . . . . . . . . . $[\text{kg}\cdot\text{m}^{-2}\cdot\text{s}^{-2}]$

$K$ Drag function . . . . . . . . . . . . . . . . . . . . . . . . . . . . $[\text{kg}\cdot\text{m}^{-2}\cdot\text{s}^{-2}]$

$m^*$ Relative mass, $m^* = m_1 m_2/(m_1 + m_2)$ . . . . . . . . . . . . . [kg]

$m_a$ Added mass . . . . . . . . . . . . . . . . . . . . . . . . . . . . . [kg]

$m_c$ Mass of material volume within continuum phase . . . . . . . . . [kg]

$m_p$ Mass of a single particle . . . . . . . . . . . . . . . . . . . . . . [kg]

$\widehat{\underline{n}}$ Streamwise directed unit vector . . . . . . . . . . . . . . . . . . . [−]

$\underline{n}_\alpha$      $\alpha$-phase normal unit vector   . . . . . . . . . . . . . . . . . . . . . . $[-]$

$\underline{n}_c$      Continuum normal unit vector   . . . . . . . . . . . . . . . . . . . . . $[-]$

$\underline{\widetilde{n}}_c$      Unit vector parallel to interstitial flow direction . . . . . . . . . . $[-]$

$\underline{n}_p$      Particle normal unit vector   . . . . . . . . . . . . . . . . . . . . . . $[-]$

$N_p$      Number density of particles per unit volume of mixed fluid . . . $[\mathrm{m}^{-3}]$

$\underline{\mathcal{P}}$      Linear momentum . . . . . . . . . . . . . . . . . . . . . . . . . . $[\mathrm{kg \cdot m \cdot s^{-1}}]$

$p_{coll}$      Collisional pressure   . . . . . . . . . . . . . . . . . . . . . . . . $[\mathrm{Pa}]$

$p_{kin}$      Kinetic pressure   . . . . . . . . . . . . . . . . . . . . . . . . . . $[\mathrm{Pa}]$

$p_p$      Particle pressure . . . . . . . . . . . . . . . . . . . . . . . . . . . . $[\mathrm{Pa}]$

$\underline{r}$      Position vector . . . . . . . . . . . . . . . . . . . . . . . . . . . . $[\mathrm{m}]$

$s$      Shifting parameter for asymptotic matching   . . . . . . . . . . . $[-]$

$S^x$      Source term for $x$-component of momentum conservation equation $[\mathrm{kg \cdot m^{-3} \cdot s^{-1}}]$

$S^y$      Source term for $y$-component of momentum conservation equation $[\mathrm{kg \cdot m^{-3} \cdot s^{-1}}]$

$Sc_c^x$      Constant of linearised $S^x$ term for the continuum . . . . . . . . . $[\mathrm{kg \cdot m^{-3} \cdot s^{-1}}]$

$Sc_c^y$      Constant of linearised source $S^y$ for the continuum . . . . . . . . $[\mathrm{kg \cdot m^{-3} \cdot s^{-1}}]$

$Sc_p^x$      Constant of linearised $S^x$ term for the particles   . . . . . . . . . $[\mathrm{kg \cdot m^{-3} \cdot s^{-1}}]$

$Sc_p^y$      Constant of linearised source $S^y$ for the particles . . . . . . . . . $[\mathrm{kg \cdot m^{-3} \cdot s^{-1}}]$

$Sp$      Gradient for both $S^x$ and $S^y$ . . . . . . . . . . . . . . . . . . . . $[\mathrm{kg \cdot m^{-3} \cdot s^{-1}}]$

$\underline{\underline{\mathcal{S}}}_c$      Strain rate tensor   . . . . . . . . . . . . . . . . . . . . . . . . . $[\mathrm{kg \cdot m^{-1} \cdot s^{-2}}]$

$S_{pc}$      Particle-continuum interface of RUC . . . . . . . . . . . . . . . . $[\mathrm{m}^2]$

$S_{face}$      RUC surface exposed upstream . . . . . . . . . . . . . . . . . . . $[\mathrm{m}^2]$

$\mathcal{S}_{CV}$      Surface area of the the control volume, $\mathcal{V}_{CV}$   . . . . . . . . . . . . $[\mathrm{m}^2]$

$\mathcal{S}^{\perp}$     Projected area of impact normal to the incoming velocity  . . . .  $[\,\mathrm{m}^2\,]$

$\mathcal{S}_{k(i)}$     Surface area of particle $i$, contained within REV  . . . . . . . . . .  $[\,\mathrm{m}^2\,]$

$\mathcal{S}_{pc(i)}$     Particle-continuum interface of particle $i$   . . . . . . . . . . .  $[\,\mathrm{m}^2\,]$

$\mathcal{S}_{pp(i)}$     Particle-particle interface of particle $i$   . . . . . . . . . . .  $[\,\mathrm{m}^2\,]$

$S_{\|}$     Parallel interface of RUC . . . . . . . . . . . . . . . .  $[\,\mathrm{m}^2\,]$

$S_{\perp}$     Transverse interface of RUC . . . . . . . . . . . . . . .  $[\,\mathrm{m}^2\,]$

$t$     Time  . . . . . . . . . . . . . . . . . . . . .  $[\,\mathrm{s}\,]$

$\underline{u}_{c}^{pore}$     Velocity profile within RUC channel for single-phase flow  . . . .  $[\,\mathrm{m{\cdot}s}^{-1}\,]$

$\underline{u}_{pc}^{pore}$     Velocity profile within RUC channel for two-phase flow  . . . . .  $[\,\mathrm{m{\cdot}s}^{-1}\,]$

$\mathcal{U}_{AEV}$     Total volume of AEV  . . . . . . . . . . . . . . . .  $[\,\mathrm{m}^3\,]$

$U_{o}$     Total volume of RUC  . . . . . . . . . . . . . . . .  $[\,\mathrm{m}^3\,]$

$\mathcal{U}_{o}$     Total volume of REV  . . . . . . . . . . . . . . . .  $[\,\mathrm{m}^3\,]$

$U_{c}$     Continuum volume of RUC   . . . . . . . . . . . . . .  $[\,\mathrm{m}^3\,]$

$U_{p}$     Particulate volume of RUC   . . . . . . . . . . . . . .  $[\,\mathrm{m}^3\,]$

$U_{\|}$     Streamwise volume of RUC   . . . . . . . . . . . . . .  $[\,\mathrm{m}^3\,]$

$\mathcal{V}_{c}$     Material volume within continuum  . . . . . . . . . . . . . .  $[\,\mathrm{m}^3\,]$

$\mathcal{V}_{CV}$     Control volume . . . . . . . . . . . . . . . . . . .  $[\,\mathrm{m}^3\,]$

$\underline{v}_{c}$     Continuum velocity  . . . . . . . . . . . . . . . . .  $[\,\mathrm{m{\cdot}s}^{-1}\,]$

$\underline{v}_{m}$     Mixture velocity  . . . . . . . . . . . . . . . . . .  $[\,\mathrm{m{\cdot}s}^{-1}\,]$

$\underline{v}_{p}$     Particle velocity  . . . . . . . . . . . . . . . . . .  $[\,\mathrm{m{\cdot}s}^{-1}\,]$

$\underline{v}_{r}$     Relative velocity, $\underline{v}_{r} = \underline{v}_{c} - \underline{v}_{p}$  . . . . . . . . . . . .  $[\,\mathrm{m{\cdot}s}^{-1}\,]$

$\underline{x}_{o}$     Centre of REV  . . . . . . . . . . . . . . . . . . .  $[\,\mathrm{m}\,]$

$w_c$      Streamwise average pore speed within RUC . . . . . . . . . . . . . $[\mathrm{m \cdot s^{-1}}]$

$w_{pc}$      Average streamwise relative pore speed . . . . . . . . . . . . . . . $[\mathrm{m \cdot s^{-1}}]$

## Greek symbols

$\beta$      Momentum transfer coefficient . . . . . . . . . . . . . . . . . . . . . $[\mathrm{kg \cdot m^{-3} \cdot s^{-1}}]$

$\beta_o^{\mathrm{flow\ by}}$      Viscous momentum transfer coefficient for high porosities . . . $[\mathrm{kg \cdot m^{-3} \cdot s^{-1}}]$

$\beta_o^{\mathrm{flow\ through}}$      Viscous momentum transfer coefficient for low porosities . $[\mathrm{kg \cdot m^{-3} \cdot s^{-1}}]$

$\beta_\infty$      Momentum transfer coefficient for two-phase inertial flow . . . . $[\mathrm{kg \cdot m^{-3} \cdot s^{-1}}]$

$\epsilon_c$      Continuum volume fraction . . . . . . . . . . . . . . . . . . . . . . $[-]$

$\epsilon_p$      Particle volume fraction or concentration . . . . . . . . . . . . . . $[-]$

$\mu_\alpha$      Dynamic viscosity of the $\alpha$-phase . . . . . . . . . . . . . . . . . . $[\mathrm{kg \cdot m^{-1} \cdot s^{-1}}]$

$\mu_c$      Continuum dynamic viscosity . . . . . . . . . . . . . . . . . . . . . $[\mathrm{kg \cdot m^{-1} \cdot s^{-1}}]$

$\mu_{mix}$      Mixture dynamic viscosity . . . . . . . . . . . . . . . . . . . . . . $[\mathrm{kg \cdot m^{-1} \cdot s^{-1}}]$

$\mu_p$      Particle dynamic viscosity . . . . . . . . . . . . . . . . . . . . . . $[\mathrm{kg \cdot m^{-1} \cdot s^{-1}}]$

$\nu_{k|x}$      Particle volume contained within REV when centroid of particle is at position
$x_i$ . . . . . . . . . . . . . . . . . . . . . . . . . . . . . . . . . . . $[\mathrm{m^3}]$

$\nu_{p(i)}$      Volume of particle $i$ . . . . . . . . . . . . . . . . . . . . . . . . . $[\mathrm{m^3}]$

$\rho_c$      Continuum density . . . . . . . . . . . . . . . . . . . . . . . . . . $[\mathrm{kg \cdot m^{-3}}]$

$\rho_m$      Mixture density $(\rho_m = \epsilon_p \rho_p + \epsilon_c \rho_c)$ . . . . . . . . . . . . . . . . $[\mathrm{kg \cdot m^{-3}}]$

$\rho_p$      Particle density . . . . . . . . . . . . . . . . . . . . . . . . . . . $[\mathrm{kg \cdot m^{-3}}]$

$\underline{\underline{\sigma}}_c$      Continuum stress . . . . . . . . . . . . . . . . . . . . . . . . . . . $[\mathrm{N \cdot m^{-2}}]$

$\underline{\underline{\sigma}}_p$      Total particle stress due to particles and continuum . . . . . . . . $[\mathrm{N \cdot m^{-2}}]$

$\underline{\underline{\sigma}}_{pp}$      Particle stress due to particle presence . . . . . . . . . . . . . . . $[\mathrm{N \cdot m^{-2}}]$

$\underline{\underline{\sigma}}_{pp}^{f}$     Frictional particles stress . . . . . . . . . . . . . . . . . . . . . . . $[\,\mathrm{N \cdot m^{-2}}\,]$

$\underline{\underline{\sigma}}_{pp}^{kc}$     Kinetic-collisional particles stress . . . . . . . . . . . . . . . . . . $[\,\mathrm{N \cdot m^{-2}}\,]$

$\xi_{\alpha}$     Bulk viscosity of the alpha phase . . . . . . . . . . . . . . . . . $[\,\mathrm{N \cdot m^{-2}}\,]$

$\underline{\underline{\tau}}_{c}$     Shear stress for single-phase flow . . . . . . . . . . . . . . . . . $[\,\mathrm{N \cdot m^{-2}}\,]$

$\tau_{c}^{w}$     Wall shear stress for the RUC . . . . . . . . . . . . . . . . . . . $[\,\mathrm{N \cdot m^{-2}}\,]$

$\tau_{c}^{\|}$     Parallel component of shear stress for single-phase flow . . . . . . $[\,\mathrm{N \cdot m^{-2}}\,]$

$\tau_{c}^{\perp}$     Transverse component of shear stress for single-phase flow . . . . $[\,\mathrm{N \cdot m^{-2}}\,]$

$\tau_{pc}^{w}$     Wall shear stress two phase flow for the RUC . . . . . . . . . . . $[\,\mathrm{N \cdot m^{-2}}\,]$

$\underline{\underline{\tau}}_{pc}$     Particle-continuum shear stress . . . . . . . . . . . . . . . . . . $[\,\mathrm{N \cdot m^{-2}}\,]$

$\tau_{S}$     Stokes relaxation time . . . . . . . . . . . . . . . . . . . . . . . $[\,\mathrm{s}\,]$

$\chi$     Tortuosity . . . . . . . . . . . . . . . . . . . . . . . . . . . . . $[\,-\,]$

## Acronyms

AEV     Arbitrary Elementary Volume . . . . . . . . . . . . . . . . . . . . $[\,-\,]$

EV     Elementary Volume . . . . . . . . . . . . . . . . . . . . . . . . . $[\,-\,]$

REV     Representative Elementary Volume . . . . . . . . . . . . . . . . . . $[\,-\,]$

RUC     Representative Unitary Cell . . . . . . . . . . . . . . . . . . . . . $[\,-\,]$

## Abbreviations

$Re$     Reynolds number for single-phase flow . . . . . . . . . . . . . . . $[\,-\,]$

$Re_{pc}$     Reynolds number for two-phase flow . . . . . . . . . . . . . . . . $[\,-\,]$

# Chapter 1

# Introduction

## 1.1   Motivation

Two-phase flow is becoming increasingly significant in engineering design and technology. In addition to its pertinent applications in engineering and prevailing scientific problems it is also relevant to the interpretation of natural phenomena and thus warrants further investigation.

Empirical methods are required to emulate a number of diverse factors, such as apparatus geometry and physical fluid properties. It is therefore vital that engineers and scientists grasp the underlying physics and theoretical modelling fundamental to these applications in order to design equipment accurately.

Currently, various Computational Fluid Dynamics (CFD) packages (e.g. FLUENT, CFX) employ two-fluid models to predict the behaviour of particles immersed in a fluid. The expressions that these two-fluid systems use to model the drag, due to the relative velocity between the two phases, are often based on empirical models, derived from pressure-drop experiments in fluidised beds. This presents the need for an alternative model, based purely on the physics of the interactions.

## 1.2   Background

The following sections give a brief overview of the necessary background theory for this study and define the concepts that will be used in later stages of this work. A complete literature review is given in Chapter 2.

## 1.2.1   Classification of modelling procedures

Ishii (1975), Enwald *et al.* (1997) and Loth (2006) divided the modelling procedures for two-phase flows into three categories: Boltzmann -, Lagrangian -, and Eulerian methods. Since the Boltzmann methods are not directly applied to this study, they will only be discussed briefly in Chapter 2. For the time being it suffices to distinguish between the Lagrangian and Eulerian strategies.

### 1.2.1.1   Particle phase methodologies

Based on the frame of reference, modelling procedures for the particle phase are divided into two categories namely *Lagrangian* or *Eulerian.*

Lagrangian models treat the fluid phase as a continuum and calculate particle trajectories. This is done by either tracking each individual particle (i.e. trajectory calculation) or by tracking groups of similar particles (i.e. simultaneous particle tracking).

The Eulerian description, when applied to the dispersed phase, generally assumes the characteristics of the particles (e.g. velocity) can be described as a continuum.

Eulerian methods may be further subdivided into mixed- and separated-fluid approaches. The former assumes a negligible relative velocity between phases and describes the motion with a single set of conservation equations, whereas the latter assumes that phase velocities differ and the motion is modelled with two sets of momentum- and mass conservation expressions: one set for each phase.

## 1.2.2   Interphase coupling

Both Lagrangian and Eulerian treatments require a description for the interaction between the phases. The interphase coupling force, $\underline{\mathcal{F}}_{pc}$, is a force acting on a single particle due to pressure and viscous stresses which are the result of disturbances caused in the flow due to the presence of the particle.

Such a force is equal in magnitude and opposite in direction to the hydrodynamic particle force acting on the continuous phase. It amounts to the hydrodynamic surface forces, $\underline{F}_{surf}$, minus the contributions from the undisturbed flow stresses, $F_c$. The undisturbed stresses, $\underline{F}_c$, refer to the stress gradient forces within the continuum, which occur independent of the presence of the particle. The coupling force may be

expressed by

$$\underline{\mathcal{F}}_{pc} \; = \; \underline{F}_{surf} - \underline{F}_{c} = \underline{F}_{D} + \underline{F}_{TR} + \underline{F}_{AM} + \underline{F}_{HI}, \qquad (1.2.1)$$

where $\underline{F}_{D}$, $\underline{F}_{TR}$, $\underline{F}_{AM}$, and $\underline{F}_{HI}$, denote the drag-, transverse or lift forces, the added mass force and the history force, respectively (Kleinstreuer (2003), Crowe *et al.* (1998)).

For heavy particles ($\rho_p \gg \rho_c$), the interphase force is often simplified to include only the particle drag (neglecting lift, added mass, and history effects, since they are proportional to $\rho_c$) i.e. $\underline{\mathcal{F}}_{pc} = \underline{F}_{D}$. For light particles ($\rho_p \ll \rho_c$) with negligible collisions, the particle acceleration and body force can be neglected.

As the number of particles increases, collisions become more important, leading to dense flows. The key aspect for these flows is the proper incorporation of the particle-particle effects on the particle phase fluid dynamics. In particular, the particle collisions cause effective stresses, which should be incorporated into the particle transport equation.

## 1.3   Objectives of this study

The main objective of this study is to create a mathematical model that can predict the motion of particle mixtures in a Newtonian fluid with the potential to be modified in future work to incorporate additional flow regimes (e.g. a non-Newtonian continuum or multiple phases). The integration of such a model into an existing code could increase prediction capabilities for industrial applications, while the process of its derivation contributes to an improved comprehension of the underlying physics that govern them. It is also the objective of this work to provide a model that is capable of predicting a particle viscosity and stress based on first principles, thus eliminating the need for estimating these parameters.

## 1.4   Contributions and publications

A novel method is used to average the particle phase and the existing Representative Unit Cell (RUC) model has been modified to include the case of variable particle volume fractions. The current model includes particle-particle interactions and is valid for a wide range of Reynolds numbers and particle volume fractions.

A simulation code was developed in Fortran and the two-phase flow equations were solved numerically. These results compared well with data obtained from settling tube experiments at the Council for Scientific and Industrial Research (CSIR).

The application of these new modelling methods, as applied to low particle volume fractions ($\epsilon_p \ll 1$), was presented at the *International Conference of Numerical Analysis and Applied Mathematics* (ICNAAM) during September 2009 (Wilms *et al.* (2009)). It was expanded into a full article and published in *Applied mathematics and computation* (Smit *et al.* (2010)). Extension of the drag term to include the particle interaction effects was presented during September 2010 at ICNAAM (Wilms *et al.* (2010)).

## 1.5   Overview of this work

Theoretically the motion of solid particles suspended in a Newtonian fluid is completely determined by requiring the Navier-Stokes equations to be satisfied at each point of the fluid, and equating each particle's rate of change of linear and angular momenta to the resultant force and the resultant torque applied to it. Termed a Lagrangian description, the extensive processing power required by such an approach has proved viable only for low Reynolds number scenarios comprising of a relatively small numbers of particles. Hence, the need for equations based on averaged flow properties.

Averaged expressions, which are valid for all points in the flow domain, are developed in Chapter 3. Although too complex for a direct solution, they provide a good starting point for the development of much needed averaging procedures which are discussed in Chapter 4.

Following Bachmat and Bear (1986), the microscopic Navier-Stokes expressions, as derived in Chapter 3, are averaged over a Representative Elementary Volume (REV) in Chapter 4, yielding equations in volume averaged form. A summation-based averaging method for the discrete phase is used to cope with the discontinuous nature of the particles to provide macroscopic expressions for the dispersed phase.

A coupling mechanism exists between the particles for instances of increased particle volume fractions which result in particle-particle collisions. Following the work of Clark (2009), Bird *et al.* (2002), and Soo (1990), the closure of such an interaction term is dealt with in Chapter 5, using the principle of momentum conservation in a Centre Of Mass (COM) reference frame in conjunction with a collision sphere model.

However, the process of averaging leaves a number of terms indeterminate. The problem of closure for the particle-continuum interaction is discussed in Chapter 6 and yields an expression in terms of averaged variables by employing an extension of the Representative Unitary Cell (RUC) model. The adaptation to the RUC is required since it is a simplification of the REV and was introduced by Du Plessis and Masliyah (1988) for the averaging of single phase flow through *stationary* porous media. Chapter 6 concludes the development of the dispersed two-phase flow model.

Chapter 7 is dedicated to a discussion of the development of a simulation code which numerically solves the expressions derived in Chapter 6. The results obtained from this program are illustrated in Chapter 8 and compared to experimental work conducted at the CSIR in Chapter 9.

In addition to the aforementioned experimental verification, the model is tested against experimental data obtained by Richardson and Zaki (1954) in Chapter 10. The work is concluded with Chapter 11 wherein conclusions are given and recommendations made for future research topics.

# Chapter 2

# Literature review

## 2.1 Introduction

There have been many contributors to the advancement of two-phase flow. This chapter attempts to provide a background of the history of this research area and to get the reader acquainted with terminology, enabling them to distinguish between the various classifications schemes used in two-phase flow.

Detailed derivations of existing two-phase flow averaging identities, presented in this part of the work, are done in preparation for envisaging ideas presented in subsequent chapters.

## 2.2 Computational Fluid Dynamics (CFD) development

An account of the history of multi-phase Computational Fluid Dynamics (CFD) is given by Lyckowski (2010) in which the initiation and development of multi-phase CFD from 1970 to 2010 are discussed. A synopsis of the key contributors is given here and the reader is referred to Enwald *et al.* (1997) for a detailed summary on fluidised bed simulations up until 1997.

Up until the 1970's, nuclear reactor licensing software applied the Homogeneous Equilibrium Model (HEM), which meant that both phases were modelled as one. This status quo already began to change during the early 1960's when Solbrig, a student of

Gidaspow, set out to develop a new set of equations for two-phase flow which would be equivalent to those developed for single-phase flow by Bird and his team (Bird *et al.* (2002)). In 1971 Solbrig succeeded and the derivation, published in Solbrig and Hughes (1971), was incorporated into the Seriated Loop (SLOOP) software.

In parallel to these developments, Los Alamos Scientific Laboratory (LASL) developed a similar code called KACHINA. KACHINA was the first software to provide stable numerical solutions for multidimensional two-phase fluid dynamics (Amsden *et al.* (1999)).

During the mid 1970's, Spalding (Spalding (1980) and Runshal (2009)) who consulted with both LASL and Gidaspow, developed the Inter Phase Slip Algorithm (IPSA) (Spalding (1976)): A procedure to solve Partial Differential Equations (PDE's) similar to that published by Solbrig and Hughes (1971). The method was embedded into the PHOENICS source code in 1978.

Systems, Science and Software ($S^3$) started work in 1975 on a general computer model of fluidised bed coal gasification called CHEMFLUB, and the company, JAYCOR, started on a similar source code in the early 1980's called FLAG. These were transient, two-dimensional programs which contained PDE's similar to those in SLOOP (later, STUBE (Solbrig *et al.* (1976))) and KACHINA source codes and included viscous stress terms and an expression for the solids pressure. Work terminated on the $S^3$ software before it was documented.

KFIX was source code used by LASL for modelling two-dimensional flow in Loss-of-Fluid Tests (LOFT). Gidaspow had an idea to develop KFIX for the simulation of a fluidised bed and acquired the source code in 1977 from LASL. It was subsequently modified by Gidaspow, Lyckowski and Galloway, and installed at the Illinois Institute of Technology (IIT).

Modifications to KFIX involved the addition of a stabilising solids pressure term to prevent over compaction. The addition of this term is discussed in Bouillard *et al.* (1992). KFIX would later be known as FLUFIX which in turn was coupled with the EROSION/MOD1 software and was designated FLUFIX/MOD2. This was followed by FORCE2, developed by Babcock and Wilcox (Ding *et al.* (1993)). These source codes are available from the Energy Science and Technology Software Centre (ESTSC) at `www.osti.gov/estsc`.   Additional modifications were made to FLUFIX for the

modelling of dense suspension (i.e. slurry) flows.

In 1985 development on the CFDLIB software started at LASL under Kashiwa (1987). It was only in 1991 that the first International Conference on Multi-phase Flow (ICMF) was held in Tsukuba, Japan. It was the first of many with the 2010 ICMF held in Tampa, USA.

In 1991, O'Brien and Syamlal started development on the open source code called MFIX (Multi-phase Flow model with Interphase Exchanges). Their objective being the development of a code that could yield a reliable model of fluidised bed reactors. The first version of MFIX applied numerical techniques found in early versions of the previously mentioned IIT code. MFIX was completed in 1993 and is maintained by Oak Ridge National Laboratory (ORNL) in partnership with the National Energy Technology Laboratory (NETL) in the United States. It is available at `www.mfix.org` and the latest version was released in 2007.

After completing his Ph.D. under Gidaspow in 1985, Syamlal joined Fluent, Inc. where he took part in furthering the development of the FLUENT package which was started in 1983 by a small group at Creare Inc near Fluent Inc.'s present headquarters in Lebanon, New Hampshire, USA. It was originally created by Swithenbank at Sheffield University in the U.K.

Work on the code has continued and is presently known as ANSYS FLUENT 12.0. ANSYS also acquired the CFX code, formerly FLOW3D, which was developed at Harwell in the U.K. It is now named ANSYS CFX.

The Open Source Field Operation and Manipulation (OpenFOAM), C++ based, source code is another application that may be used to model multiple-phase flows. It is produced by the UK company, OpenCFD Ltd., and is based on equations similar to those used in its ANSYS CFX counterpart. Most fluid dynamics solver applications in OpenFOAM use the pressure-implicit split-operator (PISO) or semi-implicit method for pressure-linked equations (SIMPLE) algorithms. These algorithms are iterative procedures for solving equations for velocity and pressure, PISO being used for transient problems and SIMPLE for steady-state (Barton (1998)).
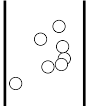
The majority of source codes mentioned above utilise a two-fluid approach as modelling procedure. Methods applied in formulating the equations for the two-fluid method are discussed in the following sections.

## 2.3   Classification of multi-phase flows

The numerical schemes, applied in the source codes discussed in Section 2.2, have been documented and categorised by Enwald *et al.* (1997) in accordance with Ishii (1975) as a guide line.

Ishii set up a classification which depended on the topology of the flow and distinguished between three classes: *separated, mixed* and *dispersed* flows. For the purpose of understanding the current work on the motion of particles in a Newtonian fluid, only the subcategories of dispersed flows are listed in Table 2.1.

**Table 2.1:** Different regimes for two-phase dispersed flows according to Ishii (1975).

| Class | Typical regimes | Geometry | Configuration | Examples |
|---|---|---|---|---|
| Dispersed flow | Bubbly flow | | Gas bubbles in liquid | Chemical reactors |
| | Droplet flow | | Liquid droplets in gas | Spray cooling |
| | Particulate flow | | Solid particles in gas or liquid | Sedimentation |

According to this classification scheme, dispersed media are divided into bubbly-, droplet-, and particulate flows: Bubbly flow physically manifests as gas bubbles in liquid, which includes the everyday soda drink or the physical processes in chemical reactors. Flows in which liquid droplets coincide within a gas is classified as droplet flow while particulate flow, which forms the focus of this study, consists of particles dispersed within a gas or a liquid.

Following Kleinstreuer (2003), Crowe *et al.* (1998), and Ishii (1975), the flow of particles and droplets in fluids can be seen as a subset of multi-component, multi-phase flows. Crowe *et al.* (1998), defines a *component* as a chemical species such as nitrogen, oxygen or water whereas *phase* refers to the solid, liquid or vapour state of the matter. Examples of single-phase, single-component flows include water- and nitrogen flows, whereas multi-phase single-component examples include steam-water flow. Multi-component examples of single- and multi-phase flows are given by air flow and air-water flow, respectively. These examples are listed in Table 2.2.

**Table 2.2:** Examples of single- and multi-component, multi-phase flows (Crowe *et al.* (1998)).

|  | Single-component | Multi-component |
|---|---|---|
| **Single-phase** | Water flow <br> Nitrogen flow | Air flow <br> Flow of emulsions |
| **Multi-phase** | Steam-water flow | Air-water flow <br> Slurry flow |

The study of particles in water may therefore be qualified as a multi-component example, since there are two separate chemical species involved (i.e. silicon ($Si$) particles in water ($H_2O$)). Moreover it may be qualified as multi-phase flow due to the silicon particles being in a solid state and the water being in a liquid state. It follows that the focus in this work is placed on multi-phase, multi-component regimes and concerns itself with the motion of dispersed matter (i.e. a particulate phase) in a carrier fluid (i.e. a continuum phase).

Multi-phase, multi-component flows may further be divided into subclasses on the basis of how the components interact with the carrier phase and with each other. These interactions are termed *coupling mechanisms* by various authors (e.g. Loth (2006), Crowe *et al.* (1998) and Kleinstreuer (2003)) and the classification of the particle phase is most aptly described, following Loth (2006), in Figure 2.1.

The broadest division is between dispersed and dense flows and is based on whether it is the continuum or dispersed phase that dominates the overall motion of the particles. Dispersed flow is partitioned into sparse flow: where the dispersed-phase motion is affected by the continuous phase, but not vice versa; and dilute flow which combines the

aforementioned with instances where the particle effects on the fluid become significant through interphase coupling (e.g. drag force).
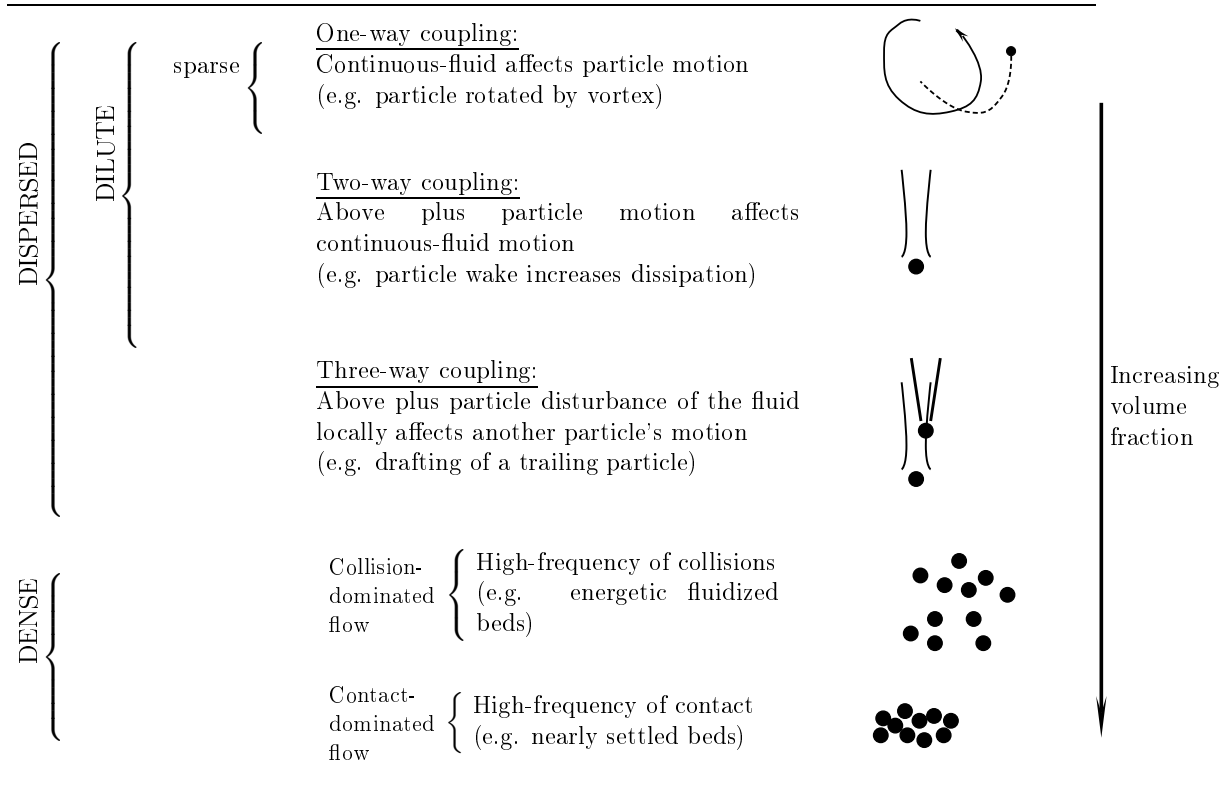


**Figure 2.1:** Dilute, dispersed, and dense flow conditions (Loth (2006)).

As the particle volume fraction increases, dispersed flow is subject to three-way coupling where the particle wakes and other local continuum disturbances affect the motion of nearby particles. A further increase in particle volume fraction induces the last level of the dispersed regime where four-way coupling dominates as particle collisions occur in combination with all of the aforementioned interactions.

When the particle-particle interactions dominate, the flow is considered dense. These interactions can refer to two separate mechanisms: particle-particle collisions and particle-particle dynamic interactions. The former refers to interactions where particles can rebound, shatter or coalesce, whereas the latter refers to cases where the particles glide upon each other, causing friction.

Once the flow domain has been categorised, using classification procedures listed in Table 2.2 and Figure 2.1, a decision needs to be made as to which modelling method

should be applied to adequately represent its motion. The various types of modelling methods available in literature are subsequently described.

## 2.4 Classification of modelling procedures

Ishii (1975) divided the modelling procedures for two-phase flows into three categories, namely Boltzmann, Lagrangian, and Eulerian methods.

Boltzmann theory uses a method analogous to dilute gas kinetic theory to describe the interactions present in gas-particle systems (Ahmadi and Ma (1990), Ding and Gidaspow (1990)). This method defines a molecular distribution function for the continuum phase and another for the particulate phase. However, accounting for size distribution and the collision processes of the solid particles with each other and with the gas molecules, proves challenging.

The motion of a suspension can be viewed in two ways: In the fields of fluidisation and gas-particle transport, separate equations of motion are sought for each of the phases, whereas those interested in the rheology of suspensions often view the suspension as a whole. The two viewpoints should however be equivalent (Gidaspow (1986), Jackson (1997)). These diverse modelling approaches mainly involve the particle phase and a concise discussion follows in the next section.

## 2.5 Particle-phase methodologies

Based on the frame of reference, the particle phase is divided into two classification schemes as *Eulerian* or *Lagrangian*. The Eulerian approach can be further classified into *mixed* or *point-force* approaches, while the Lagrangian method is grouped into *point-force* or *resolved-surface* approaches. Table 2.3 shows the various modelling approaches for the two-phase medium.

### 2.5.1 Lagrangian method

The Lagrangian method, often referred to as the *discrete method,* assumes that each particle (or group of particles) is represented separately. The properties (such as velocity) are updated along the path of individual (or cloud of similar) particles.

**Table 2.3:** Forms of the incompressible unsteady Navier-Stokes momentum equations (Loth (2006)).

| Dispersed phase approach | Dispersed phase momentum | Continuous phase momentum |
| --- | --- | --- |
| Eulerian with mixed fluid treatment | $\partial(\rho_m \underline{v}_m)/\partial t + \nabla \cdot (\rho_m \underline{v}_m \underline{v}_m) = \rho_m \underline{g} - \nabla p + \mu_m \nabla^2 \underline{v}_m$ where $\rho_m = \epsilon_p \rho_p + \epsilon_c \rho_c$ Applied throughout domain | |
| Eulerian with point-force treatment | $\rho_p \frac{\partial}{\partial t}(\epsilon_p \underline{v}_p) + \rho_p \nabla \cdot (\epsilon_p \underline{v}_p \underline{v}_p) = \epsilon_p \rho_p \underline{g} - \epsilon_p \nabla(p + p_{coll}) + \epsilon_p \mu_c \nabla^2 \underline{v}_p + \epsilon_p \underline{\mathcal{F}}_{pc}/\mathcal{U}_p$ Applied throughout the domain | $\rho_c \frac{\partial}{\partial t}(\epsilon_c \underline{v}_c) + \rho_c \nabla \cdot (\epsilon_c \underline{v}_c \underline{v}_c) = \epsilon_c \rho_c \underline{g} - \epsilon_c \nabla p + \epsilon_c \mu_c \nabla^2 \underline{v}_c - \epsilon_p \underline{\mathcal{F}}_{pc}/\mathcal{U}_p$ Applied throughout the domain |
| Lagrangian with point-force treatment | $m_p \frac{\partial \underline{v}_p}{\partial t} = F_{Vol} + F_{Surf}$ Applied along particle trajectories | $\rho_c \frac{\partial}{\partial t}(\epsilon_c \underline{v}_c) + \rho_c \nabla \cdot (\epsilon_c \underline{v}_c \underline{v}_c) = \epsilon_c \rho_c \underline{g} - \epsilon_c \nabla p + \epsilon_c \mu_c \nabla^2 \underline{v}_c - N_p \underline{\mathcal{F}}_{pc}$ Applied throughout the domain |
| Lagrangian with resolved-surface treatment | $m_p \frac{\partial \underline{v}_p}{\partial t} = \underline{F}_{Vol} + \underline{F}_{Surf} + \underline{F}_{pp}$ where $F_{Surf} = \int_{\mathcal{S}}[-p + \tau_{pc}]n d\mathcal{S}$ and does not contain $\underline{F}_{pp}$ Applied along particle trajectories | $\rho_p \frac{\partial \underline{v}_c}{\partial t} + \rho_c \underline{v}_c \nabla \cdot \underline{v}_c = \rho_c \underline{g} - \nabla p + \mu_c \nabla^2 \underline{v}_c$ Applied outside of particle volume |

Note: In the above, $N_p$ is the number density of particles per unit volume of mixed fluid, $\underline{\mathcal{F}}_{pc}$ is the interphase force between particles and the continuum, $\underline{F}_{pp}$ is the coupling force between the particles, $p_c$ is the hydrostatic continuum pressure, $p_{coll}$ is the particle collisional pressure and $\tau_{pc}$ is the shearing stress between the particle and the continuum. The mixture, particle and continuum velocities are respectively denoted by $\underline{v}_m$, $\underline{v}_p$ and $\underline{v}_c$ with the corresponding densities given by $\rho_m$, $\rho_p$ and $\rho_c$. The particle and continuum volume fractions are denoted by $\epsilon_p$ and $\epsilon_c$, respectively and the combined volume of particles is given by $U_p$.

In contrast, the Eulerian method averages particle properties over a computational volume. In brief, the Eulerian reference frame is a stationary measurement of the average of the system whilst the Lagrangian frame moves with the element it is measuring.

For the treatment of surface forces, the point-force method represents the flow over the particle with empirical and theoretical methods (e.g. by specifying a drag coefficient) to obtain the force on the particle. For the resolved-surface approach, the fluid dynamics (e.g. pressure and shear stress distributions) are fully resolved over the entire particle's surface and then integrated to obtain the overall hydrodynamic forces. Hence, for the resolved-surface treatment, high spatial resolution of the continuous phase is thus required over the particle surface. Therefore, this method is sometimes called *direct simulation*. Conversely, the continuous-flow grid scale can be course with respect to the particle size for the point-force approach, such that it is much less demanding in

terms of computational resources. Following Loth (2006), the difference between these two approaches is illustrated in Figures 2.2a and 2.2b.



**(a)** Point-force treatment.   **(b)**  Resolved-surface treatment.
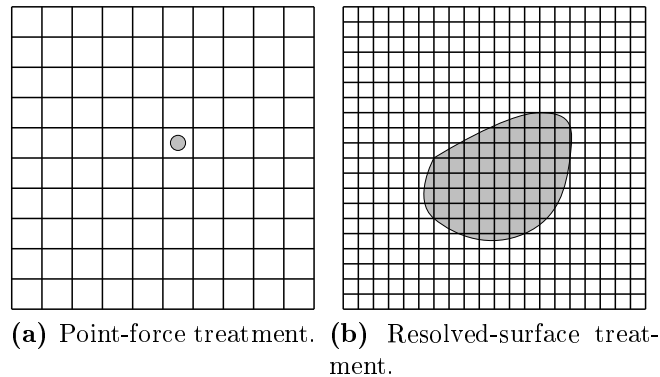
**Figure 2.2:** Different representations for particle treatment where the shaded area represents the particle and the grid represents the computational resolution for the continuous phase solution (Loth (2006)).

Lagrangian models treat the fluid phase as a continuum and calculates particle trajectories. Typical techniques which may be applied to solve Lagrangian models include (Wassen and Frank (2000)):

**Trajectory Calculation (TC)** A large number of particle trajectories are sequentially computed. The average properties of the trajectory segments that cross a computational cell are determined in order to derive macroscopic properties for the discrete phase. The TC method is however limited to steady flows. Particle-particle collisions have been accounted for by Oesterle and Petitjean (1993).

**Simultaneous Particle Tracking (SPT)** The motions of a representative number of particles are calculated simultaneously. Each simulated particle represents a certain number of real particles with similar characteristics. The macroscopic properties of the particulate phase for a certain grid cell are obtained at any time by averaging over all particles that are located in that cell at that time. Particle-particle collisions were accounted for by Tanaka and Tsuji (1991). In the majority of applications, collisions are treated stochastically using Direct Simulation Monte Carlo (DSMC) methods since deterministic models are computationally too expensive.

### 2.5.2   Eulerian method

The Eulerian description, applied to the dispersed phase, generally assumes the characteristics of the particles (e.g. velocity) may be described as a continuum. As listed in Table 2.3, Eulerian techniques are subdivided into mixed- and separated-fluid approaches.

#### 2.5.2.1   Mixed-fluid model

In the mixed-fluid approach, the assumption is made that the differences in velocity and temperature between the two phases are small in comparison to variations in the field as a whole. The use of these models results in a single set of momentum conservation equations for the flow mixture as opposed to one set for the continuous phase and one set for the dispersed phase. The approach is numerically uncomplicated and, moreover, is able to cope with both dispersed and dense conditions.

#### 2.5.2.2   Separated-flow model

The separated-fluid approach for a Eulerian description of the particle phase with the point force assumption assumes that both the carrier fluid and the particles comprise two separate, but intermixed, continua. Therefore, two sets of momentum equations are required: one for the continuous phase and the other for the dispersed phase. The separated fluid method is also called the *two-fluid method.* Here the relative velocity between the phases are taken into account and the equations will generally be coupled. Such an approach will be applied in this work and the following section is devoted to introducing the reader to the approaches followed by various authors in setting up appropriate models.

## 2.6   Modelling procedures for two-fluid models

Generally, the continuum phase is modelled with the Navier-Stokes momentum- and mass conservation equations. The construction of a model for the discrete phase is, however, approached either with the Navier-Stokes expressions or, alternatively, by using the kinetic theory of particles. Even though these two approaches differ widely, the results obtained are almost identical.

The application of the Navier-Stokes relations to the particulate phase requires the formulation of descriptions for various variables which are well defined from the molecular theory for fluids, but are relatively unknown for solids. These include the definition of the solid stress term which in turn requires expressions for the discrete phase viscosity and pressure.

Alternatively, the discrete phase may be modelled using a kinetic theory approach: The momentum equation for a single sphere is constructed using Newton's second law of motion and extended to account for a single particle in suspension (Clift *et al.* (1978), Soo (1990), and Enwald *et al.* (1997)).

## 2.6.1   Traditional two-fluid formulation

In the absence of mass transfer, the continuity and momentum equations for both phases are respectively given by

$$\frac{\partial \rho_\alpha}{\partial t} + \nabla \cdot (\rho_\alpha \, \underline{v}_\alpha) \;\; = \;\; 0, \tag{2.6.1}$$

and

$$\frac{\partial \rho_\alpha \, \underline{v}_\alpha}{\partial t} + \nabla \cdot \rho_\alpha \, \underline{v}_\alpha \, \underline{v}_\alpha - \nabla \cdot \underline{\underline{\sigma}}_\alpha - \rho_\alpha \, \underline{g} \;\; = \;\; \underline{0}, \tag{2.6.2}$$

where the discrete (or particulate) and continuum phases are respectively denoted by $\alpha = p$ and $\alpha = c$. Density and stress are denoted by $\rho_\alpha$ and $\underline{\underline{\sigma}}_\alpha$ respectively. The local velocity is denoted by $\underline{v}_\alpha$.

As mentioned earlier, the ordinary differential equation for each particle may be solved using a Lagrangian approach. Since this is computationally expensive the alternative is to apply an averaging operator action on the local instantaneous equations.

Averaging models may be divided into volume, time, and ensemble averaging methods and are discussed in Appendix B. Volume averaging, which, due to its physical interpretability, is the preferred method of averaging in this work, is applied to the mass and momentum conservation expressions in the following sections.

The averaging procedures for the mass- and momentum conservation equations, by way of the application of identities given by Equations (B.6.20) to (B.6.25), are reviewed in the following sections.

### 2.6.1.1   Averaging of the mass conservation equation

Applying the volume averaging technique to the mass conservation equation, yields

$$\frac{\partial}{\partial t}\left\langle\epsilon_\alpha\rho_\alpha\right\rangle + \nabla\cdot\left\langle\rho_\alpha\,\underline{v}_\alpha\right\rangle \;=\; 0. \tag{2.6.3}$$

### 2.6.1.2   Averaging of the momentum conservation equation

The averaging process for the momentum equation yields various terms which require further modelling in order to achieve closure. The first step is to apply the definition of volume averaging to each term in the momentum conservation equation:

$$\left\langle\frac{\partial\rho_\alpha\,\underline{v}_\alpha}{\partial t}\right\rangle + \left\langle\nabla\cdot\rho_\alpha\,\underline{v}_\alpha\,\underline{v}_\alpha\right\rangle - \left\langle\nabla\cdot\underline{\underline{\sigma}}_\alpha\right\rangle - \left\langle\rho_\alpha\,\underline{g}\right\rangle \;=\; \underline{0}. \tag{2.6.4}$$

This is followed by the application of Rules (B.6.23), (B.6.24) and (B.6.20) to the averages of derivatives, to give

$$\frac{\partial}{\partial t}\left\langle\rho_\alpha\,\underline{v}_\alpha\right\rangle + \nabla\cdot\left\langle\rho_\alpha\,\underline{v}_\alpha\,\underline{v}_\alpha\right\rangle - \nabla\cdot\left\langle\underline{\underline{\sigma}}_\alpha\right\rangle - \left\langle\rho_\alpha\,\underline{g}\right\rangle \;=$$
$$\frac{1}{\mathcal{U}_o}\int\limits_{\mathcal{S}_{\alpha\beta}}\rho_\alpha\,\underline{v}_\alpha\,\underline{w}_{\alpha\beta}\cdot\underline{n}_\alpha d\mathcal{S} - \frac{1}{\mathcal{U}_o}\int\limits_{\mathcal{S}_{\alpha\beta}}\rho_\alpha\,\underline{v}_\alpha\,\underline{v}_\alpha\cdot\underline{n}_\alpha d\mathcal{S} + \frac{1}{\mathcal{U}_o}\int\limits_{\mathcal{S}_{\alpha\beta}}\underline{\underline{\sigma}}_\alpha\cdot\underline{n}_\alpha d\mathcal{S}. \tag{2.6.5}$$

In the absence of combustion or condensation (i.e. when the interface velocity, $\underline{w}_{\alpha\beta}$, equals that of the velocity of the phase itself, $\underline{v}_\alpha$) Equation (2.6.5) will simplify to

$$\frac{\partial}{\partial t}\left\langle\rho_\alpha\,\underline{v}_\alpha\right\rangle + \nabla\cdot\left\langle\rho_\alpha\,\underline{v}_\alpha\,\underline{v}_\alpha\right\rangle - \nabla\cdot\left\langle\underline{\underline{\sigma}}_\alpha\right\rangle - \left\langle\rho_\alpha\,\underline{g}\right\rangle \;=\; \frac{1}{\mathcal{U}_o}\int\limits_{\mathcal{S}_{\alpha\beta}}\underline{\underline{\sigma}}_\alpha\cdot\underline{n}_\alpha d\mathcal{S}. \tag{2.6.6}$$

### 2.6.1.3   Reynolds decomposition

Equation (2.6.6) cannot be solved directly as it contains averages of products of the dependent variables. To obtain a solvable set of equations, it must first be rewritten into expressions containing products of the averaged variables. This is done by employing Reynolds decomposition. Reynolds decomposition of variables is typically used in the field of single-phase turbulence modelling in order to separate the fluctuating components of the variables from the time-averaged variables. In this instance however, the main purpose of the decomposition is to separate the averages of products

into products of averages. The procedure will result in extra terms in the equations, containing products of the fluctuating components. These extra terms are analogous to the Reynolds stress terms in the case of single-phase turbulence modelling (Enwald *et al.* (1997)). Administering Reynolds decomposition to a general variable, $\Omega_\alpha$, yields

$$\Omega_\alpha = \langle \Omega_\alpha \rangle_\alpha + \widetilde{\Omega}_\alpha, \tag{2.6.7}$$

where the definition of the intrinsic phase average is given by Equation (B.5.4). The average of the deviation term is assumed to be zero, which corresponds with the notion that the volume over which averaging is done is indeed a sensible representation of the macroscopic average

$$\left\langle \widetilde{\Omega}_\alpha \right\rangle = 0. \tag{2.6.8}$$

When Reynolds decomposition is applied to Equation (2.6.5) it yields

$$\frac{\partial}{\partial t} \langle \rho_\alpha \underline{v}_\alpha \rangle + \nabla \cdot (\rho_\alpha \langle \underline{v}_\alpha \rangle_\alpha \langle \underline{v}_\alpha \rangle_\alpha) + \nabla \cdot \langle \rho_\alpha \widetilde{\underline{v}}_\alpha \widetilde{\underline{v}}_\alpha \rangle - \nabla \cdot \left\langle \underline{\underline{\sigma}}_\alpha \right\rangle - \langle \rho_\alpha \underline{g} \rangle =$$
$$\frac{1}{\mathcal{U}_o} \int\limits_{\mathcal{S}_{\alpha\beta}} \underline{\underline{\sigma}}_\alpha \cdot \underline{n}_\alpha d\mathcal{S}. \tag{2.6.9}$$

The term $\nabla \cdot \langle \rho_\alpha \widetilde{\underline{v}}_\alpha \widetilde{\underline{v}}_\alpha \rangle$ is generally referred to as the Reynolds stress term and denoted by $\underline{\underline{\sigma}}_\alpha^{Re}$ (Enwald *et al.* (1997)). The right-hand side of Equation (2.6.9) is termed the interfacial momentum transfer.

The Reynolds stress for the continuum phase is modelled using a standard Boussinesq approximation. For a more detailed account of this approach the reader is referred to the work of Enwald *et al.* (1997), Simonin and Viollet (1989) and Simonin (1995).

Turbulence models for the particulate phase available in literature are based on the kinetic theory of granular flow. Such an approach to the modelling of the particulate phase uses classical results from kinetic theory of dense gases, cf. Dartevelle (2003), Chapman and Cowling (1970) in combination with Grad's theory, cf. Grad (1949), and a linear theory developed by Jenkins and Richman (Jenkins and Richman (1985)).[1]

It remains to be shown how the viscous stress term, $\underline{\underline{\sigma}}_\alpha$, is modelled for the continuum and discrete phases following the traditional approach.

---

[1] As given in Enwald *et al.* (1997).

**2.6.1.4   The viscous stress, $\underline{\underline{\sigma}}_\alpha$**

The viscous stress in Equation (2.6.9) is divided into a pressure, $p_\alpha$, and a viscous *shear stress* term, $\underline{\underline{\tau}}_\alpha$, i.e.

$$\underline{\underline{\sigma}}_\alpha \;\; = \;\; p_\alpha \underline{\underline{I}} + \underline{\underline{\tau}}_\alpha. \tag{2.6.10}$$

In the following two sections these two terms are discussed.

**2.6.1.5   Viscous shear stress**

The stress tensor for both phases is often modelled using the Newtonian strain-stress relation:

$$\underline{\underline{\tau}}_\alpha \;\; = \;\; \xi_\alpha (\nabla \cdot \underline{v}_\alpha)\underline{\underline{I}} + 2\mu_\alpha (\underline{\underline{S}}_\alpha - \frac{1}{3}(\nabla \cdot \underline{v}_\alpha)\underline{\underline{I}}), \tag{2.6.11}$$

where the strain-rate tensor is defined by

$$\underline{\underline{S}} \;\; = \;\; \frac{1}{2}\left(\nabla \underline{v}_\alpha + (\nabla \underline{v}_\alpha)^T\right). \tag{2.6.12}$$

In accordance with Stokes' assumption, the bulk viscosity, $\xi_\alpha$, is commonly set to zero in both phases (Panton (1984)). In practice, the reason for neglecting the bulk viscosity is the lack of reliable measurement techniques (Pritchett *et al.* (1978)). A theoretical expression is however possible using the kinetic theory of granular flow.

From the assumption that there is no mass transfer between the phases, it follows that $\nabla \cdot \underline{v}_\alpha = 0$. The remaining dynamic viscosity, $\mu_\alpha$, is easy to specify for the continuum phase with molecular theory but proves difficult for the discrete phase.

The particle viscosity may be modelled as a function of the particle volume fraction (Enwald *et al.* (1997)). However, the majority of viscosity models available are for mixture viscosities only. Examples of such viscosity formulae are listed in Table 2.4.

It is not obvious how the mixture viscosity is related to the phase viscosities, but often a linear relationship is assumed and the viscosities are weighted as

$$\mu_{\mathrm{mix}} \;\; = \;\; \epsilon_c \mu_c + \epsilon_p \mu_p. \tag{2.6.13}$$

Pressure in the continuum phase is simply the static continuum pressure. The pressure in the particle phase is more difficult to interpret.

**Table 2.4:** Mixture viscosities proposed by various authors.

| Source | Mixture viscosity | Constants |
|---|---|---|
| Einstein (1906), Einstein (1911) | $\mu_{mix} = \mu_c \left(1 + 2.5\epsilon_p\right))$ | $\epsilon_p \leq 0.03$ |
| Brinkman (1952), Roscoe (1952) | $\mu_{mix} = \mu_c(1 - \epsilon_p)^{-2.5}$ | |
| Frankel and Acrivos (1967) | $\mu_{mix} = \mu_c \frac{9}{8}\left[\frac{\left(\epsilon_p/\epsilon_{p,max}\right)^{1/3}}{1 - \left(\epsilon_p/\epsilon_{p,max}\right)^{1/3}}\right]$ | $\epsilon_p/\epsilon_{p,max} \to 1$ |
| Vand (1948) | $\mu_{mix} = \mu_c \left[\frac{2.5\epsilon_p + 2.7\epsilon_p^2}{1 - 0.609\epsilon_p}\right]$ | |
| Eilers (1943) | $\mu_{mix} = \mu_c \frac{25}{16}\left[\frac{\epsilon_p^2}{(1 - \epsilon_p/\epsilon_{p,max})^2}\right]$ | |
| Graham (1981) | $\mu_{mix} = \left[\frac{9}{4}\left(\frac{1}{1+0.5\psi}\right)\left(\frac{1}{\psi} - \frac{1}{1+\psi} - \frac{1}{1+\psi}^2\right) + 1 + 2.5\epsilon_p\right]$ | $\psi = \frac{1 - (\epsilon_p/\epsilon_{p,max})^{1/3}}{\epsilon_{p,max})^{1/3}}$ |
| Ishii (1977) | $\mu_{mix} = \mu_c(1 - \epsilon_p/\epsilon_{p,max})^{-2.5\epsilon_{p,max}}$ | $\mu_p \gg \mu_c$ |

Note: In the above, $\mu_{mix}$ and $\mu_p$ denote the mixture and particle viscosities, respectively. The particle- and continuum volume fractions are respectively denoted by $\epsilon_p$ and $\epsilon_c$, and $\epsilon_{p,max}$ is the maximum particle volume fraction obtainable, which usually falls in the range of 40% (i.e. $\epsilon_{p,max} \approx 0.4$).

In literature two different ways of formulating expressions for the particle pressure exist. One is based on the kinetic theory of granular flow, the other is described below:

The pressure is assumed to consist of the sum of three effects: The first corresponds to momentum transport caused by particle velocity fluctuations, $p_{p,kin}$. The second is due to particle interactions (i.e. collisions), $p_{p,coll}$ and the third is a contribution from the continuum phase pressure. The pressure gradient in the particulate phase is thus

$$\nabla(\epsilon_p p_p) \quad = \quad \nabla(\epsilon_p p_{kin}) + \nabla(\epsilon_p p_{coll}) + \nabla(\epsilon_p p_c). \qquad (2.6.14)$$

The first term on the right-hand side is neglected in traditional models. The second term is referred to as the particle collisional pressure gradient. The collisional component is the dominant pressure in dense regions. This pressure transmits a force both by short collisional impacts and by long-duration particle-particle contacts. In Section 2.4 it was stated that the aforementioned modelling methods may be applied to fluidised beds: Experimental results by Campbell and Wang (1991) showed that the particle collisional pressure is highest if the bed is not fluidised and particles rest on each other, when the long duration contact force is high. As continuum flow increases

towards the minimum fluidisation velocity, the particle collisional pressure decreases as the drag force starts to dominate over the long-duration contact force. Further increase in the continuum velocity above the minimum fluidisation velocity, causes the particle collisional pressure to increase again, now as a result of an increasing frequency of the short-duration collisional impacts.

The continuum pressure gradient enters into the momentum equations as a buoyant effect, i.e. if there is a continuum pressure gradient through a collective of particles, it exerts a force on the particles and thus the particle pressure gradient will be reduced or increased depending on the direction of the gas pressure gradient.

Several models for the particle collisional pressure-gradient term presented in literature are based on the following formulation

$$\nabla(\epsilon_p p_{p,coll}) \quad = \quad -G(\epsilon_c)\nabla\epsilon_c, \tag{2.6.15}$$

where $G(\epsilon_c)$ is the equivalent of a modulus of elasticity used in molecular theory for the particulate phase. The particle collisional pressure-gradient is often referred to as the particle-particle interaction force. The main effect of the particle-particle interaction force is only to prevent the discrete phase from becoming too densely packed (Enwald *et al.* (1997)).

This discussion concludes the traditional modelling process for the constitutive laws which specify how the physical parameters of a phase interact with one another. It remains to describe the transport of mass, momentum and energy across the interface between the phases. In the following section, interfacial momentum transfer is described, whereas interfacial mass and energy transfer have been excluded from this study.

### 2.6.1.6  Momentum transfer

The term under consideration here is the interfacial momentum transfer from the $\alpha$- to the $\beta$-phase which is given by the right-hand side of Equation (2.6.9)

$$\underline{M}_{\alpha\beta} \quad = \quad \frac{1}{\mathcal{U}_o} \int_{\mathcal{S}_{\alpha\beta}} \underline{\underline{\sigma}}_\alpha \cdot \underline{n}_\alpha d\mathcal{S}. \tag{2.6.16}$$

For the momentum conservation equation of the $\beta$-phase, the unit vector is given by, $\underline{n}_\beta = -\underline{n}_\alpha$. It follows that the momentum transfer from the $\beta$- to the $\alpha$-phase is

$$\underline{M}_{\beta\alpha} \;\; = \;\; -\underline{M}_{\alpha\beta}. \tag{2.6.17}$$

For a dispersed flow, $\underline{M}_{\alpha\beta}$ is the generalised drag force per unit of volume on a suspension of particles of mean diameter $d_p$ and it is normally divided as (Kleinstreuer (2003), Soo (1990), Croce *et al.* (2006) and Enwald *et al.* (1997))

$$\underline{M}_{\alpha\beta} \;\; = \;\; n_p \left( \underline{F}_D + \underline{F}_{TR} + \underline{F}_{AM} + \underline{F}_{HI} + \underline{F}_{OT} \right), \tag{2.6.18}$$

where $n_p$ is the number of particles per unit volume. The forces on the right-hand side of Equation (2.6.18) respectively denote the drag force, the transverse or lift force, the added mass force, the history force and other forces that are yet to be determined. These forces and their contributions to the total momentum transfer, are discussed in Appendix A.

Currently, the stationary drag force at the interface is the only one considered in the traditional two-fluid model. Empirical correlations account for this force, by which momentum transport at the interface is modelled. It is normal to consider the interface drag force as a combination of both the shape and the skin drag in a single empirical parameter (e.g. van Wachem *et al.* (2004)).

Most of the data used for drag force correlation in many multi-particle systems were obtained in uniform fluidisation and sedimentation studies: Typically, the drag force is determined through experimental measurement of the pressure gradient. Usually the experimental measurements are used to calculate the so-called *drag function* at the interface, $K$, either in a straightforward way, where $K = f(\Delta P)$, or as a function of the drag coefficient for a single particle in the suspension, $C_{ds}$, so $K = f(C_{ds}(\Delta P))$ (Gomez and Milioli (2004)).

By making use of this methodology, various correlations for $K$ have been proposed in the literature and a detailed account of such methods may be viewed in Mazzei and Lettieri (2007). For instance, Ergun (1952) measured pressure gradients in a fixed liquid-solid bed and developed an expression for $\Delta P$. This correlation was later used to calculate $K$ in a straightforward way, i.e. $K = f(\Delta P)$. Wen and Yu (1966) developed experiments on the sedimentation of solid particles in a liquid for a large range of solid volumetric fraction values. They considered their own data as well as data from other

researchers and derived a correlation for $C_{Ds}$, valid for $0.01 < \epsilon_p < 0.63$.  Later this correlation was used to indirectly calculate $K$, giving rise to an expression of the type $K = f(C_{Ds}(\Delta P))$.  Along with work done by Lewis *et al.* (1949) and Kmiec (1982), these equations serve as the prevalent equations of closure employed to model the drag force in uniformly dispersed emulsions of solid particles.

The drag force acting on a single particle in a suspension can be written as

$$\underline{F}_D \quad = \quad \frac{1}{2} C_{Ds} \rho_c |\underline{v}|\, \underline{v} (\pi d_p^2/4), \tag{2.6.19}$$

where $\underline{v}$ is either the apparent relative velocity or the relative interstitial velocity, depending on the velocity on which the drag coefficient $C_{Ds}$ is based.  The contributory effect of the stationary drag to the generalised drag is given by

$$n_p\, \underline{F}_D \quad = \quad \frac{3}{4 d_p}(1 - \epsilon_c) C_D \rho_c |\underline{v}|\, \underline{v}. \tag{2.6.20}$$

To solve averaged momentum equations numerically, the stationary drag force is usually written as

$$n_p\, \underline{F}_D \quad = \quad K\, \underline{v}_r, \tag{2.6.21}$$

where $K$ is referred to as the drag function.  Table 2.5 lists various drag functions used in literature.

**Table 2.5:** Drag functions by various authors.

| Author | Drag function, $K$ | Constants |
|---|---|---|
| Gidaspow (1986) | $\frac{3}{4d_p}C_{Ds}(1-\epsilon_c)\rho_c|\underline{v}_c - \underline{v}_p|\epsilon_c^{-1.65}$ | $C_{Ds} = \begin{cases} 24 & \text{if } Re < 1000 \\ 0.44 & \text{if } Re > 1000 \end{cases}$ |
| Ishii (1977) | $\frac{3}{4d_p}C_{Ds}(1-\epsilon_c)\rho_c|\underline{v}_c - \underline{v}_p|\epsilon_c$ | $C_D = 24(1 + 0.1(Re)^{0.75})/Re,$ <br> $Re = \rho_c|\underline{v}_p - \underline{v}_c|d_p/\mu_{mix}$ <br> $\mu_{mix}$ : from Ishii (1977) in Table 2.4 |
| Syamlal and O'Brien (1989) | $\frac{3}{4d_p}c_d\rho_c\frac{1}{R_t^2}\epsilon_c(1-\epsilon_c)|\underline{v}_p - \underline{v}_c|$ | $2R_t = C_1(\epsilon_c) - 0.06Re + \big[(0.06Re)^2 +$ <br> $0.12Re\,(2C_2(\epsilon_c) - C_1(\epsilon_c)) + C_1^2(\epsilon_c)\big]^{0.5}$ <br> $C_1(\epsilon_c) = \epsilon_c^{4.14}$ <br> $C_2(\epsilon_c) = \begin{cases} 0.8\epsilon_c^{1.28} & \text{if } \epsilon_c < 0.85 \\ \epsilon_c^{2.65} & \text{if } \epsilon_c > 0.85. \end{cases}$ <br> $C_D = \left(0.63 + 4.8\sqrt{\frac{R_t}{Re}}\right)^2$ Dallavalle (1948) <br> $Re = \rho_c|\underline{v}_p - \underline{v}_c|d_p/\mu_c$ |
| Di Felice (1994) | $\frac{3}{4d_p}C_{Ds}(1-\epsilon_c)\rho_c|\underline{v}_p - \underline{v}_c|\epsilon_c^{2-\beta}$ | $C_{Ds} = \left(0.63 + 4.8\sqrt{\frac{1}{Re}}\right)^2$ <br> $\beta = 3.7 - 0.65exp\left[-(1.5 - \log(Re))^2/2\right]$ |
| Gidaspow (1994) (based on Ergun) | $150\frac{(1-\epsilon_c)^2\mu_c}{\epsilon_c(\phi d_p)^2} + 1.75\frac{(1-\epsilon_c)\rho_c|\underline{v}_p - \underline{v}_c|}{\phi d_p}$ | $\epsilon_c < 0.8$ |
| Gibilaro *et al.* (1985) | $K = \left(\frac{17.3}{Re} + 0.336\right)\frac{\rho_c|\underline{v}_p - \underline{v}_c|}{d_p}(1-\epsilon_c)\epsilon_c^{-1.8}$ | $Re$ from Ishii and Zuber (1979) |

## 2.6.2   Contemporary discrete phase modelling methods

The equation of motion for a single sphere, moving in an unsteady non-uniform compressible fluid, was proposed by Maxey and Riley (1983) for the case of low particle Reynolds number, $Re = \rho_c d_p|\underline{v}_p - \underline{v}_c|/\mu_c < 1$. It is generally accepted (Enwald *et al.* (1997)) that the equation of motion for a single sphere can be generalised, in the case

of incompressible flows at higher Reynolds numbers, as

$$
\begin{aligned}
\rho_p \frac{\pi d_p^3}{6} \frac{d\,\underline{v}_p}{dt} &= \frac{1}{2}\rho_c C_{Ds} \frac{\pi d_p^2}{4}|\underline{v}'_c - \underline{v}_p|(\underline{v}'_c - \underline{v}_p) + \frac{1}{2}\rho_c \frac{\pi d_p^3}{6}\Delta_A \frac{d}{dt}(\underline{v}'_c - \underline{v}_p) \\
&\quad + \frac{3d_p^2}{2}\sqrt{\pi\rho_c\mu_c}\Delta_H \int_0^t \frac{d}{d\tau}(\underline{v}'_c - \underline{v}_p)\frac{d\tau}{\sqrt{t-\tau}} - \frac{\pi d_p^3}{6}\nabla p' + \rho_p \frac{\pi d_p^3}{6}\underline{g},
\end{aligned}
$$

$$(2.6.22)$$

where $d_p$ denotes the particle diameter, $\underline{v}'_c$ and $p'$ are the undisturbed continuum velocity and static continuum pressure at the particle location, respectively, i.e. the velocity and pressure of the continuum phase if the particle was not present. The terms on the right-hand side are identified as the stationary drag, the added mass force the history force, the pressure gradient and the gravity force, respectively. Different correlations for the drag coefficient for a single sphere, $C_{Ds}$, in an infinite fluid and for the correction coefficients for the added mass and the history forces, $\Delta_A$ and $\Delta_H$, can be found in Clift *et al.* (1978).

It can be shown that the history force is negligible for continuum-particle flows, provided that $\rho_c/\rho_p < 0.002$ and $d_p > 1\mu m$ (Liang and Michaelides (1992) and Vojir and Michaelides (1994)). Liang and Michaelides (1992) also concluded that the added mass effect can be neglected because the added mass term is proportional to the density ratio. It is generally assumed that these conclusions can be extended to a single particle in a suspension. Therefore, Equation (2.6.22) can be expressed in the following Eulerian form

$$
\frac{\partial}{\partial t}(\rho_p \underline{v}_p) + \nabla \cdot (\rho_p \underline{v}_p \underline{v}_p) = \frac{\rho_p}{\tau_{Gp}^X}(\underline{v}'_c - \underline{v}_p) - \nabla p' + \rho_p \underline{g} + \underline{F}_{PP}, \quad (2.6.23)
$$

where the particle relaxation time $\tau_{Gp}^X$ is

$$
\tau_{Gp}^X = \frac{3}{4d_p}\frac{\rho_c}{\rho_p}C_D|\underline{v}_p - \underline{v}'_c|, \quad (2.6.24)
$$

and $\underline{F}_{PP}$ represents the force exerted by other particles during collisions. The particle relaxation time is a characteristic time for the entrainment of particles by the surrounding continuum.

Applying the averaging identities in combination with a Reynolds decomposition and $p' = p + \tilde{p}$, yields the following averaged form of the particulate phase momentum

conservation equation (Enwald *et al.* (1997)):

$$\frac{\partial}{\partial t}(\epsilon_p \rho_p \, \underline{v}_p) + \nabla \cdot (\epsilon_p \rho_p \, \underline{v}_p \, \underline{v}_p) \;\; = \;\; -\epsilon_p \nabla p + \nabla \cdot (\epsilon_p \underline{\underline{\tau}}_p^{Xp} + \epsilon_p \underline{\underline{\sigma}}_p^{Re}) + \epsilon_p \rho_p \, \underline{g} + \underline{M}_{pI}. \tag{2.6.25}$$

The interfacial momentum transfer, $\underline{M}_{cp}$, is given by $K(\underline{v}_c - \underline{v}_p)$. To close the momentum equations, models for the collisional and kinetic terms $(\epsilon_k \underline{\underline{\tau}}_k^{X_k} + \epsilon_k \underline{\underline{\sigma}}_k^{Re})$ are acquired by employing the Maxwell-Boltzmann equation. This method is described in detail in Enwald *et al.* (1997) and only a brief outline of the procedure and the final results for the closed form of the gradient of the particle stress will be given here.

### 2.6.3 Turbulence models for the particulate phase

The effective stress tensor is derived using Boltzmann theory, the Boussinesq approximation, the closure model of Jenkins and Richman (1985) and expressions put forward for the turbulent viscosity by Simonin (1995) and Peirano and Leckner (1998). It is given by Enwald *et al.* (1997) as

$$\epsilon_p(\underline{\underline{\tau}}_p + \underline{\underline{\sigma}}_p^{Re}) \;\; = \;\; -\left(P_p - \xi_p \nabla \cdot \underline{v}_p\right)\underline{\underline{I}} + 2\mu_p\left(\underline{\underline{S}}_p - \frac{1}{3}(\nabla \cdot \underline{v}_p)\underline{\underline{I}}\right). \tag{2.6.26}$$

In Equation (2.6.26) the effective pressure is

$$p_p \;\; = \;\; \epsilon_p \rho_p T \left(1 + 2\epsilon_p g_0(1 + e)\right), \tag{2.6.27}$$

where $e$ is the restitution coefficient which represents the loss of energy during collisions and varies between zero and one. The bulk viscosity, $\xi$, in Equation (2.6.26) is given by

$$\xi_p \;\; = \;\; \frac{4}{3}\epsilon_p^2 \rho_p d_p g_0(1 + e)\sqrt{\frac{T}{\pi}}. \tag{2.6.28}$$

The radial distribution function, $g_0$, describes the probability of finding two particles in close proximity. Its main purpose is to prevent over-compaction of granular matter as it acts as a repulsion function between particles when they are close to each other. This function is equal to unity for very low particle volume fractions ($\epsilon_p \ll 1$) but increases for highly concentrated particulate systems. The function is, however, not well known for granular matter and many possible definitions exist (Dartevelle (2003)).

One such a definition is given by Lun and Savage (1986) as[2]

$$g_0 \;=\; (1 - \epsilon_p/\epsilon_{p,max}). \tag{2.6.29}$$

The shear viscosity is given as the sum of a turbulent viscosity and a collisional viscosity, $\mu_p = \epsilon_p \rho_p \left\langle \nu_p^t + \nu_p^c \right\rangle$ and expressions for the turbulent viscosity is given by Enwald *et al.* (1997) as

$$\nu_p^t \;=\; \frac{\left(\frac{1}{3}\tau_{cp}^t k_{cp} + \frac{1}{2}\tau_{cp}T(1 + \epsilon_p g_0 \phi_c)\right)}{1 + \frac{\tau_{cp}}{2}\frac{\sigma_c}{\tau_p}}, \tag{2.6.30}$$

where $k_{cp}$ denotes kinetic energy whilst $\sigma_c$ and $\phi_c$ are defined by $(1+e)(3-e)/5$ and $2(1+e)(3e-1)/5$, respectively. The interaction time between particle motion and continuum phase fluctuations is denoted by $\tau_{cp}^t$ and $\tau_{cp}$ is the particle relaxation time. The expression for the collisional viscosity, $\nu_p^c$, is defined by

$$\nu_p^c \;=\; \frac{4}{5}\epsilon_p g_0 (1 + e)\left(\nu_p^t + d_p\sqrt{\frac{T}{\pi}}\right). \tag{2.6.31}$$

Finally, a transport equation for the granular temperature, or for the turbulent kinetic energy, $T$, of the particulate phase, $k_p = 3T/2$, is required. This is given by

$$\begin{aligned}
\epsilon_p \rho_p \frac{D}{Dt}(k_p) \;=\;& \nabla\left(\epsilon_p \rho_p (K_p^t + K_p^c)\nabla k_p\right) - \left(-\epsilon_p(\underline{\underline{\tau}}_p + \underline{\underline{\sigma}}_p^{Re})\right)\nabla \cdot \underline{v}_p \\
& - \frac{2\epsilon_p \rho_p}{\tau_{cp}}(2k_p - k_{cp}) + \epsilon_p \rho_p \frac{e^2 - 1}{3\tau_p^c}k_p,
\end{aligned} \tag{2.6.32}$$

where $K_p^t$ and $K_p^c$ are the turbulent and collisional diffusivity coefficients, respectively and the time scale $\tau_p^c = (d_p/23g_0\epsilon_p)\sqrt{\pi/T}$ is the particle-particle collision time, i.e. the time between two consecutive binary collisions for a given particle. The continuum-particle covariance, $k_{cp}$, is defined as $\left\langle \tilde{\underline{v}}_p \tilde{\underline{v}}_c \right\rangle$. Various models for continuum-particle covariance may be found in Yu and Lee (2009).

The turbulent diffusivity is modelled as

$$K_p^t \;=\; \frac{\frac{3\tau_{cp}^t}{5\tau_{cp}}k_{cp} + T(1 + \epsilon_p g_0 \varsigma_c)}{\frac{9}{5\tau_{cp}} + \frac{\xi_c}{\tau_p^c}}, \tag{2.6.33}$$

where $\varsigma_c = 3(1+e)^2(2e-1)/5$ and $\xi_c = (1+e)(49-33e)/100$. The collisional diffusivity, $K_p^c$, is defined by

$$K_p^c \;=\; \epsilon_p g_0 (1 + e)\left(\frac{6}{5}K_p^t + \frac{4}{3}d_p\sqrt{\frac{T}{\pi}}\right). \tag{2.6.34}$$

---

[2]This resembles the viscosity equation given in Table 2.4 by Ishii (1977).

Semi-empirical models have been suggested by Simonin (1995) to solve Equation (2.6.32) and the reader is referred to Enwald *et al.* (1997) for a detailed example and review of turbulence models.

It is clear that the Boltzmann method for determining particle viscosities and pressures is complex and still relies on empirical data. This may be one of the reasons why the simplicity of the two-fluid model has proved more popular in the development of source codes to model two-phase flow.

# Chapter 3

# Conservation equations

## 3.1 Introduction

The development of an alternative to existing two-phase flow models requires obtaining and averaging the conservation expressions for the continuum and discrete phases. In order to guide the reader from start to finish, a brief review is given of the well known Navier-Stokes momentum conservation equations for the continuum phase, followed by a discussion on the development of momentum- and mass conservation expressions for the particle phase.

## 3.2 Mass conservation for the continuum phase

The mass, $m_c$, of an arbitrary material volume, $V_c$, within the continuum phase is given by the integral

$$m_c = \iiint\limits_{\mathcal{V}_c} \rho_c d\mathcal{V}, \tag{3.2.1}$$

where $\rho_c$ is the density of the continuum. Conservation of mass requires that

$$\frac{dm_c}{dt} = \frac{d}{dt} \iiint\limits_{\mathcal{V}_c} \rho_c d\mathcal{V} = 0. \tag{3.2.2}$$

Application of the Reynolds transport theorem, which may be viewed as a three-dimensional generalisation of the Leibniz theorem which is used to differentiate under

29

the integral sign, to Equation (3.2.2), yields

$$\iiint\limits_{\mathcal{V}_c} \left[ \frac{\partial \rho_c}{\partial t} + \nabla \cdot (\rho_c \, \underline{v}_c) \right] d\mathcal{V} \;\; = \;\; 0. \tag{3.2.3}$$

The integrand in Equation (3.2.3) should however be zero for any material volume, even if the size of such a volume should tend to zero. It follows that locally at any point within a continuum, for which mass conservation holds, the following continuity expression holds

$$\frac{\partial \rho_c}{\partial t} + \nabla \cdot (\rho_c \, \underline{v}_c) \;\; = \;\; 0. \tag{3.2.4}$$

Equation (3.2.4) concludes the derivation and is the mass conservation equation *per unit volume* for the continuum.

## 3.3 Momentum conservation for the continuum phase

External forces that influence a continuum via vector fields, such as gravitation, work on each individual mass point of the continuum. It is therefore called body forces. Let $\underline{f}_b$ be the total body force per unit mass at any point within the continuum. The resulting body force, $\underline{F}_b^{res}$, on a volume $\mathcal{V}_c$ of the continuum is therefore given by

$$\underline{F}_b^{res} \;\; = \;\; \iiint\limits_{\mathcal{V}_c} \rho_c \, \underline{f}_b \, d\mathcal{V}. \tag{3.3.1}$$

When a conceptual volume is defined, the effect of the surrounding surface forces on such a volume should be taken into consideration. These contact forces per unit area of the continuum are defined as stress and will be denoted by the stress dyad, $\underline{\underline{\sigma}}_c$. The resulting surface force on a volume $\mathcal{V}_c$ of the continuum is therefore given by

$$\underline{F}_{Surf} \;\; = \;\; \oiint\limits_{\partial \mathcal{V}_c} \underline{n}_c \cdot \underline{\underline{\sigma}}_c \, d\mathcal{S}. \tag{3.3.2}$$

For a general description of the motion of a continuum the volume $\mathcal{V}_c$ is considered to be a material volume. The internal forces at every point in a deformable body are

not necessarily equal, and therefore there exists a distribution of stresses throughout the body. Newton's second law of motion for the conservation of linear and angular momentum governs this variation of internal forces throughout the body. These laws are usually applied to a rigid particle but, for the purpose of continuum mechanics are extended to a body of continuously distributed mass and are referred to as Euler's equations of motion. Euler's first axiom or law (law of balance of linear momentum or balance of forces) states that:

> In an inertial frame, the time rate of change of linear momentum, $\underline{\mathcal{P}}$, of an arbitrary portion of a continuum body is equal to the total applied force, $\underline{\mathcal{F}}$, acting on the considered portion.

It may be expressed as

$$\underline{\mathcal{F}} \;=\; \frac{d\underline{\mathcal{P}}}{dt}. \tag{3.3.3}$$

Following Euler's linear momentum principle, as applied on $\mathcal{V}_c$, yields

$$\frac{d}{dt}\iiint\limits_{\mathcal{V}_c} \rho_c\,\underline{v}_c\,d\mathcal{V} \;=\; \iiint\limits_{\mathcal{V}_c}\rho_c\,\underline{f}_b\,d\mathcal{V} + \oiint\limits_{\partial\mathcal{V}_c}\underline{n}_c\cdot\underline{\underline{\sigma}}_c\,d\mathcal{S}. \tag{3.3.4}$$

The divergence theorem is applied to the surface integral in Equation (3.3.4), yielding

$$\iiint\limits_{\mathcal{V}_c}\frac{d}{dt}(\rho_c\,\underline{v}_c - \rho_c\,\underline{f}_b - \nabla\cdot\underline{\underline{\sigma}}_c)d\mathcal{V} \;=\; \underline{0}. \tag{3.3.5}$$

The material volume, however, was chosen arbitrarily and Equation (3.3.5) therefore holds for any volume $\mathcal{V}_c$. It follows that, at any point within the continuum

$$\frac{d}{dt}\left(\rho_c\,\underline{v}_c\right) \;=\; \rho_c\,\underline{f}_b + \nabla\cdot\underline{\underline{\sigma}}_c. \tag{3.3.6}$$

Equation (3.3.6) is commonly known as Cauchy's differential equation for the motion of any continuum. It holds in general and may be applied to rigid bodies, elastic objects and fluids (i.e. liquids or gasses).

Applying the definition of the total derivative yields

$$\frac{\partial}{\partial t}\left(\rho_c\,\underline{v}_c\right) + \nabla\cdot\left(\rho_c\,\underline{v}_c\,\underline{v}_c\right) \;=\; \nabla\cdot\underline{\underline{\sigma}}_c + \rho_c\,\underline{f}_b. \tag{3.3.7}$$

Equation (3.3.7) is the momentum conservation equation *per unit volume* for the continuum phase.

## 3.4   Mass conservation for the particle phase

Consider a moving particle with changing mass as shown in Figure 3.1.
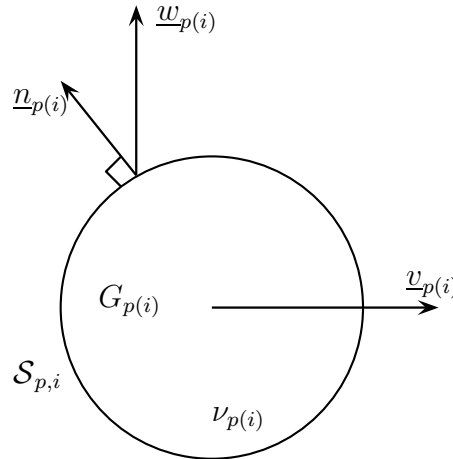


**Figure 3.1:** Solid particle.

Here $G_{p(i)}$ is the centre of mass of the solid particle $i$ moving with velocity $\underline{v}_{p(i)}$, $\nu_{p(i)}$ is the volume of the particle and $\underline{w}_{p(i)}$ is the velocity of a point on the boundary of particle $i$. Let $m_{p(i)}(t)$ denote the mass of particle $i$ at time $t$. In the absence of sources and/or sinks within the particle, mass-change is only due to a mass flux across its boundary, i.e. combustion or condensation. The change of mass with respect to time is therefore given by

$$\frac{dm_{p(i)}(t)}{dt} \;\; = \;\; \int\limits_{\mathcal{S}_{p(i)}} \rho_{p(i)} \left( \underline{w}_{p(i)} - \underline{v}_{p(i)} \right) \cdot \underline{n}_{p(i)} d\,\mathcal{S}, \tag{3.4.1}$$

where $\rho_{p(i)}$ is the density distribution of particle $i$. In Equation (3.4.1) the velocity difference, given by $\underline{w}_{p(i)} - \underline{v}_{p(i)}$, is the velocity of the particle boundary relative to its centre of mass, $G_{p(i)}$. The mass of the particle is a function of time only, therefore

$$\frac{dm_{p(i)}}{dt} \;\; = \;\; \frac{\partial m_{p(i)}}{\partial t} + \frac{dx_{p(i)}}{dt}\frac{\partial m_{p(i)}(t)}{\partial x_{p(i)}} \;\; = \;\; \frac{\partial m_{p(i)}}{\partial t}. \tag{3.4.2}$$

From Equations (3.4.2) and (3.4.1) it therefore follows that

$$\frac{\partial m_{p(i)}(t)}{\partial t} \;=\; \int\limits_{\mathcal{S}_{p(i)}} \rho_{p(i)} \left( \underline{w}_{p(i)} - \underline{v}_{p(i)} \right) \cdot \underline{n}_{p(i)} d\,\mathcal{S}. \tag{3.4.3}$$

Equation (3.4.3) is the mass conservation equation for a *single particle*.

## 3.5  Momentum conservation equation for the particle phase

From Newton's second law the following holds for each particle:

$$m_{p(i)} \frac{d\,\underline{v}_{p(i)}}{dt} \;=\; \underline{\mathcal{F}}, \tag{3.5.1}$$

where $\underline{\mathcal{F}}$ is the resultant force exerted on the particle. Generally, $\underline{\mathcal{F}}$ includes the gravitational force, aerodynamic drag, buoyancy, the added mass force, the Basset force, the Magnus effect, and the Saffman lift force. These forces and their relative contributions to the momentum of the particles are discussed by Fan and Zhu (1998) and Kleinstreuer (2003). According to Ding and Gidaspow (1990), the last four effects may be assumed negligible. The remaining three are grouped into surface forces, $\underline{F}_{surf}$, and volume forces, $\underline{F}_{vol}$[1]:

$$m_{p(i)} \frac{d\,\underline{v}_{p(i)}}{dt} \;=\; \underline{F}_{vol} + \underline{F}_{surf}. \tag{3.5.2}$$

It is assumed in the current work that the only significant volume force affecting the motion of a particle is the weight, $\underline{F}_W = m_{p(i)}\,\underline{g}$, and that the surfaces forces may be combined and written in terms of a stress tensor, $\underline{\underline{\sigma}}_{p(i)}$, integrated over the outer surface area of the particle. It then follows that

$$m_{p(i)} \frac{d\,\underline{v}_{p(i)}}{dt} \;=\; m_{p(i)}\,\underline{g} + \int\limits_{\mathcal{S}_{p(i)}} \underline{\underline{\sigma}}_{p(i)} \cdot \underline{n}_{p(i)} d\,\mathcal{S}. \tag{3.5.3}$$

Multiplying Equation (3.4.3) by the particle velocity, $\underline{v}_{p(i)}$, rewriting the particle mass, $m_{p(i)}$, as a product of its volume, $\nu_{p(i)}$ and density, $\rho_{p(i)}$, and adding the resulting

---

[1]For a detailed discussion on surface and volume forces, the reader is referred to Appendix A.

expression to Equation (3.5.3), yield

$$\rho_{p(i)}\nu_i \frac{d\,\underline{v}_{p(i)}}{dt} + \underline{v}_{p(i)}\frac{\partial \rho_{p(i)}\nu_i}{\partial t} = \nu_i \rho_{p(i)}\,\underline{g} + \int\limits_{\mathcal{S}_{p(i)}} \underline{\underline{\sigma}}_{p(i)} \cdot \underline{n}_{p(i)} d\,\mathcal{S} +$$

$$\underline{v}_{p(i)} \int\limits_{\mathcal{S}_{p(i)}} \rho_{p(i)} \left( \underline{w}_{p(i)} - \underline{v}_{p(i)} \right) \cdot \underline{n}_{p(i)} d\,\mathcal{S}. \quad (3.5.4)$$

The chain rule of differentiation is applied to the first term on the left-hand-side of Equation (3.5.4)

$$\frac{d}{dt}\,\underline{v}_{p(i)}(\underline{r},t) = \frac{\partial}{\partial t}\,\underline{v}_{p(i)}(\underline{x},t) + \frac{dx}{dt}\frac{\partial\,\underline{v}_{p(i)}}{\partial x} + \frac{dy}{dt}\frac{\partial\,\underline{v}_{p(i)}}{\partial y} + \frac{dz}{dt}\frac{\partial\,\underline{v}_{p(i)}}{\partial z}, \quad (3.5.5)$$

which may be expressed as

$$\frac{d}{dt}\,\underline{v}_{p(i)}(\underline{r},t) = \frac{\partial}{\partial t}\,\underline{v}_{p(i)}(\underline{r},t) + \underline{v}_{p(i)} \cdot \nabla\,\underline{v}_{p(i)}. \quad (3.5.6)$$

Substitution of Equation (3.5.6) into Equation (3.5.4), yields

$$\frac{\partial}{\partial t} \left( \underline{v}_{p(i)}\rho_{p(i)}\nu_i \right) + \rho_{p(i)}\nu_i\,\underline{v}_{p(i)} \cdot \nabla\,\underline{v}_{p(i)} = \nu_i \rho_{p(i)}\,\underline{g} +$$

$$\int\limits_{\partial \nu_{p(i)}} \underline{\underline{\sigma}}_{p(i)} \cdot \underline{n}_{p(i)} d\,\mathcal{S} + \underline{v}_{p(i)} \int\limits_{\mathcal{S}_{p(i)}} \rho_{p(i)} \left( \underline{w}_{p(i)} - \underline{v}_{p(i)} \right) \cdot \underline{n}_{p(i)} d\,\mathcal{S}, \quad (3.5.7)$$

where $m_{p(i)} = \rho_{p(i)}\nu_{p(i)}$ and the chain rule has again been applied to the left-hand side of the expression.

Equation (3.5.7), which is valid for each particle, describes the change in momentum of a particle with mass $m_{p(i)} = \rho_{p(i)}\nu_{p(i)}$. The first term on the left-hand side of Equation (3.5.7) is the transient term which constitutes the change in the velocity and density of a single particle over time. It describes the effect of acceleration or deceleration as well as time dependent combustion or condensation on the momentum of the particle. The second term, commonly designated the convective term in continuum dynamics, indicates how the momentum of the particle is affected by a change in the velocity of the particle with a change in its position. The third term, known as the body force term, describes the effect on the momentum of the particle from outside forces which act on the centre of mass of the particle.

The first integral represents the stresses on the particle's boundary surface. The second integral describes the change of momentum of the particle due to mass flow across the particle boundary (i.e. combustion or condensation).

# Chapter 4

# Averaging

## 4.1 Introduction

The objectives of this chapter are to quantify the concept and size range of the Representative Elementary Volume (REV) and to subsequently apply the REV to derive rules for modelling the transport of various quantities in dispersed media at the macroscopic level. These averaging rules are then applied to the Navier-Stokes momentum and the mass conservation equations which were formulated in Chapter 3.

## 4.2 Arbitrary and Representative Elementary Volumes

Solving the transport phenomena in a two-phase flow domain can be done at microscopic level. This is however impractical since a) it is computationally expensive to determine and b) quantities cannot be measured at this level and experimental data for comparative purposes therefore do not exist. These difficulties may however be avoided by considering each phase as a continuum. The actual two-phase discrete/continuum medium, in which each phase fills only a portion of the spatial domain, is replaced by a virtual model in which the continuum phase fills the entire domain.

In contrast to the traditional volume averaging models, where both phases are described as separate continuums (Bachmat and Bear (1986), Whitaker (1967)), the discrete phase remains separated in this work. And the discrete nature is dealt with by replacing the integral definition, customarily used for continuum averaging, with a summation

36

procedure and a detailed discussion follows in Section 4.6.

Average values over Elementary Volumes (EV) are designated as macroscopic values of variables. For both the discrete and continuum, these macroscopic entities are defined and allocated to the centroid of the EV, regardless of whether the centroid coincides with that phase. Fields of macroscopic variables may be obtained by traversing the EV over the entire domain.

Any Arbitrary Elementary Volume (AEV) may in principle be selected as an averaging volume for passing from the microscopic to the macroscopic regime. Different AEV's will however yield different averages depending on the size of the AEV and therefore need to be labelled to the particular AEV used for its averaging. This predicament is circumvented by introducing the concept of a Representative Elementary Volume (REV) (Whitaker (1967), Hassanizadeh and Gray (1979), and Bachmat and Bear (1986)).

The REV is chosen such that averaged properties of the continuum or discrete phase are statistically meaningful, i.e. representative of measured values. It follows that averaged values of properties obtained from averaging with an REV are independent of the size of the averaging volume.

Irrespective of its placement within a domain, the REV should contain both continuum and particle phases and be representative of the entire domain. The criteria given in the work of Bachmat and Bear (1986), Whitaker (1967), and Hassanizadeh and Gray (1979) for the selection of sensible general REV dimensions are subsequently discussed.

### 4.2.1 Selection of REV size

Bachmat and Bear (1986) stresses that the values of all averaged geometrical characteristics of the microstructure of the porous material at any point in the porous medium domain be single valued functions of the location of that point and of time only, but independent of the size of the REV. It follows that the volume of an AEV, $\mathcal{U}_{AEV}$, may be regarded as the volume of an REV, $\mathcal{U}_o$, if the porosity, $\epsilon_c$, satisfies the following constraint

$$\frac{\partial \epsilon_c}{\partial \mathcal{U}_{AEV}} = 0, \tag{4.2.1}$$

where $\epsilon_c = \frac{\mathcal{U}_c}{\mathcal{U}_o}$, and $\mathcal{U}_c$ is the volume occupied by the continuum. The size of the

REV in a domain (D) is thus determined by the porosity (Bachmat and Bear (1986)). Figure 4.1 illustrates the variations of the ratio $\mathcal{U}_c/\mathcal{U}_{AEV}$ as $\mathcal{U}_{AEV}$ increases in size.
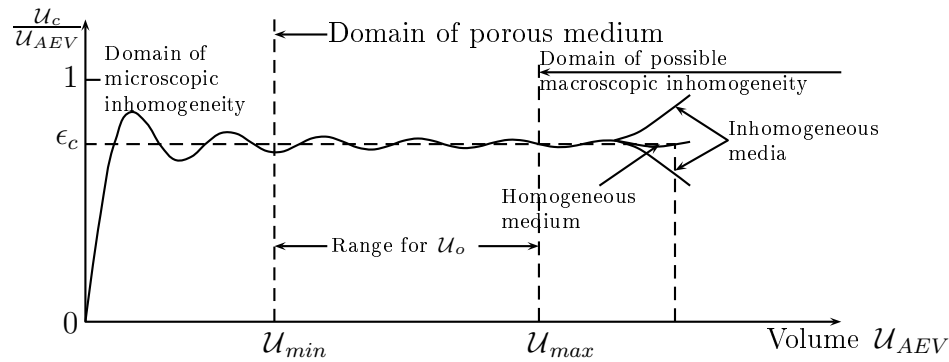


**Figure 4.1:** Variation of porosity in the neighbourhood of a point as a function of the average volume.

For small values of $\mathcal{U}_{AEV}$ the ratio, $\mathcal{U}_c/\mathcal{U}_{AEV}$, is one or zero, depending on whether the centroid of the REV, $\underline{x}_o$, falls inside the continuum or the discrete phase. As the volume of $\mathcal{U}_{AEV}$ increases, large fluctuations in $\mathcal{U}_c/\mathcal{U}_{AEV}$ occur. However, as $\mathcal{U}_{AEV}$ continues to grow, these fluctuations gradually abate, until, above some value $\mathcal{U}_{AEV} = \mathcal{U}_{min}$, it decays, leaving only small amplitude fluctuations around some constant value.

As illustrated in Figure 4.1, the REV is *that* volume, $\mathcal{U}_o$, within the range of $\mathcal{U}_{min} < \mathcal{U}_{AEV} < \mathcal{U}_{max}$ that will make the ratio, $\mathcal{U}_c/\mathcal{U}_o$, independent of $\mathcal{U}_{AEV}$, and hence a single valued function of $x_o$ only. There usually exists a number of relevant variables. The continuum description of the process described by such variables can be employed only if a common range of the REV can be found for all of these.

All average properties are assigned to the centroid of the REV, $x_{REV}$, which is illustrated in Figure 4.2. In Figure 4.2 the REV volume is given by $\mathcal{U}_o$. The section of the REV boundary surface which separates the continuum phase volume, $\mathcal{U}_c$, contained within the REV, from the continuum phase outside of the REV, is denoted by $\mathcal{S}_{cc}$. Sections of the REV boundary surface which cut through particles and points on particle surfaces where particles connect with each other, are given by $\mathcal{S}_{pp(i)}$. Similarly, the surfaces which separate the particle volumes, $\nu_{p(i)}$, from the continuum are given

by $\mathcal{S}_{pc(i)}$. The inward facing normal unit vectors for the particle and the continuum phases are denoted by $\underline{n}_{p(i)}$ and $\underline{n}_{c(i)}$, respectively.
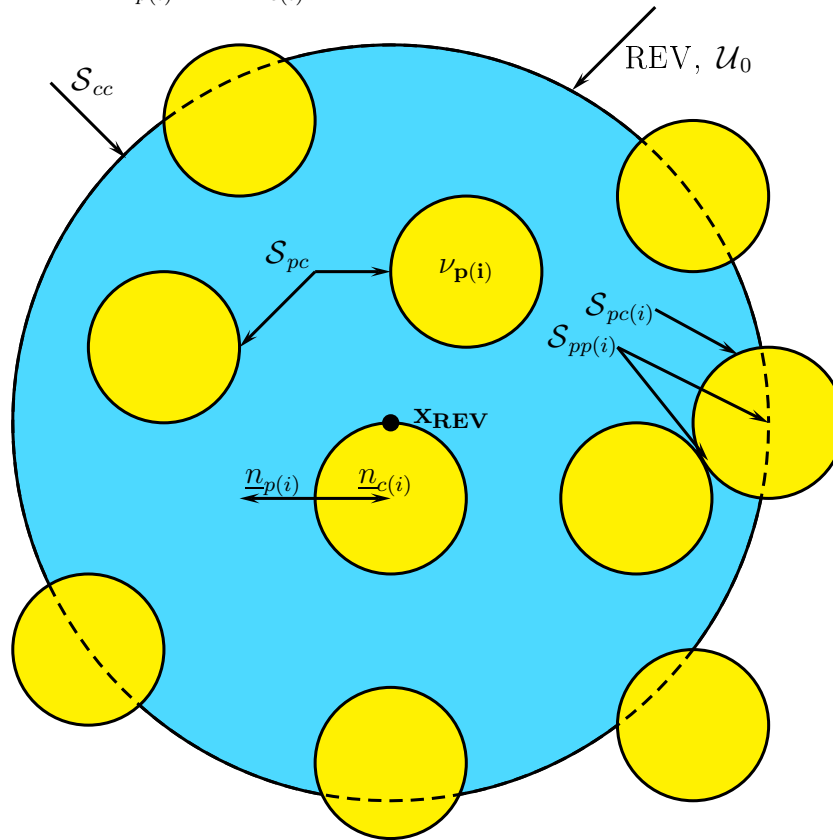


**Figure 4.2:** The Representative Elementary Volume (REV).

The initial averaging procedure, which applies the concept of an REV, averages the mass conservation equations completely but yields an integral term in the momentum conservation expressions in which microscopic variables remain.

## 4.3    Averaging rules for the continuum phase

Volume averaging for a continuum, as applied by Whitaker (1967), has been referred to in Chapter 2 and the rules that apply to such an averaging method have been derived in Appendix B. These averaging rules are repeated here in order that the reader may compare them with the averaging rules for the particulate phase that will be discussed in Section 4.6.

Let $\phi$ be a property of the continuum phase, which may be a scalar, vector or dyad and is assumed to be finite, continuous and differentiable within an REV with volume $\mathcal{U}_o$. Using an REV, the following definitions are made: The phase average of any continuum property, $\phi$, is defined as (Whitaker (1969))

$$\langle\phi\rangle \;=\; \frac{1}{\mathcal{U}_o}\int_{\mathcal{U}_c}\phi d\mathcal{U}, \tag{4.3.1}$$

and yields the average of any property $\phi$ over the entire REV volume, $\mathcal{U}_o$. The average of a property taken solely over the continuum section of the REV, $\mathcal{U}_c$, is denoted by

$$\langle\phi\rangle_c \;=\; \frac{1}{\mathcal{U}_c}\int_{\mathcal{U}_c}\phi d\mathcal{U}, \tag{4.3.2}$$

and is related to the phase average presented in Equation (4.3.1) by

$$\langle\phi\rangle \;=\; \epsilon_c\langle\phi\rangle_c, \tag{4.3.3}$$

where, $\epsilon_c = \mathcal{U}_c/\mathcal{U}_o$, signifies the fraction of the total REV volume which is occupied by the continuum phase. At any point within $\mathcal{U}_c$, the deviation of $\phi$ from the intrinsic phase average, $\langle\phi\rangle_c$, is defined by

$$\tilde{\phi} \;=\; \phi - \langle\phi\rangle_c. \tag{4.3.4}$$

The aforementioned definitions are used to derive averaging rules which are listed in Table 4.1 for the continuum phase. In Table 4.1 the velocity, $\underline{w}$, refers to the velocity at which the continuum-particle interface, $\mathcal{S}_{pc}$, is being displaced and $\underline{n}_c$ is the unit vector normal to the continuum phase on $\mathcal{S}_{pc}$, directed into the particle phase.

## 4.4 Averaging of the continuum mass conservation equation

The averaging rules, listed in Table 4.1, are applied to the equation for mass conservation of the continuum phase, given by Equation (3.2.4). A methodical approach is applied to the averaging process: The transient, convective and mass flux terms of Equation (3.2.4) are respectively labelled as Term 1, Term 2 and Term 3

$$\underbrace{\left\langle\frac{\partial\rho_c}{\partial t}\right\rangle}_{\text{Term 1}} + \underbrace{\langle\nabla\cdot(\rho_c\,\underline{v}_c)\rangle}_{\text{Term 2}} \;=\; \underbrace{\langle 0\rangle}_{\text{Term 3}}. \tag{4.4.1}$$

**Table 4.1:** Averaging rules for the continuum phase

| | |
|---|---|
| $i$ | $\langle \phi \rangle = \epsilon_c \langle \phi \rangle_c$ |
| $ii$ | $\langle \phi_1 + \phi_2 \rangle = \langle \phi_1 \rangle + \langle \phi_2 \rangle$ |
| $iii$ | $\langle \alpha \phi \rangle = \alpha \langle \phi \rangle,$ where $\alpha$ is a constant |
| $iv$ | $\langle \phi_1 \phi_2 \rangle_c = \langle \phi_1 \rangle_c \langle \phi_2 \rangle_c + \left\langle \tilde{\phi}_1 \tilde{\phi}_2 \right\rangle_c$ |
| $v$ | $\langle \nabla \phi \rangle = \nabla \langle \phi \rangle + \frac{1}{\mathcal{U}_o} \int_{\mathcal{S}_{pc}} \underline{n}_c \phi d\,\mathcal{S}$ |
| $vi$ | $\langle \nabla \phi \rangle = \epsilon_c \nabla \langle \phi \rangle_c + \frac{1}{\mathcal{U}_o} \int_{\mathcal{S}_{pc}} \underline{n}_c \tilde{\phi} d\,\mathcal{S}$ |
| $vii$ | $\langle \nabla \cdot \phi \rangle = \nabla \cdot \langle \phi \rangle + \frac{1}{\mathcal{U}_o} \int_{\mathcal{S}_{pc}} \underline{n}_c \cdot \phi d\,\mathcal{S}$ |
| $viii$ | $\left\langle \frac{\partial \phi}{\partial t} \right\rangle = \frac{\partial \langle \phi \rangle}{\partial t} - \frac{1}{\mathcal{U}_o} \int_{\mathcal{S}_{pc}} \underline{n}_c \cdot \underline{w} \phi d\,\mathcal{S}$ |

Rules $viii$ and $i$ are applied to Term 1, yielding

$$\left\langle \frac{\partial \rho_c}{\partial t} \right\rangle = \frac{\partial \epsilon_c \langle \rho_c \rangle_c}{\partial t} - \frac{1}{\mathcal{U}_o} \int_{\mathcal{S}_{pc}} \underline{n}_c \cdot \underline{v}_c \rho_c d\,\mathcal{S}, \tag{4.4.2}$$

where the velocity, $\underline{w}$, of the interface, $\mathcal{S}_{pc}$, has been replaced by the velocity, $\underline{v}_c$, of the continuum phase since it is assumed that these two are equivalent in the absence of combustion or condensation.

For the averaging of Term 2, application of averaging Rules $vii$ and $i$ is succeeded by

the use of *vi* and it follows that

$$
\begin{aligned}
\langle \nabla \cdot (\rho_c \, \underline{v}_c) \rangle \;=\;& \nabla \cdot \langle \rho_c \, \underline{v}_c \rangle + \frac{1}{\mathcal{U}_o} \int\limits_{\mathcal{S}_{pc}} \underline{n}_c \cdot \rho_c \, \underline{v}_c d\,\mathcal{S}, \\[2mm]
=\;& \nabla \cdot (\epsilon_c \, \langle \rho_c \, \underline{v}_c \rangle_c) + \frac{1}{\mathcal{U}_o} \int\limits_{\mathcal{S}_{pc}} \underline{n}_c \cdot \rho_c \, \underline{v}_c d\,\mathcal{S}, \\[2mm]
=\;& \nabla \cdot [\epsilon_c \, (\langle \rho_c \rangle_c \, \langle \underline{v}_c \rangle_c + \langle \tilde{\rho}_c \, \tilde{\underline{v}}_c \rangle_c)] + \frac{1}{\mathcal{U}_o} \int\limits_{\mathcal{S}_{pc}} \underline{n}_c \cdot \rho_c \, \underline{v}_c d\,\mathcal{S}. \quad (4.4.3)
\end{aligned}
$$

In constructing the mass conservation equation for the continuum phase, it was assumed that continuum mass would remain unchanged, hence the absence of a mass flux term and the zero value on the right-hand side of Equation (3.2.4). The average of Term 3 is given by

$$\langle 0 \rangle \;=\; 0. \tag{4.4.4}$$

Equations (4.4.2), (4.4.3) and (4.4.4) are assembled, and it follows that

$$\frac{\partial \langle \rho_c \rangle}{\partial t} + \nabla \cdot [\epsilon_c \, (\langle \rho_c \rangle_c \, \langle \underline{v}_c \rangle_c + \langle \tilde{\rho}_c \, \tilde{\underline{v}}_c \rangle_c)] \;=\; 0. \tag{4.4.5}$$

The added assumption of a constant continuum density, $\rho_c$, yields further simplification of Equation (4.4.5)

$$\frac{\partial \epsilon_c}{\partial t} + \nabla \cdot \epsilon_c \, \langle \underline{v}_c \rangle_c \;=\; 0, \tag{4.4.6}$$

which embodies a description for the conservation of continuum mass in terms of macroscopic state variables.

## 4.5  Averaging of the continuum momentum conservation equation

The approach followed in averaging the mass conservation equation for the continuum is repeated here. The momentum conservation equation for the continuum phase was given earlier by Equation (3.3.7) and is repeated here:

$$\underbrace{\frac{\partial \rho_c \, \underline{v}_c}{\partial t}}_{\text{Term 1}} + \underbrace{\nabla \cdot (\rho_c \, \underline{v}_c \, \underline{v}_c)}_{\text{Term 2}} \;=\; \underbrace{\nabla \cdot \underline{\underline{\sigma}}_c}_{\text{Term 3}} + \underbrace{\rho_c \, \underline{g}}_{\text{Term 4}}. \tag{4.5.1}$$

Under the assumption that the continuum density is constant, the application of Rules
*viii* and *i* to the transient term, labelled Term 1 in Equation (4.5.1), yields

$$\rho_c \left\langle \frac{\partial \underline{v}_c}{\partial t} \right\rangle = \rho_c \frac{\partial \epsilon_c \langle \underline{v}_c \rangle_c}{\partial t} - \rho_c \frac{1}{\mathcal{U}_o} \int_{\mathcal{S}_{pc}} \underline{n}_c \cdot \underline{v}_c \underline{v}_c d\mathcal{S}. \tag{4.5.2}$$

Application of averaging Rules *vii* and *i* to the convection term, labelled Term 2, yields

$$\rho_c \langle \nabla \cdot (\underline{v}_c \underline{v}_c) \rangle = \rho_c \nabla \cdot \langle \underline{v}_c \underline{v}_c \rangle + \rho_c \frac{1}{\mathcal{U}_o} \int_{\mathcal{S}_{pc}} \underline{n}_c \cdot \underline{v}_c \underline{v}_c d\mathcal{S},$$

$$= \rho_c \nabla \cdot \left[ \epsilon_c \left( \langle \underline{v}_c \rangle_c \langle \underline{v}_c \rangle_c + \underline{\langle \tilde{\underline{v}}_c \tilde{\underline{v}}_c \rangle_c} \right) \right] + \rho_c \frac{1}{\mathcal{U}_o} \int_{\mathcal{S}_{pc}} \underline{n}_c \cdot \underline{v}_c \underline{v}_c d\mathcal{S}. \tag{4.5.3}$$

The gradient of the underlined term in Equation (4.5.3) is denoted by Enwald *et al.*
(1997) as the *Reynolds stress* and has been discussed in Chapter 2. Following the
"traditional two-fluid derivation" by Enwald *et al.* (1997) and Hassanizadeh and Gray
(1979) in their assumption that the continuum flow remains laminar, Equation (4.5.3)
simplifies to

$$\rho_c \langle \nabla \cdot (\underline{v}_c \underline{v}_c) \rangle = \rho_c \nabla \cdot (\epsilon_c \langle \underline{v}_c \rangle_c \langle \underline{v}_c \rangle_c) + \rho_c \frac{1}{\mathcal{U}_o} \int_{\mathcal{S}_{pc}} \underline{n}_c \cdot \underline{v}_c \underline{v}_c d\mathcal{S}. \tag{4.5.4}$$

Rules *vii* and *i* are used in the averaging of the continuum stress contribution to the
momentum, and it follows that Term 3 is given by

$$\left\langle \nabla \cdot \underline{\underline{\sigma}}_c \right\rangle = \nabla \cdot \left( \epsilon_c \left\langle \underline{\underline{\sigma}}_c \right\rangle_c \right) + \frac{1}{\mathcal{U}_o} \int_{\mathcal{S}_{pc}} \underline{n}_c \cdot \underline{\underline{\sigma}}_c d\mathcal{S}. \tag{4.5.5}$$

The acceleration in the body force, given by Term 4, is assumed to be gravitational
acceleration, $\underline{g}$, and it follows that

$$\rho_c \left\langle \underline{g} \right\rangle = \rho_c \underline{g} \epsilon_c. \tag{4.5.6}$$

From Equations (4.5.2), (4.5.4), (4.5.5) and (4.5.6), it then follows that

$$\rho_c \frac{\partial \epsilon_c \langle \underline{v}_c \rangle_c}{\partial t} + \rho_c \nabla \cdot (\epsilon_c \langle \underline{v}_c \rangle_c \langle \underline{v}_c \rangle_c) = \rho_c \underline{g} \epsilon_c + \nabla \cdot \epsilon_c \left\langle \underline{\underline{\sigma}}_c \right\rangle_c + \frac{1}{\mathcal{U}_o} \int_{\mathcal{S}_{pc}} \underline{n}_c \cdot \underline{\underline{\sigma}}_c d\mathcal{S}, \tag{4.5.7}$$

which is the REV averaged form for the conservation of momentum for the continuum
phase.

## 4.6 Averaging rules for the particle phase

The particle phase is composed of discrete, solid, rigid particles which are, apart from when they collide, completely surrounded by the continuum phase. Due to the disjoint nature of the particles, the averaging procedures developed in Section 4.3 need to be adapted for the particulate phase.

Define a volumetric average of $n$ discrete particles as

$$\overline{\gamma} \;=\; \frac{1}{\mathcal{U}_o} \sum_{i=1}^{n} \gamma_{p(i)} \nu_{p(i)}, \tag{4.6.1}$$

and define the intrinsic phase average as,

$$\overline{\gamma}^{\,p} \;=\; \frac{1}{\mathcal{U}_p} \sum_{i=1}^{n} \gamma_{p(i)} \nu_{p(i)}. \tag{4.6.2}$$

The deviation from such an averaged quantity is defined as

$$\tilde{\gamma} \;=\; \gamma_{p(i)} - \overline{\gamma}^{\,p}. \tag{4.6.3}$$

The particle volume fraction, $\epsilon_p$, is linked to the continuum volume fraction, $\epsilon_c$, by

$$\epsilon_p \;=\; \frac{\mathcal{U}_p}{\mathcal{U}_o} = 1 - \epsilon_c \;=\; \overline{1} = \frac{1}{\mathcal{U}_o} \sum_{i=1}^{n} 1 \nu_{p(i)}, \tag{4.6.4}$$

where $\mathcal{U}_p = \sum_{i=1}^{n} \nu_{p(i)}$ is the total solid volume contained within the REV.

Although the particles are separated, the average values obtained are assumed to be defined at the centre of the REV, $\underline{x}_{REV}$. The averaging rules for the particle phase are listed in Table 4.2.

The set of rules given in Table 4.2 differs from those given in Table 4.1 in that Rules *vii*, *viii*, and *ix* do not contain integral terms. This is due to the fact that differentiation is additive and may therefore be taken out of the summation procedure used for averaging the discrete phase whereas the Leibniz theorem needs to be applied in order to differentiate under an integral sign in the case of the continuum phase.

**Table 4.2:** Averaging rules for the discrete phase.

| | |
|---|---|
| $i$ | $\overline{\gamma} = \epsilon_p \overline{\gamma}^{\,p}$ |
| $ii$ | $\overline{\gamma + \beta} = \overline{\gamma} + \overline{\beta}$ |
| $iii$ | $\overline{\mathrm{constant}\gamma} = \mathrm{constant}\overline{\gamma}$ |
| $iv$ | $\overline{\overline{\gamma}} = 0 = \overline{\tilde{\gamma}}$ |
| $v$ | $\overline{\tilde{\tilde{\gamma}}} = \tilde{\gamma}$ |
| $vi$ | $\overline{\gamma\beta}^{\,p} = \overline{\gamma}^{\,p}\overline{\beta}^{\,p} + \overline{\tilde{\gamma}\tilde{\beta}}^{\,p}$ |
| $vii$ | $\overline{\nabla \cdot \underline{\gamma}} = \nabla \cdot \overline{\underline{\gamma}}$ |
| $viii$ | $\overline{\nabla\underline{\gamma}} = \nabla\overline{\underline{\gamma}}$ |
| $ix$ | $\overline{\frac{\partial \gamma}{\partial t}} = \frac{\partial}{\partial t}\overline{\gamma}$ |

## 4.7 Averaging of the particle mass conservation equation

Equation (3.4.3) is summed over all particles contained either partially or fully within the REV:

$$\sum_{i=1}^{n} \frac{\partial m_{p(i)}(t)}{\partial t} = \sum_{i=1}^{n} \int_{\mathcal{S}_{(i)}} \rho_{p(i)} \left( \underline{w}_{p(i)} - \underline{v}_{p(i)} \right) \cdot \underline{n}_{p(i)} d\,\mathcal{S}_{(i)}. \qquad (4.7.1)$$

The term on the right-hand side of the integral is the sum of the surface integrals over each solid particle's surface. The surface, however, consists of both a particle-continuum interface, $\mathcal{S}_{pc(i)}$, and a particle-particle interface, $\mathcal{S}_{pp(i)}$, as was illustrated in Figure 4.2. The particle-particle boundary results due to a particle being contained

only partially within the REV. It follows that Equation (4.7.1) may be expressed as

$$
\sum_{i=1}^{n} \frac{\partial m_{p(i)}(t)}{\partial t} = \sum_{i=1}^{n} \left( \int_{\mathcal{S}_{pc(i)}} \rho_{p(i)} \left( \underline{w}_{p(i)} - \underline{v}_{p(i)} \right) \cdot \underline{n}_{p(i)} d\mathcal{S}_{(i)} + \int_{\mathcal{S}_{pp(i)}} \rho_{p(i)} \left( \underline{w}_{p(i)} - \underline{v}_{p(i)} \right) \cdot \underline{n}_{p(i)} d\mathcal{S}_{(i)} \right). \quad (4.7.2)
$$

The velocity of the particle boundary does however not exist over the $\mathcal{S}_{pp(i)}$ interface and it follows that

$$
\sum_{i=1}^{n} \frac{\partial m_{p(i)}(t)}{\partial t} = \sum_{i=1}^{n} \left( \int_{\mathcal{S}_{pc(i)}} \rho_{p(i)} \left( \underline{w}_{p(i)} - \underline{v}_{p(i)} \right) \cdot \underline{n}_{p(i)} d\mathcal{S}_{(i)} - \int_{\mathcal{S}_{pp(i)}} \rho_{p(i)} \underline{v}_{p(i)} \cdot \underline{n}_{p(i)} d\mathcal{S}_{(i)} \right). \quad (4.7.3)
$$

In order to evaluate the integral over the particle-particle interface, the spacial averaging theorem of Slattery (Whitaker (1967)) is applied to a single particle:

Consider a solid particle $i$ crossing the boundary of the REV as shown in Figure 4.3. The REV boundary moves a distance $\Delta x$ relative to the particle centre in time $\Delta t$. Let $\nu_{p(i)|x}$ denote the volume of the particle contained within the REV when the particle is at position $x_i$ and let $\nu_{p(i)|(x_i + \Delta x)}$ be the volume at position $x_i + \Delta x$. Let $\mathcal{S}_{pp(i)}$ be the surface area obtained by the intersection of the REV boundary with the particle.
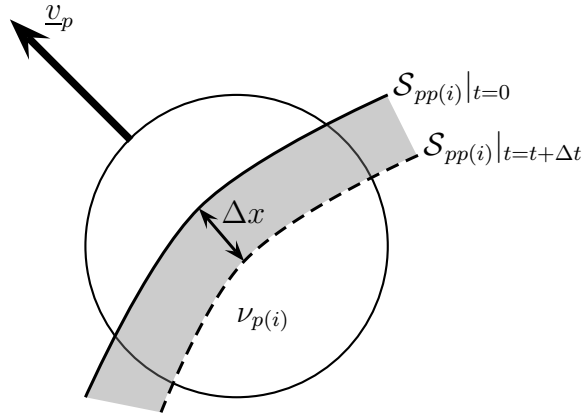
**Figure 4.3:** Solid particle at the REV boundary.

Referring to the Figure 4.3 and expressing the differentiation in terms of a limit, for a general variable $\phi$ it follows that

$$
\frac{\partial}{\partial x} \int_{\nu_{p(i)}} \phi d\nu_p = \lim_{\Delta x \to 0} \frac{1}{\Delta x} \left[ \int_{\nu_{p(i)}|_{x_i+\Delta x}} \phi d\nu_i - \int_{\nu_{p(i)}|_{x_i}} \phi d\nu_{p(i}} \right]
$$

$$
= \lim_{\Delta x \to 0} \frac{1}{\Delta x} \int_{\nu_i|_{x_i+\Delta x} - \nu_{p(i)}|_{x_i}} \phi d\nu_i. \tag{4.7.4}
$$

In the limiting case of $\Delta x \to 0$, the incremental volume element may be expressed as $d\nu_i = \Delta x\, d\,\mathcal{S}_i$ and Equation (4.7.4) reduces to

$$
\frac{\partial}{\partial x} \int_{\nu_{p(i)}} \phi d\nu_i = \lim_{\Delta x \to 0} \frac{1}{\Delta x}\Delta x \int_{\mathcal{S}_{pp(i)}} \phi d\,\mathcal{S}_i, \tag{4.7.5}
$$

which, in three-dimensions, may be written as

$$
\nabla \int_{\nu_{p(i)}} \phi d\nu_p = \int_{\mathcal{S}_{pp(i)}} \phi\, \underline{n}_{p(i)} d\,\mathcal{S}_i, \tag{4.7.6}
$$

where $\underline{n}_{p(i)}$ is an outward directed unit vector, perpendicular to $\mathcal{S}_{pp(i)}$.

Equation (4.7.6) is applied to Equation (4.7.3), yielding

$$
\underbrace{\sum_{i=1}^{n} \frac{\partial m_{p(i)}(t)}{\partial t}}_{\text{Term 1}} = \underbrace{\sum_{i=1}^{n} \int_{\mathcal{S}_{pc(i)}} \rho_{p(i)} \left( \underline{w}_{p(i)} - \underline{v}_{p(i)} \right) \cdot \underline{n}_{p(i)} d\,\mathcal{S}_i}_{\text{Term 2}} - \underbrace{\sum_{i=1}^{n} \nabla \cdot \int_{\nu_{p(i)}} \rho_{p(i)}\, \underline{v}_{p(i)} d\nu_i}_{\text{Term 3}}.
$$

$$(4.7.7)$$

From the definition of volumetric averaging of a non-connected medium given by Equation (4.6.1), Term 1 may be written as

$$
\sum_{i=1}^{n} \frac{\partial m_{p(i)}(t)}{\partial t} = \frac{\partial}{\partial t} \sum_{i=1}^{n} \rho_{p(i)} \nu_{p(i)}
$$
$$
= \mathcal{U}_o \frac{\partial \overline{\rho_p}}{\partial t}, \tag{4.7.8}
$$

which, after applying the definition for the intrinsic average for the particle phase, given by Equation (4.6.2), yields

$$
\sum_{i=1}^{n} \frac{\partial m_{p(i)}(t)}{\partial t} = \mathcal{U}_o \frac{\partial}{\partial t} \left( \epsilon_p \overline{\rho_p}^{\,p} \right). \tag{4.7.9}
$$

Since the sum of integrals, each of which is taken over the particle-continuum interface of a single particle, may also be written as

$$
\sum_{i=1}^{n} \int_{\mathcal{S}_{(i,pc)}} \rho_{p(i)} \left( \underline{w}_{p(i)} - \underline{v}_{p(i)} \right) \cdot \underline{n}_{p(i)} d\,\mathcal{S}_i \equiv \int_{\sum \mathcal{S}_{pc(i)}} \rho_{p(i)} \left( \underline{w}_{p(i)} - \underline{v}_{p(i)} \right) \cdot \underline{n}_{p(i)} d\,\mathcal{S},
$$

$$(4.7.10)$$

and since the particle-continuum interface, $\mathcal{S}_{pc}$, of the REV is constructed from the particle-continuum interfaces of all particles, contained within the REV, combined:

$$
\mathcal{S}_{pc} = \sum_i \mathcal{S}_{pc(i)}, \tag{4.7.11}
$$

it follows that Term 2 may be simplified as

$$
\sum_{i=1}^{n} \int_{\mathcal{S}_{pc(i)}} \rho_{p(i)} \left( \underline{w}_{p(i)} - \underline{v}_{p(i)} \right) \cdot \underline{n}_{p(i)} d\,\mathcal{S}_i \equiv \int_{\mathcal{S}_{pc}} \rho_{p(i)} \left( \underline{w}_{p(i)} - \underline{v}_{p(i)} \right) \cdot \underline{n}_{p(i)} d\,\mathcal{S}.
$$

$$(4.7.12)$$

It is assumed that the properties of the particle are defined at its centre: The velocity and density of each discrete element are therefore by definition regarded as constants for each individual element and the particles are regarded homogeneous. It follows that Term 3 may be expressed as

$$\sum_{i=1}^{n} \nabla \cdot \int_{\nu_{p(i)}} \rho_{p(i)} \, \underline{v}_{p(i)} d\nu_i \;=\; \sum_{i=1}^{n} \nabla \cdot \rho_{p(i)} \, \underline{v}_{p(i)} \nu_i. \tag{4.7.13}$$

Equation (4.6.1) is applied to Equation (4.7.13) and it follows that

$$\sum_{i=1}^{n} \nabla \cdot \int_{\nu_{p(i)}} \rho_{p(i)} \, \underline{v}_{p(i)} d\nu_p \;=\; \mathcal{U}_o \overline{\nabla \cdot \rho_p \, \underline{v}_p}. \tag{4.7.14}$$

Finally, the averaging rules are applied, yielding

$$\sum_{i=1}^{n} \nabla \cdot \int_{\nu_{p(i)}} \rho_{p(i)} \, \underline{v}_{p(i)} d\nu_i \;=\; \mathcal{U}_o \nabla \cdot \epsilon_p \overline{\rho_p}^{\,p} \overline{\underline{v}_p}^{\,p} + \mathcal{U}_o \nabla \cdot \overline{\tilde{\rho}_p \, \underline{\tilde{v}}_p}. \tag{4.7.15}$$

It follows that Equation (4.7.7) may then be written as

$$\frac{\partial}{\partial t} \left( \epsilon_p \overline{\rho_p}^{\,p} \right) + \nabla \cdot \epsilon_p \overline{\rho_p}^{\,p} \overline{\underline{v}_p}^{\,p} + \nabla \cdot \overline{\tilde{\rho}_p \, \underline{\tilde{v}}_p} \;=\; \frac{1}{\mathcal{U}_o} \int_{\mathcal{S}_{pc}} \rho_{p(i)} \left( \underline{w}_{p(i)} - \underline{v}_{p(i)} \right) \cdot \underline{n}_{p(i)} d\mathcal{S}.$$
$$\tag{4.7.16}$$

Equation (4.7.16) describes the change of the (volumetric weighted average) mass per unit volume of all particles in the REV. It is defined at the centroid of the REV. The integral term represents the flux of mass across the continuum-particle interface.

If the assumption is made that there are no sudden changes in the mean particle velocity and density within the REV, the third term on the left-hand side of Equation (4.7.16) may be neglected. Equation (4.7.16) may then be written as

$$\frac{\partial}{\partial t} \left( \epsilon_p \overline{\rho_p}^{\,p} \right) + \nabla \cdot \epsilon_p \overline{\rho_p}^{\,p} \overline{\underline{v}_p}^{\,p} \;=\; \frac{1}{\mathcal{U}_o} \int_{\mathcal{S}_{pc}} \rho_{p(i)} \left( \underline{w}_{p(i)} - \underline{v}_{p(i)} \right) \cdot \underline{n}_{p(i)} d\mathcal{S}.$$
$$\tag{4.7.17}$$

If, in addition to previous assumptions, it is assumed that the mass flux across the solid surface is zero (i.e. combustion and/or condensation does not occur), and that the particles within the REV have the same densities, the averaged equation for mass conservation of the discrete phase is given by

$$\frac{\partial}{\partial t}\left(\epsilon_p \overline{\rho_p}^{\,p}\right) + \nabla \cdot \left(\epsilon_p \overline{\underline{v}_p}^{\,p}\right) \;=\; 0. \tag{4.7.18}$$

## 4.8   Averaging of the particle momentum conservation equation

Equation (3.5.7) describes the change in momentum of a particle with mass $m_{p(i)} = \rho_{p(i)} \nu_{p(i)}$. In order to obtain the overall momentum of the particles in the REV, Equation (3.5.7) is summed for all $n$ particles:

$$\sum_{i=1}^{n} \frac{\partial}{\partial t}\left(\underline{v}_{p(i)} \rho_{p(i)} \nu_{p(i)}\right) + \underbrace{\sum_{i=1}^{n} \rho_{p(i)} \nu_{p(i)}\, \underline{v}_{p(i)} \cdot \nabla\, \underline{v}_{p(i)}} \;=\; \sum_{i=1}^{n} \nu_{p(i)} \rho_{p(i)}\, \underline{g} \;+$$

$$\sum_{i=1}^{n} \underset{\partial \nu_{p(i)}}{\int} \underline{\underline{\sigma}}_{p(i)} \cdot \underline{n}_{p(i)} d\mathcal{S} + \underbrace{\sum_{i=1}^{n} \underline{v}_{p(i)} \underset{\mathcal{S}_{p(i)}}{\int} \rho_{p(i)}\left(\underline{w}_{p(i)} - \underline{v}_{p(i)}\right) \cdot \underline{n}_{p(i)} d\mathcal{S}}_{\text{Term 1}}.$$

$$\tag{4.8.1}$$

The same argument that was used for the mass flux term in Equation (4.7.1) is now applied to the integral term, i.e.

$$\text{Term 1} \;=\; \sum_{i=1}^{n} \underline{v}_{p(i)} \left[\underset{\mathcal{S}_{pc(i)}}{\int} \rho_{p(i)}\left(\underline{w}_{p(i)} - \underline{v}_{p(i)}\right) \cdot \underline{n}_{p(i)} d\mathcal{S} + \underset{\mathcal{S}_{pp(i)}}{\int} \rho_{p(i)}\left(\underline{w}_{p(i)} - \underline{v}_{p(i)}\right) \cdot \underline{n}_{p(i)} d\mathcal{S}\right]$$

$$=\; -\sum_{i=1}^{n} \underline{v}_{p(i)} \underset{\mathcal{S}_{pp(i)}}{\int} \rho_{p(i)}\, \underline{v}_{p(i)} \cdot \underline{n}_{p(i)} d\mathcal{S}$$

$$=\; -\sum_{i=1}^{n} \underline{v}_{p(i)} \nabla \cdot \underset{\nu_{p(i)}}{\int} \rho_{p(i)}\, \underline{v}_{p(i)} d\nu. \tag{4.8.2}$$

It was assumed that the density and velocity of the particle are defined at its centre of mass and may therefore be removed from the integral term in Equation (4.8.2). It follows that

$$\text{Term 1} \;=\; -\sum_{i=1}^{n} \underline{v}_{p(i)} \nabla \cdot \rho_{p(i)}\,\underline{v}_{p(i)} \nu_{p(i)}. \tag{4.8.3}$$

Combination of the above result for Term 1 and the underlined term in Equation (4.8.1), yields

$$\frac{\partial}{\partial t}\sum_{i=1}^{n}\left(\underline{v}_{p(i)}\rho_{p(i)}\nu_{p(i)}\right) + \nabla \cdot \sum_{i=1}^{n}\left(\rho_{p(i)}\,\underline{v}_{p(i)}\,\underline{v}_{p(i)}\right)\nu_{p(i)} \;=\; \sum_{i=1}^{n}\nu_{p(i)}\rho_{p(i)}\,\underline{g} + $$

$$\sum_{i}\int_{\mathcal{S}_{p(i)}} \underline{\underline{\sigma}}_{p(i)}\cdot\underline{n}_{p(i)}d\mathcal{S}.$$

$$\tag{4.8.4}$$

The underlined integral term in Equation (4.8.4) is split into its particle-continuum and particle-particle components and written in condensed form:

$$\int_{\mathcal{S}_{p(i)}} \underline{\underline{\sigma}}_{p(i)}\cdot\underline{n}_{p(i)}d\mathcal{S} \;=\; \int_{\mathcal{S}_{pc(i)}} \underline{\underline{\sigma}}_{p(i)}\cdot\underline{n}_{p(i)}d\mathcal{S} + \int_{\mathcal{S}_{pp(i)}} \underline{\underline{\sigma}}_{p(i)}\cdot\underline{n}_{p(i)}d\mathcal{S}.$$

$$\tag{4.8.5}$$

Substitution of Equation (4.8.5) and application of the definition of volume averaging then yield the following volume averaged momentum conservation equation for the particulate phase:

$$\frac{\partial}{\partial t}\overline{\underline{v}_p\rho_p} + \nabla \cdot \overline{\rho_p\,\underline{v}_p\,\underline{v}_p} \;=\; \overline{\rho_p\,\underline{g}} + \frac{1}{\mathcal{U}_o}\int_{\mathcal{S}_{pc}} \underline{\underline{\sigma}}_{p(i)}\cdot\underline{n}_{p(i)}d\mathcal{S} + \frac{1}{\mathcal{U}_o}\int_{\mathcal{S}_{pp}} \underline{\underline{\sigma}}_{p(i)}\cdot\underline{n}_{p(i)}d\mathcal{S}.$$

$$\tag{4.8.6}$$

Recall that, during the averaging of the discrete phase mass equation, it was assumed that all particles have the same density and that the density is assumed to remain constant with regard to both time and position. Implementing these assumptions and

applying the averaging rules given in Table 4.2 to the terms in Equation (4.8.6), yield

$$
\rho_p \frac{\partial}{\partial t} \epsilon_p \overline{\underline{v}_p}^{\,p} + \rho_p \nabla \cdot \epsilon_p \overline{\underline{v}_p}^{\,p} \overline{\underline{v}_p}^{\,p} + \rho_p \nabla \cdot \overline{\widetilde{\underline{v}_p \, \underline{v}_p}} = \epsilon_p \rho_p \, \underline{g} + \frac{1}{\mathcal{U}_o} \int\limits_{\mathcal{S}_{pc}} \underline{\underline{\sigma}}_{p(i)} \cdot \underline{n}_{p(i)} d\mathcal{S} +
$$

$$
\frac{1}{\mathcal{U}_o} \int\limits_{\mathcal{S}_{pp}} \underline{\underline{\sigma}}_{p(i)} \cdot \underline{n}_{p(i)} d\mathcal{S}. \qquad (4.8.7)
$$

The average of the product of the velocity deviations was termed the Reynolds stress in Section 2.6.1.3. The assumptions made for the continuum phase presumably holds for the discrete phase as well and the Reynolds stress is considered negligible. It follows that

$$
\rho_p \frac{\partial}{\partial t} \epsilon_p \overline{\underline{v}_p}^{\,p} + \rho_p \nabla \cdot \epsilon_p \overline{\underline{v}_p}^{\,p} \overline{\underline{v}_p}^{\,p} = \epsilon_p \rho_p \, \underline{g} + \frac{1}{\mathcal{U}_o} \int\limits_{\mathcal{S}_{pc}} \underline{\underline{\sigma}}_{p(i)} \cdot \underline{n}_{p(i)} d\mathcal{S} +
$$

$$
\frac{1}{\mathcal{U}_o} \int\limits_{\mathcal{S}_{pp}} \underline{\underline{\sigma}}_{p(i)} \cdot \underline{n}_{p(i)} d\mathcal{S}. \qquad (4.8.8)
$$

Equation (4.8.8) represents the final form for the particle momentum conservation equation and additional modelling procedures are required for the remaining integral terms to be expressed in terms of averaged properties.

## 4.9   Summary and conclusions

In this chapter the concept of an REV has been introduced and used to derive averaging rules for both phases. These rules have been applied to the conservation equations that were presented in Chapter 3. Additional modelling procedures, required for the expression of the stress terms $\underline{\underline{\sigma}}_c$ and $\underline{\underline{\sigma}}_p$ in Equations (4.5.7) and (4.8.8) in terms of macroscopic flow properties, are discussed in Chapter 5.

# Chapter 5

# Constitutive modelling

## 5.1 Introduction

The derivation of closure laws is pivotal to accurate modelling procedures. Following Enwald *et al.* (1997), these laws are divided into two categories, namely *Constitutive laws* which specify the interaction of physical parameters *within* phases and *Transfer laws* which qualify the interactions *between* phases.

Constitutive laws entail the modelling of the continuum and particulate stress terms, appearing in Equations (4.5.7) and (4.8.8), in terms of fluid properties. The transfer laws are discussed in Chapter 6.

## 5.2 Continuum stress

The continuum stress, $\underline{\underline{\sigma}}_c$, is split into a continuum pressure, $p_c$, and a continuum shear stress term, $\underline{\underline{\tau}}_c$, and is expressed as

$$\underline{\underline{\sigma}}_c = -p_c \underline{\underline{I}} + \underline{\underline{\tau}}_c.$$

(5.2.1)

The continuum pressure is taken as the hydrostatic pressure and the shear stress is modelled using the Newtonian strain-stress relation:

$$\underline{\underline{\tau}}_c = \xi_c \nabla \cdot \underline{v}_c \underline{\underline{I}} + 2\mu_c \left( \underline{\underline{S}}_c - \frac{1}{3} \nabla \cdot \underline{v}_c \underline{\underline{I}} \right),$$

(5.2.2)

where $\xi_c$ denotes the bulk viscosity and the strain-rate tensor, $\underline{\underline{S}}_c$, is defined by

$$\underline{\underline{S}}_c = \mu_c \left( \nabla \underline{v}_c + (\nabla \underline{v}_c)^T \right).$$

(5.2.3)

In Equation (5.2.3), $\mu_c$ is the viscosity of the continuum and $T$ denotes the transpose operator. From the assumption of a constant continuum density,[1] it follows that $\nabla \cdot \underline{v}_c = 0$ and the shear stress therefore simplifies to

$$\underline{\underline{\tau}}_c \;=\; \mu_c \left( \nabla \underline{v}_c + (\nabla \underline{v}_c)^T \right). \tag{5.2.5}$$

Substitution of Equation (5.2.5) into Equation (5.2.1) yields

$$\underline{\underline{\sigma}}_c \;=\; -p_c \underline{\underline{I}} + \mu_c \left( \nabla \underline{v}_c + (\nabla \underline{v}_c)^T \right), \tag{5.2.6}$$

which is an expression for the internal continuum shear stress in terms of fluid properties.

## 5.3  Particle stress

When calculating the total force exerted on a particle by a surrounding continuum and neighbouring particles, as was done in Appendix A, the work of Kleinstreuer (2003), Enwald *et al.* (1997), Soo (1990) and Crowe *et al.* (1998) were followed in assuming that these forces may be added linearly. For this reason it is assumed in this work that the particle stress, $\underline{\underline{\sigma}}_p$, is a linear combination of the stress induced by the continuum encompassing it, $\underline{\underline{\sigma}}_c$, and the stress, $\underline{\underline{\sigma}}_{pp}$, instigated by neighbouring particles

$$\underline{\underline{\sigma}}_p \;=\; \underline{\underline{\sigma}}_c + \underline{\underline{\sigma}}_{pp}. \tag{5.3.1}$$

The continuum stress has already been discussed in Section 5.2 and it remains to be shown how the particle induced stress is modelled.

### 5.3.1  Particle induced stress

The form of viscous dissipation and stresses, experienced by randomly fluctuating particles in the dilute sections of the flow domain, are referred to as *kinetic* stresses. An increase in the particle volume fraction results in particle collisions and generate collisional stresses which, in addition to the kinetic stresses, will influence the motion of

---

[1]For variable densities (i.e. compressible flow) these terms are usually also neglected by the application of Stokes' assumption, which states that

$$\xi_c + \frac{2}{3}\mu_c \;=\; 0. \tag{5.2.4}$$

In the event of a change of volume there would therefore not exist a resistance force that could subdue such a change.

the particulate matter. However, a further increase in the particle volume fraction induces protracted sliding or abrasive inter-particle contacts, yielding a frictional stress which will dominate as individual particle motions are progressively limited. These interactions are illustrated in Figure 5.1.
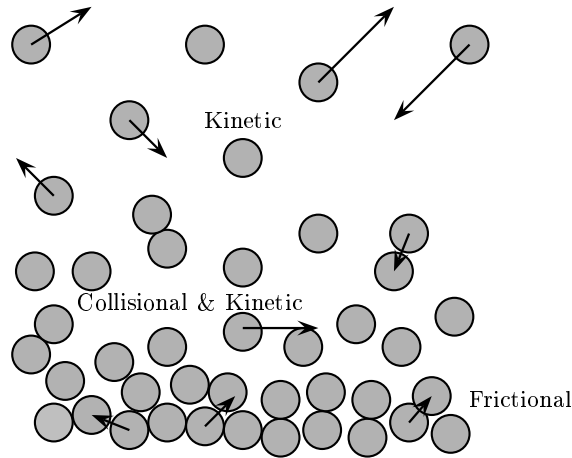


**Figure 5.1:**  The three main forms of viscous dissipation within granular flow:  kinetic, kinetic-collisional, and frictional.

It follows that the particle induced stress may be decomposed into a kinetic-collisional component, $\underline{\underline{\sigma}}^{kc}_{pp}$, and a frictional component, $\underline{\underline{\sigma}}^{f}_{pp}$. This observation was used by Dartevelle (2003) to construct the following expression for the particle induced stress

$$\underline{\underline{\sigma}}_{pp} \quad = \quad \underline{\underline{\sigma}}^{kc}_{pp} + \underline{\underline{\sigma}}^{f}_{pp}, \tag{5.3.2}$$

which in the limiting case of dilute flow, simplifies to

$$\underline{\underline{\sigma}}_{pp} \quad = \quad \underline{\underline{\sigma}}^{kc}_{pp}. \tag{5.3.3}$$

Following Enwald *et al.* (1997) and Dartevelle (2003), $\underline{\underline{\sigma}}^{kc}_{pp}$ may be expressed as a combination of kinetic-collisional particle pressure, $p^{kc}_p$, and a kinetic-collisional particle shear stress, $\underline{\underline{\tau}}^{kc}_p$, as

$$\underline{\underline{\sigma}}^{kc}_{pp} \quad = \quad -p^{kc}_p \underline{\underline{I}} + \underline{\underline{\tau}}^{kc}_p. \tag{5.3.4}$$

For the purpose of the current work it is assumed that the small grain size and dilute concentrations yield a particle pressure which, when compared to the shear, may be considered small enough to be omitted. It follows that the particle stress term is given

by substitution of Equations (5.2.6) and (5.3.4) into Equation (5.3.1) which yields the following expression for the particle shear stress:

$$\underline{\underline{\sigma}}_p \quad = \quad -p_c\underline{\underline{1}} + \underline{\underline{\tau}}_c + \underline{\underline{\tau}}_p^{kc}. \tag{5.3.5}$$

# 5.4   Application of constitutive laws

The constitutive laws for the continuum- and the particle phases are given by Equations (5.2.6) and (5.3.5), respectively. In Sections 5.4.1 and 5.4.2, these equations are substituted into the averaged momentum equations, given in Chapter 4 by Equations (4.5.7) and (4.8.8) for the continuum and particle phases, respectively. In doing so, the stress terms are replaced by fluid properties.

## 5.4.1   The continuum

Substitution of Equation (5.2.1) into the averaged momentum equation for the continuum phase, given by Equation (4.5.7), yields

$$\rho_c\frac{\partial \epsilon_c \left\langle \underline{v}_c \right\rangle_c}{\partial t} + \rho_c\nabla \cdot (\epsilon_c \left\langle \underline{v}_c \right\rangle_c \left\langle \underline{v}_c \right\rangle_c) \quad = \quad \rho_c\,\underline{g}\epsilon_c - \nabla\left(\epsilon_c \left\langle p_c \right\rangle_c\right) + \nabla \cdot \left(\epsilon_c \left\langle \underline{\underline{\tau}} \right\rangle_c\right) +$$
$$\frac{1}{\mathcal{U}_o}\int_{\mathcal{S}_{pc}} \underline{n}_c \cdot (-p_c\underline{\underline{I}} + \underline{\underline{\tau}}_c)d\,\mathcal{S}. \tag{5.4.1}$$

When the chain rule is applied to the pressure gradient term, $\nabla(\epsilon_c \left\langle p \right\rangle_c)$, it follows that

$$\rho_c\frac{\partial \epsilon_c \left\langle \underline{v}_c \right\rangle_c}{\partial t} + \rho_c\nabla \cdot (\epsilon_c \left\langle \underline{v}_c \right\rangle_c \left\langle \underline{v}_c \right\rangle_c) \quad = \quad \rho_c\,\underline{g}\epsilon_c - \epsilon_c\nabla \left\langle p_c \right\rangle_c - \left\langle p_c \right\rangle_c \nabla\epsilon_c + \nabla \cdot \left(\epsilon_c \left\langle \underline{\underline{\tau}} \right\rangle_c\right) +$$
$$\frac{1}{\mathcal{U}_o}\int_{\mathcal{S}_{pc}} \underline{n}_c \cdot \left(-p_c\underline{\underline{I}} + \underline{\underline{\tau}}_c\right)d\,\mathcal{S}. \tag{5.4.2}$$

Noting that the third term on the right-hand side of Equation (5.4.2) contains the gradient of the porosity, Equation (5.4.2) may be simplified, with the application of

Slattery's averaging theorem and expressed as [2]

$$
\rho_c \frac{\partial \epsilon_c \left\langle \underline{v}_c \right\rangle_c}{\partial t} + \rho_c \nabla \cdot (\epsilon_c \left\langle \underline{v}_c \right\rangle_c \left\langle \underline{v}_c \right\rangle_c) \;=\; \rho_c \, \underline{g} \epsilon_c - \epsilon_c \nabla \left\langle p_c \right\rangle_c + \nabla \cdot \left( \epsilon_c \left\langle \underline{\underline{\tau}} \right\rangle_c \right) +
$$
$$
\frac{1}{\mathcal{U}_o} \int_{\mathcal{S}_{pc}} \underline{n}_c \cdot \left( (-p_c + \left\langle p_c \right\rangle_c) \underline{\underline{I}} + \underline{\underline{\tau}}_c \right) d\,\mathcal{S}. \quad (5.4.4)
$$

By applying the definition of the deviation in terms of microscopic and averaged values, given by Equation (4.3.4), Equation (5.4.4) may finally be expressed as

$$
\rho_c \frac{\partial \epsilon_c \left\langle \underline{v}_c \right\rangle_c}{\partial t} + \rho_c \nabla \cdot (\epsilon_c \left\langle \underline{v}_c \right\rangle_c \left\langle \underline{v}_c \right\rangle_c) \;=\; \rho_c \, \underline{g} \epsilon_c - \epsilon_c \nabla \left\langle p_c \right\rangle_c + \nabla \cdot \left( \epsilon_c \left\langle \underline{\underline{\tau}} \right\rangle_c \right) +
$$
$$
\frac{1}{\mathcal{U}_o} \int_{\mathcal{S}_{pc}} \underline{n}_c \cdot \left( -\tilde{p}_c \underline{\underline{I}} + \underline{\underline{\tau}}_c \right) d\,\mathcal{S}. \quad (5.4.5)
$$

The averaging procedure, discussed in Appendix C, is applied to the expression for the shear stress in terms of velocity, as given by Equation (5.2.5). This allows for the gradient of the continuum averaged shear stress, which appears on the right-hand side of Equation (5.4.5), to be written as

$$
\nabla \cdot \epsilon_c \left\langle \underline{\underline{\tau}}_{pc} \right\rangle_c \;=\; \mu_c \nabla \cdot \left[ \epsilon_c \nabla \left\langle \underline{v}_c \right\rangle_c \right], \quad (5.4.6)
$$

and the averaged form of Equation (5.4.5) is thus given by

$$
\rho_c \frac{\partial \epsilon_c \left\langle \underline{v}_c \right\rangle_c}{\partial t} + \rho_c \nabla \cdot (\epsilon_c \left\langle \underline{v}_c \right\rangle_c \left\langle \underline{v}_c \right\rangle_c) \;=\; \rho_c \, \underline{g} \epsilon_c - \epsilon_c \nabla \left\langle p_c \right\rangle_c + \mu_c \nabla \cdot \left[ \epsilon_c \nabla \left\langle \underline{v}_c \right\rangle_c \right] +
$$
$$
\frac{1}{\mathcal{U}_o} \int_{\mathcal{S}_{pc}} \underline{n}_c \cdot \left( -\tilde{p}_c \underline{\underline{I}} + \underline{\underline{\tau}}_c \right) d\,\mathcal{S}. \quad (5.4.7)
$$

The remaining surface integral term which appears in Equation (5.4.5) will be closed in Chapter 6.

---

[2] Averaging Rule *vi* in Table 4.1 is applied and it is noted that $\left\langle p_c \right\rangle_c$ is an average and may therefore be combined with the integrand as follows

$$
\left\langle p_c \right\rangle_c \nabla \epsilon_c \;=\; \left\langle p_c \right\rangle_c \left( \left\langle \nabla 1 \right\rangle - \int_{\mathcal{S}_{pc}} 1 \, \underline{n}_c d\mathcal{S} \right)
$$
$$
\;=\; -\int_{\mathcal{S}_{pc}} \left\langle p_c \right\rangle_c \underline{n}_c d\mathcal{S}. \quad (5.4.3)
$$

### 5.4.2   The discrete phase

Substitution of Equation (5.3.5) into Equation (4.8.8), yields

$$\rho_p \frac{\partial}{\partial t} \epsilon_p \overline{\underline{v}_p}^{\,p} + \rho_p \nabla \cdot \epsilon_p \overline{\underline{v}_p}^{\,p} \overline{\underline{v}_p}^{\,p} \;=\; \epsilon_p \rho_p\, \underline{g} + \frac{1}{\mathcal{U}_o} \int\limits_{\mathcal{S}_{pc}} \left( -p_c \underline{\underline{1}} + \underline{\underline{\tau}}_c + \underline{\underline{\tau}}_p^{kc} \right) \cdot \underline{n}_{p(i)} d\mathcal{S} +$$

$$\frac{1}{\mathcal{U}_o} \int\limits_{\mathcal{S}_{pp}} \left( -p_c \underline{\underline{1}} + \underline{\underline{\tau}}_c + \underline{\underline{\tau}}_p^{kc} \right) \cdot \underline{n}_{p(i)} d\mathcal{S}. \qquad (5.4.8)$$

The kinetic-collisional shear, $\underline{\underline{\tau}}_p^{kc}$, can physically only occur where particles come into contact with each other. It follows that such a term will only exist on a particle-particle interface, $\mathcal{S}_{pp}$. Moreover, the continuum pressure, $p_c$, and shear, $\underline{\underline{\tau}}_c$, are defined only at interfaces and within volumes where the continuum phase is present. It therefore follows that Equation (5.4.8) simplifies to

$$\rho_p \frac{\partial}{\partial t} \epsilon_p \overline{\underline{v}_p}^{\,p} + \rho_p \nabla \cdot \epsilon_p \overline{\underline{v}_p}^{\,p} \overline{\underline{v}_p}^{\,p} \;=\; \epsilon_p \rho_p\, \underline{g} + \frac{1}{\mathcal{U}_o} \int\limits_{\mathcal{S}_{pp}} \left( \underline{\underline{\tau}}_p^{kc} \right) \cdot \underline{n}_{p(i)} d\mathcal{S}$$

$$+\frac{1}{\mathcal{U}_o} \int\limits_{\mathcal{S}_{pc}} \left( -p_c \underline{\underline{1}} + \underline{\underline{\tau}}_c \right) \cdot \underline{n}_{p(i)} d\mathcal{S}. \quad (5.4.9)$$

Application of Reynolds decomposition to the pressure in the integral term on the right-hand side of Equation (5.4.9), yields

$$\rho_p \frac{\partial}{\partial t} \epsilon_p \overline{\underline{v}_p}^{\,p} + \rho_p \nabla \cdot \epsilon_p \overline{\underline{v}_p}^{\,p} \overline{\underline{v}_p}^{\,p} \;=\; \epsilon_p \rho_p\, \underline{g} - \frac{1}{U_o} \int\limits_{\mathcal{S}_{pc}} \langle p_c \rangle_c\, \underline{n}_p d\mathcal{S} + \frac{1}{\mathcal{U}_o} \int\limits_{\mathcal{S}_{pp}} \underline{\underline{\tau}}_p^{kc} \cdot \underline{n}_{p(i)} d\mathcal{S}$$

$$-\frac{1}{\mathcal{U}_o} \int\limits_{\mathcal{S}_{pc}} \left( -\tilde{p}_c \underline{\underline{1}} + \underline{\underline{\tau}}_c \right) \cdot \underline{n}_c d\mathcal{S}, \qquad (5.4.10)$$

where the negative sign in front of the last term on the right-hand side appears due to the relation between the particulate unit vector and the corresponding continuum unit vector, $\underline{n}_p = -\underline{n}_c$. The divergence theorem is applied to the second term on the

right-hand side of Equation (5.4.10) and it follows that

$$
\rho_p \frac{\partial}{\partial t} \epsilon_p \overline{\underline{v}_p}^p + \rho_p \nabla \cdot \epsilon_p \overline{\underline{v}_p}^p \overline{\underline{v}_p}^p \;=\; \epsilon_p \rho_p \underline{g} - \epsilon_p \nabla \langle p_c \rangle_c + \frac{1}{\mathcal{U}_o} \int\limits_{\mathcal{S}_{pp}} \underline{\underline{\tau}}_p^{kc} \cdot \underline{n}_{p(i)} d\mathcal{S}
$$

$$
- \frac{1}{\mathcal{U}_o} \int\limits_{\mathcal{S}_{pc}} \left( -\tilde{p}_c \underline{\underline{1}} + \underline{\underline{\tau}}_c \right) \cdot \underline{n}_c d\mathcal{S}. \qquad (5.4.11)
$$

Note that the surface integral term which appears in Equation (5.4.5) is present in Equation (5.4.11) also, but with opposite sign. It is through these surface integrals that momentum is transferred between phases and dissimilar signs indicate that momentum dissipated from one phase is the momentum gained by another. Additional modelling procedures, needed to define the transfer laws for the closure of the preceding surface integrals, are discussed in Chapter 6.

It remains to be shown how the additional surface integral in Equation (5.4.11), which serves as the descriptor for momentum transfer *within* the particle phase, is closed.

## 5.5 Particle interaction

The particle interaction effect enters Equation (5.4.10) through the integral expression

$$
\underline{I}_p \;=\; \frac{1}{\mathcal{U}_o} \int\limits_{\mathcal{S}_{pp}} \underline{\underline{\tau}}_p^{kc} \cdot \underline{n}_{p(i)} d\mathcal{S}, \qquad (5.5.1)
$$

and since $\mathcal{S}_{pp} = \sum_i \mathcal{S}_{pp(i)}$, it follows that Equation (5.5.1) may be written as the sum of particle-particle interaction forces experienced by each particle:

$$
\underline{I}_p \;=\; \frac{1}{\mathcal{U}_o} \sum \int\limits_{\mathcal{S}_{pp(i)}} \underline{\underline{\tau}}_p^{kc} \cdot \underline{n}_{p(i)} d\mathcal{S}. \qquad (5.5.2)
$$

The integrand denotes a force, $\underline{F}_{p(i)}^{kc}$, parallel to an incremental surface element, $d\mathcal{S}$, on which it acts.

Subsequent integration over all surface elements where particles are in contact with one another, yields the following expression for the particle induced momentum con-

tribution

$$\underline{I}_p \;=\; \frac{1}{\mathcal{U}_o} \sum_{i=1}^{N} \underline{F}_{p(i)}^{kc},\tag{5.5.3}$$

where $\underline{F}_{p(i)}^{kc}$ is the resultant force acting on the $i^{th}$ particle due to multiple collisions with its neighbours. In the remainder of this section such a resultant particle interaction force, experienced by a single particle, will be modelled.

The initial derivation of a closed expression for Equation (5.5.3) is done for a one-dimensional situation. In accordance with work done by Soo (1990) and Fan and Zhu (1998), the one-dimensional model is expanded to higher dimensions. It should however be noted that the expansion is not mathematically rigourous, but a mere approximation of the aforementioned unidimensional model.

The subject matter of the following sections is aimed at obtaining an expression for the average collision force induced by collisions between a multitude of particles. In order for this to be done in a coherent manner, some definitions and terminologies are introduced and the collisional force between two particles is considered.

## 5.5.1   Two-dimensional binary elastic collisions

The application of the Centre Of Mass reference frame (COM)[3], in conjunction with an elasticity assumption, yields a significant reduction in the complexity of any task involving momentum conservation during collisions.

In the COM reference frame, the observer moves alongside the system's centre of mass and all measurements are made in reference to this position. In the absence of external forces acting on the system, the total momentum on the system in the COM reference is effectively zero at all points in time. If, in addition to the COM frame of reference, it is also assumed that kinetic energy is conserved, i.e. that all collisions are elastic, it also holds that each particle's pre- and post collisional *speed* remains unchanged. The latter seems obvious for one-dimensional head on collisions but it will be shown that it indeed holds for the two-dimensional (and for that matter multi-dimensional) collisions.

---

[3] An invaluable reference for COM theory is Chapter IV of Maxwell (1877) and may be downloaded from `www.forgottenbooks.org`. In addition to this, extensive use was made of the *OpenCourseWare lectures*, made available by MIT (Lewin (2007)).

### 5.5.1.1   The Centre Of Mass (COM)

The centre of mass possesses the property of having a constant velocity, unaffected by the changing motion of its parts. It is mathematically defined as

$$M_{tot} \, \underline{r}_{COM} \;\; = \;\; \sum_i m_i \, \underline{r}_i, \tag{5.5.4}$$

where $m_i$ is the mass of a single particle and $M_{tot}$ is the combined mass of all the particles within the system. The position of the centre of mass is given by $\underline{r}_{COM}$ whereas $\underline{r}_i$ denotes the position of each particle. It follows from Equation (5.5.4), that the constant velocity of the centre of mass, $\underline{v}_{COM}$, is given by

$$\underline{v}_{COM} \;\; = \;\; \frac{1}{M_{tot}} \sum_i m_i \, \underline{v}_{p(i)} = \frac{1}{M_{tot}} \sum_i \underline{P}_i, \tag{5.5.5}$$

where $\underline{v}_{p(i)}$ and $\underline{P}_i$ are the velocity and momentum of the $i^{th}$ particle respectively.

To an observer, placed at the centre of mass, the velocity, $\underline{v}_{COM}$, will appear to be zero. It follows that the sum of the momenta will be zero also. This is true independent of the dimensionality or elasticity of the system. It therefore holds that, in the absence of a net external force, the total momentum remains zero before and after a collision in the COM frame of reference and the velocity of the COM, $\underline{v}_{COM}$, will be unchanged.

The additional assumption of full elasticity (i.e. conservation of kinetic energy), results in an unaltered speed for each particle before and after impact with a separate particle. A derivation, supporting this statement follows.

## 5.5.2   The effect of elasticity

Consider a fully elastic collision within the COM frame of reference, as illustrated in Figure 5.2. For any collision, albeit elastic or inelastic, the following holds in the COM frame of reference *before* impact

$$\underline{P}_1 + \underline{P}_2 \;\; = \;\; m_1 \, \underline{v}_{p(1)} + m_2 \, \underline{v}_{p(2)} = \underline{0}, \tag{5.5.6}$$

where $\underline{P}_1$ and $\underline{P}_2$ are the momenta of Particles 1 and 2, respectively whilst $\underline{v}_{p(1)}$ and $\underline{v}_{p(2)}$ denote their velocities. From Equation (5.5.6) it follows that the velocities of the two particles are always in opposite directions in a COM frame and the respective speeds are inversely proportional to their masses.
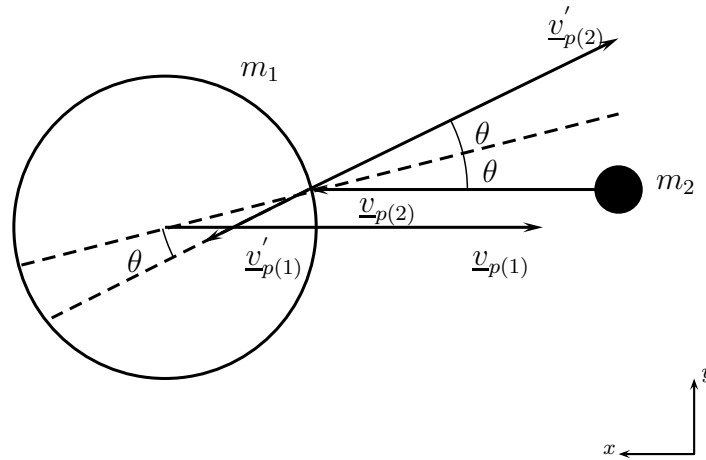
**Figure 5.2:** Elastic two-dimensional collision with specular reflection.

Let $\underline{v}_{p(1)} = u_{p(1)}\,\underline{i} + v_{p(1)}\,\underline{j}$ and let $\underline{v}_{p(2)} = u_{p(2)}\,\underline{i} + v_{p(2)}\,\underline{j}$, where $u_p$ and $v_p$ denote the $x$ and $y$ velocity components, respectively. From Equation (5.5.6) it then follows that

$$m_1 u_{p(1)} + m_2 u_{p(2)} \;\; = \;\; 0, \tag{5.5.7}$$

and

$$m_1 v_{p(1)} + m_2 v_{p(2)} \;\; = \;\; 0. \tag{5.5.8}$$

Let the $x$- and $y$-components of the momentum resulting from the motion of Particles 1 and 2 be given by,

$$
\begin{aligned}
P_{1,x} = m_1 u_{p(1)} \quad &\text{and} \quad P_{2,x} = m_2 u_{p(2)} \\
P_{1,y} = m_1 v_{p(1)} \quad &\text{and} \quad P_{2,y} = m_2 v_{p(2)}.
\end{aligned}
\tag{5.5.9}
$$

Substitution of the expressions for the momentum components, given by the equalities in (5.5.9), into Equations (5.5.7) and (5.5.8), yields the following relations

$$P_{1,x} \;\; = \;\; -P_{2,x}, \tag{5.5.10}$$

and

$$P_{1,y} \;\; = \;\; -P_{2,y}. \tag{5.5.11}$$

For any collision, elastic or inelastic, in any frame, albeit laboratory or COM, the following holds before impact

$$
\begin{aligned}
E_k &= \frac{1}{2}m_1|\underline{v}_{p(1)}|^2 + \frac{1}{2}m_2|\underline{v}_{p(2)}|^2, \\
&= \frac{1}{2}m_1\left(u^2_{p(1)} + v^2_{p(1)}\right) + \frac{1}{2}m_2\left(u^2_{p(2)} + v^2_{p(2)}\right), \\
&= \frac{1}{2m_1}m_1^2u^2_{p(1)} + \frac{1}{2m_1}m_1^2v^2_{p(1)} + \frac{1}{2m_2}m_2^2u^2_{p(2)} + \frac{1}{2m_2}m_2^2v^2_{p(2)}, \quad (5.5.12)
\end{aligned}
$$

where $E_k$ is the total kinetic energy prior to the collision. Substitution of the expressions given for the $x$- and $y$- momentum components into Equation (5.5.12), yields

$$
E_k = \frac{1}{2m_1}\left(P^2_{1,x} + P^2_{1,y}\right) + \frac{1}{2m_2}\left(P^2_{2,x} + P^2_{2,y}\right). \tag{5.5.13}
$$

If it is assumed that the collision is viewed in the COM frame of reference, Equations (5.5.10) and (5.5.11) may be substituted into Equation (5.5.13), and it follows that

$$
E_k = \left(\frac{1}{2m_1} - \frac{1}{2m_2}\right)\left(P^2_{1,x} + P^2_{1,y}\right). \tag{5.5.14}
$$

A similar expression may be obtained for the post collisional kinetic energy, $E'_k$:

$$
E'_k = \left(\frac{1}{2m_1} - \frac{1}{2m_2}\right)\left(P'^2_{1,x} + P'^2_{1,y}\right), \tag{5.5.15}
$$

where the primed variables indicate that it is taken after impact. Under the assumption that the collisions are fully elastic, Equation (5.5.14) may be set equal to Equation (5.5.15) and it follows that

$$
\left(P^2_{1,x} + P^2_{1,y}\right) = \left(P'^2_{1,x} + P'^2_{1,y}\right). \tag{5.5.16}
$$

The above may be written in the form of,

$$
(m_1|\underline{v}_{p(1)}|)^2 = (m_1|\underline{v}'_{p(1)}|)^2, \tag{5.5.17}
$$

where $|\underline{v}_{p(1)}|^2 = u^2_{p(1)} + v^2_{p(1)}$.

Equation (5.5.17) validates the statement made earlier that the pre- and post- collisional speeds are equal,

$$
|\underline{v}_{p(1)}| = |\underline{v}'_{p(1)}|. \tag{5.5.18}
$$

In a similar manner it can be shown that,

$$| \underline{v}_{p(2)} | \;\; = \;\; | \underline{v}'_{p(2)} |. \tag{5.5.19}$$

It follows that, in an elastic collision, the speed of the individual particles do not change, though their directions may change, depending on the shapes of the bodies and the point of impact.

In the following section it is shown how collisions between two moving objects may be simplified by keeping one of the objects stationary and viewing only the motion of the other. Such an approach reduces the complexity of the mathematical description of the motion between two particles significantly and therefore provides a useful tool for describing the motions of particle clouds.

### 5.5.2.1   Relative mass and velocities

With reference to Figure 5.2, it is shown that the change in the $x$-momentum component of Particle 2 may be expressed relative to that of Particle 1.

From Equation (5.5.10) it follows that

$$\Delta P_{1,x} \;\; = \;\; -\Delta P_{2,x}, \tag{5.5.20}$$

where $\Delta P_{i,x} = P_{i,x} - P'_{i,x}$ denotes the change in momentum of Particle $i$ due to the collision. The change in the $x$-momentum component of each particle is written in terms of its velocity component, yielding

$$m_1 \Delta u_{p(1)} \;\; = \;\; -m_2 \Delta u_{p(2)}. \tag{5.5.21}$$

From Equation (5.5.21) it then follows that

$$\Delta u_{p(1)} = \frac{1}{m_1} \Delta P_{1,x} \quad \text{and} \quad \Delta u_{p(2)} = -\frac{1}{m_2} \Delta P_{1,x},$$

where $\Delta u_p$ denotes the difference between the pre- and -post collisional values. Subtraction, yields

$$\Delta u_{p(1)} - \Delta u_{p(2)} \;\; = \;\; \frac{1}{m^*} \Delta P_{1,x}, \tag{5.5.22}$$

where $m^* = (m_1 m_2)/(m_1 + m_2)$ is commonly known as the *relative mass*. From Equation (5.5.22) it follows that the change in the $x$-component of momentum for Particle 2 may be written in terms of relative velocity and mass as

$$m^* \left( u_{p(rel)} \right) - m^* \left( u'_{p(rel)} \right) \;\; = \;\; \Delta P_{1,x}, \tag{5.5.23}$$

where $u_{p(rel)} = u_{p(1)} - u_{p(2)}$ and $u'_{rel} = u'_{p(1)} - u'_{p(2)}$ respectively denote the pre- and post collisional $x$-component of the relative velocity. Equation (5.5.23) is ratification for the observation made by Fan and Zhu (1998), Soo (1990) and Clark (2009) that the collision between two moving particles is equivalent to the case where a particle collides with another which possesses the same relative mass and relative velocity.

If, along with the elasticity assumption already made, it is assumed that the collisions are specular and that the initial velocity of Particle 2 is parallel to the $x$-axis, it follows from Figure 5.2 that the magnitude of the $x$-component, $u'_{p(2)}$, of Particle 2's outgoing velocity, $\underline{v}'_{p(2)}$, is given by

$$|u'_{p(2)}| \quad = \quad |\underline{v}'_{p(2)}| \cos(2\theta) = |\underline{v}_{p(2)}| \cos(2\theta), \tag{5.5.24}$$

and since $\underline{v}_{p(2)} = u_{p(2)}$, Equation (5.5.24) may be expressed as

$$|u'_{p(2)}| \quad = \quad |u_{p(2)}| \cos(2\theta). \tag{5.5.25}$$

From Figure 5.2 it is seen that the direction of $u'_{p(2)}$ is opposite to $u_{p(2)}$ and it follows that

$$u'_{p(2)} \quad = \quad -u_{p(2)} \cos(2\theta). \tag{5.5.26}$$

Similarly, the $x$-component of Particle 1's velocity is given by

$$u'_{p(1)} \quad = \quad -u_{p(1)} \cos(2\theta). \tag{5.5.27}$$

Combination of equations (5.5.26) and (5.5.27) then yields

$$u'_{p(rel)} \quad = \quad -u_{p(rel)} \cos(2\theta). \tag{5.5.28}$$

Equation (5.5.28) is substituted into Equation (5.5.23) to obtain an expression for the change in the $x$-component of the total momentum in terms of the relative mass and velocity:

$$\begin{aligned} \Delta P_{1,x} \quad &= \quad m^* u_{p(rel)} \left(1 + \cos(2\theta)\right) \\ &= \quad 2m^* u_{p(rel)} \cos^2 \theta. \end{aligned} \tag{5.5.29}$$

The $x$-component of the force exerted by Particle 2 onto Particle 1 is given by

$$f^{kc} = \frac{dP_{1,x}}{dt} \quad \approx \quad \frac{\Delta P_x}{\Delta t}. \tag{5.5.30}$$

In order to derive an expression for the average force exerted due to multiple particles colliding with one another, it is necessary to average the forces over a collision sphere. A discussion on averaging techniques, which employs the concept of a collision sphere, follows in the next section.

### 5.5.2.2   The collision sphere: a control volume formulation

When two particles of radii $r_1$ and $r_2$, possessing the same relative mass -and velocity, collide, a collisions sphere with radius $r_c = r_1 + r_2$ may be constructed to average the force exerted by one over the other (Clark (2009)). The collision sphere is a control volume analogous to the REV and is illustrated in Figure 5.3.
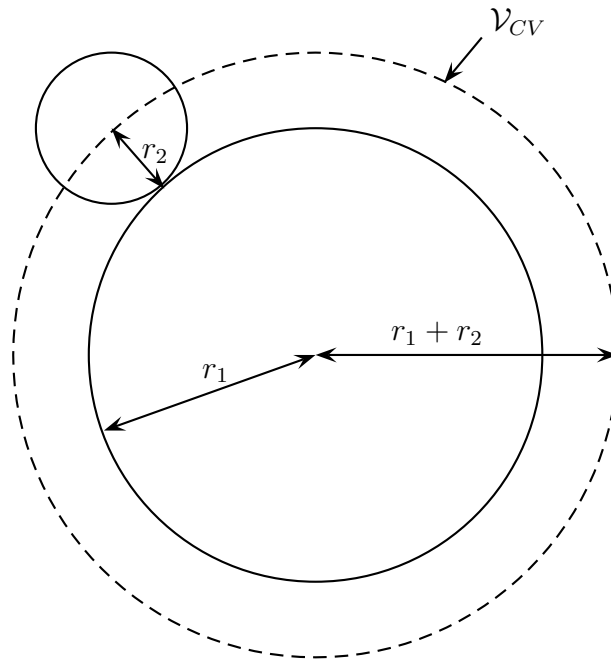


**Figure 5.3:** Two-dimensional view of a collision sphere formed around Particle 1.

The volume of the collision sphere, $\mathcal{V}_{CV}$, is indicated by the dashed line in Figure 5.3. One particle is considered to be the central particle around which the collision sphere is centred and is labelled as a particle of Type 1. Type 1 particles are made up of particles with radii equal to $r_1$, whereas Type 2 particles consist of those particles with radii equaling $r_2$. In Figure 5.3 the Type 1 particle is taken as the central sphere. Any Type 2 particle which crosses the border of the collision sphere, will inevitably make contact with the central sphere (Clark (2009)).

The force acting on the collision sphere is due to the rate of change of the momentum over the control volume and may be expressed as

$$\underline{f}^{kc} = \frac{dm^* \, \underline{v}_{p(rel)}}{dt}, \tag{5.5.31}$$

where $m^*$ is the relative or reduced mass and $\underline{v}_{p(rel)}$ denotes the velocity of the particles. Equation (5.5.31) is approximated by

$$\underline{f}^{kc} \approx \frac{\Delta \left( m^* \, \underline{v}_{p(rel)} \right)}{\Delta t}. \tag{5.5.32}$$

Equation (5.5.32) denotes the force that will be exerted by a single particle of Type 2 onto a particle of Type 1 with a relative mass, $m^*$. The total force experienced by a particle of Type 1 if $N_2$ such particles were to cross the boundary of the collision sphere is given by

$$\underline{f}^{kc} = N_2 \frac{\Delta \left( m^* \, \underline{v}_{p(rel)} \right)}{\Delta t}. \tag{5.5.33}$$

The volume average of $\underline{f}^{kc}$ over the collision sphere may then be calculated by integrating over the collision sphere and is given by

$$\underline{F}^{kc} = \frac{1}{\mathcal{V}_{CV}} \int_{\mathcal{V}_{CV}} N_2 \frac{\Delta \left( m^* \, \underline{v}_{p(rel)} \right)}{\Delta t} d\mathcal{V}. \tag{5.5.34}$$

Following Clark (2009), Soo (1990) and Fan and Zhu (1998), the volume integral is then reduced to a surface integral: [4]

$$\underline{F}^{kc} = \frac{1}{\mathcal{V}_{CV}} \int_{\mathcal{S}} N_2 \Delta \left( m^* \, \underline{v}_{p(rel)} \right) \left( \underline{v}_{p(rel)} \cdot \underline{n} \right) d\mathcal{S}. \tag{5.5.36}$$

The definition of the dot product is applied and it follows that

$$\underline{F}^{kc} = \frac{N_2}{\mathcal{V}_{CV}} \int_{\mathcal{S}^{\perp}} \Delta \left( m^* \, \underline{v}_{p(rel)} \right) |\underline{v}_{p(rel)}| d\mathcal{S}^{\perp}, \tag{5.5.37}$$

---

[4]The relation between the incremental volume element, $d\mathcal{V}$, and the corresponding surface element, $d\mathcal{S}$, is given by Krause (2005) as

$$d\mathcal{V} = (\underline{v} \cdot \underline{n}) \, d\mathcal{S} \Delta t. \tag{5.5.35}$$

where $d\mathcal{S}^{\perp}$ is the projected area of impact normal to the incoming velocity and is illustrated in Figure 5.4.

It is assumed that the flow is compliant with a simple shear regime as illustrated in Figure 5.5. The velocity therefore consists of an $x$-component only which is entirely dependent on the $y$-dimension (i.e. $\underline{v}_{p(rel)} = u(y)_{p(rel)}$) and Equation (5.5.37) may be expressed as[5]

$$F^{kc} = \frac{N_2}{\mathcal{V}_{CV}} \int_{\mathcal{S}^{\perp}} \Delta\left(m^* u_{p(rel)}\right) u_{p(rel)} d\mathcal{S}^{\perp}. \tag{5.5.38}$$

The force due to the simple shear collisions of a total of $N_2$ Type 2 particles on a centred Type 1 particle should also only have an $x$-component and it is for this reason that the vector notation is dropped in calculations to follow.
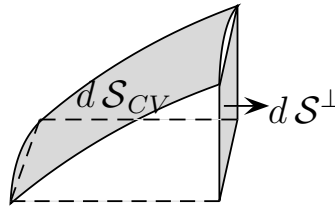


**Figure 5.4:** Projected Surface element, $\mathcal{S}^{\perp}$.

Equation (5.5.38) may thus be written in terms of the $x$-component of the momentum change due to collision, as

$$F^{kc} = \frac{N_2}{\mathcal{V}_{CV}} \int_{\mathcal{S}^{\perp}} \Delta P_x u_{p(rel)} d\mathcal{S}^{\perp}. \tag{5.5.39}$$

Substitution of Equation (5.5.29) into Equation (5.5.39), yields

$$F^{kc} = \frac{N_2}{\mathcal{V}_{CV}} \int_{\mathcal{S}^{\perp}} 2m^* u_{p(rel)}^2 \cos^2\theta d\mathcal{S}^{\perp}. \tag{5.5.40}$$

---

[5]Note that a similar result may be obtained by using the momentum theorem, discussed in Appendix D.
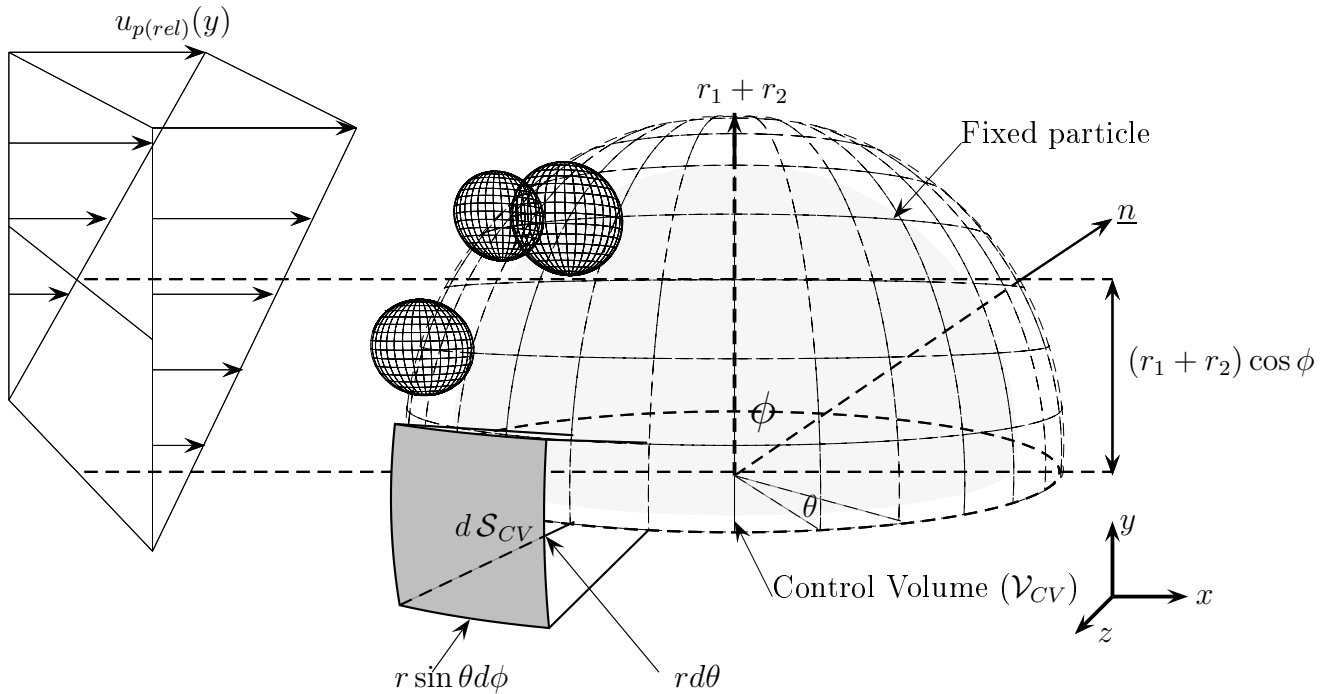
**Figure 5.5:** Sphere of Type 1 subjected to shear flow of cloud of Type 2 particles.

The incremental surface area, orientated perpendicularly to the $x$-direction, is given in spherical coordinates by

$$d\mathcal{S}^{\perp} = r^2 \sin\theta\cos\theta d\theta d\phi, \tag{5.5.41}$$

and the shear flow may be expressed as

$$u_{p(rel)} = \frac{\partial u}{\partial y}y = \frac{\partial u_{p(rel)}}{\partial y}r\sin\theta\cos\phi, \tag{5.5.42}$$

where $r$, $\theta$, and $\phi$ are as illustrated in Figure 5.5. It follows that Equation (5.5.40) may be written as

$$F^{kc} = \frac{N_2}{\mathcal{V}_{CV}}\int_{\mathcal{S}^{\perp}} 2m^*(r_1+r_2)^4\left(\frac{\partial u_{p(rel)}}{\partial y}\right)^2 \sin^3\theta\cos^2\phi\cos^3\theta d\theta d\phi. \tag{5.5.43}$$

Referring to Figure 5.5 it is seen that only the upstream half of the top half of the collision sphere is subjected to particle collisions by a simple shear influx of Type 2 particles. It follows that the collision sphere volume is given by $\mathcal{V}_{CV} = 2/3\pi(r_1 + r_2)^3$ and that integration should take place over the quarter sphere, subjected to the Type 2 particles, hence

$$F^{kc} = \frac{2N_2}{2/3\pi(r_1 + r_2)^3} \int_0^{\pi/2} \int_0^{\pi/2} 2m^*(r_1 + r_2)^4 \left(\frac{\partial u_{p(rel)}}{\partial y}\right)^2 \sin^3\theta \cos^2\phi \cos^3\theta d\theta d\phi.$$
(5.5.44)

Let the number density of a Type 2 particle cloud be the number of particles of Type 2 divided by the volume over which they have an impact. For the case of particles colliding with the top half sphere the number density is given by

$$n_2 = N_2/(2/3\pi(r_1 + r_2)^3).$$
(5.5.45)

Substitution of the number density into Equation (5.5.44) yields

$$F^{kc} = 4n_2 \int_0^{\pi/2} \int_0^{\pi/2} m^*(r_1 + r_2)^4 \left(\frac{\partial u_{p(rel)}}{\partial y}\right)^2 \sin^3\theta \cos^2\phi \cos^3\theta d\theta d\phi.$$
(5.5.46)

Integration of Equation (5.5.46) yields the force exerted by the shear flow of a particle cloud of Type 2 on a single particle of Type 1:

$$F^{kc} = \frac{\pi}{12} n_2 m^* \left(\frac{\partial u_{p(rel)}}{\partial y}\right)^2 (r_1 + r_2)^4.$$
(5.5.47)

For the case of identical particles, the relative mass is given by $m^* = m_{p(i)}/2$, and the force given in Equation (5.5.47) may be expressed as

$$F^{kc} = \frac{\pi}{24} \frac{N_2}{\mathcal{V}_{CV}} m_{p(i)} \left(\frac{\partial u_{p(rel)}}{\partial y}\right)^2 d_p^4.$$
(5.5.48)

The particle mass, $m_{p(i)}$, is expressed in terms of its density, $\rho_p$, and volume, $\nu_{p(i)}$. Hence, Equation (5.5.48) becomes

$$F^{kc} = \frac{\pi}{24} \frac{N_2}{\mathcal{V}_{CV}} \nu_{p(i)} \rho_p \left(\frac{\partial u_{p(rel)}}{\partial y}\right)^2 d_p^4.$$
(5.5.49)

The particle volume fraction is defined as $\epsilon_p = \sum_i \nu_{p(i)}/\mathcal{V}_{CV}$ and after some rearranging of the terms in Equation (5.5.49) it follows that

$$F^{kc} = \frac{\pi}{6} d_p^3 \frac{1}{4} \epsilon_p \rho_p \left(\frac{\partial u_{p(rel)}}{\partial y}\right)^2 d_p.$$
(5.5.50)

Equation (5.5.51) may be expressed as,

$$F^{kc} = \nu_p \frac{\epsilon_p \rho_p d_p}{4} \left( \frac{\partial u_{p(rel)}}{\partial y} \right)^2 .$$ (5.5.51)

The kinetic collisional force of Equation (5.5.51) is written in terms of a particle shear stress for it to be compared to particle shear stresses proposed by Haff (1983) as given by Brennen (2005).

The projected area of impact for the force in Equation (5.5.51) is the half circle perpendicular to the incoming flow over the top half of the single sphere. It follows that

$$\text{Area}_{proj} = 2 \int_0^{\pi/2} \int_0^{\pi/2} d_p^2 \sin\theta \cos\theta d\theta d\phi = \frac{\pi d_p^2}{2}.$$ (5.5.52)

If the force of Equation (5.5.51) is projected onto the half-circle perpendicular to the $y$-axis, the shear stress exerted onto a single particle by its surrounding cloud is

$$\tau_p^{kc} = \frac{\epsilon_p \rho_p d_p^2}{12} \left( \frac{\partial u_{p(rel)}}{\partial y} \right)^2 .$$ (5.5.53)

Equation (5.5.53) bares close resembles to the equations given by Brennen (2005) for the shear stress term derived by Haff (1983), namely

$$\tau_{\text{Haff}}^{kc} = g_s(\epsilon_p) \rho_p d_p^2 \left( \frac{\partial u_{p(rel)}}{\partial y} \right)^2 ,$$ (5.5.54)

here $g_s(\epsilon_p)$ is a function of the particle volume fraction. Haff (1983) required $g(\epsilon_p)$ to tend towards zero as $\epsilon_p$ approaches zero. The function for $g_s(\epsilon_p)$ for the Equation (5.5.53) is given by

$$g_s(\epsilon_p) = \frac{\epsilon_p}{12},$$ (5.5.55)

and thus the limiting condition as proposed by Haff (1983) is satisfied.

Equation (5.5.53) may be written in a similar form as Newton's law of viscosity

$$\tau_p^{kc} = \mu_p \frac{\partial u_{p(rel)}}{\partial y},$$ (5.5.56)

where the particle viscosity is given by, $\mu_p = \epsilon_p \rho_p d_p^2 / 12 \frac{\partial u_{p(rel)}}{\partial y}$.

The particle phase therefore exhibits non-Newtonian fluid properties since its viscosity is not constant but a function of the deformation tensor.

This provides a basis for the two-fluid treatment of two-phase flow, where the particle phase is not treated as discrete but as a fluid from the beginning of the derivation of the momentum expressions. In such cases the particle viscosity is, however, chosen from one of the many empirically derived viscosity expressions available (Enwald *et al.* (1997)).

Equation (5.5.56) states that the stress, $\tau^{kc}$, is proportional to the velocity gradient, $\frac{\partial u_{rel}}{\partial y}$ and the constant of proportionality is the particle viscosity, $\mu_p$. The two-dimensional shear stress and particle interaction force is derived in Appendix E and stated here as

$$\underline{F}^{kc}_{p(i)} = \frac{\epsilon_p \rho_p d_p}{4} \left( \frac{\partial u}{\partial y} + \frac{\partial v}{\partial x} \right) \left[ \left( \frac{\partial u}{\partial y} + \frac{\partial v}{\partial x} \right) \underline{i} + \left( \frac{\partial u}{\partial y} + \frac{\partial v}{\partial x} \right) \underline{j} \right] \nu_i. \quad (5.5.57)$$

Equation (5.5.57) is substituted into Equation (5.5.3) and it follows that

$$\underline{I}_p = -\frac{1}{\mathcal{U}_o} \sum_{i=1}^{N} \frac{\epsilon_p \rho_p d_p}{4} \left( \frac{\partial u}{\partial y} + \frac{\partial v}{\partial x} \right) \left[ \left( \frac{\partial u}{\partial y} + \frac{\partial v}{\partial x} \right) \underline{i} + \left( \frac{\partial u}{\partial y} + \frac{\partial v}{\partial x} \right) \underline{j} \right] \nu_i. \tag{5.5.58}$$

For a constant particle diameter and density, this may be expressed in terms of averaging notation introduced earlier in Section 4.6

$$\begin{aligned}
\underline{I}_p &= -\frac{\rho_p d_p}{4} \overline{\epsilon_p \left( \frac{\partial u}{\partial y} + \frac{\partial v}{\partial x} \right)^2} \hat{\underline{n}}. \\
&= -\frac{\epsilon_p^2 \rho_p d_p}{4} \overline{\left( \frac{\partial u}{\partial y} + \frac{\partial v}{\partial x} \right)^2}^p \hat{\underline{n}}, \tag{5.5.59}
\end{aligned}$$

where it is assumed that

$$\overline{\tilde{\epsilon}_p \left( \widetilde{\frac{\partial u}{\partial y} + \frac{\partial v}{\partial x}} \right)^2}^p = 0. \tag{5.5.60}$$

It is assumed that Equation (5.5.59) may be cast into the following form

$$\underline{I}_p = -\frac{\epsilon_p^2 \rho_p d_p}{4} \left( \frac{\partial \overline{u}^p}{\partial y} + \frac{\partial \overline{v}^p}{\partial x} \right)^2 \hat{\underline{n}}. \tag{5.5.61}$$

Substitution of Equation (5.5.61) into Equation (5.4.10), yields the following expression

for momentum conservation of the discrete phase

$$\rho_p \frac{\partial}{\partial t}\epsilon_p \overline{\underline{v}_p}^{\,p} + \rho_p \nabla \cdot \epsilon_p \overline{\underline{v}_p}^{\,p}\overline{\underline{v}_p}^{\,p} = \epsilon_p \underline{g}\rho_p - \epsilon_p \nabla \langle p_c\rangle_c - \frac{\epsilon_p^2 \rho_p d_p}{4}\left(\frac{\partial \overline{u}^{\,p}}{\partial y} + \frac{\partial \overline{v}^{\,p}}{\partial x}\right)^2 \hat{\underline{n}}$$

$$- \frac{1}{\mathcal{U}_o}\int_{\mathcal{S}_{pc}}\left(-\tilde{p}_c\underline{\underline{1}} + \underline{\underline{\tau}}_c\right)\cdot \underline{n}_c d\mathcal{S}, \qquad (5.5.62)$$

which concludes the constitutive modelling procedure.

## 5.6   Summary and conclusions

In this chapter the constitutive laws have been applied to the conservation equations that were derived in Chapter 4. Using the principles of momentum conservation and full elasticity an expression for particle-particle interaction was established. This interaction term bares close resemblance to the shear stress term derived by Haff (1983). The final averaged form of the continuum and the particle momentum equations are given by Equations (5.4.5) and (5.5.62), respectively.

# Chapter 6

# Transfer laws: The Representative Unit Cell

## 6.1  Introduction

The Representative Unit Cell (RUC) is defined as a rectangular volume of minimum dimensions into which the geometric properties of the REV may be embedded. It provides a facility to consider flow conditions within the most elementary control volume of the particular porous medium and still have all the geometrical properties of the medium at hand for modelling of physical phenomena. It is assumed that the average geometrical properties of the particle structure within the RUC can be resembled by a cube of particle material, located centrally within, and aligned with, the cubic RUC, as is shown in Figure 6.1.

A two-dimensional schematic, in which the sections of the RUC is labelled, is given in Figure 6.2. In Figure 6.2 the unit vector, $\widehat{\underline{n}}$, denotes the direction of the streamwise direction,[1] whereas $\underline{n}_c$ and $\underline{n}_p$ are outward directed unit vectors normal to the continuum and particle phases, respectively. The interstitial flow direction is given by $\tilde{\underline{n}}$. The volume of the particle phase is given by $U_p$ and that of the continuum is denoted by $U_c$. The continuum volume is further divided into a streamwise and a transverse section, which are denoted by $U_{||}$ and $U_\perp$, respectively. Surface areas parallel to the streamwise direction are denoted by $S_{||}$ and surface areas perpendicular to $\widehat{\underline{n}}$ are given

---

[1] The streamwise direction, which will be denoted by $\hat{\underline{n}}$ in this work, is the direction of the volumetric average of the microscopic velocity in the REV.

by $S_\perp$.
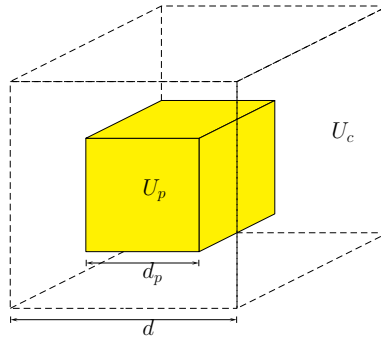


**Figure 6.1:** Representative Unit Cell (RUC).
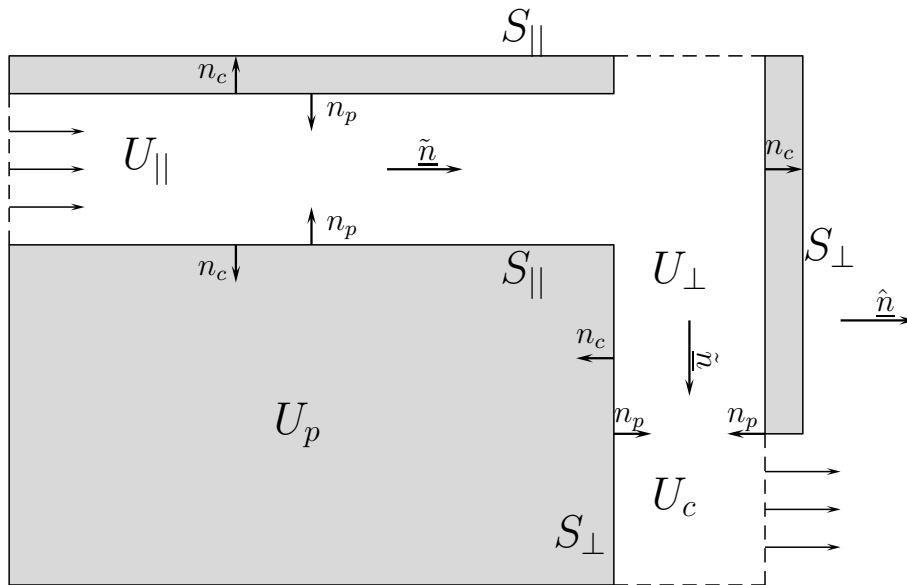


**Figure 6.2:** Two-dimensional RUC schematic.

The RUC was first developed by Du Plessis and Masliyah (1988) to model time-independent laminar flow through a rigid, isotropic and consolidated porous medium of spatially varying porosity. The 1988 version of the RUC model performed well in the

Darcy regime of very low intra-pore Reynolds number[2] flow, but its prediction of the Forchheimer inertial effect was not quantitatively correct. These shortcomings were addressed by modelling the gradual increase of Reynolds number with flow recirculation on the streamwise lee-side surface of the solid material (Du Plessis (1992)).

Experimental validation of the 1992 model by Du Plessis *et al.* (1994) showed that such a modelling procedure was capable of accurately predicting the pressure gradients for both Darcy and Forchheimer flows. With the introduction of streamwise staggering, Lloyd *et al.* (2004), adapted the RUC to predict the Darcy permeability in anisotropic media. Up to date the RUC model has continued to undergo numerous modifications in an effort to increase its predictive proficiency.

The version of the RUC model used in this work, is the 1997 rendition for a granular medium (Du Plessis and Diedericks (1997)), and not the latest version. The reason this was done is that the later modifications severely increased the complexity of the model whereas the increase in its prediction capabilities, for this work, would be overshadowed by errors made in experimental procedures.

The appeal of the RUC, and the reason for it being adopted here, is that it contains few empirical fitting parameters. The result is a model which is applicable to a broad range of physical processes.

In Section 6.2, the 1997 RUC model for single phase flow is discussed in order to acquaint the reader with its underlying assumptions. This standard model is then modified in Section 6.3 to incorporate two-phase flow and increase the range of particle volume fractions for which it may be utilised.

## 6.2   1997 RUC model

The particle-continuum surface integral in Equation (5.5.62) represents the momentum transfer between the two phases. An overview of the closure method for such an integral for a stationary porous medium is given in this section.

---

[2]The Reynolds number for flow through a stationary porous medium is defined as $Re = \rho_c \epsilon_c d_p |v_c| / \mu_c$.

The integral to be closed is given by

$$
\underline{I} \;=\; \frac{1}{U_o} \int\limits_{S_{pc}} \left( -\tilde{p}\,\underline{n}_c + \underline{\underline{\tau}}_c \cdot \underline{n}_c \right) dS. \tag{6.2.1}
$$

The relative importance of inertial and viscous effects is given by the dimensionless Reynolds number which is defined as

$$
Re \;=\; \frac{\text{Inertial forces}}{\text{Viscous forces}}. \tag{6.2.2}
$$

Small Reynolds number values indicate slow viscous flows for which it is assumed that viscous forces, arising from shearing motions of the continuum, dominate over inertial forces (associated with high pressure gradients). An increase in the Reynolds number amplifies the inertial forces until the Forchheimer regime is reached where such inertial forces dictate. An additional surge in the Reynolds number renders the flow turbulent. It is, however, assumed in this work that the flow remains laminar and "high Reynolds numbers" will refer to the upper limit of Reynolds numbers for which the flow is still laminar.

The particle-continuum interface, $\mathcal{S}_{pc}$, in Equation (6.2.1) is approximated as the particle-continuum interface, $S_{pc}$, of the RUC and partitioned into its constituent parallel and transverse regions denoted respectively by $S_{\parallel}$ and $S_{\perp}$, as illustrated in Figure 6.2:

$$
\underline{I} \;=\; \frac{1}{U_o} \int\limits_{S_{\parallel}} -\tilde{p}\,\underline{n}_c dS + \frac{1}{U_o} \int\limits_{S_{\perp}} -\tilde{p}\,\underline{n}_c dS + \frac{1}{U_o} \int\limits_{S_{\parallel}} \underline{\underline{\tau}}_c \cdot \underline{n}_c dS + \frac{1}{U_o} \int\limits_{S_{\perp}} \underline{\underline{\tau}}_c \cdot \underline{n}_c dS.
$$

$$
\tag{6.2.3}
$$

Equation (6.2.3) describes the impact that the presence of the stationary particulate material has on the momentum of the continuum traversing it. In the following sections, pressure and shearing effects will be compared to each other for the two limiting, i.e. Darcy and Forchheimer, flow regimes.

## 6.2.1 Modelling viscous flow

For the low Reynolds number limit, it is assumed that the contribution to the total surface stress is dominated by the shear component and that, in comparison, the pressure gradient effect may be considered negligible. The shear stresses in the transverse

pore sections of the RUC are directed perpendicularly to the streamwise direction and therefore have a zero contribution in the said direction. These transverse shear stresses will, however, cause interstitial pressure drops. It is assumed that the contribution to $\underline{I}$ due to such a pressure drop may be incorporated by integrating the wall shear over the total particle-continuum interface, $S_{pc}$, instead of only over the streamwise section $S_{||}$, i.e.

$$\underline{I}_o = \frac{1}{U_o} \int\limits_{S_{||}} \left( \underline{\underline{\tau}}_c \cdot \underline{n}_c \right) dS + \widehat{\underline{n}} \frac{1}{U_o} \int\limits_{S_\perp} \left( \underline{n}_c \cdot \underline{\underline{\tau}}_c \cdot \tilde{\underline{n}}_c \right) dS. \tag{6.2.4}$$

In Equation (6.2.4), $\underline{I}_o$ denotes the viscous approximation of $\underline{I}$ and $\tilde{\underline{n}}_c$ is the unit normal vector indicating the interstitial flow direction. Let $\underline{n}_c$ be the unit vector directed perpendicular from the continuum into the particle phase and let $\widehat{\underline{n}}$ be the unit vector in the streamwise direction as depicted in Figure 6.2. Under the *first face second stress* convention, the wall shear stresses in the streamwise and transverse channels are respectively expressed as

$$\underline{\underline{\tau}}_c^{||} = \tau_c^{||}(-\underline{n}_c \widehat{\underline{n}}), \tag{6.2.5}$$

and

$$\underline{\underline{\tau}}_c^\perp = -\tau_c^\perp \underline{n}_c \tilde{\underline{n}}. \tag{6.2.6}$$

Substituting Equations (6.2.5) and (6.2.6) into the relevant integrals of Equation (6.2.4) and assuming that the shear stress dyad is symmetric, yield

$$\underline{I}_0 = -\frac{1}{U_o} \int\limits_{S_{||}} \tau_c^{||} \widehat{\underline{n}} dS + \frac{1}{U_o} \int\limits_{S_\perp} -\tau_c^\perp \widehat{\underline{n}} dS. \tag{6.2.7}$$

For the low Reynolds number limit, the wall shear stress, $\tau_c^w$ (which is defined as the sum of all the wall shear stresses within the RUC, $\tau_c^w = \tau_{||} + \tau_\perp$) is assumed uniform and constant over the particle continuum interface, $S_{pc}$, in all channel sections and it follows that

$$\underline{I}_o = -\widehat{\underline{n}} \frac{S_{pc}}{U_o} \tau_c^w. \tag{6.2.8}$$

The flow is assumed Newtonian and the upstream directed shear is therefore given in terms of the pore velocity profile, $u_c^{pore}$, as

$$\tau_c^w = \mu_c \frac{du_c^{pore}}{dy}. \tag{6.2.9}$$

The velocity profile for the motion of a continuum between parallel plates for which a no-slip condition is adopted at the $S_{pc}$-interfaces, is

$$u_c^{pore}(y) = -\frac{y}{2\mu_c}\left(\frac{dp}{dx}\right)(d_c - y), \qquad (6.2.10)$$

where $d_c$ is the distance between the plates. This type of flow, generally referred to as plane Poiseuille flow, is illustrated in Figure 6.3.
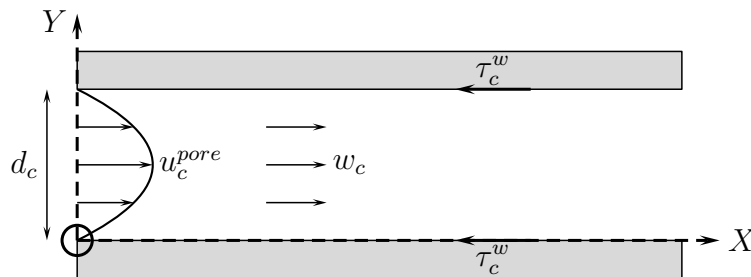


**Figure 6.3:** Plane Poiseuille flow.

Taking the derivative of Equation (6.2.10) with respect to $y$ and substituting the result into the expression for the shear, given by Equation (6.2.9), yield

$$\tau_c^w = \frac{d_c}{2}\left(-\frac{dp}{dx}\right). \qquad (6.2.11)$$

In order for the shear to be incorporated into the RUC model it needs to be expressed in terms of the streamwise *average* pore velocity, $w_c$. Such a velocity is obtained by integrating over the parabolic velocity profile given by Equation (6.2.10) and dividing the result by the width of the channel, $d_c$:

$$
\begin{aligned}
w_c &= \frac{1}{d_c}\int_0^{d_c} u_c^{pore}\,dy \\
&= \frac{d_c^2}{12\mu_c}\left(-\frac{dp}{dx}\right). \qquad (6.2.12)
\end{aligned}
$$

The pressure gradient in Equation (6.2.11) may thus be expressed in terms of $w$, yielding

$$\tau_c^w = \frac{6\mu_c w_c}{d_c}. \qquad (6.2.13)$$

Following Du Plessis (2003), the ratio of the average streamwise pore velocity, $w_c$, to the average interstitial continuum velocity, $\langle v_c\rangle_c$, is given by the ratio of the streamwise

RUC volume, $U_{||}$, to the total RUC-volume available for continuum motion, $U_c$:

$$\frac{w_c}{\langle v_c \rangle_c} \approx \frac{U_c}{U_{||}}. \tag{6.2.14}$$

It follows that Equation (6.2.13) may be expressed in terms of $\langle v_c \rangle_c$ as

$$\tau_c^w = \frac{6\mu_c \langle v_c \rangle_c}{d_c} \frac{U_c}{U_{||}}. \tag{6.2.15}$$

The ratio between the streamwise and the total continuum volume is referred to as the tortuosity and denoted by $\chi = U_c/U_{||}$. It follows that Equation (6.2.15) may be given in terms of the tortuosity as

$$\tau_c^w = \frac{6\mu_c \langle v_c \rangle_c \chi}{d_c}. \tag{6.2.16}$$

Substitution of the expression for the wall shear, given by Equation (6.2.16), into Equation (6.2.8) then yields the following closed form for the momentum surface integral in the case of low Reynolds number flow:

$$\underline{I}_o = -\frac{S_{pc}\chi}{U_o} \frac{6\mu \langle v_c \rangle_c}{d_c} \widehat{\underline{n}}_c. \tag{6.2.17}$$

Table 6.1 is a summary of the geometric coefficients for a granular medium. Substitution of the coefficients listed in Table 6.1 into Equation (6.2.17), yields the following expression for viscous flow in terms of the continuum -and particle volume fractions, respectively denoted by $\epsilon_c$ and $\epsilon_p$, and the width of the particulate volume, $d_p$:

$$\underline{I}_o = -\frac{36\mu_c}{d_p^2} \frac{\epsilon_p^{4/3}\epsilon_c}{(1 - \epsilon_p^{1/3})(1 - \epsilon_p^{2/3})} \langle v_c \rangle_c \widehat{\underline{n}}_c. \tag{6.2.18}$$

**Table 6.1:** Geometric coefficients for a granular medium.

| Coefficient | Expression |
|---|---|
| $U_o$ | $d^3$ |
| $A_c$ | $d^2 - d_p^2$ |
| $U_{\parallel}$ | $A_c d$ |
| $U_c$ | $U_o - U_p$ |
| $d_p$ | $(1 - \epsilon_c)^{1/3} d$ |
| $d_c$ | $d - d_p = d(1 - (1 - \epsilon_c)^{1/3})$ |
| $S_{pc}$ | $6d_p^2 = 6(1 - \epsilon_c)^{2/3} d^2$ |
| $S_{\parallel}$ | $4d_p^2$ |
| $S_{\perp}$ | $2d_p^2$ |
| $S_{face}$ | $d_p^2$ |
| $\chi$ | $\frac{\epsilon_c}{\left(1 - (1 - \epsilon_c)^{2/3}\right)}$ |

This concludes the closure of Equation (6.2.1) for the viscous motion of a Newtonian continuum through a stationary porous medium.

## 6.2.2   Modelling inertial flow

With an increase in Reynolds number the predominance of the pressure gradient above the shear stresses is enhanced so that the shear stress contribution in Equation (6.2.1) may be discarded, yielding the following form of the momentum transfer integral for the inertial regime:

$$\underline{I}_\infty \;=\; \frac{1}{U_o} \int\limits_{S_\perp} -\tilde{p}\,\underline{n}_c dS. \tag{6.2.19}$$

Du Plessis (1993) proposed that the integral $\underline{I}_\infty$ may be modelled by an internal form drag condition, with $c_d$ the drag coefficient and $S_{face}$ the surface exposed upstream, relative to the streamwise direction, i.e.

$$\underline{I}_\infty \;=\; -\frac{1}{U_o} c_d S_{face} \frac{1}{2} \rho w_c^2 \widehat{\underline{n}}_c. \tag{6.2.20}$$

The relationship between the average streamwise continuum pore velocity, $w_c$, and the average interstitial continuum velocity, $\langle v_c \rangle_c$ (given by Equation (6.2.14)) is applied to Equation (6.2.20) and the geometric coefficients (listed in Table 6.1) substituted, to yield

$$\underline{I}_\infty = -\frac{\rho_c c_d}{2 d_p} \frac{\epsilon_c^2 \epsilon_p}{\left(1 - \epsilon_p^{2/3}\right)^2} \langle v_c \rangle_c^2 \, \widehat{\underline{n}}_c. \tag{6.2.21}$$

This concludes the closure of Equation (6.2.1) for the inertial motion of a Newtonian continuum through a stationary porous medium.

Equations (6.2.18) and (6.2.21) describe the two limits of laminar continuum motion. They, however, do not provide information about the transition from low to high Reynolds number flows. This shortcoming is addressed by applying an asymptotic matching technique, first described by Churchill and Usagi (1972), through which an equation which embodies the range from the low to the intermediate Reynolds numbers is attained.

### 6.2.3 A general closure expression

Equations (6.2.18) and (6.2.21) are combined with the use of the asymptote matching technique (Churchill and Usagi (1972)):

$$\underline{I} = \left( \underline{I}_o^s + \underline{I}_\infty^s \right)^{\frac{1}{s}}, \tag{6.2.22}$$

where $s$ is a *shifting parameter* which, following Du Plessis (2003), is taken as unity for the closure procedure. The closed form of Equation (6.2.1) is therefore given by

$$
\begin{aligned}
\underline{I} &= -\left[ \frac{36 \mu_c}{d_p^2} \frac{\epsilon_p^{4/3} \epsilon_c}{(1 - \epsilon_p^{1/3})(1 - \epsilon_p^{2/3})} \langle v_c \rangle_c \, \widehat{\underline{n}}_c + \frac{\rho_c c_d}{2 d_p} \frac{\epsilon_c^2 \epsilon_p}{\left(1 - \epsilon_p^{2/3}\right)^2} \langle v_c \rangle \langle v_c \rangle \right] \widehat{\underline{n}}_c \\
&= -\left[ \frac{36 \mu_c}{d_p^2} \frac{\epsilon_p^{4/3} \epsilon_c}{(1 - \epsilon_p^{1/3})(1 - \epsilon_p^{2/3})} + \frac{\rho_c c_d}{2 d_p} \frac{\epsilon_c^2 \epsilon_p}{\left(1 - \epsilon_p^{2/3}\right)^2} || \langle v_c \rangle || \right] \langle \underline{v}_c \rangle_c. \tag{6.2.23}
\end{aligned}
$$

Equation (6.2.23) is the final result for the closure of Equation (6.2.1) which is relevant to limiting as well as intermediate Reynolds number flows.

This surmises the application of the 1997 RUC to the modelling of single phase Newtonian flow through a stationary porous medium and proves sufficiently accurate for

continuum volume fractions up to 0.8 (Lloyd *et al.* (2004)). Adaptations made to this model to incorporate two-phase flow are discussed, and a final closure model for the momentum transfer between phases given, in the following sections.

## 6.3    Adaptation to the 1997 RUC

In this section, the existing RUC model is modified to allow for particulate motion and to incorporate porosities exceeding the 0.8 limiting value of the 1997 rendition.

The surface integral term remaining in Equations (5.4.7) and (5.5.62) is similar to that given for single phase flow by Equation (6.2.1) and subjected to the same assumptions and modelling procedures of Section 6.2. The difference lies in the definition of the shear stress, $\underline{\underline{\tau}}_{pc}$, for two-phase flow: For the 1997 single phase RUC model, the shear stress was derived from the plane Poiseuille velocity profile between stationary plates whereas current work allows for said plates to move relative to the continuum. In sections to follow the closure procedures for the low- and high Reynolds number limits are discussed. Asymptotic matching between these extremes yields an expression for the momentum transfer integral in terms of averaged variables which is applicable to intermediate flows.

## 6.4    Two-phase viscous flow at the low Reynolds number limit

The low Reynolds number regime is treated by dividing it into two categories: Low and high continuum volume fractions. For small values of $\epsilon_c$, the drag in the medium is assumed to be due to *flow through* a particulate phase, whereas the drag for high porosity values will be regarded to originate from *flow by* a particulate phase. An asymptotic match between these two categories will then yield a closed expression for the Darcy regime.

### 6.4.1   Low Reynolds number flow at low porosities

The modelling procedure for low Reynolds numbers follows similar assumptions to those made in Section 6.2.1. The closure of the integral term is given in terms of the

relative wall shear stress, $\tau_{pc}^w$ as

$$\underline{I}_o^{\text{flow through}} = -\widehat{\underline{n}}\frac{S_{pc}}{U_o}\tau_{pc}^w. \tag{6.4.1}$$

The relative shear, $\tau_{pc}^w$, is defined in terms of the relative pore velocity, $u_{pc}^{pore}$, as

$$\tau_{pc}^w = \mu_c\frac{du_{pc}^{pore}}{dy}. \tag{6.4.2}$$

The velocity profile, $u_{pc}^{pore}$, for a continuum phase moving relatively to parallel plates, as illustrated in Figure 6.4, is given by

$$u_{pc}^{pore} = -\frac{y}{2\mu_c}\left(\frac{dp}{dx}\right)(d_c - y). \tag{6.4.3}$$

The shearing stress due to this relative velocity is derived similarly to that given by Equation (6.2.9) and may be written in terms of the pressure gradient as

$$\tau_{pc}^w = \frac{d_c}{2}\left(-\frac{dp}{dx}\right). \tag{6.4.4}$$
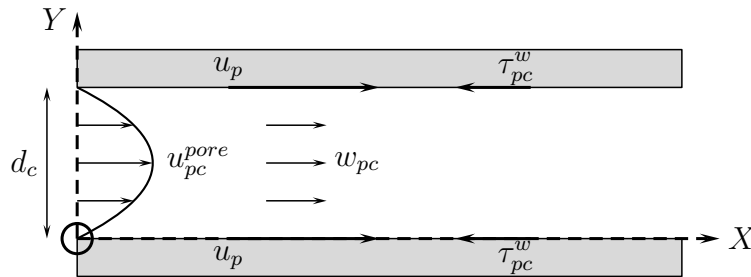


**Figure 6.4:** Plane Poiseuille flow for the adapted model.

The average streamwise relative pore velocity is given by

$$w_{pc} = \frac{1}{d_c}\int_0^{d_c} u_{pc}^{pore}dy$$
$$= \frac{d_c^2}{12\mu_c}\left(-\frac{dp}{dx}\right). \tag{6.4.5}$$

The average interstitial relative velocity is defined as

$$v_{pc} = \langle v_c\rangle_c - \overline{v_p}^{\,p}, \tag{6.4.6}$$

and is assumed to be related to $w_{pc}$ by

$$\frac{w_{pc}}{v_{pc}} \approx \frac{U_c}{U_{||}}. \tag{6.4.7}$$

It follows that the shear stress for the particle-continuum surface integral term is given by

$$\tau_{pc}^w = \frac{6\mu_c \left( \langle v_c \rangle_c - \overline{v_p}^p \right)}{d_c} \chi. \tag{6.4.8}$$

Substitution of Equation (6.4.8) into Equation (6.4.1), yields

$$\underline{I}_o^{\text{flow through}} = -\frac{36\epsilon_c(1 - \epsilon_c)^{4/3}}{d_p^2 \left( 1 - (1 - \epsilon_c)^{2/3} \right) \left( 1 - (1 - \epsilon_c)^{1/3} \right)} \mu_c \left( \langle \underline{v}_c \rangle_c - \overline{\underline{v}_p}^p \right). \tag{6.4.9}$$

Equation (6.4.9) is the drag force per RUC volume, $U_o$, that results from shear interaction between the two phases for low continuum volume fractions.

## 6.4.2   Low Reynolds number flow at high porosities

The drag force for viscous flow should, for porosity values close to unity, strive to that experienced by a single particle, i.e. Stokes drag. Equation (6.4.9), however, rapidly tends to zero as porosity tends to one and is therefore subject to modification.

This shortcoming is dealt with by first deriving an expression for Stokes drag over particles within an REV. Stokes drag is given by (p.60 Bird *et al.* (2002)) as

$$\underline{F}_{Stokes} = 3\pi d_p \mu_c \, \underline{v}_{pc}, \tag{6.4.10}$$

where $d_p$ is the particle diameter and the relative velocity, $\underline{v}_{pc}$, is once again assumed to be the average relative interstitial velocity, which is given by

$$\underline{v}_{pc} = \langle \underline{v}_c \rangle - \overline{\underline{v}_p}^p. \tag{6.4.11}$$

The average of the Stokes force over the entire REV is assumed to provide an approximation for the viscous drag within the REV due to flow by a particulate phase and will be denoted by $\underline{I}_o^{\text{flow by}}$. It is attained by adding the forces for all $N$ particles, present within the REV, and dividing through the total REV volume, $\mathcal{U}_o$:

$$\underline{I}_o^{\text{flow by}} = -\frac{1}{\mathcal{U}_o} \sum_{i=1}^{N} 3\pi d_p \mu_c \left( \langle \underline{v}_c \rangle - \overline{\underline{v}_p}^p \right). \tag{6.4.12}$$

Equation (6.4.12) is multiplied and divided by the volume of a single particle ($\nu_{p(i)} = \frac{1}{6}\pi d_p^3$) to obtain:

$$\underline{I}_o^{\text{flow by}} \quad = \quad -\frac{1}{\mathcal{U}_o}\sum_{i=1}^{N}\frac{18\mu_c\left(\langle\underline{v}_c\rangle - \overline{\underline{v}_p}^{\,p}\right)}{d_p^2}\nu_{p(i)}, \tag{6.4.13}$$

which is in the form of the definition for the particle average, given by Equation (4.6.1).

Since $\underline{v}_{pc}$ was given by Equation (6.4.6) in terms of averages it may be moved outside of the summation operator. Hence the following expression for the average Stokes force is given by

$$\underline{I}_o^{\text{flow by}} \quad = \quad -\frac{18\epsilon_p\mu_c\left(\langle\underline{v}_c\rangle - \overline{\underline{v}_p}^{\,p}\right)}{d_p^2}. \tag{6.4.14}$$

Stokes flow is only valid for Reynolds numbers below 0.1 and denotes the drag for instances where the viscous regime is described by "flow by" rather than "flow through" a particulate phase. In the next section an expression for the total viscous drag force for two-phase flow, which will be valid for low- and high porosity limits is derived.

### 6.4.3   Total Drag Force for the Darcy Regime

The total viscous drag force per unit volume for two-phase flow (which is applicable over the entire porosity range) is obtained by adding Equations (6.4.9) and (6.4.14):

$$\underline{I}_o^{pc} \quad = \quad -\frac{\mu_c\epsilon_p}{d_p^2}\left(\frac{36\epsilon_c\epsilon_p^{1/3}}{\left(1-\epsilon_p^{2/3}\right)\left(1-\epsilon_p^{1/3}\right)}+18\right)\left(\langle\underline{v}_c\rangle_c - \overline{\underline{v}_p}^{\,p}\right). \tag{6.4.15}$$

This is written in terms of the momentum transfer coefficients for the limiting porosity values, $\beta_o^{\text{flow through}}$ and $\beta_o^{\text{flow by}}$, as

$$\underline{I}_o^{pc} \quad = \quad -\left(\beta_o^{\text{flow through}} + \beta_o^{\text{flow by}}\right)\left(\langle\underline{v}_c\rangle_c - \overline{\underline{v}_p}^{\,p}\right), \tag{6.4.16}$$

where

$$\beta_o^{\text{flow through}} \quad = \quad \frac{36\epsilon_c\epsilon_p^{4/3}}{d_p^2\left(1-\epsilon_p^{2/3}\right)\left(1-\epsilon_p^{1/3}\right)}\mu_c, \tag{6.4.17}$$

and

$$\beta_o^{\text{flow by}} \quad = \quad \frac{18\epsilon_p\mu_c}{d_p^2}. \tag{6.4.18}$$

The behaviour of each of the momentum transfer coefficients of Equations (6.4.17) and (6.4.18), as well as their combined effect for porosity values that range from those of packed beds (i.e., $\epsilon_c \approx 0.4$) to porosities corresponding to dilute instances of dispersed solid material within a fluid (i.e. $\epsilon_c \approx 1$), are illustrated in Figure 6.5.
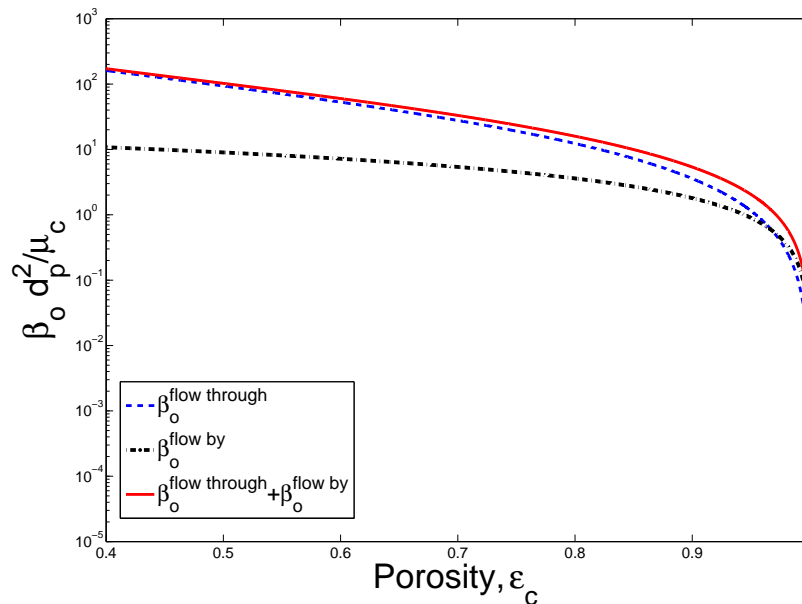


**Figure 6.5:** Flow by and flow through momentum transfer given by Equations (6.4.16) – (6.4.18).

From Figure 6.5 it is apparent that $\beta_o^{\text{flow through}}$ dominates for porosities in the range of $0.4 \leq \epsilon_c \leq 0.95$. Figure 6.6 is an enlarged view of the porosity range for $0.95 < \epsilon_c \leq 1.0$, showing that Stokes drag dictates for $\epsilon_c > 0.97$.

The solid line in both Figures 6.5 and 6.6 constitutes the effect of the combined drag, given by $\beta_o^{\text{flow through}} + \beta_o^{\text{flow by}}$, and follows the trend of Equation (6.4.17) and Equation (6.4.18) for the ranges of $0.4 \leq \epsilon_c \leq 0.95$ and $\epsilon_c > 0.97$, respectively. The addition of the Stokes drag thus reduces the rate at which the combined result tends towards zero.
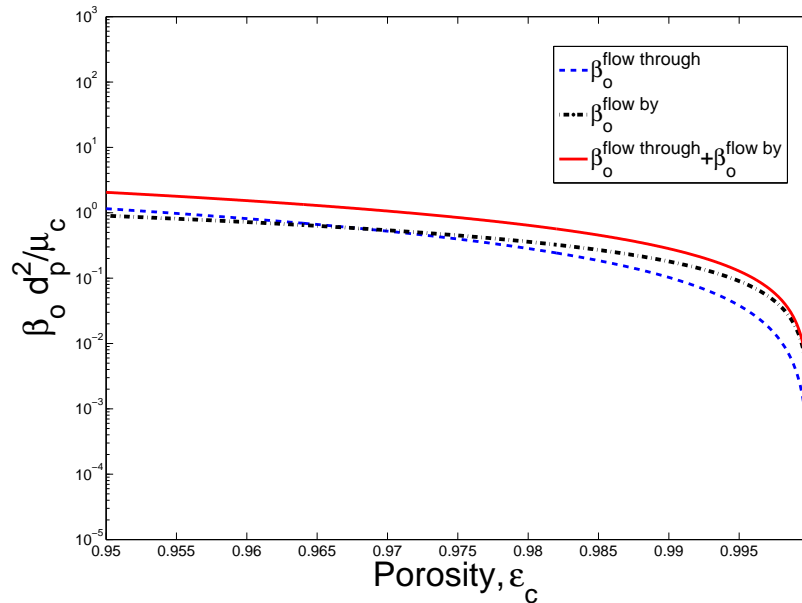
**Figure 6.6:** Flow by and flow through momentum transfer given by Equations (6.4.16) – (6.4.18) for $\epsilon_c \geq 0.95$.

## 6.5   High Reynolds number flow

Following the procedure set out in Section 6.2.2, yields the following closed form for the Forchheimer regime

$$\underline{I}_\infty^{pc} \;=\; -\frac{1}{2}\frac{c_d \rho_c}{d_p}\frac{\epsilon_p \epsilon_c^2}{\left(1-\epsilon_p^{2/3}\right)^2}\left(\langle \underline{v}_c\rangle_c - \overline{\underline{v}_p}^{\,p}\right)||\,\langle \underline{v}_c\rangle_c - \overline{\underline{v}_p}^{\,p}||, \qquad (6.5.1)$$

where the continuum velocity of Equation (6.2.21) has been replaced by the relative velocity.

## 6.6   Asymptotic matching

Asymptotic matching of Equations (6.4.15) and (6.5.1), yields a result for the momentum transfer between the particle- and the continuum phases, which is applicable to

the intermediate Reynolds numbers:

$$
\underline{I}^{pc} = -\left[\left[\frac{\mu_c \epsilon_p}{d_p^2}\left(\frac{36\epsilon_c \epsilon_p^{1/3}}{\left(1 - \epsilon_p^{2/3}\right)\left(1 - \epsilon_p^{1/3}\right)} + 18\right)\right]^s + \right.
$$
$$
\left.\left[\frac{1}{2}\frac{c_d \rho_c}{d_p}\frac{\epsilon_p \epsilon_c^2}{\left(1 - \epsilon_p^{2/3}\right)^2}||\left\langle \underline{v}_c\right\rangle_c - \overline{\underline{v}_p}^p||\right]^s\right]^{1/s}\left(\left\langle \underline{v}_c\right\rangle_c - \overline{\underline{v}_p}^p\right). \qquad (6.6.1)
$$

For simplicity the averaging notation is dropped and the final expressions for continuum- and particle momentum conservation expressions are thus given respectively by

$$
\rho_c \frac{\partial \epsilon_c \underline{v}_c}{\partial t} + \rho_c \nabla \cdot (\epsilon_c \underline{v}_c \underline{v}_c) = \rho_c \underline{g}\epsilon_c - \epsilon_c \nabla p_c + \mu_c \nabla \cdot [\epsilon_c \nabla \underline{v}_c] -
$$
$$
\left[\left[\frac{\mu_c \epsilon_p}{d_p^2}\left(\frac{36\epsilon_c \epsilon_p^{1/3}}{\left(1 - \epsilon_p^{2/3}\right)\left(1 - \epsilon_p^{1/3}\right)} + 18\right)\right]^s + \left[\frac{1}{2}\frac{c_d \rho_c}{d_p}\frac{\epsilon_p \epsilon_c^2}{\left(1 - \epsilon_p^{2/3}\right)^2}||\underline{v}_c - \underline{v}_p||\right]^s\right]^{1/s}\left(\underline{v}_c - \underline{v}_p\right),
$$
$$
(6.6.2)
$$

and

$$
\rho_p \frac{\partial}{\partial t}\epsilon_p \underline{v}_p + \rho_p \nabla \cdot \epsilon_p \underline{v}_p \underline{v}_p = \epsilon_p \underline{g}\rho_p - \epsilon_p \nabla \left\langle p_c\right\rangle_c - \frac{\epsilon_p^2 \rho_p d_p}{4}\left(\frac{\partial \overline{u}^p}{\partial y} + \frac{\partial \overline{v}^p}{\partial x}\right)^2 \hat{\underline{n}} +
$$
$$
\left[\left[\frac{\mu_c \epsilon_p}{d_p^2}\left(\frac{36\epsilon \epsilon_p^{1/3}}{\left(1 - \epsilon_p^{2/3}\right)\left(1 - \epsilon_p^{1/3}\right)} + 18\right)\right]^s + \left[\frac{1}{2}\frac{c_d \rho_c}{d_p}\frac{\epsilon_p \epsilon_c^2}{\left(1 - \epsilon_p^{2/3}\right)^2}||\underline{v}_c - \underline{v}_p||\right]^s\right]^{1/s}\left(\underline{v}_c - \underline{v}_p\right).
$$
$$
(6.6.3)
$$

The values of the drag coefficient, $c_d$, and the asymptotic matching parameter, $s$, are unknown and calculated retrospectively following comparison with existing empirical data sets.

## 6.6.1 Setting the fitting parameters

The expression for the momentum transfer between the particles and its surrounding continuum, given by Equation (6.6.1), may be written in terms of a *momentum transfer coefficient*, $\beta$, as

$$
\underline{I}_{tot} = -\beta\left(\underline{v}_c - \underline{v}_p\right), \qquad (6.6.4)
$$

where $\beta$ is given in terms of the Reynolds number for two phase flow, $Re_{pc} = \rho_c \epsilon_c d_p || \underline{v}_c - \underline{v}_p || / \mu_c$:

$$
\beta \;=\; \left[ \left[ \left[ \frac{\mu_c \epsilon_p}{d_p^2} \left( \frac{36 \epsilon_c \epsilon_p^{1/3}}{\left(1 - \epsilon_p^{2/3}\right) \left(1 - \epsilon_p^{1/3}\right)} + 18 \right) \right]^s + \left[ \frac{1}{2} \frac{c_d \mu_c}{d_p^2} \frac{\epsilon_p \epsilon_c}{\left(1 - \epsilon_p^{2/3}\right)^2} Re_{pc} \right]^s \right]^{1/s} \right. \tag{6.6.5}
$$

which, in turn, may be expressed as the sum of its Darcy, $\beta_o$, and the Forchheimer component, $\beta_\infty$, as

$$
\beta \;=\; (\beta_o^s + \beta_\infty^s)^{1/s} , \tag{6.6.6}
$$

where

$$
\beta_o \;=\; \frac{\mu_c \epsilon_p}{d_p^2} \left( \frac{36 \epsilon_c \epsilon_p^{1/3}}{\left(1 - \epsilon_p^{2/3}\right) \left(1 - \epsilon_p^{1/3}\right)} + 18 \right) , \tag{6.6.7}
$$

and

$$
\beta_\infty \;=\; \frac{1}{2} \frac{c_d \mu_c}{d_p^2} \frac{\epsilon_p \epsilon_c}{\left(1 - \epsilon_p^{2/3}\right)^2} Re_{pc}. \tag{6.6.8}
$$

The inclination of Equations (6.6.7), (6.6.8) and their combined effect, given by Equation (6.6.6), are illustrated in Figure 6.7 for a packed bed porosity, $\epsilon_c = 0.4$, and a drag coefficient value, $c_d = 1.95$. From Figure 6.7 it is seen that a decrease in the value for the shifting parameter, $s$, moves the $\beta$-curve closer to its asymptotes.

A $c_d$-value of 1.9 is recommended for packed beds ($\epsilon \approx 0.4$) by Du Plessis and Woudberg (2008). However, for the limiting values of $\epsilon_c \to 1$, that is: for extremely dilute solutions, experimental data given in Chapter 9 suggests a drag coefficient corresponding to the Stokes drag coefficient for a single particle, $c_d = 0.44$, and a shifting parameter, $s = 0.6$.
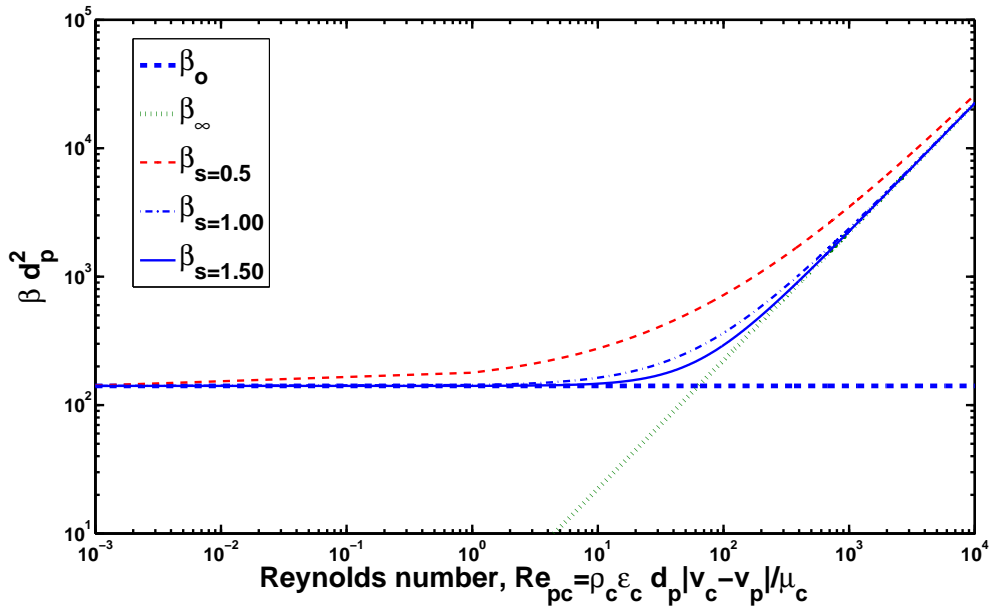
**Figure 6.7:** Influence of shifting parameter, $s$, on the momentum transfer coefficient, $\beta$.

This concludes the closure procedure for the momentum conservation equations. In Chapter 7, Equations (6.6.2) and (6.6.3) will be discretised in order to be subjected to numerical analysis in Chapter 8.

# Chapter 7

# Numerical calculation of the flow field

In this chapter the formulation for the discrete form of the conservation equations is discussed and emphasis is placed on the discretisation concept, and in particular, the control volume formulation. Attention is given to source term linearisation, interpolation methods, the upwind scheme as well as the staggered grid method of Patankar (1980) and the resulting scalar and vector control volumes are illustrated.

A detailed review of the Tridiagonal Matrix Algorithm (TDMA), used to solve the equations, is given and combined with an iterative Gauss-Seidel method. Finally, the implementation of the Semi Implicit Method for Pressure Linked Equations (SIMPLE) for two-phase flow will be described and a schematic of the algorithm given.

## 7.1   Principle of discretisation

Discretisation of the analytical equations presented in Chapter 6, is the first step taken in rendering them suitable for numerical implementation. In order to obtain a discrete representation of the conservation expressions, various methods, including finite difference, finite element, and finite volume methods, may be applied.

The current work adopts the control-volume method for which the domain is divided into a number of non-overlapping control volumes such that there is one control volume surrounding each grid point. The differential equation is integrated over each control volume. Piecewise profiles expressing the variation of the dependent variable between grid nodes are used to evaluate the required integrals. This approach yields a discrete equation which contains the values of the dependent variable for a group of grid nodes.

The discretisation equation, obtained in this manner, expresses the conservation principles for the dependent variable over a control volume, just as the differential equation expressed it for an infinitesimal differential element.

An attractive feature of the control-volume formulation is that the resulting solution would imply that the integral conservation of quantities such as mass or momentum is exactly satisfied over any group of control volumes and thus over the whole calculation domain.

Consider a two-dimensional problem and the partial grid shown in Figure 7.1.
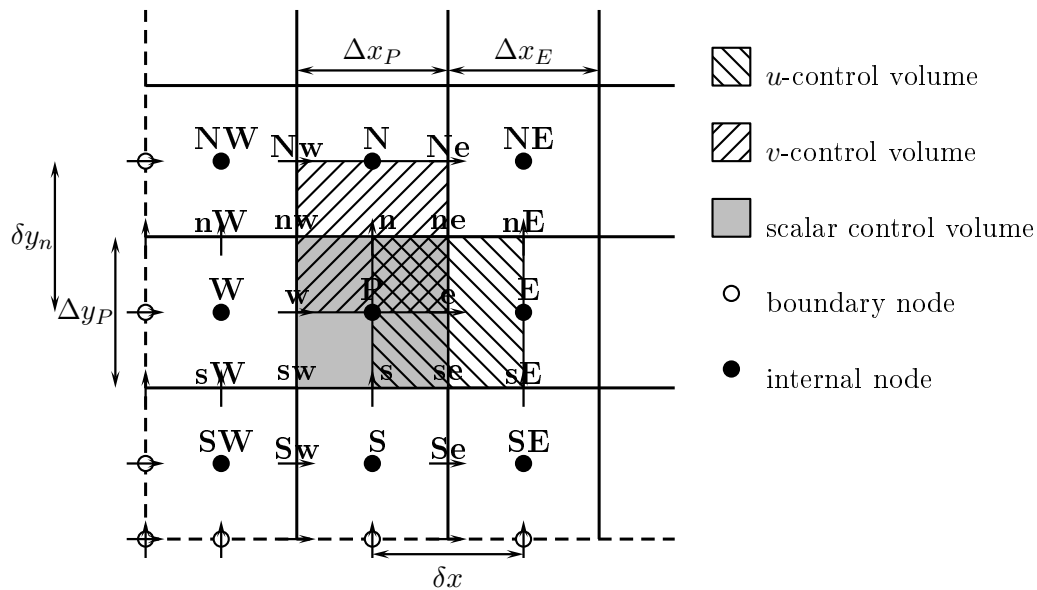


**Figure 7.1:** Grid arrangement.

The grid nodes of the calculation domain will be referred to as *boundary* nodes whereas the remainder will be known as *internal* nodes. Around each of these internal nodes a control volume exists. Following Practice B of Patankar (1980), control volumes for the scalar values, i.e. pressure- and volume fraction values, are centred around the nodes, whereas the control volumes for the vector quantities for the $x$- and $y$ directed velocities are staggered to the north and east directions of the scalar control volume, respectively, as illustrated in Figure 7.1.

Grid staggering is done to prevent wavy pressure fields to be mistaken for uniform fields since adjacent, and not alternating nodes, are used in calculations (Patankar (1980)). The velocity components are calculated for nodes that lie on the faces of the scalar control volume and consequently the difference between the pressures at nodes E and P are used to calculate the pressure force acting on the control volume for the $x$-component of the velocity.

Henceforth the control volumes for the discretisation of the pressure and the volume fraction quantities will be referred to as scalar control volumes, whereas the control volumes for the $x$- and $y$-directed velocities, indicated by the hatched areas in Figure 7.1, will be referred to as the $u$- and $v$-control volumes, respectively.

## 7.2 Discretisation for the momentum conservation equations

The unsteady convection-diffusion equations, given in Chapter 6 by Equations (6.6.2) and (6.6.3), are written in terms of their directional components and, although always implied, the averaging notation is omitted.[1] The directional components of the continuum phase are given by

$$\rho_c\epsilon_c\frac{\partial u_c}{\partial t} + \rho_c\epsilon_c u_c\frac{\partial u_c}{\partial x} + \rho_c\epsilon_c v_c\frac{\partial u_c}{\partial y} \;=\; -\epsilon_c\frac{\partial p_c}{\partial x} + \mu_c\frac{\partial}{\partial x}\left(\epsilon_c\frac{\partial u_c}{\partial x}\right) + \mu_c\frac{\partial}{\partial y}\left(\epsilon_c\frac{\partial u_c}{\partial y}\right) + S^x$$

$$(7.2.1)$$

and

$$\rho_c\epsilon_c\frac{\partial v_c}{\partial t} + \rho_c\epsilon_c u_c\frac{\partial v_c}{\partial x} + \rho_c\epsilon_c v_c\frac{\partial v_c}{\partial y} \;=\; \rho_c g\epsilon_c - \epsilon_c\frac{\partial p_c}{\partial y} + \mu_c\frac{\partial}{\partial x}\left(\epsilon_c\frac{\partial v_c}{\partial x}\right) + \mu_c\frac{\partial}{\partial y}\left(\epsilon_c\frac{\partial v_c}{\partial y}\right) + S^y.$$

$$(7.2.2)$$

The corresponding expressions for the particulate phase are

$$\rho_p\epsilon_p\frac{\partial u_p}{\partial t} + \rho_c\epsilon_p u_p\frac{\partial u_p}{\partial x} + \rho_p\epsilon_p v_p\frac{\partial u_p}{\partial y} \;=\; -\epsilon_p\frac{\partial p_c}{\partial x} - \frac{\epsilon_p^2\rho_p d_p}{4}\left(\frac{\partial u_p}{\partial y} + \frac{\partial v_p}{\partial x}\right)^2 - S^x$$

$$(7.2.3)$$

---

[1] For a full derivation the reader is referred to Appendix F.

and

$$
\rho_p \epsilon_p \frac{\partial v_p}{\partial t} + \rho_p \epsilon_p u_p \frac{\partial u_p}{\partial x} + \rho_p \epsilon_p v_p \frac{\partial u_p}{\partial y} \;\;=\;\; \epsilon_p g \rho_p - \epsilon_p \frac{\partial p_c}{\partial y} - \frac{\epsilon_p^2 \rho_p d_p}{4} \left( \frac{\partial u_p}{\partial y} + \frac{\partial v_p}{\partial x} \right)^2 - S^y.
$$

$$(7.2.4)$$

The source terms, $S^x$ and $S^y$, appearing in Equations (7.2.1) - (7.2.4), are respectively given by

$$
S^x = - \left[ \left[ \frac{\mu_c \epsilon_p}{d_p^2} \left( \frac{36 \epsilon_c \epsilon_p^{1/3}}{\left(1 - \epsilon_p^{2/3}\right)\left(1 - \epsilon_p^{1/3}\right)} + 18 \right) \right]^s + \left[ \frac{1}{2} \frac{c_d \rho_c}{d_p} \frac{\epsilon_p \epsilon_c^2}{\left(1 - \epsilon_p^{2/3}\right)^2} || \underline{v}_c - \underline{v}_p || \right]^s \right]^{1/s} (u_c - u_p)
$$

$$(7.2.5)$$

and

$$
S^y = - \left[ \left[ \frac{\mu \epsilon_p}{d_p^2} \left( \frac{36 \epsilon_c \epsilon_p^{1/3}}{\left(1 - \epsilon_p^{2/3}\right)\left(1 - \epsilon_p^{1/3}\right)} + 18 \right) \right]^s + \left[ \frac{1}{2} \frac{c_d \rho_c}{d_p} \frac{\epsilon_p \epsilon_c^2}{\left(1 - \epsilon_p^{2/3}\right)^2} || \underline{v}_c - \underline{v}_p || \right]^s \right]^{1/s} (v_c - v_p)
$$

$$(7.2.6)$$

Following Patankar (1980), each of these source terms may be written as a linear function of the dependent variable, $\phi$, under consideration,

$$
S \;\;=\;\; Sc + Sp\phi.
$$

$$(7.2.7)$$

Source term linearisations for the continuum phase in the $x$ and $y$-directions are respectively given by

$$
S^x \;\;=\;\; Sc_c^x + Spu_c,
$$

$$(7.2.8)$$

and

$$
S^y \;\;=\;\; Sc_c^y + Spv_c,
$$

$$(7.2.9)$$

where

$$
Sc_c^x \;\;=\;\; \left[ \left[ \frac{\mu_c \epsilon_p}{d_p^2} \left( \frac{36 \epsilon_c \epsilon_p^{1/3}}{\left(1 - \epsilon_p^{2/3}\right)\left(1 - \epsilon_p^{1/3}\right)} + 18 \right) \right]^s + \left[ \frac{1}{2} \frac{c_d \rho_c}{d_p} \frac{\epsilon_p \epsilon_c^2}{\left(1 - \epsilon_p^{2/3}\right)^2} || \underline{v}_c - \underline{v}_p || \right]^s \right]^{1/s} u_p,
$$

$$(7.2.10)$$

and

$$
Sc_c^y = \left[ \left[ \left[ \frac{\mu_c \epsilon_p}{d_p^2} \left( \frac{36 \epsilon_c \epsilon_p^{1/3}}{\left(1 - \epsilon_p^{2/3}\right)\left(1 - \epsilon_p^{1/3}\right)} + 18 \right) \right]^s + \left[ \frac{1}{2} \frac{c_d \rho_c}{d_p} \frac{\epsilon_p \epsilon_c^2}{\left(1 - \epsilon_p^{2/3}\right)^2} || \underline{v}_c - \underline{v}_p || \right]^s \right]^{1/s} v_p .
$$
$$(7.2.11)$$

The $Sp$ coefficient is given by,

$$
Sp = - \left[ \left[ \left[ \frac{\mu_c \epsilon_p}{d_p^2} \left( \frac{36 \epsilon_c \epsilon_p^{1/3}}{\left(1 - \epsilon_p^{2/3}\right)\left(1 - \epsilon_p^{1/3}\right)} + 18 \right) \right]^s + \left[ \frac{1}{2} \frac{c_d \rho_c}{d_p} \frac{\epsilon_p \epsilon_c^2}{\left(1 - \epsilon_p^{2/3}\right)^2} || \underline{v}_c - \underline{v}_p || \right]^s \right]^{1/s} .
$$
$$(7.2.12)$$

Source term linearisation for the particulate phase is treated in a similar manner with the linearisation components for the $x-$ and $y$-directions, respectively, given by

$$
S_p^x = -Sc_p^x - Sp u_p , \qquad (7.2.13)
$$

and

$$
S_p^y = -Sc_p^y - Sp v_p . \qquad (7.2.14)
$$

Here

$$
Sc_p^x = \left[ \left[ \left[ \frac{\mu_c \epsilon_p}{d_p^2} \left( \frac{36 \epsilon_c \epsilon_p^{1/3}}{\left(1 - \epsilon_p^{2/3}\right)\left(1 - \epsilon_p^{1/3}\right)} + 18 \right) \right]^s + \left[ \frac{1}{2} \frac{c_d \rho_c}{d_p} \frac{\epsilon_p \epsilon_c^2}{\left(1 - \epsilon_p^{2/3}\right)^2} || \underline{v}_c - \underline{v}_p || \right]^s \right]^{1/s} u_c ,
$$
$$(7.2.15)$$

and

$$
Sc_p^y = \left[ \left[ \left[ \frac{\mu_c \epsilon_p}{d_p^2} \left( \frac{36 \epsilon_c \epsilon_p^{1/3}}{\left(1 - \epsilon_p^{2/3}\right)\left(1 - \epsilon_p^{1/3}\right)} + 18 \right) \right]^s + \left[ \frac{1}{2} \frac{c_d \rho_c}{d_p} \frac{\epsilon_p \epsilon_c^2}{\left(1 - \epsilon_p^{2/3}\right)^2} || \underline{v}_c - \underline{v}_p || \right]^s \right]^{1/s} v_c ,
$$
$$(7.2.16)$$

and $Sp$ is given by Equation (7.2.12).

## 7.3  Discretisation of the momentum conservation equations

The $u$-and $v$-control volumes, illustrated in Figure 7.1, are used for the discretisation of the $x$-and $y$-components of the momentum conservation equations, respectively, and the discrete equations established from integration over such volumes will resemble

$$a_c^e \phi^e = a_c^{ee} \phi^{ee} + a_c^w \phi^w + a_c^{Ne} \phi^{Ne} + a_c^{Se} \phi^{Se} + b_c - \left[ \epsilon_c^E p_c^E - \epsilon_c^P p_c^P \right] \Delta y_P, \quad (7.3.1)$$

and

$$a_c^n \phi^n = a_c^{nE} \phi^{nE} + a_c^{nW} \phi^{nW} + a_c^{nn} \phi^{nn} + a_c^s \phi^s + b_c - \left[ \epsilon_c^{ne} p_c^{ne} - \epsilon_c^{nw} p_c^{nw} \right] \Delta x_P, \quad (7.3.2)$$

where, for example, $\phi^e$ will be the $u$-velocity across the $e$-interface shown in Figure 7.1.

### 7.3.1  The continuum phase

In this section a stepwise procedure will be presented for the discretisation of the $x$-component of the continuum momentum conservation expression given by Equation (7.2.1). The discretisation is begun by integrating each component of the equation over the $u$-control volume illustrated in Figure 7.1 as well as from time $t_0$ to time $t$. The resulting discrete form of each integral expression is listed in Table 7.1. In Table 7.1 $u_c^{0,e}$ denotes the continuum velocity across the $e$-interface at time $t = 0$.

The convection and diffusion expressions are denoted by the terms listed in Table 7.2 and are substituted into the discretised expressions given by the right-hand side column of Table 7.1. The resulting expressions are reassembled and yield the following for the $x$-component of the momentum conservation equation for the continuum phase:

$$\frac{\rho_c \epsilon_c^e \left[ u_c^e - u_c^{0,e} \right] \delta x_e \Delta y}{\Delta t} + F_c^E u_c^E - F_c^P u_c^P + F_c^{ne} u_c^{ne} - F_c^{se} u_c^{se} = -\epsilon_c^e \left[ p_c^E - p_c^P \right] \Delta y_P$$

$$+ D_c^E \left( \frac{\partial u_c}{\partial x} \right)^E \Delta x_E - D_c^P \left( \frac{\partial u_c}{\partial x} \right)^P \Delta x_P + D_c^{ne} \left( \frac{\partial u_c}{\partial y} \right)^{ne} \delta y_n - D_c^{se} \left( \frac{\partial u_c}{\partial y} \right)^{se} \delta y_s +$$

$$Sc_c^x \delta x_e \Delta y_P + Spu_c \delta x_e \Delta y_P. \quad (7.3.3)$$

**Table 7.1:** Discretised expressions for the $x$-directed continuum momentum conservation equation.

| Integral expression | Discretised expression |
|---|---|
| $\int_{se}^{ne} \int_P^E \int_{t_0}^t \rho_c \epsilon_c \frac{\partial u_c}{\partial t} dt dx dy$ | $\rho_c \epsilon_c^e \left[ u_c^e - u_c^{0,e} \right] \delta x_e \Delta y_P$ |
| $\int_{t_0}^t \int_{se}^{ne} \int_P^E \rho_c \epsilon_c u_c \frac{\partial u_c}{\partial x} dx dy dt$ | $\rho_c \left[ \epsilon_c^E u_c^{2,E} - \epsilon_c^P (u_c^P)^2 \right] \Delta y_P \Delta t$ |
| $\int_{t_0}^t \int_P^E \int_{se}^{ne} \rho_c \epsilon_c u_c \frac{\partial v_c}{\partial y} dy dx dt$ | $\rho_c \left[ \epsilon_c^{ne} v_c^{ne} u_c^{ne} - \epsilon_c^{se} v_c^{se} u_c^{se} \right] \delta x_e \Delta t$ |
| $\int_{t_0}^t \int_{se}^{ne} \int_P^E -\epsilon_c \frac{\partial p_c}{\partial x} dx dy dt$ | $-\epsilon_c^e \left[ p_c^E - p_c^P \right] \Delta y_P \Delta t$ |
| $\int_{t_0}^t \int_{se}^{ne} \int_P^E \mu_c \frac{\partial}{\partial x} \left[ \epsilon_c \frac{\partial u_c}{\partial x} \right] dx dy dt$ | $\mu_c \left[ \epsilon_c^E \left( \frac{\partial u_c}{\partial x} \right)^E - \epsilon_c^P \left( \frac{\partial u_c}{\partial x} \right)^P \right] \Delta y_P \Delta t$ |
| $\int_{t_0}^t \int_P^E \int_{se}^{ne} \mu_c \frac{\partial}{\partial y} \left[ \epsilon_c \frac{\partial u_c}{\partial y} \right] dy dx dt$ | $\mu_c \left[ \epsilon_c^{ne} \left( \frac{\partial u_c}{\partial y} \right)^{ne} - \epsilon_c^{se} \left( \frac{\partial u_c}{\partial y} \right)^{se} \right] \delta x_e \Delta t$ |
| $\int_{t_0}^t \int_{se}^{ne} \int_P^E Sc_c^x dx dy dt$ | $Sc_c^x \delta x_e \Delta y_P \Delta t$ |
| $\int_{t_0}^t \int_{se}^{ne} \int_P^E Spu_c dx dy dt$ | $Spu_c \delta x_e \Delta y_P \Delta t$ |

The remaining derivatives in Equation (7.3.3) are discretised by assuming that they may be approximated with a piecewise linear profile over the control volume. The discrete form of these differential terms are then given by

$$\left( \frac{\partial u_c}{\partial x} \right)^P \approx \frac{u_c^e - u_c^w}{\Delta x_P} \tag{7.3.4}$$

$$\left( \frac{\partial u_c}{\partial x} \right)^E \approx \frac{u_c^{ee} - u_c^e}{\Delta x_E} \tag{7.3.5}$$

$$\left( \frac{\partial u_c}{\partial y} \right)^{se} \approx \frac{u_c^e - u_c^{Se}}{\delta y_s} \tag{7.3.6}$$

$$\left( \frac{\partial u_c}{\partial y} \right)^{ne} \approx \frac{u_c^{Ne} - u_c^e}{\delta y_n}. \tag{7.3.7}$$

Substitution of the discrete approximations, given by Equations (7.3.4)-(7.3.7), into

**Table 7.2:** Convection and diffusion coefficients for the continuum momentum conservation equation.

| Convection coefficient | Diffusion coefficient |
|---|---|
| $F_c^P = \rho_c \epsilon_c^P u_c^P \Delta y_P$ | $D_c^P = \mu_c \epsilon_c^P \frac{\Delta y_P}{\Delta x_P}$ |
| $F_c^E = \rho_c \epsilon_c^E u_c^E \Delta y_P$ | $D_c^E = \mu_c \epsilon_c^E \frac{\Delta y_P}{\Delta x_E}$ |
| $F_c^{se} = \rho_c \epsilon_c^{se} v_c^{se} \delta x_e$ | $D_c^{se} = \mu_c \epsilon_c^{se} \frac{\delta x_e}{\delta y_s}$ |
| $F_c^{ne} = \rho_c \epsilon_c^{ne} v_c^{ne} \delta x_e$ | $D_c^{ne} = \mu_c \epsilon_c^{ne} \frac{\delta x_e}{\delta y_n}$ |

the remaining differential terms in Equation (7.3.3), yields

$$\frac{\rho_c \epsilon_c^e \left[ u_c^e - u_c^{0,e} \right] \delta x_e \Delta y}{\Delta t} + F_c^E u_c^E - F_c^P u_c^P + F_c^{ne} u_c^{ne} - F_c^{se} u_c^{se} = -\epsilon_c^e \left[ p_c^E - p_c^P \right] \Delta y$$

$$+ D_c^E \left( u_c^{ee} - u_c^e \right) - D_c^P \left( u_c^e - u_c^w \right) + D_c^{ne} \left( u_c^{nE} - u_c^e \right) - D_c^{se} \left( u_c^e - u_c^{Se} \right) +$$

$$S c_c^x \delta x_e \Delta y_P + S p u_c \delta x_e \Delta y_P. \tag{7.3.8}$$

Further manipulation of Equation (7.3.8) entails the use of the upwind scheme from which the convection terms are calculated under the assumption that the value of the $x$-component continuum velocity, $u_c$, at an interface is equal to its value at the grid point on the upwind side of such a face (Patankar (1980)). This implies that

$$u_c^E = u_c^e \quad \text{if} \quad F_c^E > 0$$

$$u_c^E = u_c^{ee} \quad \text{if} \quad F_c^E < 0.$$

The upwind scheme then implies that,

$$F_c^E u_c^E = [[F_c^E, 0]] u_c^e - [[-F_c^E, 0]] u_c^{ee} \tag{7.3.9}$$

$$F_c^P u_c^P = [[F_c^P, 0]] u_c^w - [[-F_c^P, 0]] u_c^e \tag{7.3.10}$$

$$F_c^{ne} u_c^{ne} = [[F_c^{ne}, 0]] u_c^e - [[-F_c^{ne}, 0]] u_c^{Ne} \tag{7.3.11}$$

$$F_c^{se} u_c^{se} = [[F_c^{se}, 0]] u_c^{Se} - [[-F_c^{se}, 0]] u_c^e, \tag{7.3.12}$$

where the double bracket notation used by Patankar (1980) is adopted to indicate the maximum of two values. The terms of the upwind scheme, listed as Equations

(7.3.9)-(7.3.12), are substituted into Equation (7.3.8) and it follows that

$$\left[ -Sp\delta x_e \Delta y_P + \frac{\rho_c \epsilon_c^e \delta x_e \Delta y_P}{\Delta t} + [[F_c^E, 0]] + D_c^E + [[-F_c^{se}, 0]] + D_c^{se} + [[-F_c^P, 0]] + D_c^P + [[F_c^{ne}, 0]] + D_c^{ne} \right] u_c^e =$$

$$\left( [[-F_c^E, 0]] + D_c^E \right) u_c^{ee} + \left( [[F_c^P, 0]] + D_c^P \right) u_c^w + \left( [[-F_c^{ne}, 0]] + D_c^{ne} u_c^{nE} \right) u_c^{Ne} + \left( [[F_c^{se}, 0]] + D_c^{se} u_c^{Se} \right) u_c^{Se} -$$

$$\epsilon_c^e \left[ p_c^E - p_c^P \right] \Delta y_P + \frac{\rho_c \epsilon_c^e u_c^{0,e} \delta x_e \Delta y_P}{\Delta t} + Sc_c^x \delta x_e \Delta y_P. \tag{7.3.13}$$

Continuity of the flow is assumed and hence $F_c^P + F_c^{se} = F_c^E + F_c^{ne}$. Application of this result to Equation (7.3.13), yields

$$a_c^e u_c^e \;=\; a_c^{ee} u_c^{ee} + a_c^w u_c^w + a_c^{Ne} u_c^{Ne} + a_c^{Se} u_c^{Se} + b_c - \epsilon_c^e \left[ p_c^E - p_c^P \right] \Delta y_P, \tag{7.3.14}$$

where

$$a_c^{ee} \;=\; [[-F_c^E, 0]] + D_c^E \tag{7.3.15}$$

$$a_c^w \;=\; [[F_c^P, 0]] + D_c^P \tag{7.3.16}$$

$$a_c^{Ne} \;=\; [[-F_c^{ne}, 0]] + D_c^{ne} \tag{7.3.17}$$

$$a_c^{Se} \;=\; [[F_c^{se}, 0]] + D_c^{se} \tag{7.3.18}$$

$$a_c^{e,0} \;=\; \frac{\rho_c \epsilon_c^e \delta x_e \Delta y}{\Delta t} \tag{7.3.19}$$

$$b_c \;=\; a_c^{e,0} u_c^{e,0} + Sc_c^x \delta x_e \Delta y \tag{7.3.20}$$

$$a_c^e \;=\; a_c^{ee} + a_c^w + a_c^{Ne} + a_c^{Se} + a_c^{e,0} - Sp. \tag{7.3.21}$$

Equations (7.3.14)-(7.3.21) conclude the derivation of the discrete approximation of the $x$-component momentum conservation equation, given by Equation (7.2.1).

## 7.3.2  The particulate phase

The $x$-component of the particle momentum expression is also discretised over the $u$-control volume, illustrated in Figure 7.1. Let $S_d = -\frac{\epsilon_p^2 \rho_p d_p}{4} \left( \frac{\partial u_p}{\partial y} + \frac{\partial v_p}{\partial x} \right)^2$, denote the particle interaction term. It is assumed that $S_d$ may be treated as a source term and it will therefore be evaluated at $e$. The discrete terms are listed in Table 7.3. Diffusion terms are absent and convection is treated in the same manner as for the continuum. The convection expressions are listed in Table 7.4.

**Table 7.3:** Discretised expressions for the $x$-directed particle momentum conservation equation.

| Integral expression | Discretised expression |
|---|---|
| $\int_{se}^{ne} \int_P^E \int_{t_0}^t \rho_p \epsilon_p \frac{\partial u_p}{\partial t} dt dx dy$ | $\rho_p \epsilon_p^e \left[ u_p^e - u_p^{0,e} \right] \delta x_e \Delta y_P$ |
| $\int_{t_0}^t \int_{se}^{ne} \int_P^E \rho_c \epsilon_p u_p \frac{\partial u_p}{\partial x} dx dy dt$ | $\rho_p \left[ \epsilon_p^E u_p^{2,E} - \epsilon_p^P (u_p^P)^2 \right] \Delta y_P \Delta t$ |
| $\int_{t_0}^t \int_P^E \int_{se}^{ne} \rho_p \epsilon_p v_p \frac{\partial u_p}{\partial y} dy dx dt$ | $\rho_p \left[ \epsilon_p^{ne} v_p^{ne} u_p^{ne} - \epsilon_p^{se} v_p^{se} u_p^{se} \right] \delta x_e \Delta t$ |
| $\int_{t_0}^t \int_{se}^{ne} \int_P^E -\epsilon_p \frac{\partial p_c}{\partial x} dx dy dt$ | $-\epsilon_p^e \left[ p_c^E - p_c^P \right] \Delta y_P \Delta t$ |
| $\int_{t_0}^t \int_{se}^{ne} \int_P^E S_d dy dx dt$ | $S_d \delta x_e \Delta y_p \Delta t$ |
| $\int_{t_0}^t \int_{se}^{ne} \int_P^E S c_p^x dx dy dt$ | $S c_p^x \delta x_e \Delta y_P \Delta t$ |
| $\int_{t_0}^t \int_{se}^{ne} \int_P^E S p u_p dx dy dt$ | $S p u_p \delta x_e \Delta y_P \Delta t$ |

**Table 7.4:** Convection coefficients for the particulate momentum equation.

**Convection coefficient**

$$F_p^P = \rho \epsilon_p^P u^P \Delta y_P$$

$$F_p^E = \rho \epsilon_p^E u^E \Delta y_P$$

$$F_p^{se} = \rho \epsilon_p^{se} v^{se} \delta x_e$$

$$F_p^{ne} = \rho \epsilon_p^{ne} v^{ne} \delta x_e$$

These convection expressions are substituted into the expressions given in Table 7.3 and the discretised expression for the particulate momentum conservation is at this stage given by

$$
\frac{\rho_p \epsilon_p^e \delta x_e \Delta y_P}{\Delta t} u_p^e + F_p^E u_p^E - F_p^P u_p^P + F_p^{ne} u_p^{ne} - F_p^{se} u_p^{se} =
$$
$$
\frac{\rho_p \epsilon_p^e \delta x_e \Delta y_P}{\Delta t} u_p^{0,e} + S_d \delta x_e \Delta y_P + S c_p^x \delta x_e \Delta y_P + S p u_c \delta x_e \Delta y_P - \epsilon_p^e \left[ p_c^E - p_c^P \right] \Delta y_P.
$$

$$(7.3.22)$$

The upwind scheme is applied to Equation (7.3.22) and it follows that

$$
a_p^e u_p^e = a_p^{ee} u_p^{ee} + a_p^w u_p^w + a_p^{Ne} u_p^{Ne} + a_p^{Se} u_p^{Se} + b_p - \epsilon_p^e \left[ p_c^E - p_c^P \right] \Delta y_P, \quad (7.3.23)
$$

where

$$
a_p^{ee} = [[-F_p^E, 0]] + D_p^E \tag{7.3.24}
$$
$$
a_p^w = [[F_p^P, 0]] + D_p^P \tag{7.3.25}
$$
$$
a_p^{Ne} = [[-F_p^{ne}, 0]] + D_p^{ne} \tag{7.3.26}
$$
$$
a_p^{Se} = [[F_p^{se}, 0]] + D_p^{se} \tag{7.3.27}
$$
$$
a_p^{e,0} = \frac{\rho_p \epsilon_p^e \delta x_e \Delta y}{\Delta t} \tag{7.3.28}
$$
$$
b_p = a_p^{e,0} u_p^{e,0} + \left( S c_p^x + S_d \right) \delta x_e \Delta y \tag{7.3.29}
$$
$$
a_p^e = a_p^{ee} + a_p^w + a_p^{Ne} + a_p^{Se} + a_p^{e,0} - Sp. \tag{7.3.30}
$$

Equations (7.3.23)-(7.3.30) represent the final discretised form of Equation (7.2.3).

The discrete forms for the $x$-components of the momentum equations for both phases have been derived in detail. The $y$-components are discretised in a similar manner but the discretisation is done over the $v$-control volume indicated in Figure 7.1. The neighbouring nodes for the $u$-control volume were given by $P$, $E$, $se$ and $ne$. The neighbouring nodes for the $v$-control volume are given by $nw$, $ne$, $P$, and $N$ and the corresponding convection and diffusion coefficients are listed in Table 7.5 where the $\alpha$-notation corresponds to $c$ or $p$ for the continuum or particulate cases, respectively.

**Table 7.5:** Convection and diffusion coefficients for $y$-continuum momentum conservation equation.

| Convection coefficient | Diffusion coefficient |
|---|---|
| $F_\alpha^{nw} = \rho_\alpha \epsilon_\alpha^{nw} u_\alpha^{nw} \delta y_n$ | $D_c^{nw} = \mu_c \epsilon_c^{nw} \frac{\delta y_n}{\delta x_w}$ |
| $F_\alpha^{ne} = \rho_\alpha \epsilon_\alpha^{ne} u_\alpha^{ne} \delta y_n$ | $D_c^{ne} = \mu_c \epsilon_c^{ne} \frac{\delta y_n}{\delta x_e}$ |
| $F_\alpha^{P} = \rho_\alpha \epsilon_\alpha^{P} v_\alpha^{P} \Delta x_P$ | $D_c^{P} = \mu_c \epsilon_c^{P} \frac{\Delta x_P}{\Delta y_P}$ |
| $F_\alpha^{N} = \rho_\alpha \epsilon_\alpha^{N} v_\alpha^{N} \Delta x_P$ | $D_c^{N} = \mu_c \epsilon_c^{N} \frac{\Delta x_P}{\Delta y_N}$ |

The $y$-component of the discrete momentum conservation equation for the continuum is given by

$$a_c^n v_c^n \;=\; a_c^{nW} v_c^{nW} + a_c^{nE} v_c^{nE} + a_c^s v_c^s + a_c^{nn} v_c^{nn} + b_c - \epsilon_c^n \left[ p_c^N - p_c^P \right] \Delta x_P, \quad (7.3.31)$$

where

$$
\begin{aligned}
a_c^{nW} &= [[F_c^{nw}, 0]] + D_c^{nw} & (7.3.32)\\
a_c^{nE} &= [[-F_c^{ne}, 0]] + D_c^{ne} & (7.3.33)\\
a_c^{s} &= [[F_c^{P}, 0]] + D_c^{P} & (7.3.34)\\
a_c^{nn} &= [[-F_c^{N}, 0]] + D_c^{N} & (7.3.35)\\
a_c^{n,0} &= \frac{\rho_c \epsilon_c^n \delta x_e \Delta y}{\Delta t} & (7.3.36)\\
b_c &= a_c^{n,0} u_c^{n,0} + \left( S c_c^y + \rho_c g \epsilon_c^n \right) \delta x_e \Delta y_P & (7.3.37)\\
a^n &= a_c^{nW} + a_c^{nE} + a_c^s + a_c^{nn} + a_c^{e,0} - Sp. & (7.3.38)
\end{aligned}
$$

The $y$-component of the discrete momentum equation for the particles is given by

$$a_p^n v_p^n \;=\; a_p^{nW} v_p^{nW} + a_p^{nE} v_p^{nE} + a_p^s v_p^s + a_p^{nn} v_p^{nn} + b_p - \epsilon_p^n \left[ p_c^N - p_c^P \right] \Delta x_P, (7.3.39)$$

where

$$a_p^{nW} \;=\; [[F_p^{nw}, 0]] \tag{7.3.40}$$

$$a_p^{nE} \;=\; [[-F_p^{ne}, 0]] \tag{7.3.41}$$

$$a_p^{s} \;=\; [[F_p^{P}, 0]] \tag{7.3.42}$$

$$a_p^{nn} \;=\; [[-F_p^{N}, 0]] \tag{7.3.43}$$

$$a_p^{n,0} \;=\; \frac{\rho_p \epsilon_p^n \delta x_e \Delta y}{\Delta t} \tag{7.3.44}$$

$$b_p \;=\; a_p^{n,0} u_p^{n,0} + \left((\rho_p - \rho_c) g \epsilon_p^n + S_d + S c_p^y\right) \delta x_e \Delta y_P \tag{7.3.45}$$

$$a^{n} \;=\; a_p^{nW} + a_p^{nE} + a_p^{s} + a_p^{nn} + a_p^{e,0} - Sp. \tag{7.3.46}$$

This concludes the discretisation for the momentum conservation equations. In the following section the discretisation for the mass conservation equation will be discussed.

## 7.4    Discretisation of the mass conservation equation

The expression for continuity of the continuum was presented in Chapter 4 by Equation (4.4.6) and is restated here:

$$\frac{\partial \epsilon_c}{\partial t} + \frac{\partial \epsilon_c u_c}{\partial x} + \frac{\partial \epsilon_c v_c}{\partial y} \;=\; 0, \tag{7.4.1}$$

where averaging notation has been omitted but is, however, always implied. A discretised expression is derived, using the scalar-control volume which is indicated by the shaded section of Figure 7.1. The terms resulting from the integration of Equation (7.4.1) over the scalar-control volume are listed in Table 7.6 and the convection coefficients are listed in Table 7.7.

**Table 7.6:** Discretised expressions for continuum mass conservation equation over $P$-control volume.

| Integral expression | Discretised expression |
|---|---|
| $\int_s^n \int_w^e \int_{t_0}^t \frac{\partial \epsilon_c}{\partial t} dt dx dy$ | $\left( \epsilon_c^P - \epsilon_c^{0,P} \right) \Delta x_P \Delta y_P$ |
| $\int_{t_0}^t \int_s^n \int_w^e \frac{\partial \epsilon_c u_c}{\partial x} dx dy dt$ | $\left[ (\epsilon_c u_c)^e - (\epsilon u_c)^w \right] \Delta y_P \Delta t$ |
| $\int_{t_0}^t \int_w^e \int_s^n \frac{\partial \epsilon_c v_c}{\partial y} dy dx dt$ | $\left[ (\epsilon_c v_c)^n - (\epsilon_c v_c)^s \right] \Delta x_P \Delta t$ |

**Table 7.7:** Convection coefficients for the continuum mass conservation equation.

**Convection coefficient**

$$F_c^e = u_c^e \Delta y_P$$

$$F_c^w = u_c^w \Delta y_P$$

$$F_c^n = v_c^n \Delta x_P$$

$$F_c^s = v_c^s \Delta x_P$$

Substitution of the convection coefficients into the expressions given on the right-hand side of Table 7.6, yields the following discrete form for mass conservation:

$$\frac{\left(\epsilon_c^P - \epsilon_c^{0,P}\right)\Delta x_P \Delta y_P}{\Delta t} + \epsilon_c^e F_c^e - \epsilon_c^w F_c^w + \epsilon_c^n F_c^n - \epsilon_c^s F_c^s \;=\; 0. \qquad (7.4.2)$$

The upwind scheme for the continuum volume fraction is given by

$$F_c^e \epsilon_c^e \;=\; [[F_c^e, 0]]\epsilon_c^P - [[-F_c^e, 0]]\epsilon_c^E \qquad (7.4.3)$$

$$F_c^w \epsilon_c^w \;=\; [[F_c^w, 0]]\epsilon_c^W - [[-F_c^w, 0]]\epsilon_c^P \qquad (7.4.4)$$

$$F_c^n \epsilon_c^n \;=\; [[F_c^n, 0]]\epsilon_c^P - [[-F_c^n, 0]]\epsilon_c^N \qquad (7.4.5)$$

$$F_c^s \epsilon_c^s \;=\; [[F_c^s, 0]]\epsilon_c^S - [[-F_c^s, 0]]\epsilon_c^P. \qquad (7.4.6)$$

Reassembling the terms given in Table 7.6 and subsequently applying the upwind expressions, yield the following discretised form of Equation (7.4.1):

$$a_c^P \epsilon^P \;=\; a_c^E \epsilon_c^E + a_c^W \epsilon_c^W + a_c^N \epsilon_c^N + a_c^S \epsilon_c^S + b_c, \qquad (7.4.7)$$

where

$$a_c^{0,P} \;=\; \frac{\Delta x_P \Delta y_P}{\Delta t}, \qquad (7.4.8)$$

$$b_c \;=\; a_c^{0,P} \epsilon_c^{0,P}, \qquad (7.4.9)$$

$$a_c^E \;=\; [[-F_c^e, 0]], \qquad (7.4.10)$$

$$a_c^W \;=\; [[F_c^w, 0]], \qquad (7.4.11)$$

$$a_c^N \;=\; [[-F_c^n, 0]], \qquad (7.4.12)$$

$$a_c^S \;=\; [[F_c^s, 0]], \qquad (7.4.13)$$

$$a_c^P \;=\; a_c^E + a_c^W + a_c^N + a_c^S + a_c^{0,P}. \qquad (7.4.14)$$

Equations (7.4.7)-(7.4.14) are the discrete form of Equation (7.4.1) and will at a later stage be used to solve the continuum volume fractions.

## 7.5   Pressure and velocity corrections

The momentum equations can be solved only when the pressure field is given or is somehow estimated. Unless the correct pressure field is employed, the resulting velocity field will not satisfy the continuity equation. Such an imperfect velocity field, based on

a guessed pressure field, $p^*$, will be denoted by $u^*$ and $v^*$. The starred velocity fields will result from the solution of the following discretisation equations:

$$a_c^e u_c^{*e} \;=\; a_c^{ee} u_c^{*ee} + a_c^w u_c^{*w} + a_c^{Ne} u_c^{*Ne} + a_c^{Se} u_c^{*Se} + b_c - \epsilon_c^e \left[p_c^{*E} - p_c^{*P}\right] \Delta y_P, \quad (7.5.1)$$

and

$$a_c^n v_c^{*n} \;=\; a_c^{nW} v_{*c}^{nW} + a_c^{*nE} v_c^{nE} + a_c^{*s} v_c^s + a_c^{*nn} v_c^{nn} + b_c - \epsilon_c^n \left[p_c^{*N} - p_c^{*P}\right] \Delta x_P. \quad (7.5.2)$$

The correct velocity field is denoted by

$$a_c^e u_c^e \;=\; a_c^{ee} u_c^{ee} + a_c^w u_c^w + a_c^{Ne} u_c^{Ne} + a_c^{Se} u_c^{Se} + b_c - \epsilon_c^e \left[p_c^E - p_c^P\right] \Delta y_P, \quad (7.5.3)$$

and

$$a_c^n v_c^n \;=\; a_c^{nW} v_c^{nW} + a_c^{nE} v_c^{nE} + a_c^s v_c^s + a_c^{nn} v_c^{nn} + b_c - \epsilon_c^n \left[p_c^N - p_c^P\right] \Delta x_P. \quad (7.5.4)$$

The aim is to improve the guessed pressure $p^*$ such that the resulting starred velocity field will progressively satisfy the continuity equation more accurately. This is achieved by introducing the following relations,

$$p_c \;=\; p_c^* + p_c^{'} \qquad\qquad (7.5.5)$$

$$u_c \;=\; u_c^* + u_c^{'}, \qquad\qquad (7.5.6)$$

where starred entities are approximations which are subtracted from the real values to yield the primed correction terms. Subtracting Equation (7.5.1) from Equation (7.5.3), yields

$$a_c^e u_c^{'e} \;=\; a_c^{ee} u_c^{'ee} + a_c^w u_c^{'w} + a_c^{Ne} u_c^{'Ne} + a_c^{Se} u_c^{'Se} - \epsilon_c^e \left[p_c^{'E} - p_c^{'P}\right] \Delta y_P. \qquad (7.5.7)$$

Following Patankar (1980), all entries on the right hand side of Equation (7.5.7), except for the pressure correction terms, are dropped. (An extensive discussion on the omission of these terms is given by Patankar (1980).) The resulting correction equation is given by

$$a_c^e u_c^{'e} \;=\; \epsilon_c^e \left[p_c^{'P} - p_c^{'E}\right] \Delta y_P, \qquad\qquad (7.5.8)$$

and may be rewritten as

$$u_c^{'e} \;=\; d_c^e \left[p_c^{'P} - p_c^{'E}\right], \qquad\qquad (7.5.9)$$

where $d_c^e = \left(\epsilon_c^e \Delta y_P\right) / \left(a_c^e\right)$. Substitution of Equation (7.5.6) into Equation (7.5.9) yields the velocity-correction formula:

$$u_c^e = u_c^{*e} + d_c^e \left[p_c^{'P} - p_c^{'E}\right]. \qquad (7.5.10)$$

Similar equations may be deduced for the neighbouring control volumes. These are given by Equations (7.5.11)-(7.5.13):

$$u_c^w = u_c^{*w} + d_c^w \left[p_c^{'W} - p_c^{'P}\right] \qquad (7.5.11)$$

$$v_c^n = v_c^{*n} + d_c^n \left[p_c^{'P} - p_c^{'N}\right] \qquad (7.5.12)$$

$$v_c^s = v_c^{*s} + d_c^s \left[p_c^{'S} - p_c^{'P}\right]. \qquad (7.5.13)$$

The velocity correction formulae for the particulate phase are derived in a similar manner and are given by

$$u_p^e = u_p^{*e} + d_p^e \left[p_c^{'P} - p_c^{'E}\right] \qquad (7.5.14)$$

$$u_p^w = u_p^{*w} + d_p^w \left[p_p^{'W} - p_p^{'P}\right] \qquad (7.5.15)$$

$$v_p^n = v_p^{*n} + d_p^n \left[p_p^{'P} - p_p^{'N}\right] \qquad (7.5.16)$$

$$v_p^s = v_p^{*s} + d_p^s \left[p_p^{'S} - p_p^{'P}\right], \qquad (7.5.17)$$

where $d_p^e$, in Equation (7.5.14), is given by $d_p^e = \left(\epsilon_p^e \Delta y_P\right) / \left(a_p^e\right)$. Similar equations hold for $d_p^w$, $d_p^n$, and $d_p^s$.

By integrating Equation (7.4.1) over the scalar-control volume, illustrated in Figure 7.1, the continuity equation for the continuum may now be used to construct an equation for the pressure correction. The result is given by

$$\frac{\left(\epsilon_c^P - \epsilon_c^{0,P}\right) \Delta x_P \Delta y_P}{\Delta t} + \epsilon_c^e u_c^e \Delta y_P - \epsilon_c^w u_c^w \Delta y_P + \epsilon_c^n v_c^n \Delta x_P - \epsilon_c^s v_c^s \Delta x_P = 0. \ (7.5.18)$$

Equations (7.5.10)-(7.5.13) are substituted into Equation (7.5.18) and it follows that

$$a_c^P p_c^{'P} = a_c^E p_c^{'E} + a_c^W p_c^{'W} + a_c^N p_c^{'N} + a_c^S p_c^{'S} + b_c, \qquad (7.5.19)$$

where

$$a_c^E = \epsilon_c^e \Delta y_P d_c^e \tag{7.5.20}$$

$$a_c^W = \epsilon_c^w \Delta y_P d_c^w \tag{7.5.21}$$

$$a_c^N = \epsilon_c^n \Delta x_P d_c^n \tag{7.5.22}$$

$$a_c^S = \epsilon_c^s \Delta x_P d_c^s \tag{7.5.23}$$

$$a_c^P = a_c^E + a_c^W + a_c^N + a_c^S \tag{7.5.24}$$

$$b_c = \frac{\left(\epsilon_c^{0,P} - \epsilon_c^P\right)\Delta x_P \Delta y_P}{\Delta t} - \Delta y_P \left(\epsilon_c^e u_c^{*e} - \epsilon_c^w u_c^{*w}\right) - \Delta x_P \left(\epsilon_c^n v_c^{*n} - \epsilon_c^s v_c^{*s}\right). \tag{7.5.25}$$

Equations (7.5.19)-(7.5.25) conclude the derivation of the pressure correction equation.

Where calculations of the coefficients for the discrete equations require the values for variables at locations where they are not explicitly specified, interpolation between neighbouring known values are used to approximate them. In this work, velocities for the convection coefficients were calculated using the arithmetic mean between its neighbours whereas porosities were approximated using the harmonic mean of their adjacent values.

## 7.6 Relaxation

The omission of the neighbouring velocity terms in the derivation of the $p'$-equation leads to exaggerated pressure corrections. To remedy this, Patankar (1980) recommends underrelaxation in the momentum equations: The momentum equations may be written in truncated form as

$$a^e u_\alpha^e = a^{nb} u^{nb} + \beta \tag{7.6.1}$$

and expressed as

$$u^e = \frac{a^{nb} u^{nb} + \beta}{a^e}, \tag{7.6.2}$$

where the $nb$ superscript indicates the neighbouring nodi of $e$.

If $u^{*e}$ is added to and subtracted from the right-hand side of Equation (7.6.2), it yields

$$u^e = u^{*e} + \left(\frac{a^{nb} u^{nb} + \beta}{a^e} - u^{*e}\right), \tag{7.6.3}$$

where the contents of the parentheses represent the change in $u^e$ produced by the current iteration. This change is modified by the introduction of a relaxation factor $\alpha$, so that

$$u^e \;=\; u^{*e} + \alpha\left(\frac{a^{nb}u^{nb} + \beta}{a^e} - u^{*e}_\alpha\right), \qquad (7.6.4)$$

or

$$\frac{a^e}{\alpha}u^e \;=\; a^{nb}u^{nb} + \beta + (1 - \alpha)\frac{a^e}{\alpha}u^{*e}. \qquad (7.6.5)$$

A suitable value of $\alpha$ is found by experience and from exploratory computations for a given problem. The pressure correction is underrelaxed by replacing Equation (7.5.5) with

$$p_c \;=\; \alpha_p p_c^{'} + p_c^{*}, \qquad (7.6.6)$$

where Patankar (1980) recommends $\alpha_p = 0.8$.


## 7.7   Solution of the discretised equations

In previous sections, methods were discussed to discretise the governing equations of two-phase flow. This process resulted in a system of linear algebraic equations which needs to be solved. The complexity of computation depends on the dimensionality of the problem, the number of grid nodes and the discretisation practice.

Any valid procedure can be used to solve the algebraic equations, but available computer resources set a constraint. The solution methods may be divided into the categories of *direct* and *indirect* (or *iterative*) methods. Direct methods include Cramer's matrix inversion and Gaussian elimination. The number of operations required for the solution of a system of $N$ equations with $N$ unknowns with a direct method is of the order of $N^3$. It is also required that all $N^2$ coefficients of the set of equations are stored. The computational time is therefore higher than desired.

On the contrary, iterative methods are based on the repeated application of a relatively simple algorithm which, after a number of repetitions, yields a converged result. Examples of such methods include the Jacobi and Gauss-Seidel point-by-point iteration methods. The total number of operations are typically in the order of $N$ iterations per cycle. Convergence is subject to the system of equations complying to fairly exact

criteria. The main advantage of these iterative solution methods is that only non-zero coefficients of the equations need to be stored in memory and thus such methods are generally more economical than their direct counterparts.

Jacobian and Gauss-Seidel iterative methods are easy to implement but can be slow to converge when the system is large, and are deemed ill-suited for general CFD procedures. An alternative method, developed by L.H. Thomas in 1949, known as the Thomas- or the Tridiagonal Matrix Algorithm (TDMA) is used instead (Conte and de Boor (1972)). The TDMA is a direct method for one-dimensional situations, but can be applied iteratively to solve multi-dimensional problems and therefore became a popular method for CFD codes. In the following section the TDMA method is discussed.

### 7.7.1   The Tridiagonal matrix algorithm

The designation, TDMA, refers to the fact that when the matrix of the coefficients of the equations is written, all the nonzero coefficients align along three diagonals of the matrix. The TDMA on its own is a direct method and will be described as one in this section of the work. It is later combined with the Gauss-Seidel method to form part of an iterative (or indirect) method for the calculation of grid node values.

Consider a system of equations that has a tridiagonal form:

$$
\begin{aligned}
\phi_1 &= C_1 \\
-\beta_2\phi_1 +D_2\phi_2 -\alpha_2\phi_3 &= C_2 \\
-\beta_3\phi_2 +D_3\phi_3 -\alpha_3\phi_4 &= C_3 \\
-\beta_4\phi_3 +D_4\phi_4 \quad -\alpha_4\phi_5 &= C_4 \\
&\cdots \quad = \quad \cdots \\
-\beta_n\phi_{n-1} \quad +D_n\phi_n -\alpha_n\phi_{n+1} &= C_n \\
\phi_{n+1} &= C_{n+1}
\end{aligned}
$$
(7.7.1)

The values of $\phi_1$ and $\phi_{n+1}$ are known boundary values. Each entry in the set given by Equation (7.7.1) may be written in the following general form:

$$
-\beta_j\phi_{j-1} + D_j\phi_j - \alpha_j\phi_{j+1} = C_j,
$$
(7.7.2)

and the set given by Equation (7.7.1) may then be expressed as:

$$\phi_2 \;=\; \frac{\alpha_2}{D_2}\phi_3 + \frac{\beta_2}{D_2}\phi_1 + \frac{C_2}{D_2} \tag{7.7.3}$$

$$\phi_3 \;=\; \frac{\alpha_3}{D_3}\phi_4 + \frac{\beta_3}{D_3}\phi_2 + \frac{C_3}{D_3} \tag{7.7.4}$$

$$\phi_4 \;=\; \frac{\alpha_4}{D_4}\phi_5 + \frac{\beta_4}{D_4}\phi_3 + \frac{C_4}{D_4} \tag{7.7.5}$$

$$... \;=\; ... \tag{7.7.6}$$

$$\phi_n \;=\; \frac{\alpha_n}{D_n}\phi_{n+1} + \frac{\beta_n}{D_n}\phi_{n-1} + \frac{C_n}{D_n}. \tag{7.7.7}$$

The set given by Equations (7.7.3)-(7.7.7) is solved by *forward elimination* and then by *back substitution*.

The forward eliminations commence with the elimination of $\phi_2$ from Equation (7.7.4) by substituting Equation (7.7.3) into Equation (7.7.4) and subsequently yielding

$$\phi_3 \;=\; \frac{\alpha_3}{D_3}\phi_4 + \frac{\beta_3}{D_3}\left[\frac{\alpha_2\phi_3 + \beta_2\phi_1 + C_2}{D_2}\right] + \frac{C_3}{D_3} \tag{7.7.8}$$

$$=\; \left[\frac{\alpha_3}{D_3 - \beta_3\frac{\alpha_2}{D_2}}\right]\phi_4 + \left[\frac{\beta_3\left(\frac{\beta_2}{D_2}\phi_1 + \frac{C_2}{D_2}\right) + C_3}{D_3 - \beta_3\frac{\alpha_2}{D_2}}\right]. \tag{7.7.9}$$

If the following notation is employed

$$A_2 = \frac{\alpha_2}{D_2} \quad \text{and} \quad C_2' = \frac{\beta_2}{D_2} + \frac{C_2}{D_2}, \tag{7.7.10}$$

Equation (7.7.9) may be written as

$$\phi_3 \;=\; \left[\frac{\alpha_3}{D_3 - \beta_3 A_2}\right]\phi_4 + \left[\frac{\beta_3 C_2' + C_3}{D_3 - \beta_3 A_2}\right]. \tag{7.7.11}$$

Letting

$$A_3 = \frac{\alpha_3}{D_3 - \beta_3 A_2} \quad \text{and} \quad C_3' = \frac{\beta_3 C_2' + C_3}{D_3 - \beta_3 A_2}, \tag{7.7.12}$$

allows for Equation (7.7.11) to be written as,

$$\phi_3 \;=\; A_3\phi_4 + C_3'. \tag{7.7.13}$$

The back-substitution process begins with the formulation of a general form for the recurrence relationship of Equation (7.7.13):

$$\phi_j \;=\; A_j\phi_{j+1} + C_j', \tag{7.7.14}$$

where

$$A_j \;=\; \frac{\alpha_j}{D_j - \beta_j A_{j-1}} \tag{7.7.15}$$

$$C_j' \;=\; \frac{\beta_j C_{j-1}' + C_j}{D_j - \beta_j A_{j-1}}. \tag{7.7.16}$$

These formulae comply to the boundary nodes, $j = 1$ and $j = n + 1$, by setting

$$A_1 = 0 \quad \text{and} \quad C_1' = \phi_1$$

$$A_{n+1} = 0 \quad \text{and} \quad C_{n+1}' = \phi_{n+1}.$$

For a system of equations to be solved it is required that they be arranged in the form of Equation (7.7.2) and expressions for $\alpha_j$, $\beta_j$, $D_j$ and $C_j'$ are identified from the discretised expressions. The values of $A_j$ and $C_j'$ are calculated starting at $j = 2$ and going up to $j = n$ by applying Equation (7.7.16).

Since the value for $\phi_{n+1}$ is a specified boundary value, the values for $\phi_j$ can be obtained in reverse order by means of the recurrence formula given in Equation (7.7.14).

## 7.7.2   Iterative application of the TDMA

In this section it is illustrated how the TDMA may be applied iteratively to solve a system of equations. Consider the grid illustrated in Figure 7.2 in conjunction with a general discrete equation of the form

$$a^P \phi^P \;=\; a^W \phi^W + a^E \phi^E + a^S \phi^S + a^N \phi^N + b. \tag{7.7.17}$$

The system is solved by applying the TDMA along a chosen line, for example north-south lines. The discrete equation is rearranged in the form,

$$-a^S \phi^S + a^P \phi^P - a^N \phi^N \;=\; a^W \phi^W + a^E \phi^E + b. \tag{7.7.18}$$

The right-hand side of Equation (7.7.18) is assumed to be temporarily known. Equation (7.7.18) is in the form of Equation (7.7.2) where $\alpha_j \equiv a^N$, $\beta_j \equiv a^S$, $D_j \equiv a^P$ and $C_j \equiv a^W \phi^W + a^E \phi^E + b$.

It is now possible to solve in the north-south-direction of the chosen line for values $j = 2, 3, 4, ..., n$ as shown in Figure 7.2.
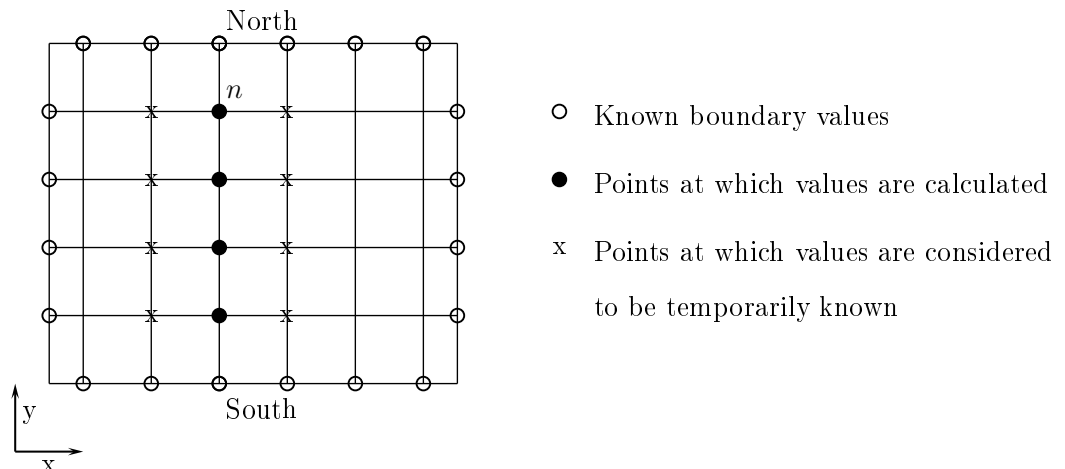
**Figure 7.2:** Representation of the line-by-line method.

# 7.8   Assembly of a complete method

The SIMPLE algorithm gives a method of calculating pressure and velocities. Generally SIMPLE is applied to solve a single velocity value, however, in this work the continuum and particle velocities are solved together, as illustrated in the schematic illustrated in Figure 7.3. The solution procedure can be surmised as follows:

The pressure and velocities are initialised and the $x$-component momentum equations for the continuum and the particulate phase, given by Equations (7.3.14) and (7.3.23), respectively, are solved. This is followed by solving the $y$-component momentum equations for the continuum and the particulate phase, given by Equations (7.3.31) and (7.3.39), respectively. The pressure correction is then obtained from Equation (7.5.19) and the pressure and continuum velocities are updated. The process is repeated until the relative percentage difference between velocity values for two successive iterations falls below 0.1 %– a criterion that for a time step of 0.05 s is usually satisfied within the order of a 100 cycles.

The relative percentage difference is obtained by calculating the sum of the velocities for each grid row and then determining the mean of these values for the relevant time step. The same is done for the next time step and the percentage difference of these two values, $x_1$ and $x_2$, is calculated by dividing the absolute difference of the two values by the average value of the same two values as shown in the equation below:

$$\%\text{Diff} \;=\; \frac{|x_1 - x_2|}{|(x_1 + x_2)/2|} \times 100. \tag{7.8.1}$$

The final velocity values are then used to calculate the continuum volume fractions from Equation (7.4.7) whereafter the particle volume fractions follow since $\epsilon_c + \epsilon_p = 1$. The time is updated with a user-specified time step and the new volume fractions are used to solve the next round of momentum conservation equations.
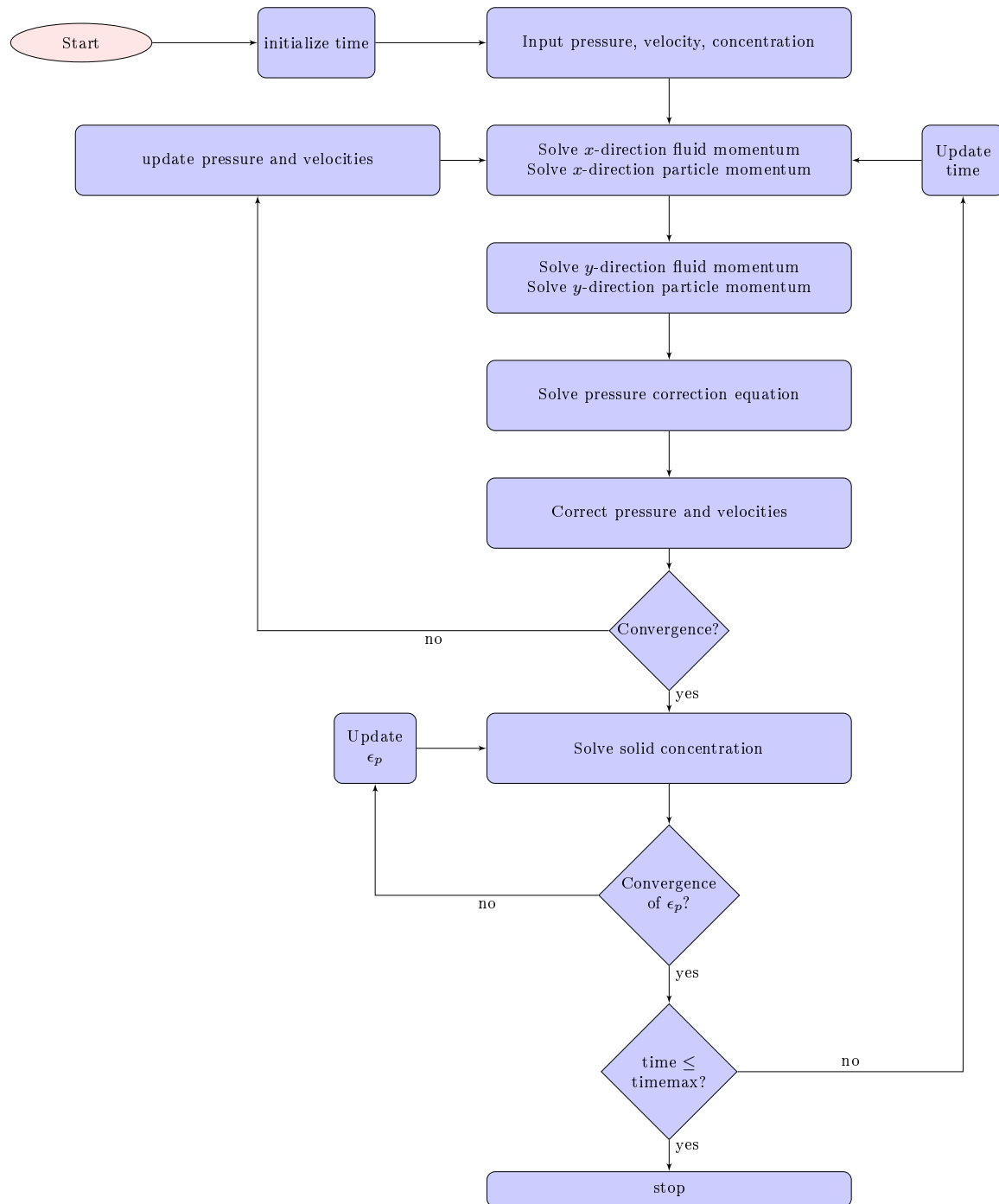
**Figure 7.3:** Adapted SIMPLE algorithm for two-phase flow.

## 7.9   Implementation of boundary conditions

Consider a two-dimensional problem and the partial grid shown in Figure 7.4.
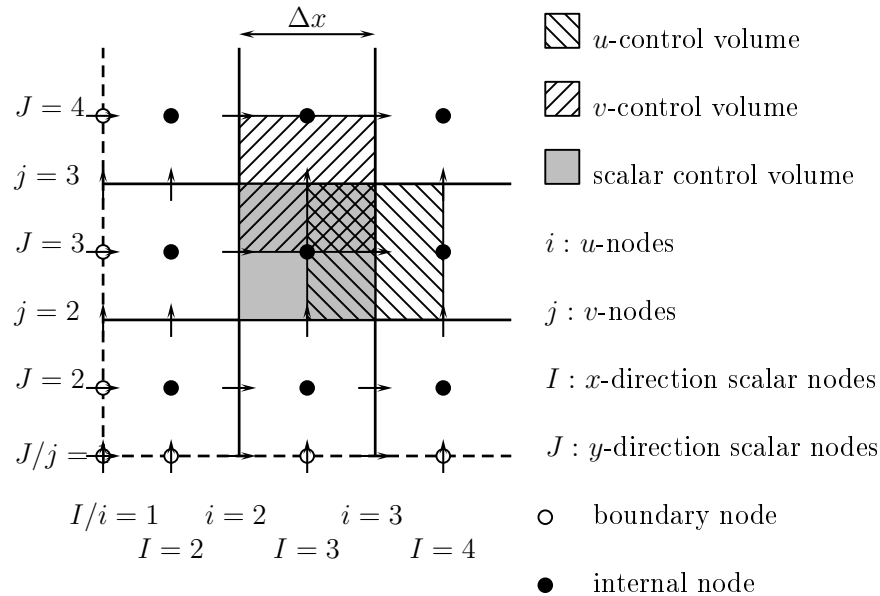


**Figure 7.4:** Grid arrangement.

Around each of the internal nodes a control volume exists and Equation (7.7.17) provides the necessary equations for all the unknown values at the internal grid nodes. For a line along each dimension, two of these equations will however involve the boundary nodes. Following Patankar (1980), attention is focused on the left-hand $x$-direction boundary nodes adjacent to the internal nodes, $I = 2$ as illustrated in Figure 7.4. For the boundary control volume used in Practice B (Patankar (1980)), where grid nodes are placed at the centres of control volumes, the length of the first control volume is zero, i.e. $\Delta x_{I=1} = 0$.

In this work the boundary conditions will consist either of, given values, or a given gradient between the boundary and its internal neighbour. The equation for the left-hand side boundary node is given by,

$$\phi_1 \;=\; B_{in}\phi_2 + C_{in}, \tag{7.9.1}$$

and the boundary expression for the right-hand side boundary is given by,

$$\phi_N \;=\; B_{out}\phi_{N-1} + C_{out}. \tag{7.9.2}$$

If the boundary value is known, $B$ and $C$ are set to zero and the given value, respectively. In case of a zero gradient condition $B = 1$ and $C = 0$. In determining a boundary expression for the pressure the fact that the pressure gradient between any two nodes is constant is used: In the current program it is taken into account that the pressure gradient between nodes $I = 1$ and $I = 2$ is equal to the pressure gradient between nodes $I = 2$ and $I = 3$. It follows that,

$$P(1) \;\; = \;\; P(2) - [P(3) - P(2)]\frac{\delta x_e(1)}{\delta x_e(2)}. \tag{7.9.3}$$

The expression is modified in order to include the option of a given pressure value. It follows that the resulting boundary expression for the inlet pressure is given by

$$P(1) \;\; = \;\; B_{in}\left[P(2) - [P(3) - P(2)]\frac{\delta x_e(1)}{\delta x_e(2)}\right] + C_{in}, \tag{7.9.4}$$

and the outlet pressure, $P(N)$, is defined using the same gradient requirements,

$$P(N) \;\; = \;\; B_{out}\left[P(N-1) + [P(N-1) - P(N-2)]\frac{\delta x_e(N-1)}{\delta x_e(N-2)}\right] + C_{out}. \tag{7.9.5}$$

Equations (7.9.1) and (7.9.2) are used to specify the boundary conditions for the velocity and volume fractions, whereas Equations (7.9.4) and (7.9.5) will be used for pressure calculations.

A similar procedure is followed for the "top" and "bottom" boundaries.

## 7.10  Conclusions

The discretised equations and the TDMA method along with the SIMPLE algorithm, illustrated in Figure 7.3, can now be implemented. In this work simulations were done in the Fortran programming language and the simulation code was designated *Two-phase motion simulation* (2PMS). The results from these simulations are discussed in Chapter 8.

# Chapter 8

# Numerical simulations

## 8.1 Introduction

The discrete expressions for momentum and mass transfer, derived and implemented into the SIMPLE algorithm in Chapter 7, were implemented in Fortran and designated Two-Phase Motion Simulation (2PMS).

In the first part of this chapter the emphasis is placed on the validation of 2PMS for elementary flow simulations to evaluate the functionality of the code. This will be followed by the validation of the mathematical model, derived in Chapters 3-6, for horizontal and vertical two-phase flow conditions and, where applicable, the comparison of said simulated results to analytical expressions.

In Chapter 9, vertical simulations, which are performed here for various particle sizes, grid geometries, time-steps, and initial volume fraction values, will also be verified with physical experiments performed at the Council for Scientific and Industrial Research (CSIR) in Stellenbosch.

## 8.2 Basic flow simulations

Simulations were done to ensure that 2PMS correctly predicts the motion of a fluid between parallel plates, over a porous bed and through an isotropic porous medium. Horizontal flow simulations were conducted with a $200 \times 30$ size grid over a flow domain measuring 200 cm in length and 2 cm in width.

### 8.2.1   Plane Poiseuille flow

The program was first validated for plane Poiseuille flow: The input velocity at the left side of the domain, illustrated in Figure 8.1, was set to $u_c = 0.1$ cm/s and the density of the fluid was set to approximate that of water at room temperature: $\rho_c = 1000$ kg/m$^3$.
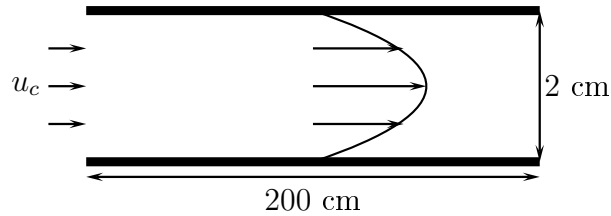


**Figure 8.1:** Setup for plane Poiseuille flow simulation.

A simulation was done for an open channel with no-slip boundary conditions at the upper and lower edges, and zero gradient conditions were applied to the in- and outlets. The fully developed velocity profile obtained from this simulation is compared to the analytical equation for plane Poiseuille flow in Figure 8.4 from which it can be seen that the numerical approximation followed the results of the analytical solution closely.

### 8.2.2   Flow through a stationary porous medium

For the same input conditions, dimensions and boundary conditions, a simulation was done in a medium with an isotropic particle volume fraction of, $\epsilon_p = 0.5$, consisting of granular material with a 1 mm diameter and with a density of 2500 kg/m$^3$. The setup for the simulation is shown in Figure 8.2.
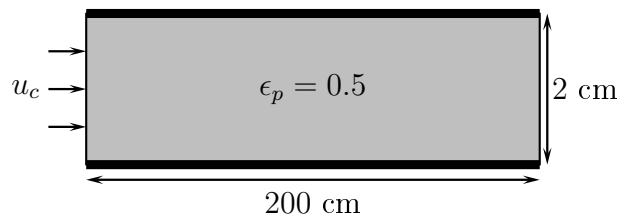


**Figure 8.2:** Setup for flow simulation through a stationary porous medium.

The drag approximation for slow viscous flow, given by Equation (6.4.15), was assumed to govern and was applied to yield the following expression for flow through a stationary porous medium:

$$\mu_c \epsilon_c \frac{\partial^2 u_c}{\partial y^2} = \epsilon_c \frac{\partial p_c}{\partial x} + \frac{\mu \epsilon_p}{d_p^2} \left[ \frac{36 \epsilon_c \epsilon_p^{1/3}}{\left(1 - \epsilon_p^{2/3}\right)\left(1 - \epsilon_p^{1/3}\right)} + 18 \right] u_c. \qquad (8.2.1)$$

Only the Darcy part of the drag equation was used since the Forchheimer component renders the partial differential equation analytically unsolvable. The aforementioned omission is justified by the choice of input velocity which yields a Reynolds number, $Re \approx 1$, which is well within the viscous regime.

The pressure gradient was obtained from the numerical pressure output as 0.0013 Pa and the partial differential expression given in Equation (8.2.1) was solved to obtain

$$u_c = \frac{\frac{dp}{dx} \exp\left[-\frac{\sqrt{A}y}{\sqrt{\mu \epsilon_c}}\right] \left[-1 + \exp\left[\frac{\sqrt{A}y}{\mu \epsilon_c}\right]\right] \left[-\exp\left[\frac{2\sqrt{A}}{\mu \epsilon_c}\right] + \exp\left[\frac{\sqrt{A}y}{\mu \epsilon_c}\right]\right]}{A \left[1 + \exp\left[\frac{2\sqrt{A}}{\sqrt{\mu \epsilon_c}}\right]\right]}, \quad (8.2.2)$$

where the constant $A$ in Equation (8.2.2) is given by

$$A = \frac{\mu \epsilon_p}{d_p^2} \left[ \frac{36 \epsilon_c \epsilon_p^{1/3}}{\left(1 - \epsilon_p^{2/3}\right)\left(1 - \epsilon_p^{1/3}\right)} + 18 \right]. \qquad (8.2.3)$$

As for the plane Poiseuille simulation, the results are illustrated in Figure 8.4 from which it follows that the numerical values yielded is an accurate approximation to the analytical solution, given by Equation (8.2.2).

### 8.2.3   Flow past a stationary porous medium

The final verification for the program was done by examining results yielded for the $x$-component fluid velocity profile when the boundary to the channel is not a solid, but consists of a porous medium, as illustrated in Figure 8.3.

The analytical solution to this problem can be obtained from Neale and Nader (1974) but falls outside the scope of this research. Their solution is, however, illustrated along with the simulated results in Figure 8.4 for flow past a porous medium with a particle volume fraction of 0.5. The simulated result appears to be a good approximation of that given by Neale and Nader (1974).
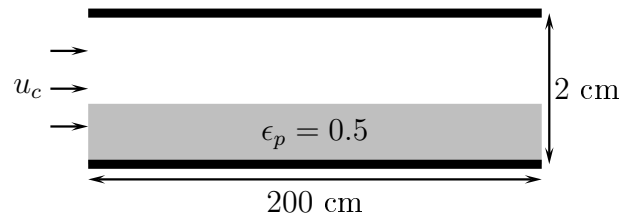
**Figure 8.3:** Setup for flow simulation past and through a porous medium.
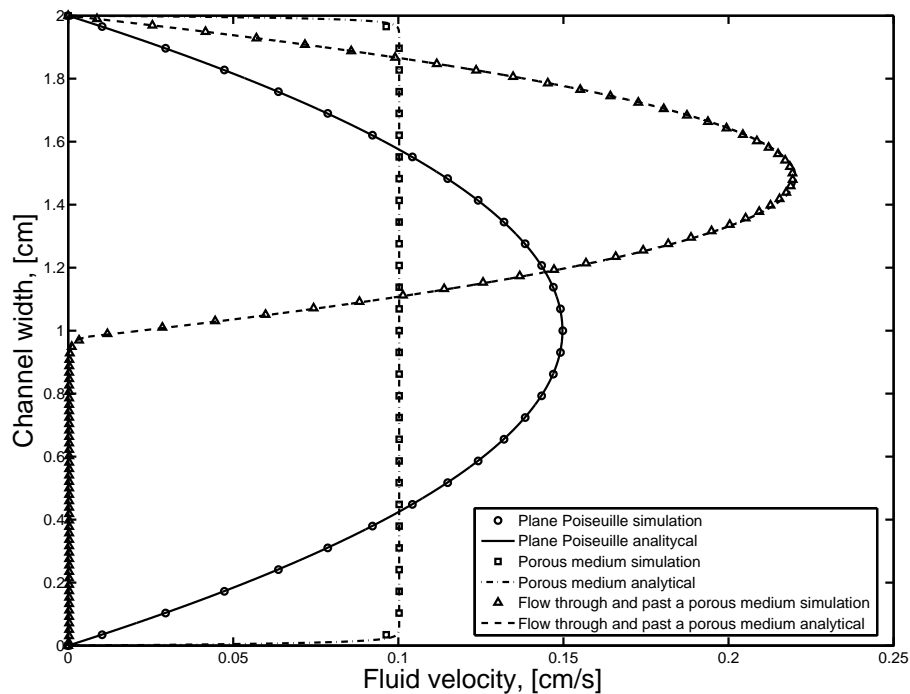


**Figure 8.4:** Simulated and analytical velocity profiles for flow in between parallel plates, flow through a porous bed and flow over and through a porous bed.

Following the satisfactory results obtained for flow profiles through an open channel as well as past and through a porous medium, experiments were done for cases where the bed did not remain stationary.

## 8.3  Two-phase flow

In order to illustrate a simple two-phase flow example, a deposit, of which the constituent particles have a diameter of 1 mm and a density of $\rho_p = 2500$ kg/m$^3$, was placed at the centre of a stationary continuum, with a density of $\rho_c = 1000$ kg/m$^3$, and allowed to settle under the influence of gravity alone. The setup for the simulation is illustrated in Figure 8.5.
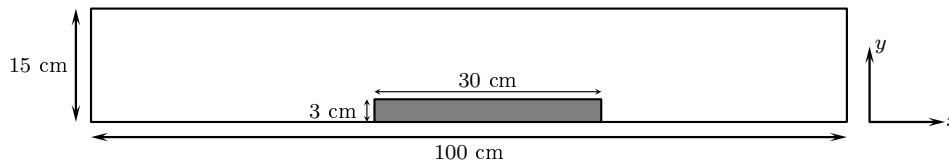


**Figure 8.5:** Setup for horizontal two-phase flow.

For the volume fraction-, velocity profile- and interaction force simulations, illustrated in Figures 8.6-8.10, a grid of $500 \times 500$ nodes in the $x-$ and $y-$directions, respectively, was used and all values at the edges of the simulation domain were set to zero.

Initially the continuum and particles are at rest and only gravitation is applied to the system resulting in the downward motion of the particles. At the edges of the deposit the continuum moves upward as the particle phase displaces it. These phenomena at the initiation of the settling process are illustrated at the top of Figures 8.6a, 8.7a, 8.8a, 8.9a and 8.10a. The interaction forces between the particles as well as those forces between the particles and the continuum enveloping them, for this stage, are shown at the top of Figures 8.9a and 8.10a, respectively. The scale on these figures show the order of magnitude of the forces per unit volume and from Figures 8.9a and 8.10a the interactions between phases, which are in the order of $10^1$, dominate the particle-particle interaction which are in the order of $10^{-2}$.

As the settling motion continues, slopes are formed at the edges of the deposit as the particles spread to the bottom and the sides, pulling the continuum along with it as shown in the lower half of Figures 8.6a, 8.7a and 8.8a. Both the interaction forces between the phases and the interaction force between the particles themselves increase, since these forces are proportional to the velocity. The interaction forces are visibly larger at the sides than in the middle of the deposit since there is very little motion at the centre. The edges of the deposit therefore settles faster than its centre, resulting

in the steepening of the slope and the widening of the base as illustrated in the upper half of Figures 8.6b-8.10b.

However, as the slope increases, so does the downward velocity of the particles at the centre of the deposit, resulting in the flattening of the deposit as illustrated in the bottom half of Figure 8.6b. Where the deposit reaches the lateral boundaries of the domain it can be seen from Figure 8.9b and 8.10b that the particle-particle- and the particle-continuum interaction forces sharply increase where collisions occur with the stationary boundary.
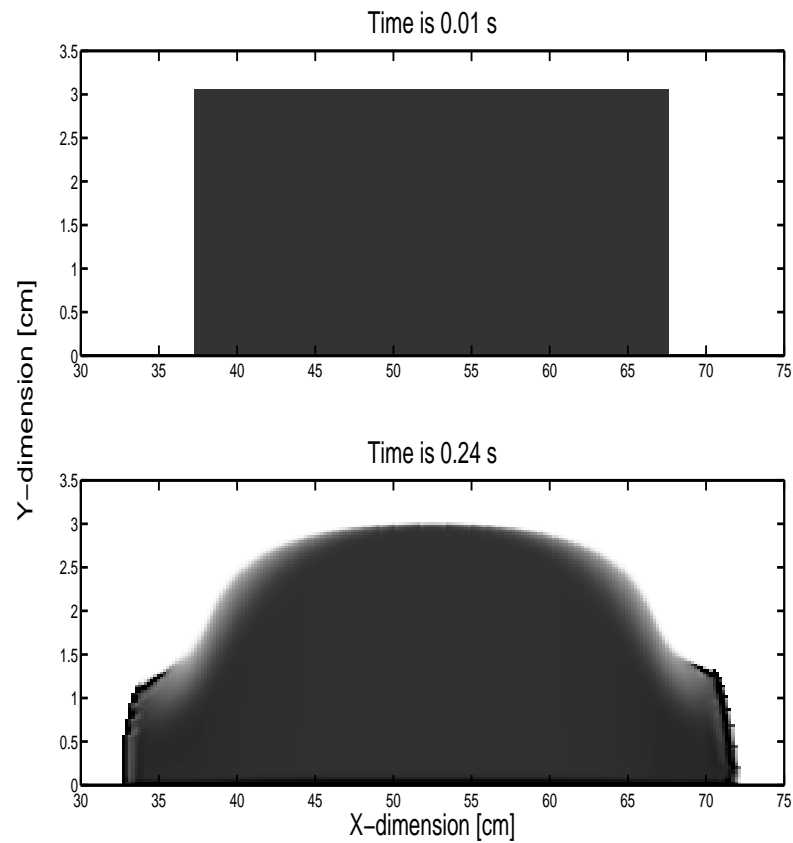
(a) Particle volume fractions at t=0.01 s and t=0.24 s.
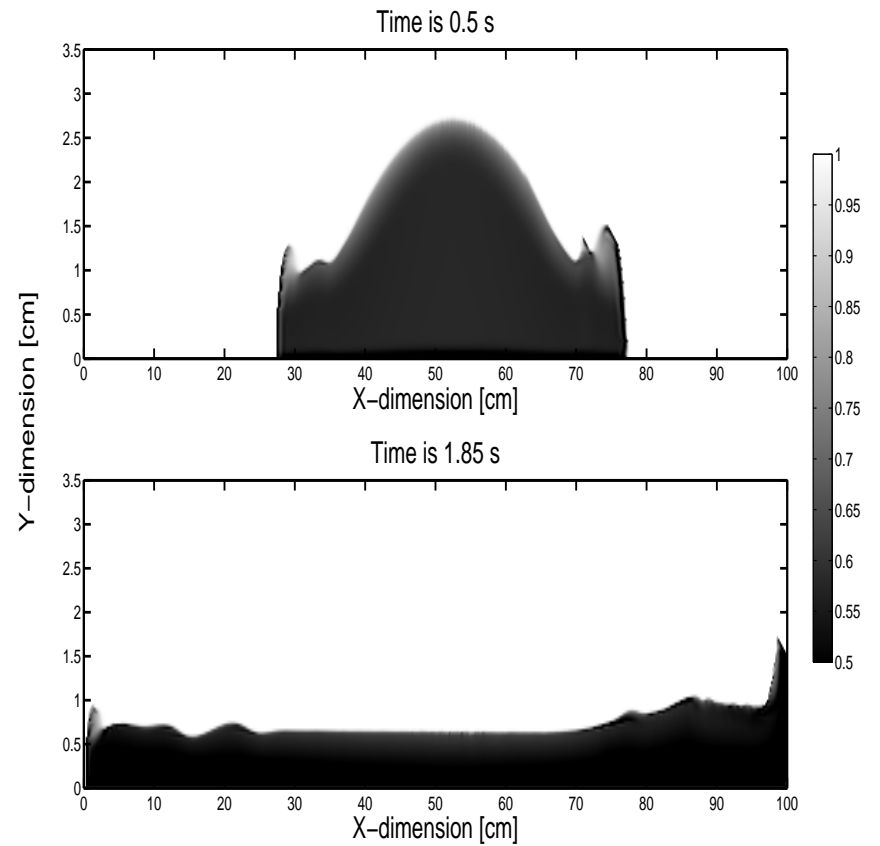
(b) Particle volume fractions at t=0.50 s and t=1.85 s.

**Figure 8.6:** Change in particle volume fraction with time.
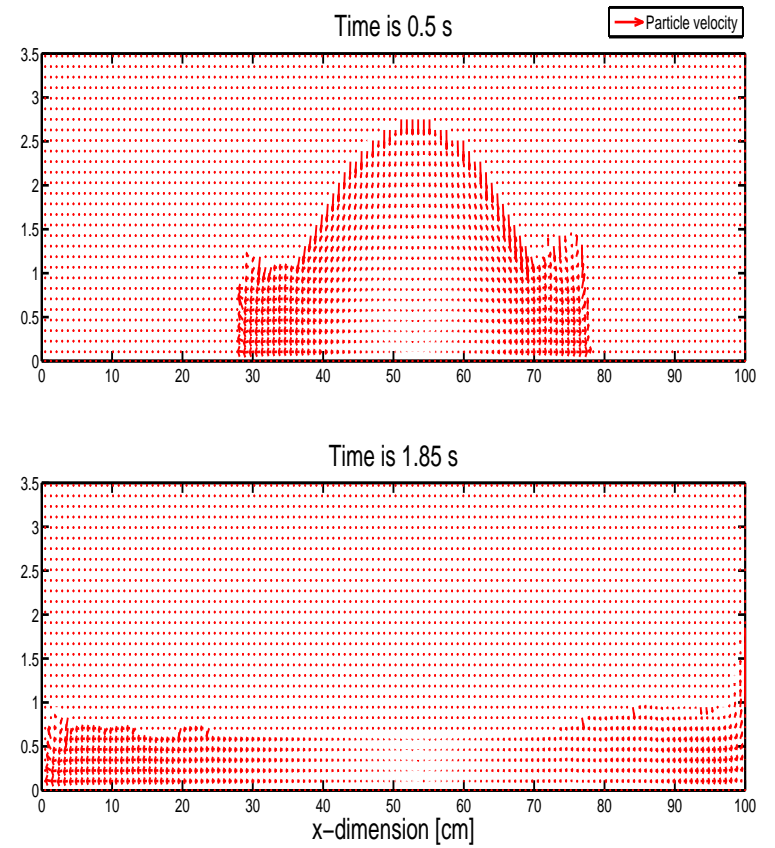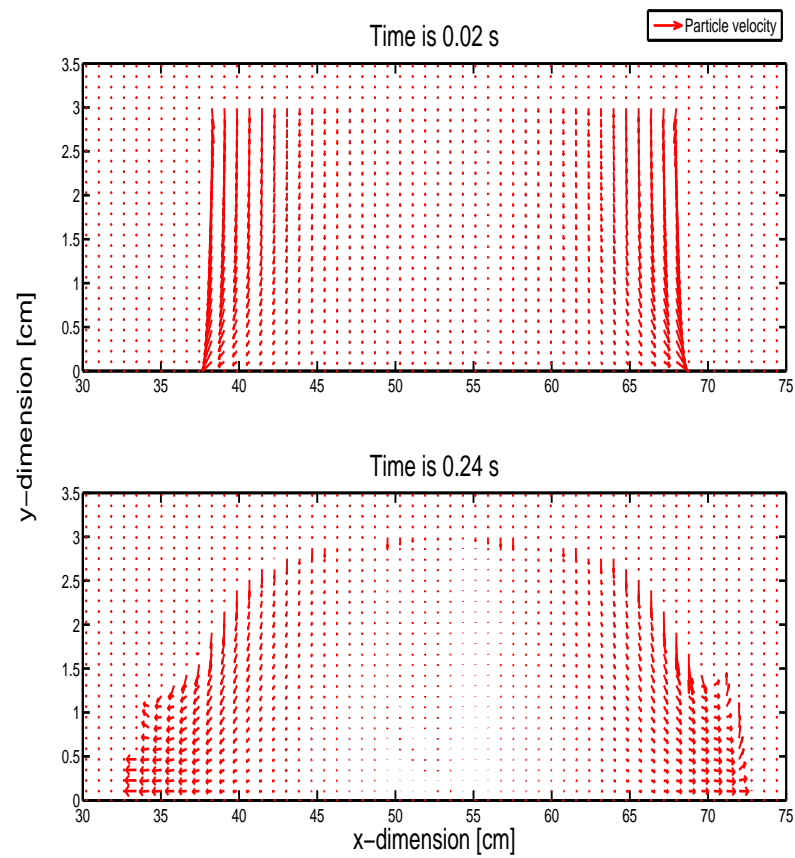
**(a)** Particle velocities at t=0.01 s and t=0.24 s.

**(b)** Particle velocities at t=0.50 s and t=1.85 s.

**Figure 8.7:** Change in particle velocity profile with time.
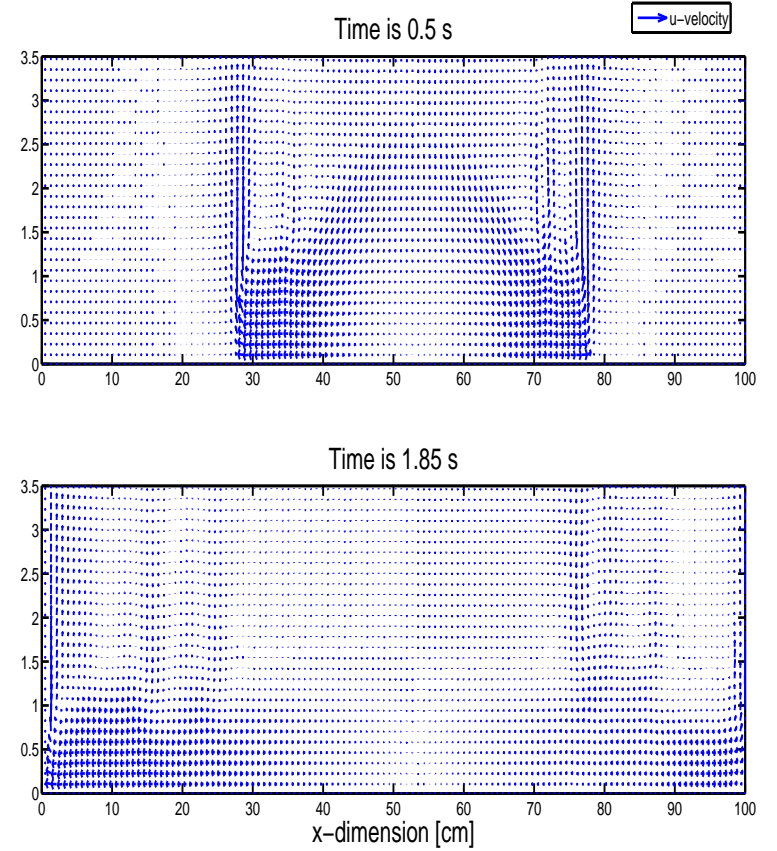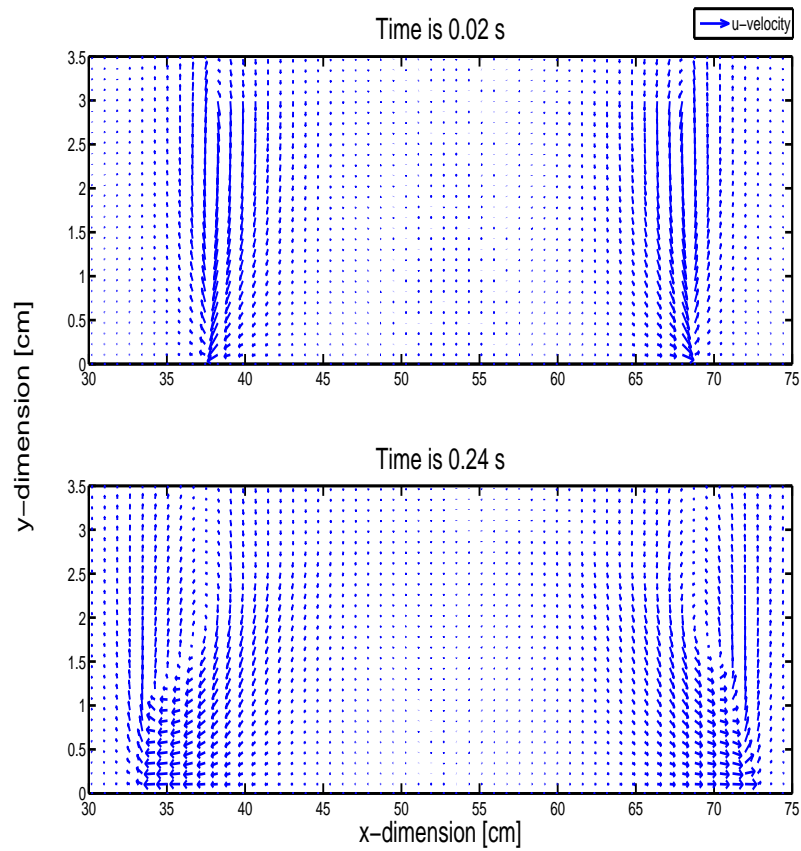
**(a)** Continuum velocities at t=0.01 s and t=0.24 s.     **(b)** Continuum velocities at t=0.50 s and t=1.85 s.

**Figure 8.8:** Change in continuum velocity profile with time.
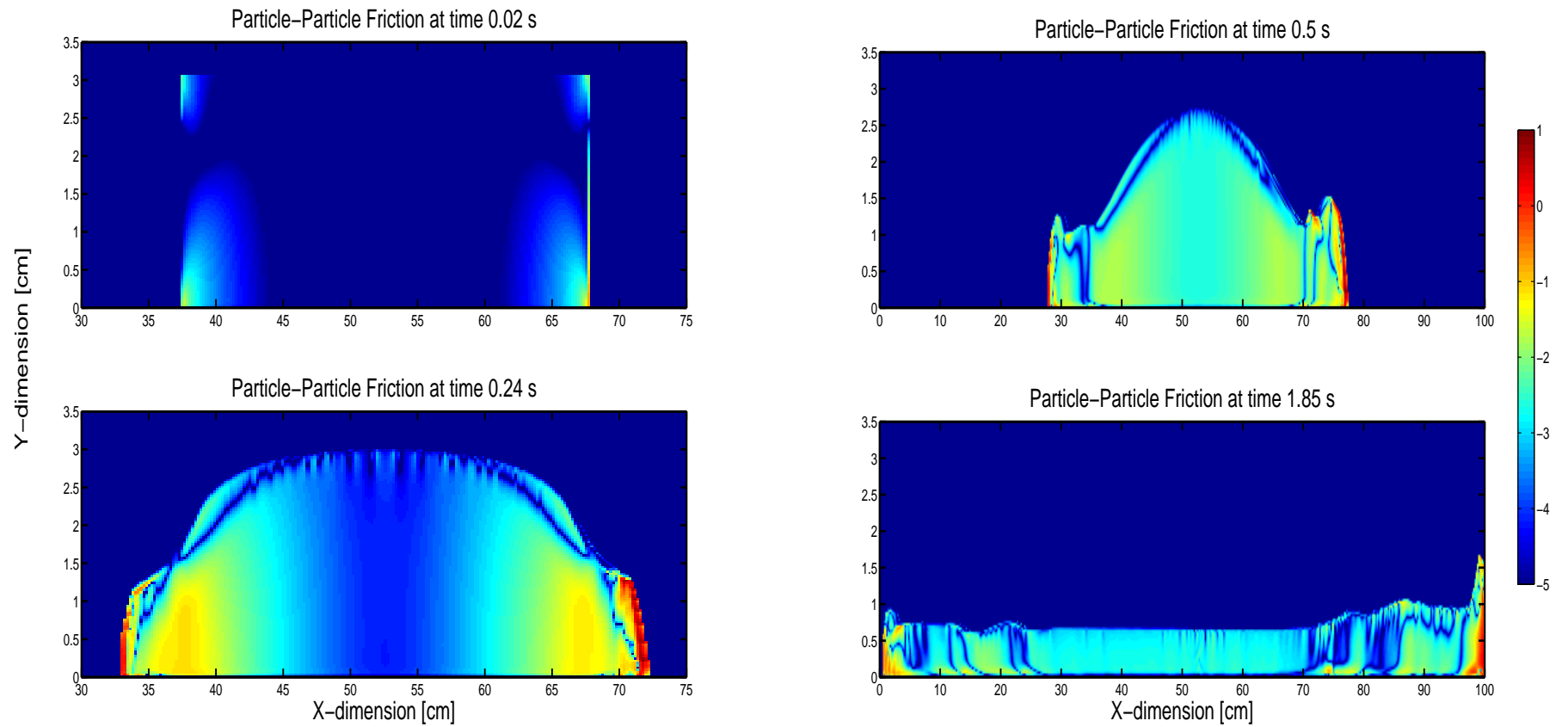
(a) Particle-particle forces at t=0.01 s and t=0.24 s.

(b) Particle-particle forces at t=0.50 s and t=1.85 s.

**Figure 8.9:** Changes in the order of magnitude of particle-particle interaction forces per unit volume as a deposit collapses within a continuum.
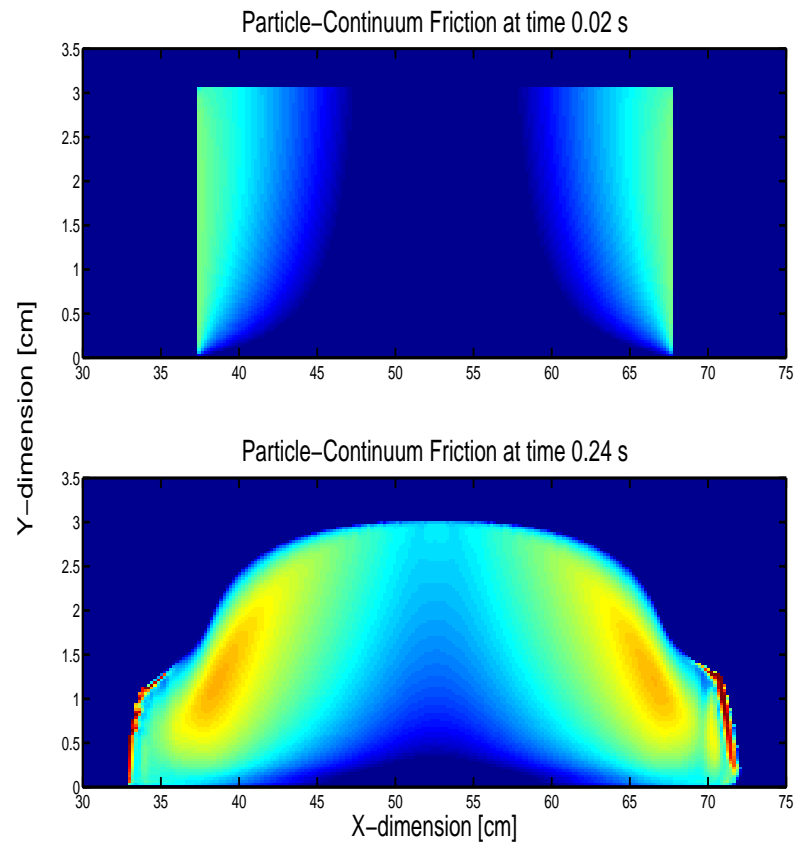
**(a)** Particle-continuum forces at t=0.01 s and t=0.24 s.
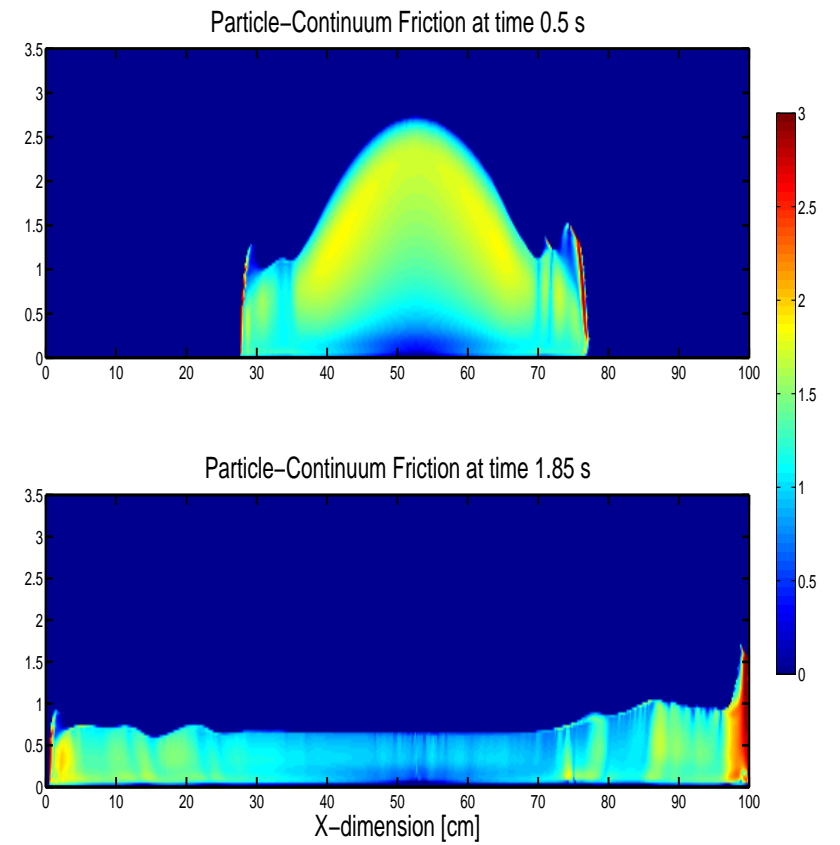
**(b)** Particle-continuum forces at t=0.50 s and t=1.85 s.

**Figure 8.10:** Changes in the order of magnitude of particle-continuum interaction forces per unit volume as a deposit collapses within a continuum.

# 8.4   Vertical motion

Simulations were done in order to predict the vertical settling motion of an evenly distributed 3.6 g sample of silicon particles with a density of $\rho_p = 2500$ kg/m$^3$ through water with a density of $\rho_c = 1000$ kg/m$^3$. The depth and width of the water column through which the particles fell were set to 1.7 m and 0.150 m, respectively and the setup for the simulation is illustrated in Figure 8.11.
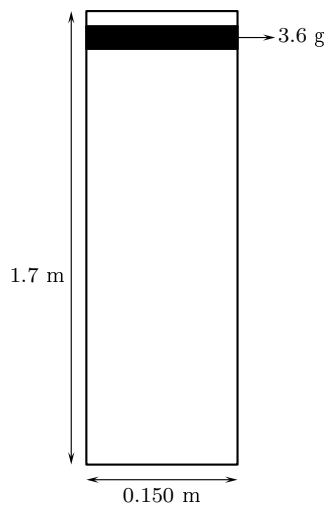


**Figure 8.11:** Setup for vertical settling simulation.

The vertical settling simulations done with 2PMS are verified against experimental data obtained from settling tube experiments in Chapter 9. In the following sections the boundary conditions applied for the setup of the simulation as well as its stability with regard to the selection of grid size and time step intervals are discussed.

## 8.4.1   Boundary conditions

At the left- and right boundaries of the setup shown in Figure 8.11 it was assumed that both the particles and the continuum were at rest (i.e. a no-slip boundary condition was applied). At the upper boundary it was assumed that a zero-gradient boundary condition existed and at the bottom it was assumed that the particles and the continuum would be stationary to be representative of the settling tube experiments performed in Chapter 9.

The particle volume fraction, $\epsilon_p$, was assumed to be zero at the upper edge of the setup and was assumed to be equal to one at the left-, right- and base sides. Over all, a zero-gradient pressure condition was applied.

The initial guess for the pressure values was set to zero. The input condition for the particle volume fraction proved problematic since the simulation had to represent the physical settling tube experiments for which this value could not be measured. It was however known that for each of the physical experiments a mass of 3.6 g particles were inserted in the form of a single layer into the settling tube. To make the simulations comparable to these conditions the particle volume fraction was changed according to the selection of the grid size to always ensure that a single layer entry would be representative of a particle mass of 3.6 g. The following was used to determine the particle volume fraction:

$$\epsilon_p \;\; = \;\; \frac{m_p}{\rho_p \Delta x \Delta y (N_x - 2)}, \tag{8.4.1}$$

where $m_p$ and $\rho_p$ denote the mass and density of the particles and $\Delta x$, $\Delta y$ and $N_x$ are the grid dimensions for a single cell in the $x$- and $y$-directions and the total number of grid nodes in the horizontal direction, respectively. The subtraction is done to eliminate the two cells at the boundaries which were assumed to have a zero particle volume fraction.

The particles were released with a zero initial velocity and the fluid too was assumed at rest at initiation.

## 8.4.2 Grid geometry and time steps

The stability of 2PMS with regard to grid and time step selection was analysed using three grid sizes of $85 \times 15$, $170 \times 30$, and $340 \times 60$ on a domain 170 cm $\times$ 15 cm in size. Three time step intervals of 0.005 s, 0.01 s and 0.05 s were applied to each of the grid allotments and simulations were performed for particles 1 mm, 0.75 mm, 0.50 mm, and 0.30 mm in diameter.

### 8.4.2.1 Convergence within a time step

During each time step, the program was iterated until the percentage relative difference between the average group velocities of two successive iterations was less than 0.1%.
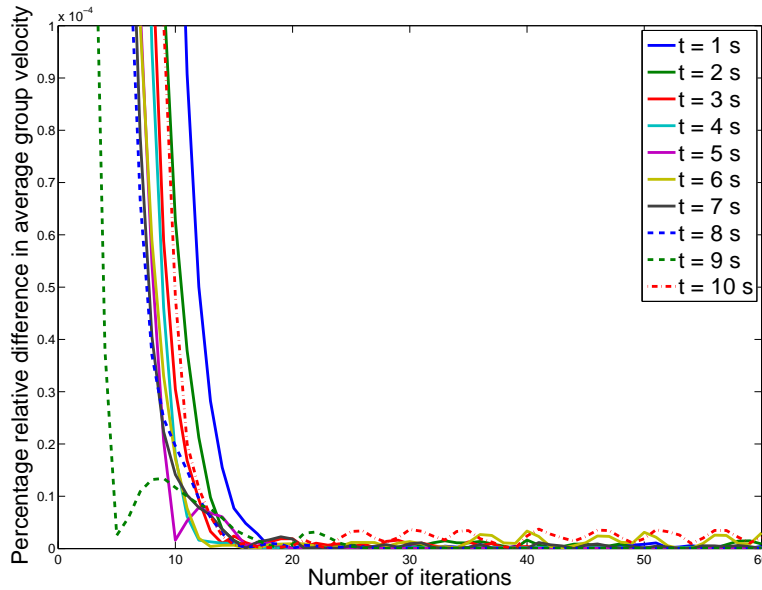
**Figure 8.12:** Convergence within a time step.

This was done by calculating the average group velocity for each iteration as

$$u_p^{avg}(j) \;=\; \frac{\sum u_p(i,j)\epsilon_p(i,j)}{\sum \epsilon_p(i,j)}, \tag{8.4.2}$$

which yielded the average velocity of each column of the grid, the mean of which is the average group velocity. The percentage relative difference between the average group velocity for two successive iterations, $I-1$ and $I$, was then obtained as

$$\%DIFF \;=\; \frac{2|u_p^{avg}(I,t) - u_p^{avg}(I-1,t)|}{|u_p^{avg}(I,t) + u_p^{avg}(I-1,t)|}100. \tag{8.4.3}$$

In Figure 8.12 an example of the relative difference criteria, given by Equation (8.4.3), at various time steps for a 1 mm-diameter particle and a time step of 0.01 s is illustrated.

### 8.4.2.2 Grid and time step stability

Following Patankar (1980), the fully implicit scheme was used to ensure that the result for a simulation is independent of the grid or the time step interval choices. Grid independence for a time step of 0.01 s is illustrated in Figure 8.13 and time step independence is shown in Figure 8.14. Figures 8.13 and 8.14 also show that a terminal group velocity is reached for each of the simulations after a period of 10 s.
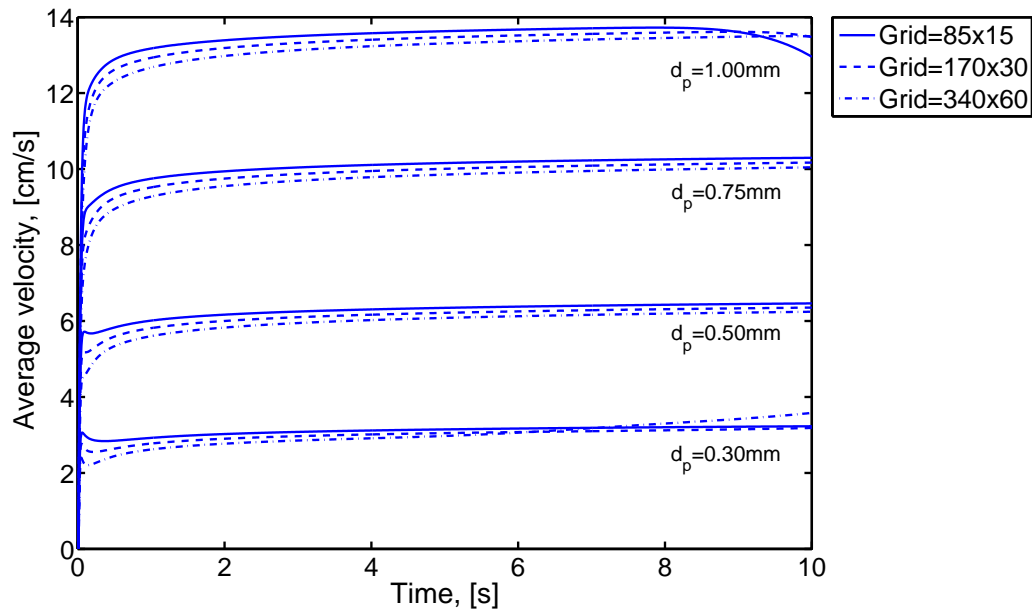
**Figure 8.13:** Grid analysis for vertical settling simulations.
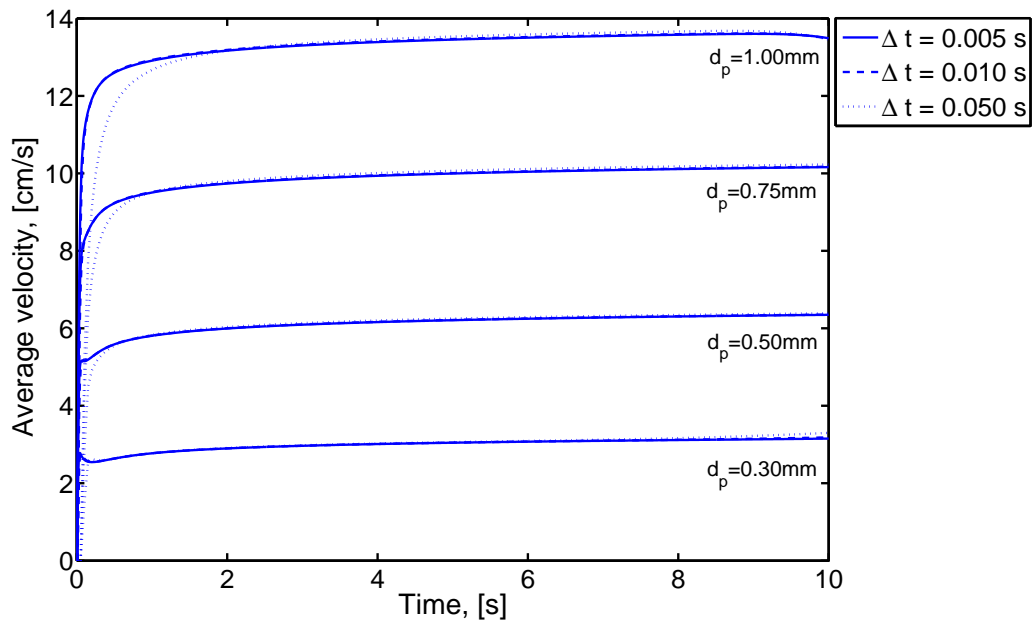


**Figure 8.14:** Time analysis for vertical settling simulations.

It was however found that numerical diffusion increased rapidly as the grid was made coarser. The numerical diffusion for a 1 mm particle simulation over a $340{\times}60$, $170{\times}30$, and a $85 \times 15$ grid is illustrated in Figures 8.15-8.17.
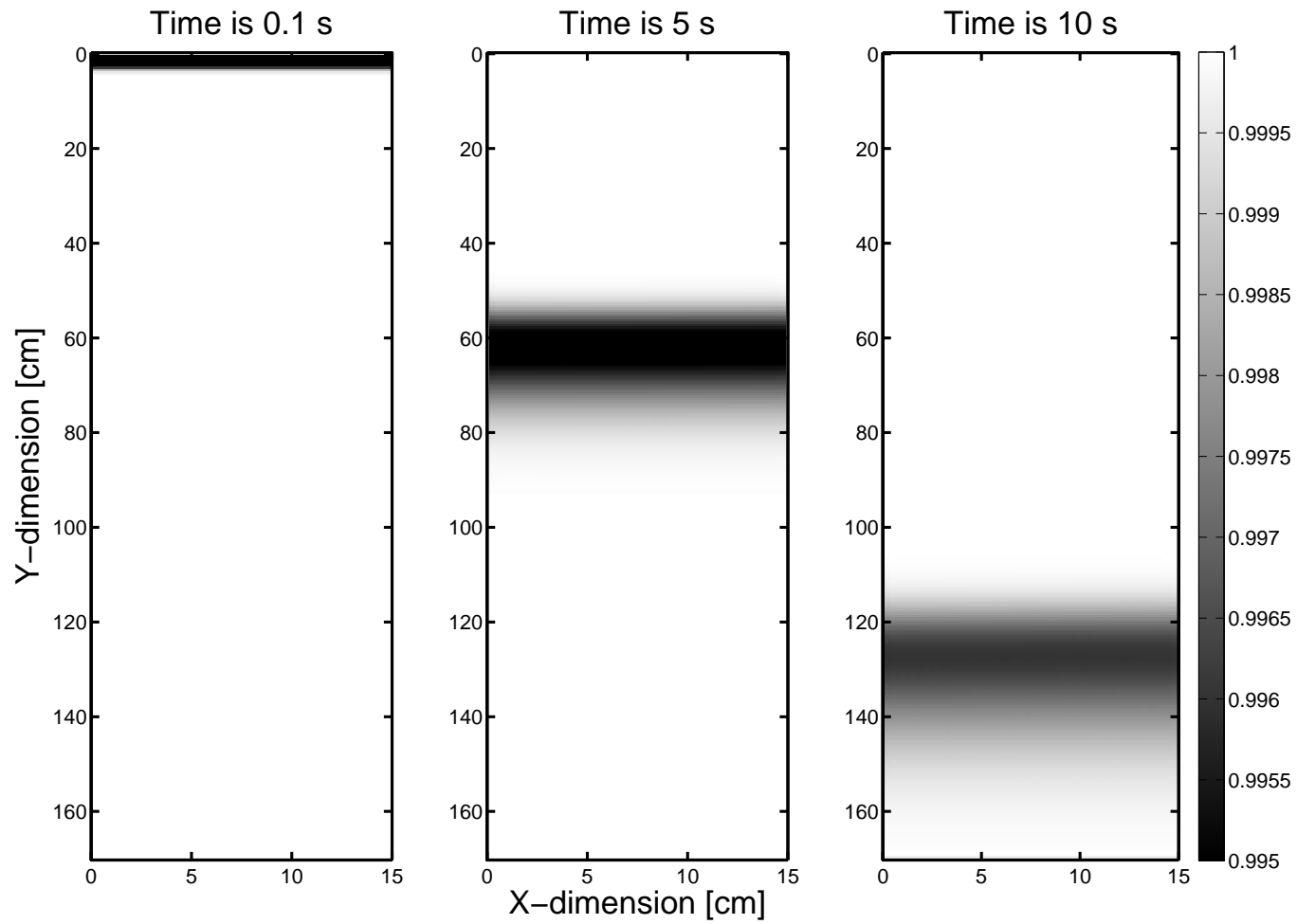
**Figure 8.15:** Particle volume fraction of a 3.6 g sample of 1 mm particles over a $340 \times 60$ grid.
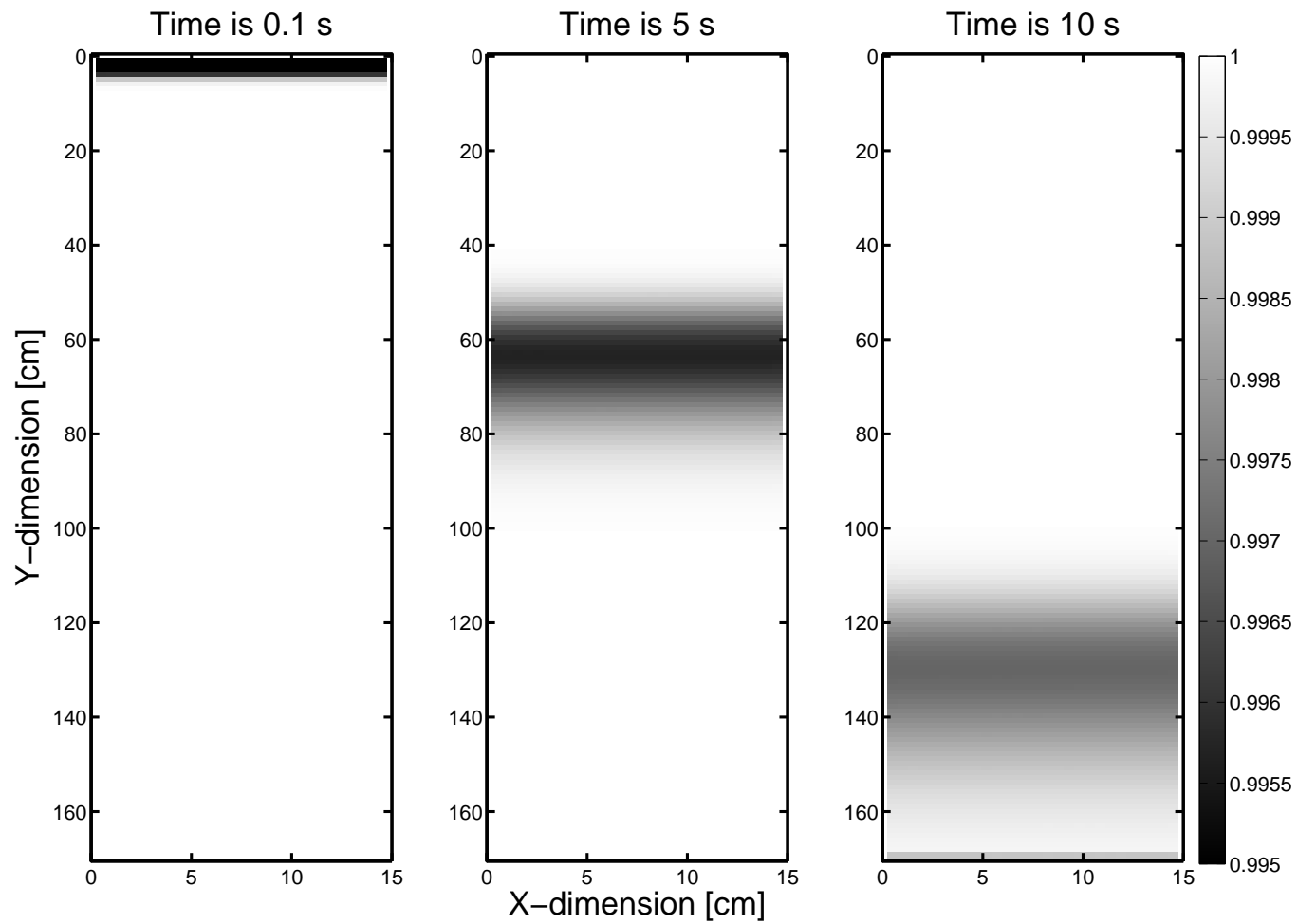
**Figure 8.16:** Particle volume fraction of a 3.6 g sample of 1 mm particles over a $170 \times 30$ grid.
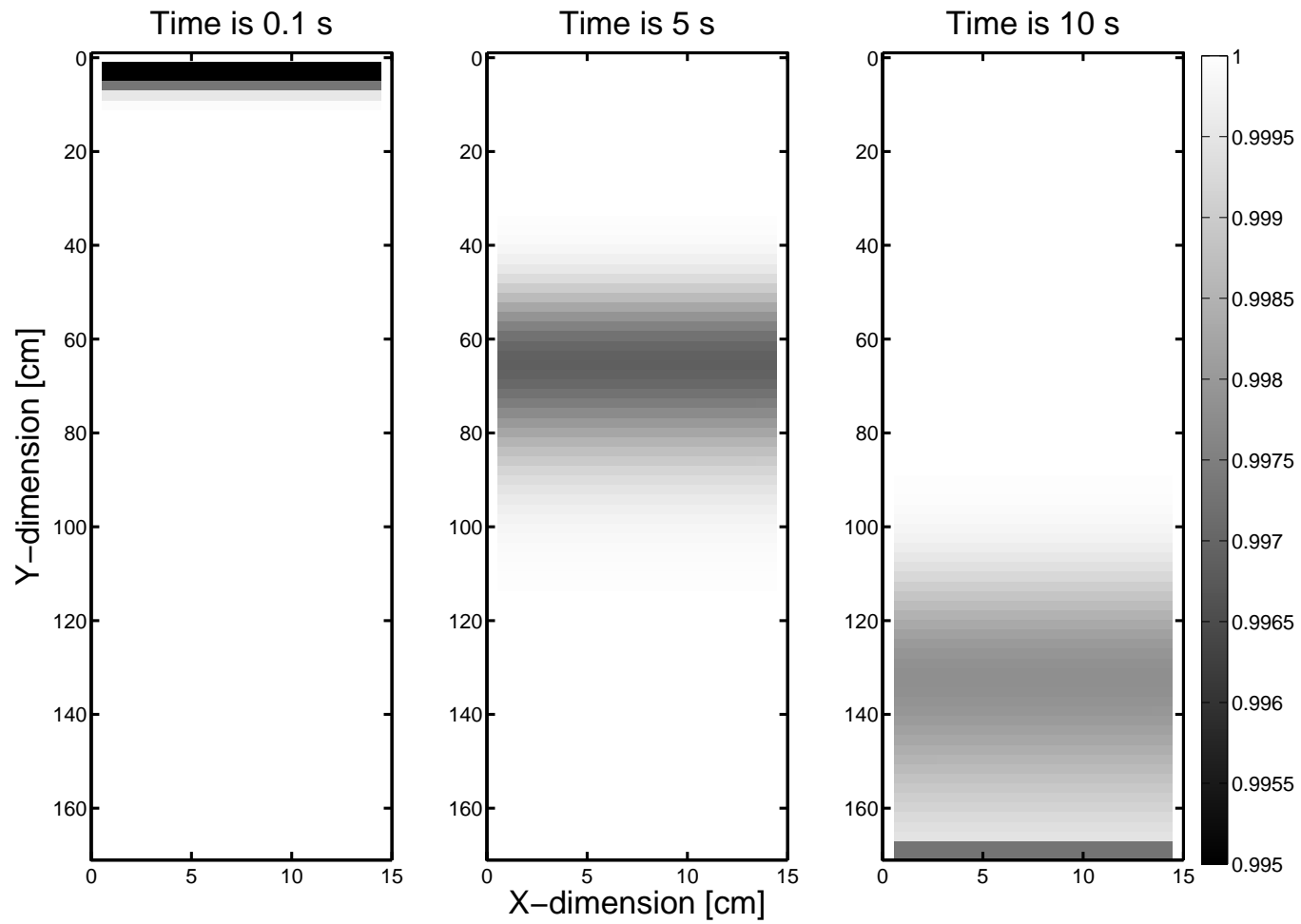
**Figure 8.17:** Particle volume fraction of a 3.6 g sample of 1 mm particles over a 85 × 15 grid.

Following Rafael and Mahaffy (1998), a truncation error analysis of the fully implicit time integration on a staggered mesh yields an equation of the form (for mesh cell $i$ and time step $n+1$):

$$\frac{\partial \phi}{\partial t}\Big|_i^{n+1} + \frac{\partial}{\partial x}(\phi u_c)\Big|_i^{n+1} = \frac{\partial}{\partial x}\left\{0.5\left(|u_c|\Delta x + \Delta t u_c^2\right)\frac{\partial \phi}{\partial t}\right\}\Big|_i^{n+1}. \qquad (8.4.4)$$

The second term on the right-hand side of Equation (8.4.4) represents a diffusive transport.

According to Rafael and Mahaffy (1998), Equation (8.4.4) is not approximating the original expression given by

$$\frac{\phi \rho_c}{\partial t} + \nabla\left(\phi \rho_c u_c\right) = 0, \qquad (8.4.5)$$

but is in fact approximating, with second order accuracy, the transport equation

$$\frac{\partial \phi}{\partial t} + \frac{\partial}{\partial x}\left(\phi u_c\right) = \frac{\partial}{\partial x}\left(K_{impl}\frac{\partial \phi}{\partial t}\right), \qquad (8.4.6)$$

which physically describes a convective-diffusive transport of the scalar $\phi$ with a diffusion coefficient, $K_{impl}$, given by

$$K_{impl} = 0.5\left(|u|\Delta x + \Delta t u^2\right). \qquad (8.4.7)$$

Thus, the first order upwind scheme will always yield a diffusive solution if implicit time differencing is used, the magnitude of which will grow both with increasing time step, $\Delta t$, and cell sizes $\Delta x$ as illustrated by Figures 8.15-8.17.

An additional source of numerical diffusion appears in multidimensional flows when the velocity field is skewed with respect to the computational grid (Patankar (1980), Rafael and Mahaffy (1998)). In such cases, the upwind formulation introduces additional diffusive terms proportional to the cross gradients of the scalar being transported.

According to the expression obtained in Equation (8.4.7) for the false numerical diffusion coefficients introduced by the upwind solution, it is clear that grid size plays an important role in the magnitude of the diffusion affecting the convective solution. Therefore, one could, in principle, diminish the influence of the diffusive terms in the solution by means of grid refinement.

### 8.4.3 Convergence of the average group velocity over time

Results show that the particles accelerate from their initial stationary state under the influence of gravity. During this acceleration period the particles spread out considerably. As the particle group falls, the surrounding fluid is also set into motion. The fluid caught within the group moves faster than the fluid at the front end of the group and, due to the nature of the equations discussed previously, this results in the front end of the cloud being exposed to less drag than the internal sections, causing it to move faster. The effect is an increase in the size of the cloud and a decrease in its concentration. However, numerical instabilities, discussed in the previous section, also contribute to the diffusion phenomenon. Figure 8.18 shows how the group velocity of the particles tend to zero as the particles reach the lower boundary of the simulation setup. The rate at which the velocity decreases appears to be proportional to the size of the groups' constituent particles.

Although the spread of the particle cloud in physical experiments may be ascribed to a difference in particle size and the initial surface tension forces between the particles and the fluid matter, this can not be used to explain the diffusion seen in the numerical experiments since the particles are assumed to be of equal size and surface tension is not included in the expressions used to simulate the motion.

At each time step the simulation data for the particle velocities and the particle volume fractions were captured and inserted into a Matlab routine (for which an example is given below) to determine the average velocity of the cloud. This average was determined by multiplication of each grid point velocity with its corresponding concentration and dividing by the sum of the concentrations, as given by Equation (8.4.2) and from Figures 8.13 and 8.14 it is apparent that for each particle size, the cloud reached a terminal velocity value after a lapse of 10 s. These terminal velocity values will be compared to those obtained via experiments with a settling tube in Chapter 9.

```
X=[340       170.00000
  339      169.74895
      ...
    2        0.25148
    1        0.00000];

Y=[  60       15.00000
         ...
    2        0.12931
```

```
          1         0.00000];

fid1 = fopen('Por.bin', 'r');
fid2 = fopen('Us.bin', 'r');
UsAVG = [];
TIME = [];
for i=1:1000
    [Por,count] = fread(fid1,[63,340], 'float32');  %read one time step
    [Us,count] = fread(fid2,[63,339], 'float32');  %read one time step
    Por = reshape(Por, [63,340]);
    %construct matrix
    Us = reshape(Us, [63,339]);
    Por = Por(3:end-1,:)';
    Us = Us(3:end-1,:)';
    %calculate average velocity
    usavg=mean(sum(Us(:,2:end-1).*Por(1:end-1,2:end-1))./sum(Por(1:end-1,2:end-1)));
    UsAVG=[UsAVG usavg ];
    %calculate time step
    time=i.*0.01;
    TIME = [TIME time];
end
plot(flipud(TIME),UsAVG,'-.')
xlabel('time [s]')
ylabel('Average particle velocity [cm/s]')
```
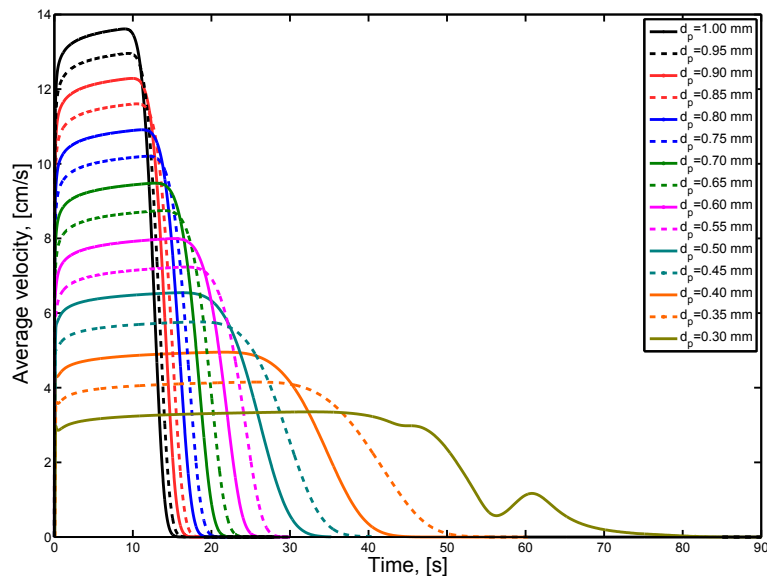


**Figure 8.18:** Average group velocities for vertical particle motion.

### 8.4.4 Comparison between analytical and numerical results

The numerical results were compared to results obtained when the particle momentum conservation equation at terminal velocity, given by Equation (6.6.3), was solved with Matlab's fzero procedure which uses a combination of bisection, secant, and inverse quadratic interpolation methods to obtain the roots for an expression. In deriving the solution to the particle momentum conservation equation it was assumed that the pressure gradient may be approximated with the buoyancy term:

$$\nabla p = \rho_c \, \underline{g}. \tag{8.4.8}$$

However, the former assumption, validated in Appendix A.3.1, should only be applied to cases where the direction of the predominant pressure difference coincides with that of the gravitational force acting on the particles. It was furthermore assumed that terminal velocity was reached. Application of the aforestated assumptions to Equation (6.6.3) yielded the following for the terminal particle velocity:

$$\underline{0} = \epsilon_p \, \underline{g} \, (\rho_p - \rho_c) - \left[ \left[ \frac{\mu \epsilon_p}{d_p^2} \left( \frac{36 \epsilon \epsilon_p^{1/3}}{\left(1 - \epsilon_p^{2/3}\right)\left(1 - \epsilon_p^{1/3}\right)} + 18 \right) \right]^s + \right.$$
$$\left. \left[ \frac{1}{2} \frac{c_d \rho_c}{d_p} \frac{\epsilon_p \epsilon_c^2}{\left(1 - \epsilon_p^{2/3}\right)^2} || \underline{v}_c - \underline{v}_p || \right]^s \right]^{1/s} (\underline{v}_c - \underline{v}_p). \tag{8.4.9}$$

Comparisons between the results obtained by 2PMS and those obtained by solving the terminal velocity expression, given by Equation (8.4.9), with Matlab's fzero algorithm, are illustrated in Figure 8.19 for asymptotic fitting parameters, $s = 0.5$, $s = 0.6$, and $s = 0.7$. From Figure 8.19 it follows that an increase in the value of $s$, increases the magnitude of the group velocity with respect to the particle diameter.

The relative error between the results determined with the fzero procedure in Matlab and those obtained via 2PMS was determined by

$$\%Error = \frac{Val_{Matlab} - Val_{2PMS}}{Val_{Matlab}} \times 100, \tag{8.4.10}$$

for which the maximum error was determined as 0.248%. With this small relative error, the predictive capability of the code was validated.
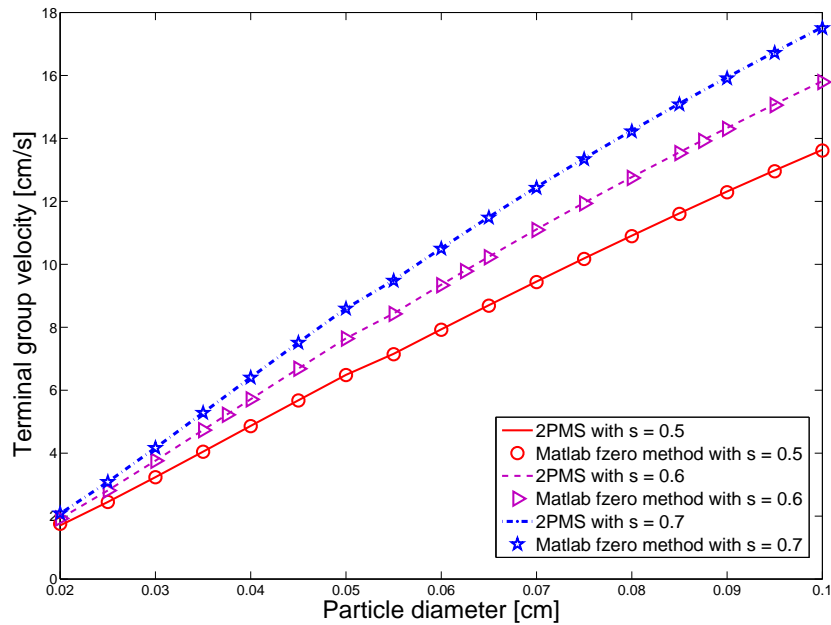
**Figure 8.19:** Comparison of Matlab's fzero terminal velocity solution to results for terminal velocity obtained with 2PMS for different values of the asymptotic fitting parameter, $s$.

## 8.5   Conclusions

In the absence of experimental procedures to verify the precision of numerical predictions for horizontal two phase motion, discussed in Section 8.2, only the simulations for which analytical results were made available is regarded as reliable. Results were not verified for the settling of a deposit within a continuum. However, the trend shown by these horizontal runs do seem to simulate expected physical behaviour.

Results obtained for vertical two-phase motion upheld those produced with Matlab's fzero method. In the next chapter it will also be shown that these results correspond well with physical data obtained through settling tube experiments and the program is therefore regarded as a reliable prediction mechanism.

# Chapter 9

# Physical experiments

In order to further verify the validity of Equations (6.6.2) and (6.6.3), the terminal fall velocity of a group of silica particles were determined with a settling tube which is illustrated in Figure 9.2. A settling tube is an instrument that is used to determine the natural velocity with which a group of particles settles through a water column. In addition to the settling tube, a camera was placed adjacent to the tube and a video was made of the particles as they fell through the lower section of the settling tube. The camera- and the settling tube results were then compared. In the following sections the settling tube components, the experimental procedure, the sample characteristics and results obtained for the terminal settling of silica particles are discussed.

## 9.1   Settling tube components

The settling tube used in this study is illustrated in Figures 9.2 and 9.3. It measures 1.7 m in length with an inner diameter of 15 cm and consists of the following main components:

1. A clear acrylic Sample Insertion Plate (SIP) for inserting the sample;

2. A rotating cradle used to hold and lower the insertion plate at the top of the tube;

3. A DIP-switch that activates the timer;

4. A weighing pan at the bottom of the tube;

**143**

5. The weighing pan is suspended by three thin, copper wires from a strain gauge that is mounted to the wall;

6. A strain gauge amplifier, for amplifying the strain gauge signal;

7. An analogue to digital converter card that accepts the amplifier and DIP-switch signals and is housed in a PC;

8. Software to process the digitised strain signals.

### 9.1.1   Experimental method

Experiments with the settling tube were performed, following a procedure set out by Soltau (2009): A 3.6 g sample of each of the categories of silicon beads, presented in Table 9.1, was spread evenly onto the SIP in a layer of approximately one grain thickness. Water was applied to the SIP and its sample to ensure adhesion of the particles to the plate. The insertion plate and sample were subsequently inverted and placed into the cradle/collar at the top of the tube, the camera was activated and the cradle was lowered smoothly by rotation until the insertion plate and sample made contact with the water. Contact between the sample and the water, broke the adhesive forces and the beads started to fall. Simultaneously, the dip switch triggered the timer.

After falling the length of the tube, the particles settled on the weighing pan and the strain gauge registered the increasing strain due to the accumulation of particles on the plate. The captured strain provided an instantaneous readout of the sample accumulation. An example result from Soltau (2009) is illustrated in Figure 9.1 where the increasing strain is shown as a function of time after insertion. A completed experiment has the appearance of an $S$ shaped curve. In Figure 9.1, the lower upward curve of the $S$, signals the first arrival of material on the pan at approximately 10 seconds and indicates the largest particles which have settled the fastest. This is followed by a steep slope which denotes rapid settling of the trailing particles. Flattening of the slope occurs after about 40-50 seconds as the smallest particles accumulate on the pan. After 157 seconds the entire sample has settled and the strain reading is constant.

In the example in Figure 9.1, fifty percent of the strain was measured after 34 seconds, signifying that fifty percent of the sample had settled at this stage. The velocity for each of the percentiles is determined by

$$\text{Settling velocity(m/s)} \quad = \quad \text{distance particle falls(m)/time taken(s)}, \quad (9.1.1)$$
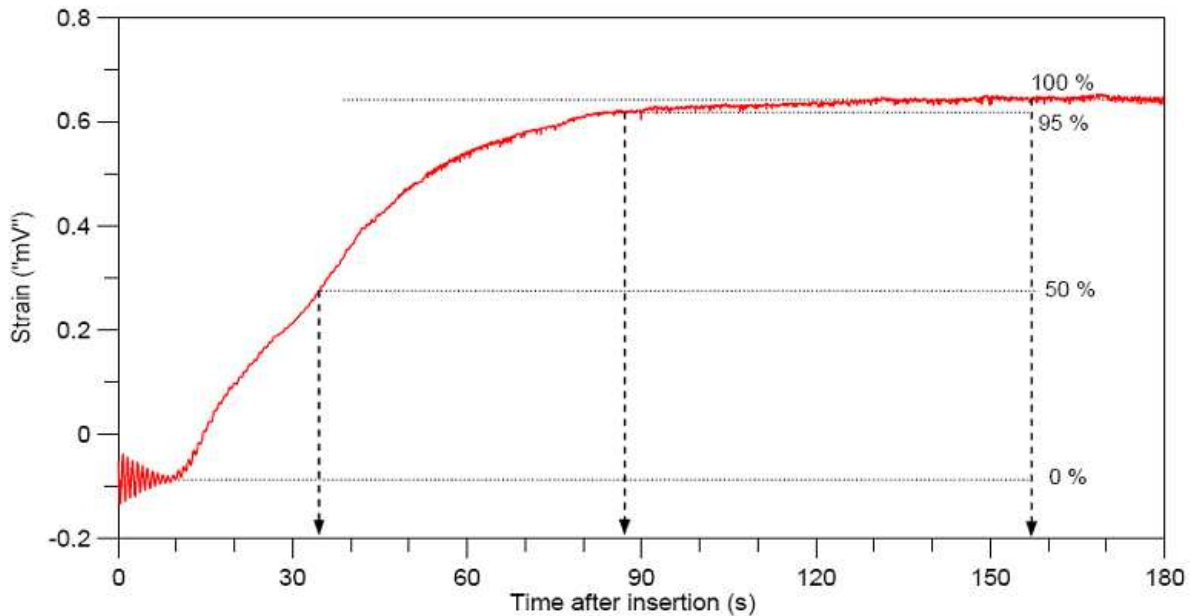
**Figure 9.1:** Strain output.

and the median settling velocity for the $50^{th}$ percentile would therefore be 1.7 m/34 s = 0.05 m/s. The instability seen in the strain record in Figure 9.1 during the first few seconds is due to a slight disturbance of the strain gauge when the sediment is inserted and rapidly diminishes. An example of the output of one of the experiments done during this study with the $0.015 - 0.025$ mm beads is given in Table 9.2. The particle size was determined by the CSIR via an in house developed program. The program calculates the particle size from the *Standard Relation Curve* which is an empirical curve, developed by Fromme in 1977 (Soltau (2009)) and improved by Schoonees (Soltau (2009)), which relates particle size to settling velocity as,

$$D_x \;\; = \;\; 29730w_x^2 + 4173w_x + 67.38, \tag{9.1.2}$$

where $D_x$ is the $x^{th}$ percentile grain size (in μm) and $w_x$ denotes the $x^{th}$ percentile settling velocity (in m/s). The results of Equation (9.1.2) are given in the fourth column of Table 9.2.
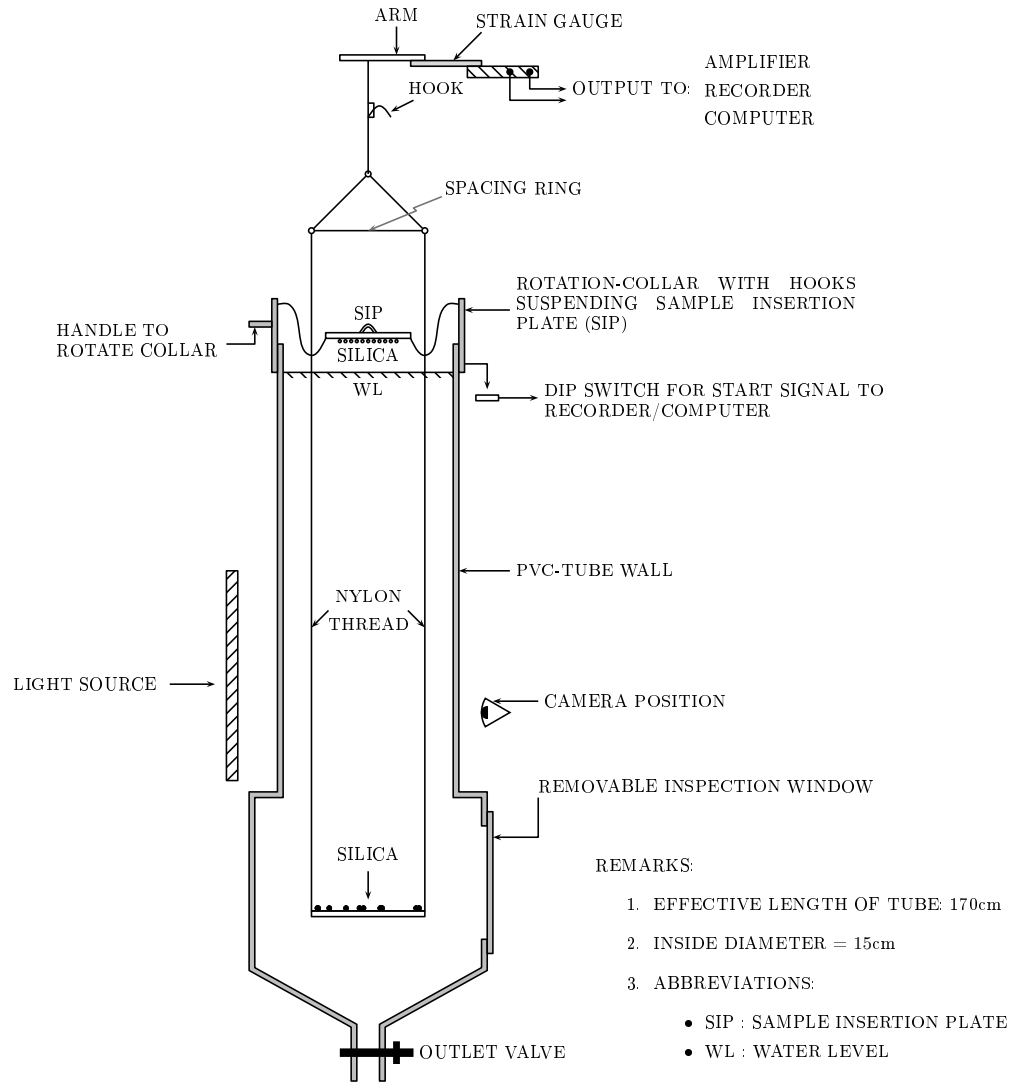
**(a)** Schematic of the settling tube



**(b)** Settling tube

**Figure 9.2:** Settling tube.

(a) Upper mechanism of settling tube

(b) Lower mechanism of settling tube
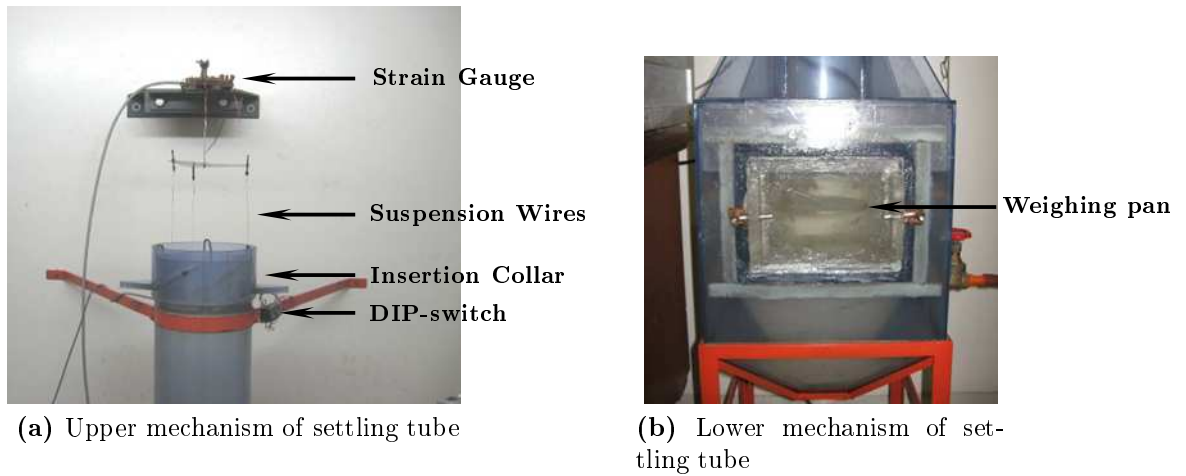
**Figure 9.3:** Mechanisms of settling tube.

The settling tube data were corroborated by making a video of the motion of each of the experiments.

## 9.2 Camera setup

A PowerShot A560 Canon camera was placed adjacent to the settling tube, as shown in Figure 9.4, and the falling particles were photographed on a macro setting at 30 fps.
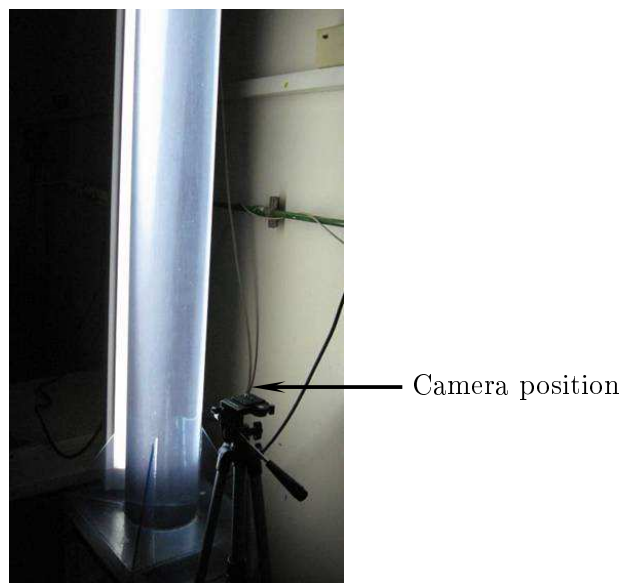


**Figure 9.4:** Light and camera positions.

Reference markings were made on the tube and the speeds of the particles were calculated using Photron FASTCAM viewer software.

## 9.3   Sample characteristics

Spherical glass beads, ranging from 0.15 mm to 1.0 mm in diameter, were used in the experiments and the average size of each sample was regarded as the representative sample size for the purpose of comparison between experimental, simulated and analytical measurements as shown in Figure 9.4.

**Table 9.1:** Particle sizes.

| Size Range [mm] | Average [mm] |
| --- | --- |
| 0.15-0.25 | 0.2 |
| 0.20-0.30 | 0.25 |
| 0.25-0.50 | 0.375 |
| 0.50-0.75 | 0.625 |
| 0.75-1.00 | 0.875 |

The silicon beads were supplied by the company, Sigmund Lindner (SiLi), which provided the chemical composition as 72.5% $SiO_2$, 13% $Na_2O$, 9.06% CaO, 4.22% MgO and 0.58% $Al_2O_3$. The specific weight of the beads were given as 2.50kg/l (i.e. 2.50g/cc) and the three larger samples are shown in Figure 9.5.



**(a)** $0.25 - 0.50$ mm   **(b)** $0.50 - 0.75$ mm   **(c)** $0.75 - 1.00$ mm
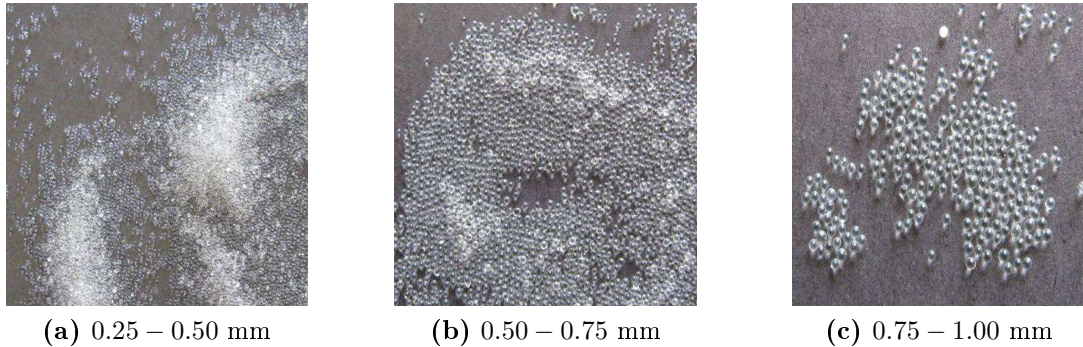
**Figure 9.5:** Silicon beads used for the experiments.

## 9.4 Experimental results and processing

An example of the strain data for a 3.6 g sample of particles, ranging from 0.015 mm to 0.025 mm in diameter, is given in Table 9.2.

**Table 9.2:** Output for strain data for a 3.6g $0.015 - 0.025$ mm sample.

| Percentage in suspension | Percentage on pan | Velocity (m/s) | Size (μ) |
|---|---|---|---|
| 95 | 5 | 0.0308 | 224.37 |
| 90 | 10 | 0.0301 | 220.12 |
| 84 | 16 | 0.0295 | 216.15 |
| 75 | 25 | 0.0289 | 212.88 |
| 50 | 50 | 0.0269 | 201.10 |
| 25 | 75 | 0.0245 | 187.41 |
| 16 | 84 | 0.0234 | 181.29 |
| 10 | 90 | 0.0218 | 172.74 |
| 5 | 95 | 0.0200 | 162.68 |

The percentages listed in the first column of the table are interpreted as the percentage of the total amount of particles which remain in suspension and therefore have a corresponding velocity equal to or slower than those given by the third column.

The percentages listed in the second column correspond with those portrayed in Figure 9.1 and indicate those portions of the total amount of particles that have settled onto the weighing pan and thus have a velocity equal to or faster than the velocity values given by the third column.

The fourth column in Table 9.2 indicates the sizes of the particles that fall in the percentile categories listed in columns 1 and 2 according to Equation (9.1.2). Since the particle sizes are known, the data given by the fourth column was not used for this work. It is, however, apparent from the grain size results for the $0.015 - 0.025$ mm sample, listed in Table 9.2 that the empirical curve provided a fairly accurate estimate of the particle sizes in that it yielded a size range of $0.016 - 0.022$ mm for the given range of $0.015 - 0.025$ mm.

For each of the sample sizes a minimum of 5 experimental runs were made, the results of which are illustrated in Figure 9.6. From the close correlation between the runs it follows that the experimental procedure was successful and that the experiments are repeatable.

The percentage values indicated on the $x$-axis of Figures 9.6a-9.6e denote the percentage of particles which fell slower than the corresponding velocity value on the $y$-axis. The average velocity for each sample set was calculated using the trapezium rule to obtain the entire area underneath the graph for each run and dividing the said area by the 90 units it spans on the $x$-axes. These results are illustrated in Figure 9.8.

As discussed previously, digital images of the falling particles were taken. The positions of a portion of the particles were digitised relative to markings that have been made on the tube, and the speeds of the particles were calculated (using the Photron FAST-CAM viewer software). For various particles within a single experiment, the distance traversed by a particle along with the time required for the distance to be completed was recorded, as illustrated in Figure 9.7. The average of the speeds obtained was then assumed to denote the average speed of the group of particles for that specific experimental run.

Various experiments were done for each of the particle size ranges, listed in Table 9.1, the average of which was used for comparative purposes in Figure 9.8. Example photographs taken for the $0.75 - 1.00$ mm sample are shown in Figure 9.7. The data obtained from the photographic experiments are listed in Appendix G in Table G.1

and the average velocity results for each sample is shown in conjunction with the settling tube experiments in Figure 9.8 from which it follows that close correlation between photographic, settling tube, numerical and analytical results were obtained. The values of the average data obtained for the settling tube and camera data along with the relative difference between the results obtained by these methods are listed in Table 9.3.
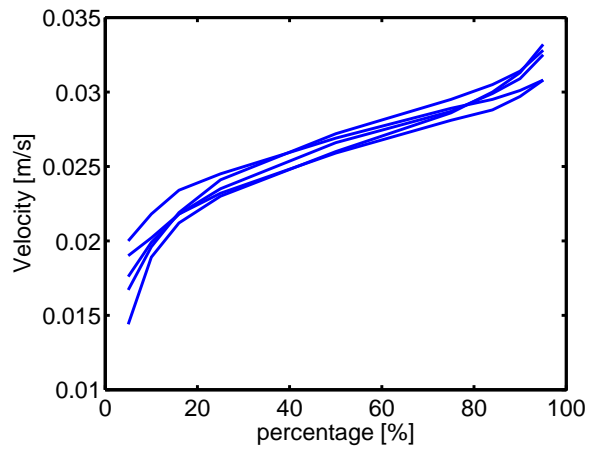
(a) Particle size: $0.15 - 0.25$ mm
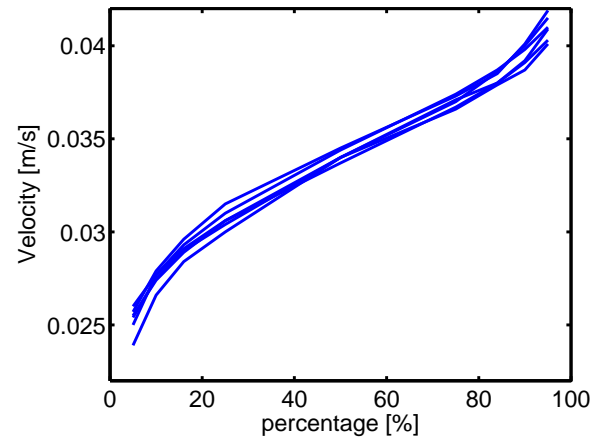
(b) Particle size: $0.20 - 0.30$ mm
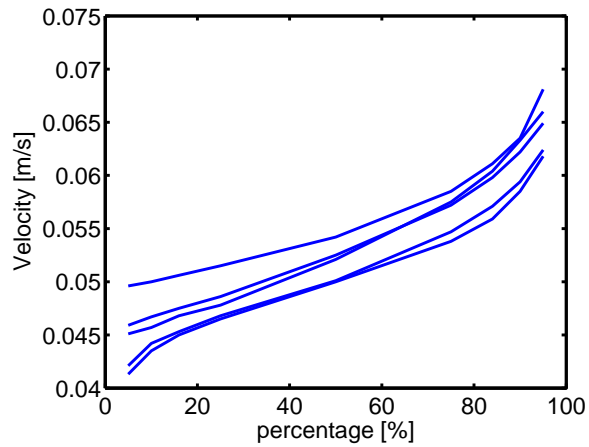
(c) Particle size: $0.25 - 0.50$ mm
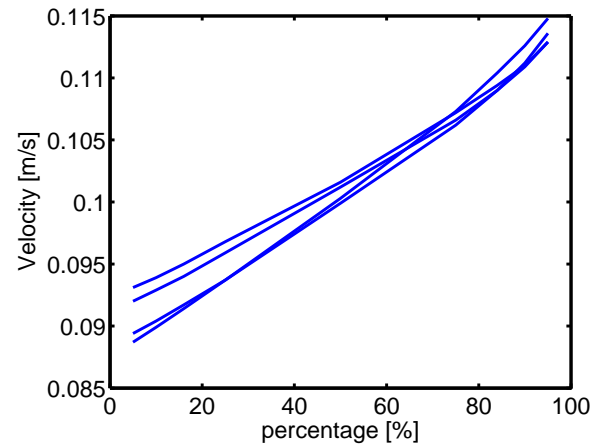
(d) Particle size: $0.50 - 0.75$ mm
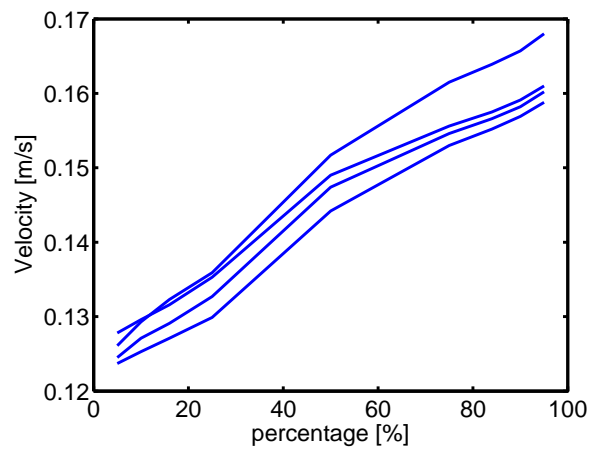
(e) Particle size: $0.75 - 1.00$ mm

**Figure 9.6:** Settling tube data.
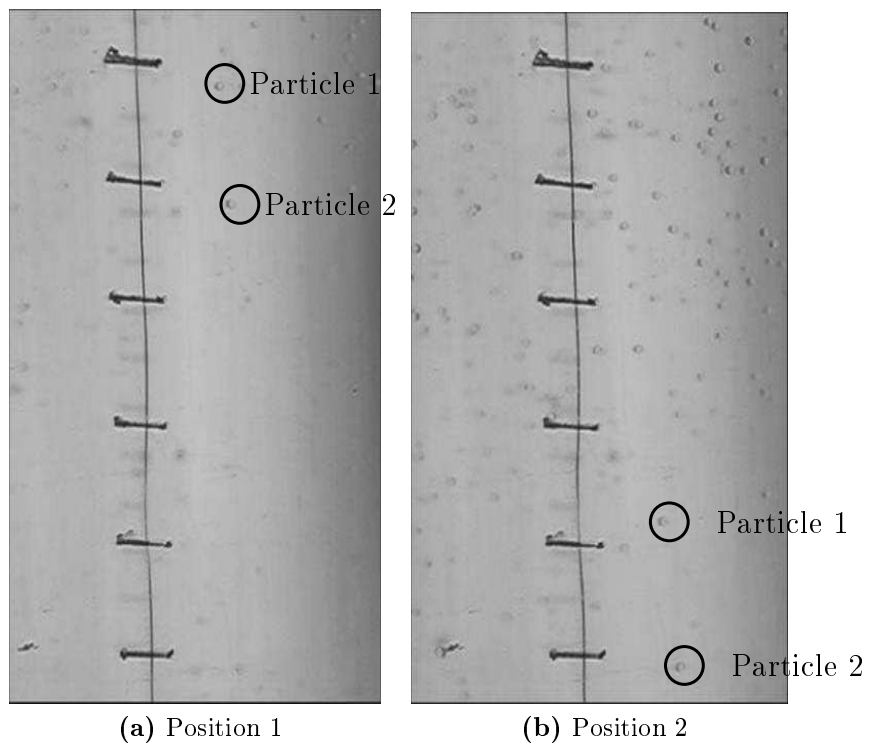
**Figure 9.7:** Particle positions.

**Table 9.3:** Comparison between camera and settling tube data.

| Particle diameter | Average of settling tube data | Average of camera data | Average of numerical data, $s = 0.6$ | Relative difference: settling tube vs camera | Relative difference: settling tube vs numerical | Relative difference: settling tube vs numerical |
|---|---|---|---|---|---|---|
| [mm] | [cm/s] | [cm/s] | [cm/s] | [%] | [%] | [%] |
| 0.02 | 2.47 | 2.61 | 1.93 | 5.61 | 24.8 | 30.3 |
| 0.025 | 3.20 | 3.32 | 2.81 | 3.51 | 13.0 | 16.5 |
| 0.0375 | 4.98 | 5.00 | 5.22 | 0.319 | 4.69 | 4.40 |
| 0.0625 | 9.58 | 9.68 | 9.78 | 1.12 | 2.13 | 1.00 |
| 0.0875 | 13.53 | 13.3 | 13.9 | 1.75 | 2.88 | 4.63 |
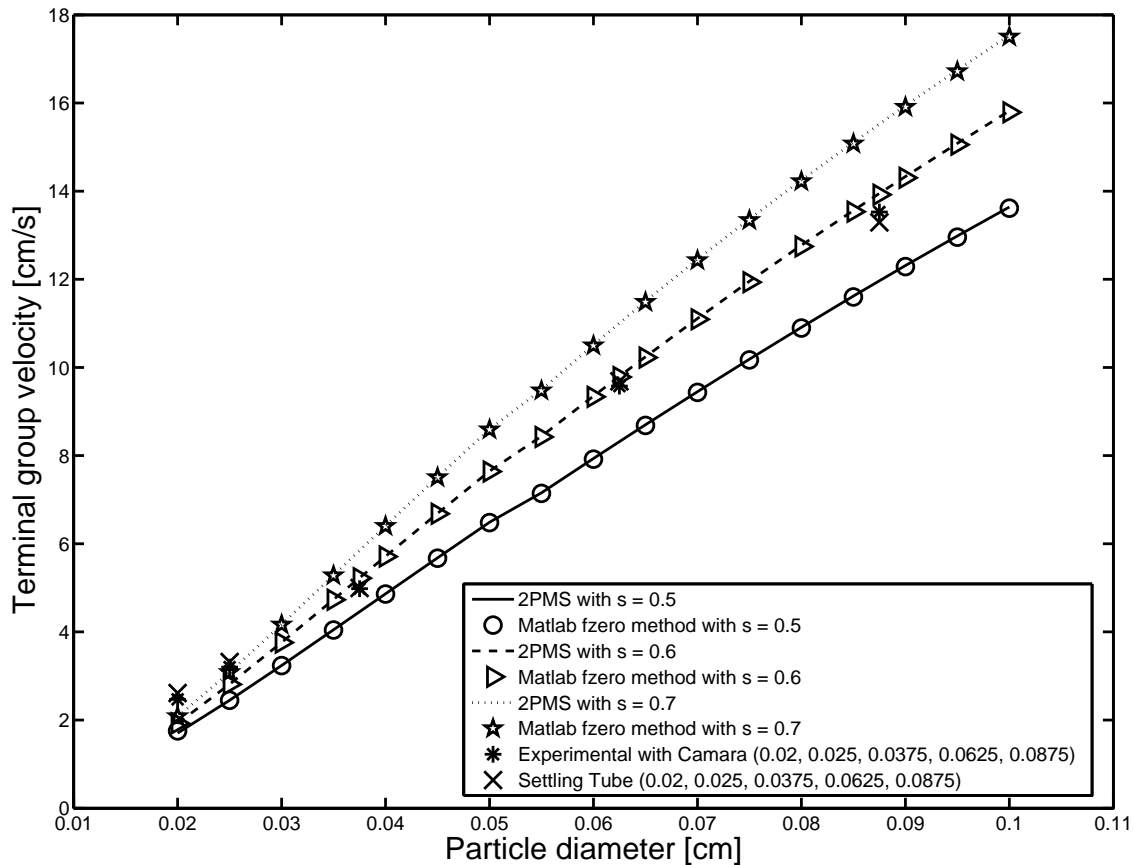
**Figure 9.8:** Correlation between numerical simulations, analytical solution and experiments.

## 9.5   Conclusions

In Table 9.3, results given by 2PMS, the fzero Matlab procedure, as well as camera- and settling tube experimental procedures are compared to each other. For each particle size range, used for experiments and listed in Table 9.1, an average was calculated and associated with the the average obtained from all the experimental results for both the camera and settling tube experiments. These averaged values for the settling tube and camera experiments are listed in columns two and three of Table 9.3, respectively and the relative differences between these two methods are listed in column five. The largest discrepancy was obtained for a particle diameter of $d_p = 0.2$ mm.

From Figure 9.8 it can be seen that the numerical results generated by 2PMS for a fitting coefficient $s = 0.6$, corresponds best to both settling tube- and camera exper-

imental values and the relative percentage differences are listed in columns six and seven of Table 9.3, respectively. As with the comparison between the settling tube and the camera experiments, the greatest difference was found for particles with an average particle diameter of $d_p = 0.2$ mm.

It should be noted that the results obtained numerically are very much dependent on the choice of $s$ of which the physical significance is yet to be determined. However, the numerical output from 2PMS yielded the correct trend when compared to experimental data. Experiments with smaller particles proved more difficult than those done for larger particles since these were influenced most by surface tension at the beginning of the experiment and showed a much more diffusive nature as it spread over nearly the total length of the settling tube during the experiments. This made it difficult to determine a value for the average group velocity since they did not show group behaviour. Experimental results obtained for larger particles are thus deemed more accurate and correlated well with simulations.

# Chapter 10

# Discussion and recommendations

In Chapter 9 the physical results from experiments done at the CSIR were compared to predictions made for the group terminal velocity of different particle sizes. In this chapter the predictions made by Equation (6.6.3) for the group terminal velocity are tested against the widely referenced experimental work of Richardson and Zaki (1954). The results of these experiments were summarised by Concha (2009) in a table relating the ratio between the group- and the Stokes velocities of a single particle to the particle diameters. In this chapter, the actual values of the group velocity obtained by Richardson and Zaki (1954) in relation to the particle diameters and those predicted by Equation (6.6.3) are given.

The prediction capabilities of our model is also compared to the empirically models set forth by Ergun, lewis, Wen and Yu, and Kmiec (Mazzei and Lettieri (2007)).

## 10.1   Empirical work by Richardson and Zaki (1954)

Richardson and Zaki (1954) examined experimentally the effect of the volume fraction of suspended particles upon the rate of settlement of the particles. They confined the experimental work to uniformly sized spherical particles, greater than 100 μm in diameter. The sedimentation experiments were made with suspensions contained in flat-bottomed Pyrex tubes about 10 cm in height with internal diameters of 1.9, 2.8, 3.2, 4.8, and 5 cm. After the tube and its contents attained the temperature of the chamber, the suspension was agitated and the tube was then orientated in the vertical position. The rate at which the sludge line fell was observed. The temperature of the

liquid was maintained at 20 °C. The physical characteristics of the materials used are listed in Table 10.1.

Group velocities obtained for the settling of various types of spherical particles in different types of fluids are listed in Tables 10.2 and 10.3, respectively and graphs of these values can be seen in Appendix H.

Correlations between the experimental data of Richardson and Zaki (1954) and those values predicted by Equation (6.6.3) for terminal velocities, are shown in Figure 10.1. For a perfect correlation between the empirical and theoretical result, the points would be centred on the 45° line. Points that lie above this line are due to the theoretical model yielding higher values than the experiments and those that occur below the line are under-predicting the empirical data.

Figures 10.1a to 10.1j show the correlation between the experimentally obtained group settling velocity of different sized spherical particles at ten separate particle volume fractions in the range of $0 < \epsilon_p \leq 0.585$ performed by Richardson and Zaki (1954). In each case two theoretical approximations are made: Both of which are the solution to Equation (6.6.3) for the scenario of a terminal velocity scenario but differ with regard to the drag coefficient, $c_d$, and the shifting parameter, $s$.

The first approximation was made by choosing the shifting factor $s = 0.6$ and the drag coefficient $c_d = 0.44$. The value for $c_d$ is chosen here to be the value for the drag coefficient of a single sphere and $s$ is based on the best fit that was achieved on the basis of inspection with data obtained during experiments discussed in Chapter 9. The drawback of this choice of shifting parameter is that Equation (6.6.3) is not analytical solvable, but the terminal velocity may readily be achieved by using any numerical integration technique. In this case the fzero method was applied in Matlab.

The second theoretical approximation is based on a shifting factor $s = 1.0$ and a drag coefficient $c_d = 2.05$ which are based on investigations done on foams (Du Plessis (1992), Du Plessis and Masliyah (1988)). This choice of $s$ has the benefit of rendering a quadratic equation for which analytical solutions are easily obtainable.

The higher the value of $s$, the more closely the solution traces the asymptotic expressions, i.e. the more abrupt the transition (Churchill and Usagi (1972)). Conversely a gradual change-over between extremal solutions will signify that a small $s$ be used. Hence, $s$, is indicative of the rate of transition between the constituent predictive equa-

tions. The afore mentioned influence of the shifting parameter was also discussed in Section 6.6.1 and shown in Figure 6.7. Churchill and Usagi (1972) recommends that experiments should be set up so as to investigate the behaviour in region of the point where the asymptotes of the extreme behaviours meet in order for correct approximations to be made. It is further recommended in this work that the Forchheimer regime be treated in a similar manner to the Darcy regime, i.e. that it should be split into a low particle volume fraction (or single particle) and a high volume fraction (or porous bed) part and that these should then be matched in a manner similar to that used to match the high and low particle volume fraction scenarios for the Darcy regime.

For particle volume fractions tending to zero, both theoretical models coincide well with the values obtained by Richardson and Zaki (1954) for velocities up to 10 cm/s. Once this limit is exceeded the theoretical model with $s = 1$ and $c_d = 2.05$ however tends to under-predict the experimental values as is shown in Figure 10.1a. From Figures 10.1b to 10.1f it can be seen that for velocities up to 1 cm/s both models under-predict the results whereas for higher velocities the model with $c_d = 2.05$ and $s = 1.0$ tends to under predict whilst its counter part matches the data well. As the particle volume fraction increases further so does the accuracy of both models as can be seen from Figures 10.1g and 10.1h but tends to over prediction of the experimental values as the particle volume fraction increases above $\epsilon_p = 0.500$ in Figures 10.1i and 10.1j.

## 10.2    Comparisons to empirical models

In the following sections, the predictions made by Equation (6.6.3) for the group terminal velocity are tested against the empirical Ergun equation (Ergun (1952)) as well as empirical models by Lewis, Wen and Yu, and Kmiec (Mazzei and Lettieri (2007)) which are based on the aforementioned experimental data of Richardson and Zaki (1954).

### 10.2.1    The Ergun equation

The empirical Ergun model is given by

$$\underline{F}_{ERGUN} \;=\; \left( \frac{150 \mu_c \epsilon_p^2}{d_p^2 \epsilon^2} + \frac{1.75 \rho_c \epsilon_p || \, \underline{v}_c - \underline{v}_p ||}{d_p \epsilon_c} \right) \left( \underline{v}_c - \underline{v}_p \right). \qquad (10.2.1)$$

The Ergun equation was developed only for packed beds and was never meant to account for large variations in concentration as is found in sedimentation problems.

In spite of this limitation, it is commonly employed by many researchers over a wide range of particle volume fractions. It is used in the multiphase flow model, proposed by Gidaspow (1994), which has been adopted as default in the majority of commercial CFD codes used to date (e.g. Fluent). This correlation is used for values of the continuum volume fraction up to 0.80.

## 10.2.2 Lewis, Wen and Yu, and Kmiec drag force closures

The most widespread and popular equations of closure employed to model the drag force in uniformly dispersed emulsions of solid particles are those based on the work by Kmiec (1982), Lewis et al. (1949), and Wen and Yu (1966). In particular, the equation developed by Lewis is usually adopted as default correlation in most commercial CFD codes when the continuum volume fraction of the suspension exceeds the threshold value of 0.80 (a limit suggested by Gidaspow (1994)). Following Mazzei and Lettieri (2007), all three these closure relationships can be expressed in the following form:

$$\underline{F}(\epsilon_c, ||\underline{v}_c - \underline{v}_p||) = \frac{3}{4} C_D(Re) \frac{\rho_c ||\underline{v}_c - \underline{v}_p||(1 - \epsilon_c)}{d_p} \epsilon_c^{-\alpha}. \qquad (10.2.2)$$

Here the Reynolds number is defined as,

$$Re(\epsilon_c, ||\underline{v}_c - \underline{v}_p||) = \frac{\rho_c \epsilon d_p}{\mu_c} ||\underline{v}_c - \underline{v}_p||, \qquad (10.2.3)$$

and the drag coefficient $C_D(Re)$ is calculated using the expression suggested by Schiller and Naumann (1935):

$$C_D(Re) = \begin{cases} \frac{24}{Re}\left(1 + 0.15Re^{0.687}\right) & \text{for } Re < 1000 \\ \\ 0.44 & \text{for } Re \geq 1000. \end{cases}$$

The drag is calculated for the limiting values of the viscous and inertial regimes and an expression for the intermediate range is derived following the asymptotic matching technique introduced by Churchill and Usagi (1972),

$$\underline{F}_{tot}(\epsilon_c, ||\underline{v}_c - \underline{v}_p||) = \frac{18\mu_c(1 - \epsilon_c)\epsilon_c^{-\alpha}}{\epsilon_c d_p^2} + 0.33 \frac{\rho_c ||\underline{v}_c - \underline{v}_p||\epsilon_p}{d_p}\epsilon_c^{-\alpha}. \quad (10.2.4)$$

The respective values for $\alpha$, as proposed by Lewis et al., Wen and Yu, and Kmiec, are 2.65, 2.70 and 2.78, respectively. The drag force closures, given by Equations (10.2.1) and (10.2.4) were implemented in 2PMS and the results were compared to

those obtained for our model in Figure 10.2. From Figure 10.2 it can be seen that the models proposed by Lewis and Wen and Yu, yield almost identical results. Both, however, overestimate the experimental data. The Ergun equation overestimates the velocities of the smaller particles and underestimates the velocities yielded for larger particle diameters. The results were also compared with the settling tube equation, by solving Equation (9.1.2) for the velocity and obtaining the following expression for the fall velocity in terms of the particle diameter:

$$v_{settle} \;=\; \left(-0.702*10^{-1} + 0.336*10^{-5}\left(235027485 + 2973000 d_p\right)^{1/2}\right)100,$$
$$(10.2.5)$$

where the multiplication with 100 is due to the fact that the velocities and particle diameters in Equation (9.1.2) are in metres per second and micrometres, respectively. The results obtained for the velocities with Equation (10.2.5) yield a good approximation for the experimental trend but tend to underestimate the velocity of the larger particles. The current model yielded a good approximation of the experimental data for the entire range of particle diameters, thus exceeding the prediction capabilities of its counterparts.

## 10.3   Conclusions

The results yielded by Equation (6.6.3) produced good predictions for both the experiments done at the CSIR for this study as well as with the experimental data by Richardson and Zaki (1954) and empirical models based on this data (e.g. Lewis and Wen and Yu). The theoretical model however still remains dependent on the shifting factor $s$. An effort was made not to introduce empirical coefficients too early in the development of the model but after testing it on existing as well as new experimental data it is apparent that the introduction of certain empirical coefficients may be inevitable due to the existence of certain geometrical effects.

**Table 10.1:** Physical properties of material used for experiments done by Richardson and Zaki (1954).

| No. | $d_p$ [cm] | $\rho_p$ [g/cm$^3$] | $\mu_c \times 10^2$ [g/(cm.s)] | $\rho_c$ g/cm$^3$ |
|---|---|---|---|---|
| 1 | 0.0181 | 1.0580 | 20.8000 | 1.0340 |
| 2 | 0.0181 | 1.0580 | 20.8000 | 1.0340 |
| 3 | 0.0096 | 2.9230 | 62.0000 | 1.2080 |
| 4 | 0.0096 | 2.9230 | 62.0000 | 1.2080 |
| 5 | 0.0358 | 1.0580 | 20.8000 | 1.0340 |
| 6 | 0.0358 | 1.0580 | 20.8000 | 1.0340 |
| 7 | 0.0096 | 2.9230 | 20.8000 | 1.0340 |
| 8 | 0.0096 | 2.9230 | 20.8000 | 1.0340 |
| 9 | 0.0096 | 2.9230 | 20.8000 | 1.0340 |
| 10 | 0.0230 | 2.6230 | 62.0000 | 1.2080 |
| 11 | 0.0230 | 2.6230 | 62.0000 | 1.2080 |
| 12 | 0.0128 | 2.9600 | 1.8900 | 2.8900 |
| 13 | 0.0128 | 2.9600 | 1.8900 | 2.8900 |
| 14 | 0.0181 | 1.0580 | 1.5300 | 1.0010 |
| 15 | 0.0181 | 1.0580 | 1.5300 | 1.0010 |
| 16 | 0.0181 | 1.0580 | 1.5300 | 1.0010 |
| 17 | 0.1029 | 2.9760 | 112.9000 | 1.2210 |
| 18 | 0.1029 | 2.9760 | 112.9000 | 1.2210 |
| 19 | 0.0253 | 1.0580 | 2.9100 | 0.9350 |
| 20 | 0.0253 | 1.0580 | 2.9100 | 0.9350 |
| 21 | 0.0096 | 2.9230 | 1.6120 | 2.1700 |
| 22 | 0.0096 | 2.9230 | 1.6120 | 2.1700 |
| 23 | 0.0253 | 2.7800 | 6.0750 | 1.1350 |
| 24 | 0.0253 | 1.0600 | 1.0000 | 1.0000 |
| 25 | 0.0230 | 2.6230 | 1.8900 | 2.8900 |
| 26 | 0.0230 | 2.6230 | 1.8900 | 2.8900 |
| 27 | 0.0230 | 2.6230 | 1.8900 | 2.8900 |
| 28 | 0.0230 | 2.6230 | 1.6120 | 2.1700 |
| 29 | 0.0230 | 2.6230 | 1.6120 | 2.1700 |
| 30 | 0.0230 | 2.6230 | 1.6120 | 2.1700 |
| 31 | 0.0510 | 2.7450 | 6.0750 | 1.1350 |
| 32 | 0.1029 | 2.9760 | 10.9600 | 1.1530 |
| 33 | 0.1029 | 2.9760 | 10.9600 | 1.1530 |
| 34 | 0.1029 | 2.9760 | 10.9600 | 1.1530 |
| 35 | 0.0253 | 2.7800 | 1.0000 | 1.0000 |
| 36 | 0.1029 | 10.6000 | 15.0100 | 0.8750 |
| 37 | 0.1029 | 2.9760 | 1.8900 | 2.8900 |
| 38 | 0.1029 | 2.9760 | 1.8900 | 2.8900 |
| 39 | 0.1029 | 2.9760 | 1.8900 | 2.8900 |
| 40 | 0.1029 | 2.9760 | 1.8390 | 2.7450 |
| 41 | 0.1029 | 2.9760 | 1.8390 | 2.7450 |
| 42 | 0.1029 | 2.9760 | 1.8390 | 2.7450 |
| 43 | 0.0510 | 2.7450 | 1.0000 | 1.0000 |
| 44 | 0.1029 | 2.7450 | 1.0000 | 1.0000 |
| 45 | 0.1029 | 2.7450 | 1.0000 | 1.0000 |
| 46 | 0.4200 | 2.8900 | 15.0100 | 0.8750 |
| 47 | 0.1029 | 10.6000 | 3.8100 | 0.8180 |
| 48 | 0.2466 | 11.2500 | 15.0100 | 0.8750 |
| 49 | 0.3175 | 7.7300 | 15.0100 | 0.8750 |
| 50 | 0.4200 | 2.8900 | 6.0750 | 1.1350 |
| 51 | 0.1029 | 10.6000 | 1.0000 | 1.0000 |
| 52 | 0.4200 | 2.8900 | 1.0000 | 1.0000 |
| 53 | 0.3175 | 7.7300 | 1.0000 | 1.0000 |
| 54 | 0.6350 | 7.7400 | 1.0000 | 1.0000 |

**Table 10.2:** Empirical group velocities for various solid volume fractions and particle sizes (Richardson and Zaki (1954)).

| Nr. | Particle diameter [cm] | Reynolds number | Velocity $\epsilon_p = 0.0$ [cm/s] | Velocity $\epsilon_p = 0.01$ [cm/s] | Velocity $\epsilon_p = 0.05$ [cm/s] | Velocity $\epsilon_p = 0.1$ [cm/s] | Velocity $\epsilon_p = 0.15$ [cm/s] | Velocity $\epsilon_p = 0.2$ [cm/s] | Velocity $\epsilon_p = 0.3$ [cm/s] | Velocity $\epsilon_p = 0.4$ [cm/s] | Velocity $\epsilon_p = 0.5$ [cm/s] | Velocity $\epsilon_p = 0.585$ [cm/s] |
|---|---|---|---|---|---|---|---|---|---|---|---|---|
| 1 | 0.0181 | 0.0002 | 0.0021 | 0.0020 | 0.0017 | 0.0014 | 0.0011 | 0.0009 | 0.0005 | 0.0003 | 0.0001 | 0.0001 |
| 2 | 0.0181 | 0.0002 | 0.0021 | 0.0020 | 0.0017 | 0.0014 | 0.0011 | 0.0009 | 0.0005 | 0.0003 | 0.0002 | 0.0001 |
| 3 | 0.0096 | 0.0003 | 0.0139 | 0.0134 | 0.0115 | 0.0094 | 0.0076 | 0.0060 | 0.0036 | 0.0020 | 0.0010 | 0.0005 |
| 4 | 0.0096 | 0.0003 | 0.0139 | 0.0134 | 0.0115 | 0.0095 | 0.0077 | 0.0062 | 0.0038 | 0.0022 | 0.0011 | 0.0006 |
| 5 | 0.0358 | 0.0014 | 0.0081 | 0.0078 | 0.0066 | 0.0054 | 0.0043 | 0.0034 | 0.0020 | 0.0011 | 0.0005 | 0.0003 |
| 6 | 0.0358 | 0.0014 | 0.0081 | 0.0078 | 0.0066 | 0.0054 | 0.0043 | 0.0034 | 0.0020 | 0.0011 | 0.0005 | 0.0003 |
| 7 | 0.0096 | 0.0022 | 0.0455 | 0.0438 | 0.0375 | 0.0306 | 0.0247 | 0.0197 | 0.0119 | 0.0067 | 0.0034 | 0.0017 |
| 8 | 0.0096 | 0.0022 | 0.0455 | 0.0438 | 0.0376 | 0.0307 | 0.0249 | 0.0198 | 0.0121 | 0.0068 | 0.0035 | 0.0017 |
| 9 | 0.0096 | 0.0022 | 0.0455 | 0.0438 | 0.0377 | 0.0308 | 0.0250 | 0.0200 | 0.0122 | 0.0069 | 0.0035 | 0.0018 |
| 10 | 0.0230 | 0.0030 | 0.0659 | 0.0634 | 0.0541 | 0.0439 | 0.0352 | 0.0279 | 0.0167 | 0.0092 | 0.0046 | 0.0022 |
| 11 | 0.0230 | 0.0030 | 0.0659 | 0.0634 | 0.0542 | 0.0442 | 0.0355 | 0.0282 | 0.0170 | 0.0095 | 0.0047 | 0.0023 |
| 12 | 0.0128 | 0.0648 | 0.0331 | 0.0318 | 0.0272 | 0.0221 | 0.0177 | 0.0141 | 0.0084 | 0.0047 | 0.0023 | 0.0011 |
| 13 | 0.0128 | 0.0648 | 0.0331 | 0.0319 | 0.0274 | 0.0224 | 0.0181 | 0.0144 | 0.0088 | 0.0049 | 0.0025 | 0.0013 |
| 14 | 0.0181 | 0.0758 | 0.0640 | 0.0616 | 0.0528 | 0.0431 | 0.0347 | 0.0277 | 0.0167 | 0.0094 | 0.0047 | 0.0023 |
| 15 | 0.0181 | 0.0786 | 0.0664 | 0.0638 | 0.0544 | 0.0440 | 0.0352 | 0.0278 | 0.0165 | 0.0091 | 0.0044 | 0.0022 |
| 16 | 0.0181 | 0.0786 | 0.0664 | 0.0639 | 0.0547 | 0.0445 | 0.0359 | 0.0285 | 0.0172 | 0.0096 | 0.0048 | 0.0024 |
| 17 | 0.1029 | 0.0992 | 0.8910 | 0.8533 | 0.7146 | 0.5664 | 0.4430 | 0.3413 | 0.1922 | 0.0991 | 0.0452 | 0.0203 |
| 18 | 0.1029 | 0.0992 | 0.8910 | 0.8542 | 0.7183 | 0.5724 | 0.4502 | 0.3490 | 0.1992 | 0.1043 | 0.0485 | 0.0222 |
| 19 | 0.0253 | 0.1199 | 0.1475 | 0.1418 | 0.1205 | 0.0974 | 0.0778 | 0.0612 | 0.0362 | 0.0197 | 0.0096 | 0.0046 |
| 20 | 0.0253 | 0.1199 | 0.1475 | 0.1418 | 0.1208 | 0.0978 | 0.0783 | 0.0618 | 0.0367 | 0.0201 | 0.0099 | 0.0048 |
| 21 | 0.0096 | 0.3024 | 0.2340 | 0.2254 | 0.1932 | 0.1578 | 0.1274 | 0.1016 | 0.0616 | 0.0346 | 0.0175 | 0.0087 |
| 22 | 0.0096 | 0.3024 | 0.2340 | 0.2256 | 0.1940 | 0.1593 | 0.1293 | 0.1036 | 0.0637 | 0.0363 | 0.0186 | 0.0094 |
| 23 | 0.0253 | 0.3909 | 0.8270 | 0.7972 | 0.6858 | 0.5630 | 0.4570 | 0.3663 | 0.2250 | 0.1282 | 0.0659 | 0.0334 |
| 24 | 0.0253 | 0.4908 | 0.1940 | 0.1872 | 0.1619 | 0.1337 | 0.1093 | 0.0882 | 0.0551 | 0.0320 | 0.0168 | 0.0087 |
| 25 | 0.0230 | 1.2274 | 0.3490 | 0.3371 | 0.2924 | 0.2426 | 0.1992 | 0.1616 | 0.1020 | 0.0599 | 0.0319 | 0.0168 |
| 26 | 0.0230 | 1.2274 | 0.3490 | 0.3369 | 0.2913 | 0.2409 | 0.1970 | 0.1591 | 0.0994 | 0.0578 | 0.0304 | 0.0158 |
| 27 | 0.0230 | 1.2274 | 0.3490 | 0.3382 | 0.2971 | 0.2507 | 0.2095 | 0.1732 | 0.1139 | 0.0702 | 0.0396 | 0.0221 |
| 28 | 0.0230 | 2.0202 | 0.6525 | 0.6312 | 0.5509 | 0.4609 | 0.3816 | 0.3124 | 0.2011 | 0.1209 | 0.0662 | 0.0358 |
| 29 | 0.0230 | 2.0202 | 0.6525 | 0.6309 | 0.5495 | 0.4585 | 0.3786 | 0.3090 | 0.1975 | 0.1179 | 0.0640 | 0.0343 |
| 30 | 0.0230 | 2.0202 | 0.6525 | 0.6316 | 0.5526 | 0.4638 | 0.3854 | 0.3167 | 0.2054 | 0.1247 | 0.0691 | 0.0378 |
| 31 | 0.0510 | 2.7537 | 2.8900 | 2.7980 | 2.4500 | 2.0585 | 1.7125 | 1.4088 | 0.9164 | 0.5579 | 0.3102 | 0.1702 |
| 32 | 0.1029 | 6.5276 | 6.0300 | 5.8333 | 5.0910 | 4.2591 | 3.5269 | 2.8875 | 1.8584 | 1.1174 | 0.6122 | 0.3310 |
| 33 | 0.1029 | 6.5276 | 6.0300 | 5.8468 | 5.1514 | 4.3635 | 3.6613 | 3.0395 | 2.0173 | 1.2567 | 0.7181 | 0.4053 |
| 34 | 0.1029 | 6.5276 | 6.0300 | 5.8509 | 5.1700 | 4.3959 | 3.7032 | 3.0874 | 2.0683 | 1.3025 | 0.7538 | 0.4310 |
| 35 | 0.0253 | 8.9815 | 3.5500 | 3.4588 | 3.1084 | 2.7022 | 2.3304 | 1.9917 | 1.4094 | 0.9454 | 0.5896 | 0.3639 |
| 36 | 0.1029 | 11.7571 | 19.6000 | 19.0714 | 17.0477 | 14.7163 | 12.5973 | 10.6822 | 7.4288 | 4.8845 | 2.9747 | 1.7920 |
| 37 | 0.1029 | 18.2520 | 1.1600 | 1.1278 | 1.0048 | 0.8636 | 0.7359 | 0.6210 | 0.4273 | 0.2775 | 0.1666 | 0.0989 |
| 38 | 0.1029 | 18.2520 | 1.1600 | 1.1296 | 1.0131 | 0.8783 | 0.7553 | 0.6436 | 0.4524 | 0.3011 | 0.1861 | 0.1138 |
| 39 | 0.1029 | 18.2520 | 1.1600 | 1.1271 | 1.0017 | 0.8582 | 0.7288 | 0.6128 | 0.4182 | 0.2691 | 0.1598 | 0.0938 |
| 40 | 0.1029 | 38.0915 | 2.4800 | 2.4224 | 2.1995 | 1.9381 | 1.6955 | 1.4712 | 1.0764 | 0.7504 | 0.4898 | 0.3167 |
| 41 | 0.1029 | 38.0915 | 2.4800 | 2.4170 | 2.1748 | 1.8937 | 1.6359 | 1.4008 | 0.9952 | 0.6707 | 0.4206 | 0.2610 |
| 42 | 0.1029 | 38.0915 | 2.4800 | 2.4185 | 2.1815 | 1.9057 | 1.6520 | 1.4196 | 1.0167 | 0.6915 | 0.4384 | 0.2752 |
| 43 | 0.0510 | 41.3100 | 8.1000 | 7.9301 | 7.2691 | 6.4854 | 5.7486 | 5.0583 | 3.8163 | 2.7567 | 1.8764 | 1.2664 |
| 44 | 0.1029 | 75.6315 | 7.3500 | 7.1475 | 6.3732 | 5.4838 | 4.6781 | 3.9525 | 2.7269 | 1.7764 | 1.0701 | 0.6375 |
| 45 | 0.1029 | 75.6315 | 7.3500 | 7.1475 | 6.3732 | 5.4838 | 4.6781 | 3.9525 | 2.7269 | 1.7764 | 1.0701 | 0.6375 |
| 46 | 0.4200 | 78.1029 | 31.9000 | 31.1586 | 28.2921 | 24.9299 | 21.8088 | 18.9244 | 13.8459 | 9.6529 | 6.3006 | 4.0739 |
| 47 | 0.1029 | 79.8642 | 36.1500 | 35.4021 | 32.4916 | 29.0357 | 25.7811 | 22.7268 | 17.2154 | 12.4927 | 8.5498 | 5.8028 |
| 48 | 0.2466 | 83.5212 | 58.1000 | 56.7213 | 51.3970 | 45.1664 | 39.3994 | 34.0849 | 24.7721 | 17.1378 | 11.0843 | 7.1010 |
| 49 | 0.3175 | 101.2415 | 54.7000 | 53.5201 | 48.9379 | 43.5204 | 38.4437 | 33.7050 | 25.2260 | 18.0543 | 12.1549 | 8.1126 |
| 50 | 0.4200 | 267.1874 | 34.0500 | 33.5137 | 31.3992 | 28.8284 | 26.3390 | 23.9331 | 19.3809 | 15.1914 | 11.3890 | 8.4846 |
| 51 | 0.1029 | 488.7750 | 47.5000 | 46.8222 | 44.1408 | 40.8567 | 37.6499 | 34.5235 | 28.5223 | 22.8798 | 17.6287 | 13.5052 |
| 52 | 0.4200 | 2041.2000 | 48.6000 | 47.9546 | 45.3948 | 42.2456 | 39.1526 | 36.1200 | 30.2423 | 24.6363 | 19.3316 | 15.0884 |
| 53 | 0.3175 | 2530.4750 | 79.7000 | 78.6177 | 74.3298 | 69.0601 | 63.8955 | 58.8385 | 49.0673 | 39.7870 | 31.0495 | 24.0989 |
| 54 | 0.6350 | 7156.4500 | 112.7000 | 111.1481 | 104.9981 | 97.4494 | 90.0574 | 82.8300 | 68.8901 | 55.6896 | 43.3016 | 33.4832 |

**Table 10.3:** Theoretical group velocities for various solid volume fractions and particle sizes as approximated by Equation (6.6.3).

| Nr. | Particle diameter [cm] | Reynolds number | Velocity $\epsilon_p = 0.0$ [cm/s] | Velocity $\epsilon_p = 0.01$ [cm/s] | Velocity $\epsilon_p = 0.05$ [cm/s] | Velocity $\epsilon_p = 0.1$ [cm/s] | Velocity $\epsilon_p = 0.15$ [cm/s] | Velocity $\epsilon_p = 0.2$ [cm/s] | Velocity $\epsilon_p = 0.3$ [cm/s] | Velocity $\epsilon_p = 0.4$ [cm/s] | Velocity $\epsilon_p = 0.5$ [cm/s] | Velocity $\epsilon_p = 0.585$ [cm/s] |
|---|---|---|---|---|---|---|---|---|---|---|---|---|
| 1 | 0.0181 | 0.0002 | 0.0021 | 0.0013 | 0.0009 | 0.0007 | 0.0006 | 0.0005 | 0.0003 | 0.0002 | 0.0002 | 0.0001 |
| 2 | 0.0181 | 0.0002 | 0.0021 | 0.0013 | 0.0009 | 0.0007 | 0.0006 | 0.0005 | 0.0003 | 0.0002 | 0.0002 | 0.0001 |
| 3 | 0.0096 | 0.0003 | 0.0139 | 0.0088 | 0.0061 | 0.0046 | 0.0038 | 0.0031 | 0.0023 | 0.0017 | 0.0012 | 0.0009 |
| 4 | 0.0096 | 0.0003 | 0.0139 | 0.0088 | 0.0061 | 0.0046 | 0.0038 | 0.0031 | 0.0023 | 0.0017 | 0.0012 | 0.0009 |
| 5 | 0.0358 | 0.0014 | 0.0080 | 0.0051 | 0.0035 | 0.0027 | 0.0022 | 0.0018 | 0.0013 | 0.0010 | 0.0007 | 0.0005 |
| 6 | 0.0358 | 0.0014 | 0.0080 | 0.0051 | 0.0035 | 0.0027 | 0.0022 | 0.0018 | 0.0013 | 0.0010 | 0.0007 | 0.0005 |
| 7 | 0.0096 | 0.0022 | 0.0455 | 0.0290 | 0.0200 | 0.0153 | 0.0124 | 0.0103 | 0.0074 | 0.0055 | 0.0040 | 0.0030 |
| 8 | 0.0096 | 0.0022 | 0.0455 | 0.0290 | 0.0200 | 0.0153 | 0.0124 | 0.0103 | 0.0074 | 0.0055 | 0.0040 | 0.0030 |
| 9 | 0.0096 | 0.0022 | 0.0455 | 0.0290 | 0.0200 | 0.0153 | 0.0124 | 0.0103 | 0.0074 | 0.0055 | 0.0040 | 0.0030 |
| 10 | 0.0230 | 0.0030 | 0.0656 | 0.0418 | 0.0288 | 0.0220 | 0.0178 | 0.0149 | 0.0107 | 0.0079 | 0.0058 | 0.0044 |
| 11 | 0.0230 | 0.0030 | 0.0656 | 0.0418 | 0.0288 | 0.0220 | 0.0178 | 0.0149 | 0.0107 | 0.0079 | 0.0058 | 0.0044 |
| 12 | 0.0128 | 0.0648 | 0.0323 | 0.0208 | 0.0144 | 0.0110 | 0.0089 | 0.0074 | 0.0054 | 0.0040 | 0.0029 | 0.0022 |
| 13 | 0.0128 | 0.0648 | 0.0323 | 0.0208 | 0.0144 | 0.0110 | 0.0089 | 0.0074 | 0.0054 | 0.0040 | 0.0029 | 0.0022 |
| 14 | 0.0181 | 0.0758 | 0.0649 | 0.0417 | 0.0288 | 0.0221 | 0.0179 | 0.0150 | 0.0108 | 0.0079 | 0.0058 | 0.0044 |
| 15 | 0.0181 | 0.0786 | 0.0649 | 0.0417 | 0.0288 | 0.0221 | 0.0179 | 0.0150 | 0.0108 | 0.0079 | 0.0058 | 0.0044 |
| 16 | 0.0181 | 0.0786 | 0.0649 | 0.0417 | 0.0288 | 0.0221 | 0.0179 | 0.0150 | 0.0108 | 0.0079 | 0.0058 | 0.0044 |
| 17 | 0.1029 | 0.0992 | 0.8714 | 0.5612 | 0.3883 | 0.2975 | 0.2416 | 0.2015 | 0.1455 | 0.1071 | 0.0785 | 0.0593 |
| 18 | 0.1029 | 0.0992 | 0.8714 | 0.5612 | 0.3883 | 0.2975 | 0.2416 | 0.2015 | 0.1455 | 0.1071 | 0.0785 | 0.0593 |
| 19 | 0.0253 | 0.1199 | 0.1428 | 0.0921 | 0.0637 | 0.0488 | 0.0397 | 0.0331 | 0.0239 | 0.0176 | 0.0129 | 0.0097 |
| 20 | 0.0253 | 0.1199 | 0.1428 | 0.0921 | 0.0637 | 0.0488 | 0.0397 | 0.0331 | 0.0239 | 0.0176 | 0.0129 | 0.0097 |
| 21 | 0.0096 | 0.3024 | 0.2220 | 0.1444 | 0.1004 | 0.0771 | 0.0627 | 0.0524 | 0.0379 | 0.0279 | 0.0205 | 0.0155 |
| 22 | 0.0096 | 0.3024 | 0.2220 | 0.1444 | 0.1004 | 0.0771 | 0.0627 | 0.0524 | 0.0379 | 0.0279 | 0.0205 | 0.0155 |
| 23 | 0.0253 | 0.3909 | 0.8819 | 0.5764 | 0.4018 | 0.3091 | 0.2516 | 0.2102 | 0.1522 | 0.1123 | 0.0824 | 0.0622 |
| 24 | 0.0253 | 0.4908 | 0.1941 | 0.1272 | 0.0888 | 0.0683 | 0.0556 | 0.0465 | 0.0337 | 0.0249 | 0.0183 | 0.0138 |
| 25 | 0.0230 | 1.2274 | -0.3574 | -0.2387 | -0.1684 | -0.1304 | -0.1066 | -0.0893 | -0.0649 | -0.0480 | -0.0353 | -0.0267 |
| 26 | 0.0230 | 1.2274 | -0.3574 | -0.2387 | -0.1684 | -0.1304 | -0.1066 | -0.0893 | -0.0649 | -0.0480 | -0.0353 | -0.0267 |
| 27 | 0.0230 | 1.2274 | -0.3574 | -0.2387 | -0.1684 | -0.1304 | -0.1066 | -0.0893 | -0.0649 | -0.0480 | -0.0353 | -0.0267 |
| 28 | 0.0230 | 2.0202 | 0.6796 | 0.4608 | 0.3278 | 0.2550 | 0.2090 | 0.1756 | 0.1281 | 0.0949 | 0.0700 | 0.0530 |
| 29 | 0.0230 | 2.0202 | 0.6796 | 0.4608 | 0.3278 | 0.2550 | 0.2090 | 0.1756 | 0.1281 | 0.0949 | 0.0700 | 0.0530 |
| 30 | 0.0230 | 2.0202 | 0.6796 | 0.4608 | 0.3278 | 0.2550 | 0.2090 | 0.1756 | 0.1281 | 0.0949 | 0.0700 | 0.0530 |
| 31 | 0.0510 | 2.7537 | 3.0429 | 2.0860 | 1.4936 | 1.1661 | 0.9583 | 0.8063 | 0.5898 | 0.4380 | 0.3233 | 0.2450 |
| 32 | 0.1029 | 6.5276 | 6.7538 | 4.8214 | 3.5406 | 2.8056 | 2.3288 | 1.9742 | 1.4604 | 1.0934 | 0.8123 | 0.6183 |
| 33 | 0.1029 | 6.5276 | 6.7538 | 4.8214 | 3.5406 | 2.8056 | 2.3288 | 1.9742 | 1.4604 | 1.0934 | 0.8123 | 0.6183 |
| 34 | 0.1029 | 6.5276 | 6.7538 | 4.8214 | 3.5406 | 2.8056 | 2.3288 | 1.9742 | 1.4604 | 1.0934 | 0.8123 | 0.6183 |
| 35 | 0.0253 | 8.9815 | 4.0706 | 2.9592 | 2.1996 | 1.7560 | 1.4651 | 1.2470 | 0.9280 | 0.6980 | 0.5204 | 0.3971 |
| 36 | 0.1029 | 11.7571 | 22.8815 | 16.9090 | 12.7115 | 10.2214 | 8.5708 | 7.3237 | 5.4839 | 4.1437 | 3.1006 | 2.3725 |
| 37 | 0.1029 | 18.2520 | 1.4041 | 1.0680 | 0.8199 | 0.6684 | 0.5660 | 0.4875 | 0.3697 | 0.2821 | 0.2127 | 0.1637 |
| 38 | 0.1029 | 18.2520 | 1.4041 | 1.0680 | 0.8199 | 0.6684 | 0.5660 | 0.4875 | 0.3697 | 0.2821 | 0.2127 | 0.1637 |
| 39 | 0.1029 | 18.2520 | 1.4041 | 1.0680 | 0.8199 | 0.6684 | 0.5660 | 0.4875 | 0.3697 | 0.2821 | 0.2127 | 0.1637 |
| 40 | 0.1029 | 38.0915 | 2.9777 | 2.3721 | 1.8877 | 1.5778 | 1.3613 | 1.1909 | 0.9265 | 0.7220 | 0.5545 | 0.4325 |
| 41 | 0.1029 | 38.0915 | 2.9777 | 2.3721 | 1.8877 | 1.5778 | 1.3613 | 1.1909 | 0.9265 | 0.7220 | 0.5545 | 0.4325 |
| 42 | 0.1029 | 38.0915 | 2.9777 | 2.3721 | 1.8877 | 1.5778 | 1.3613 | 1.1909 | 0.9265 | 0.7220 | 0.5545 | 0.4325 |
| 43 | 0.0510 | 41.3100 | 9.7926 | 7.8447 | 6.2710 | 5.2585 | 4.5486 | 3.9877 | 3.1137 | 2.4342 | 1.8745 | 1.4651 |
| 44 | 0.1029 | 75.6315 | 19.2420 | 16.6715 | 14.2600 | 12.5900 | 11.3546 | 10.3317 | 8.6294 | 7.1812 | 5.8718 | 4.8230 |
| 45 | 0.1029 | 75.6315 | 19.2420 | 16.6715 | 14.2600 | 12.5900 | 11.3546 | 10.3317 | 8.6294 | 7.1812 | 5.8718 | 4.8230 |
| 46 | 0.4200 | 78.1029 | 38.0488 | 31.6614 | 26.1320 | 22.4390 | 19.7777 | 17.6253 | 14.1637 | 11.3592 | 8.9549 | 7.1298 |
| 47 | 0.1029 | 79.8642 | 43.1555 | 35.9593 | 29.7138 | 25.5372 | 22.5246 | 20.0861 | 16.1597 | 12.9737 | 10.2379 | 8.1580 |
| 48 | 0.2466 | 83.5212 | 66.5872 | 55.4966 | 45.8670 | 39.4259 | 34.7791 | 31.0173 | 24.9591 | 20.0419 | 15.8182 | 12.6064 |
| 49 | 0.3175 | 101.2415 | 64.6485 | 54.5664 | 45.5982 | 39.5280 | 35.1107 | 31.5072 | 25.6404 | 20.8063 | 16.5882 | 13.3311 |
| 50 | 0.4200 | 267.1874 | 39.4882 | 34.9092 | 30.4135 | 27.2511 | 24.8870 | 22.9109 | 19.5724 | 16.6643 | 13.9584 | 11.7199 |
| 51 | 0.1029 | 488.7750 | 52.5990 | 47.4803 | 42.1740 | 38.3909 | 35.5421 | 33.1447 | 29.0480 | 25.4066 | 21.9228 | 18.9396 |
| 52 | 0.4200 | 2041.2000 | 53.4548 | 49.9617 | 45.8572 | 42.8963 | 40.6731 | 38.8103 | 35.6399 | 32.8134 | 30.0593 | 27.6116 |
| 53 | 0.3175 | 2530.4750 | 88.8463 | 83.3427 | 76.7600 | 72.0112 | 68.4534 | 65.4799 | 60.4378 | 55.9636 | 51.6190 | 47.7623 |
| 54 | 0.6350 | 7156.4500 | 131.3540 | 124.7385 | 116.2342 | 110.1158 | 105.5862 | 101.8526 | 95.6594 | 90.3337 | 85.3202 | 80.9810 |
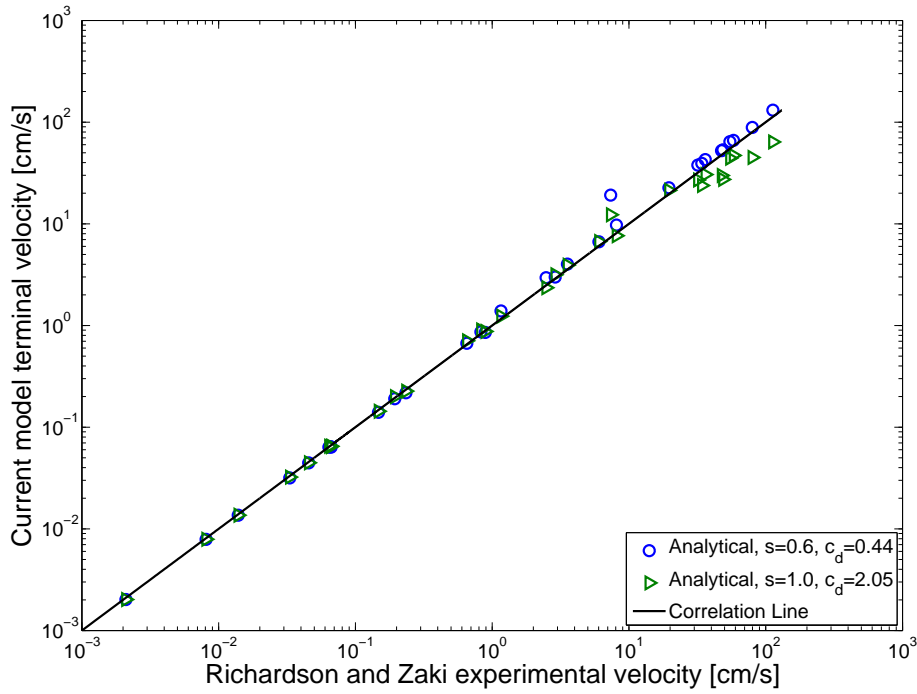
(a) Correlation for $\epsilon_p \to 0$.
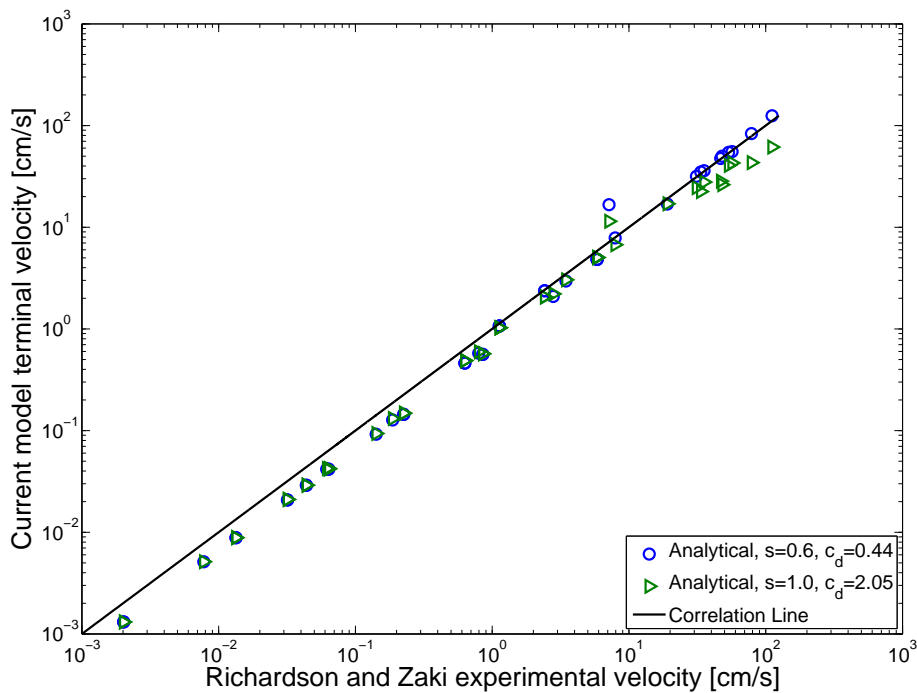


(b) Correlation for $\epsilon_p = 0.010$.

**Figure 10.1:** Correlation between empirical data from Richardson and Zaki (1954) and predictions made by Equation (6.6.3).
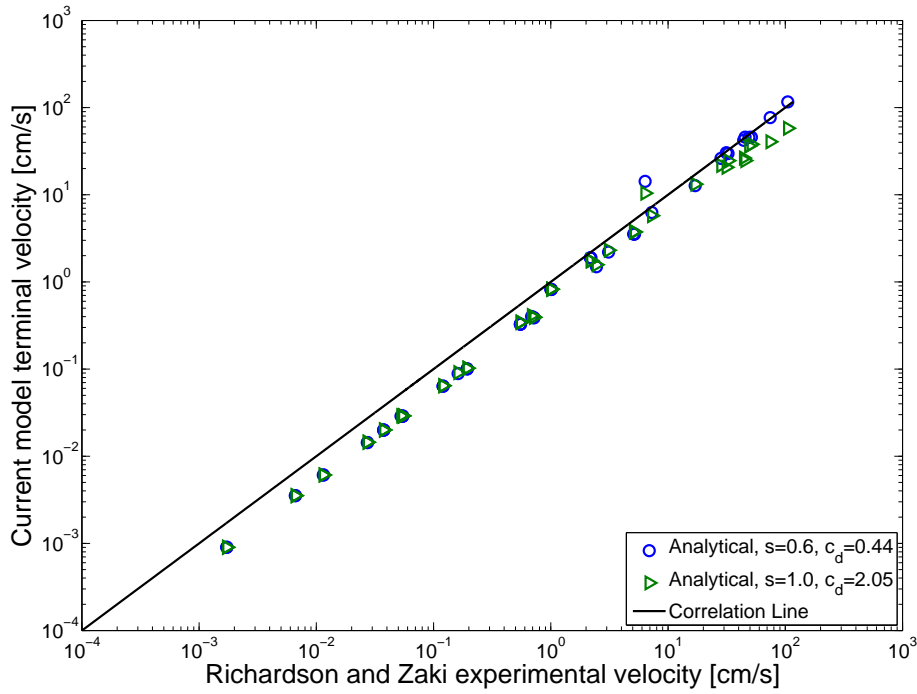
(c) Correlation for $\epsilon_p = 0.050$.
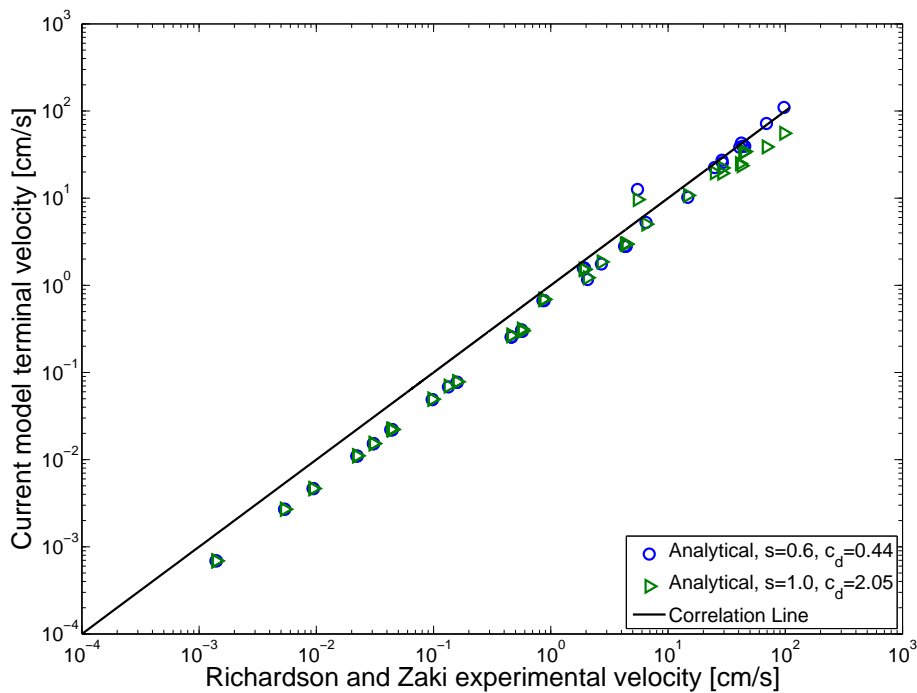


(d) Correlation for $\epsilon_p = 0.100$.

**Figure 10.1:**  Correlation between empirical data from Richardson and Zaki (1954) and predictions made by Equation (6.6.3).
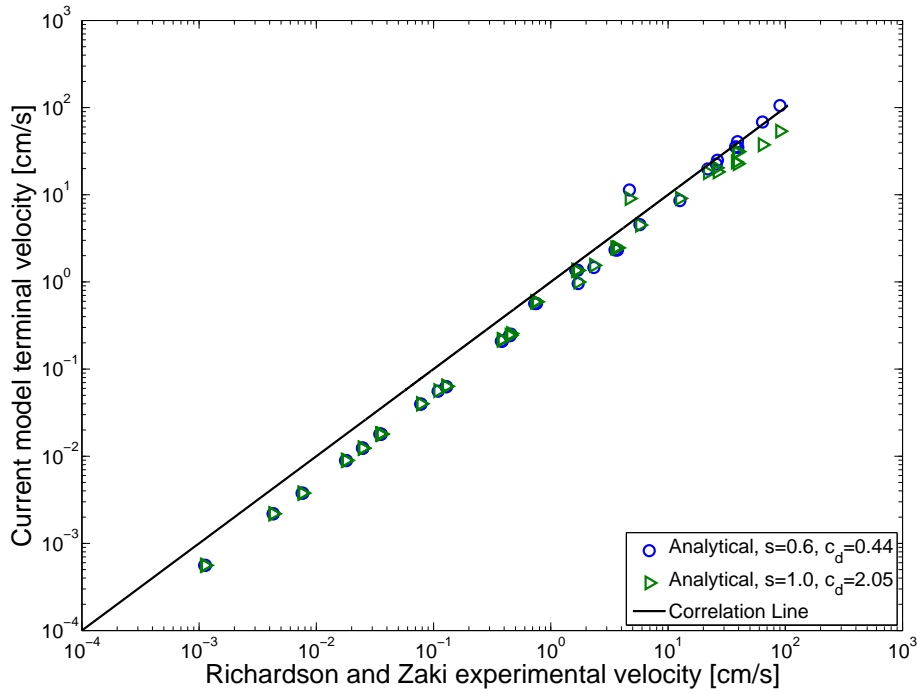
(e) Correlation for $\epsilon_p = 0.150$.
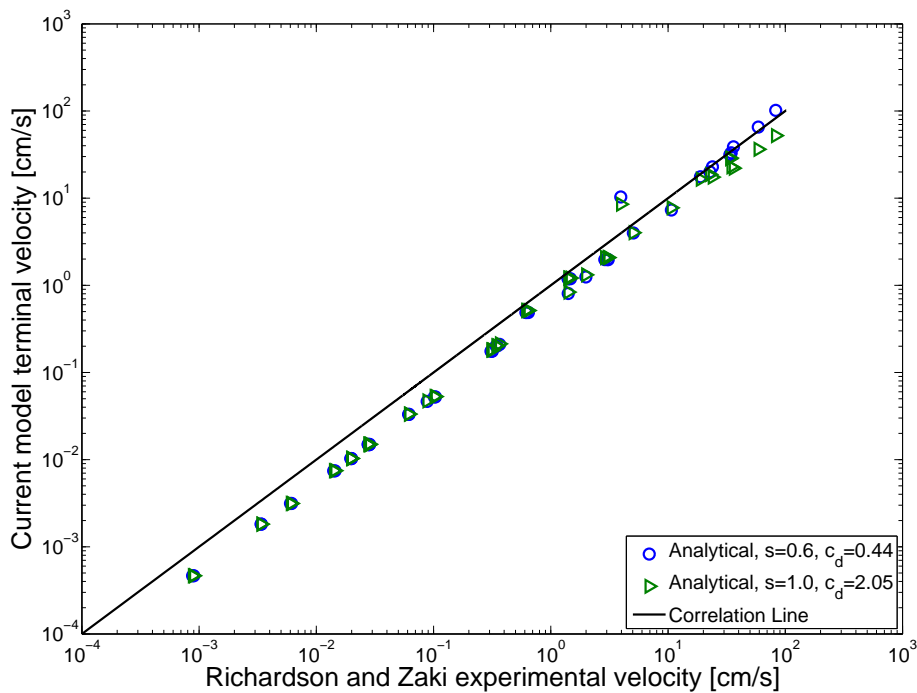


(f) Correlation for $\epsilon_p = 0.200$.

**Figure 10.1:** Correlation between empirical data from Richardson and Zaki (1954) and predictions made by Equation (6.6.3).
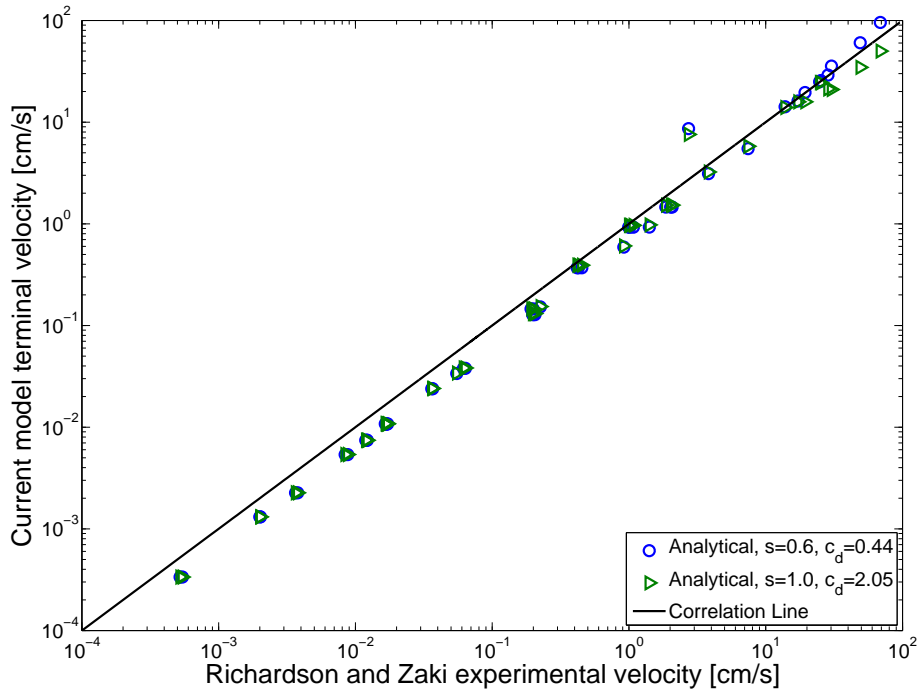
**(g)** Correlation for $\epsilon_p = 0.300$.
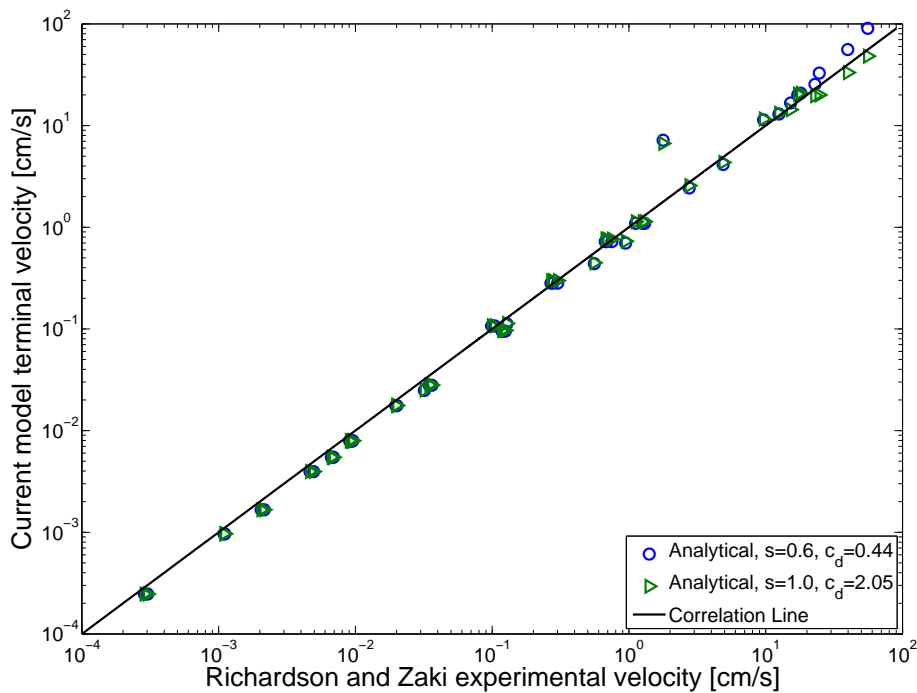


**(h)** Correlation for $\epsilon_p = 0.400$.

**Figure 10.1:**  Correlation between empirical data from Richardson and Zaki (1954) and predictions made by Equation (6.6.3).
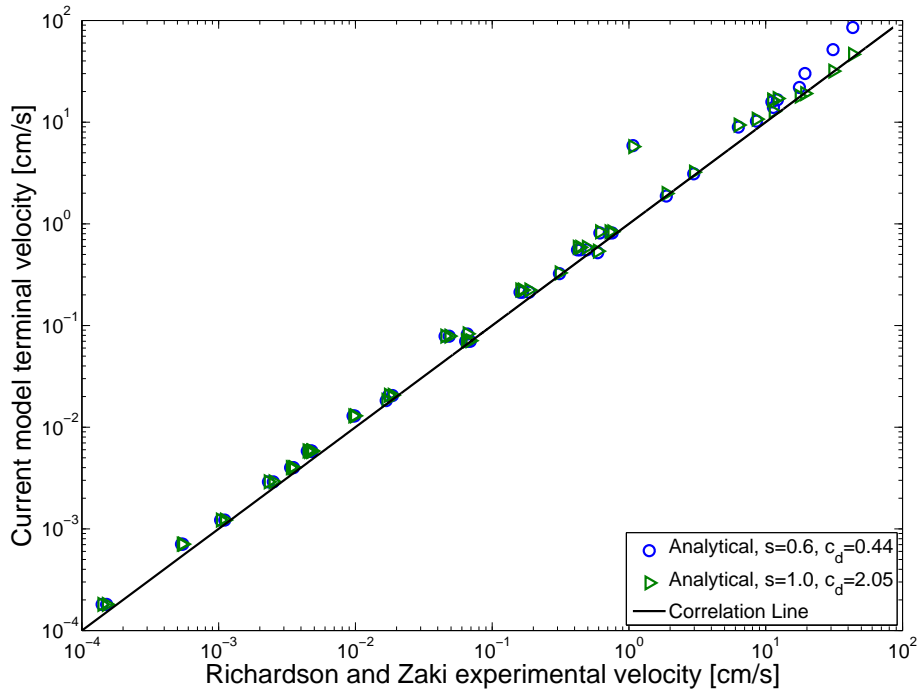
(i) Correlation for $\epsilon_p = 0.500$.
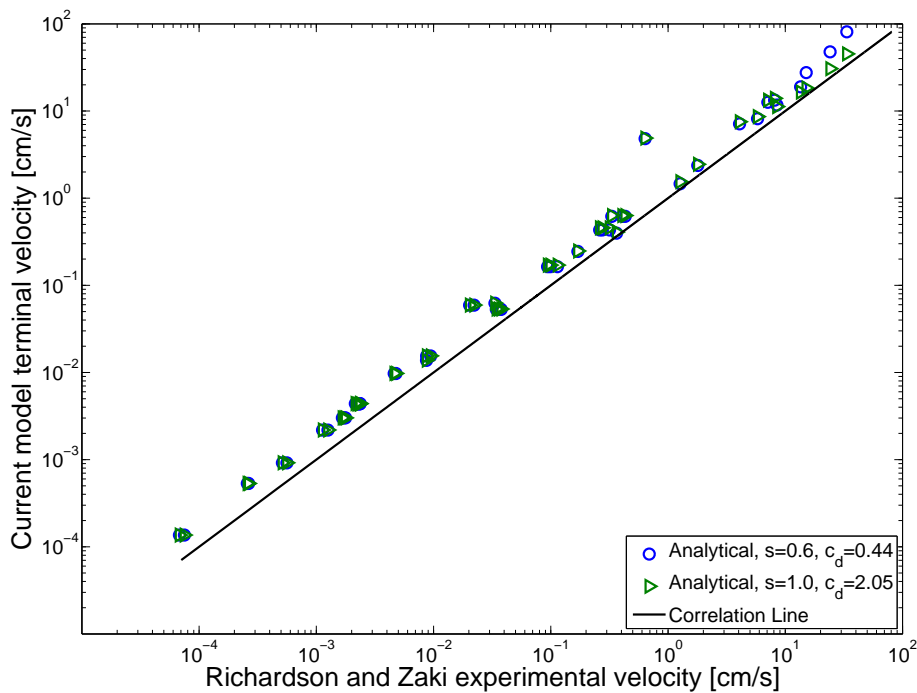


(j) Correlation for $\epsilon_p = 0.585$.

**Figure 10.1:**  Correlation between empirical data from Richardson and Zaki (1954) and predictions made by Equation (6.6.3).
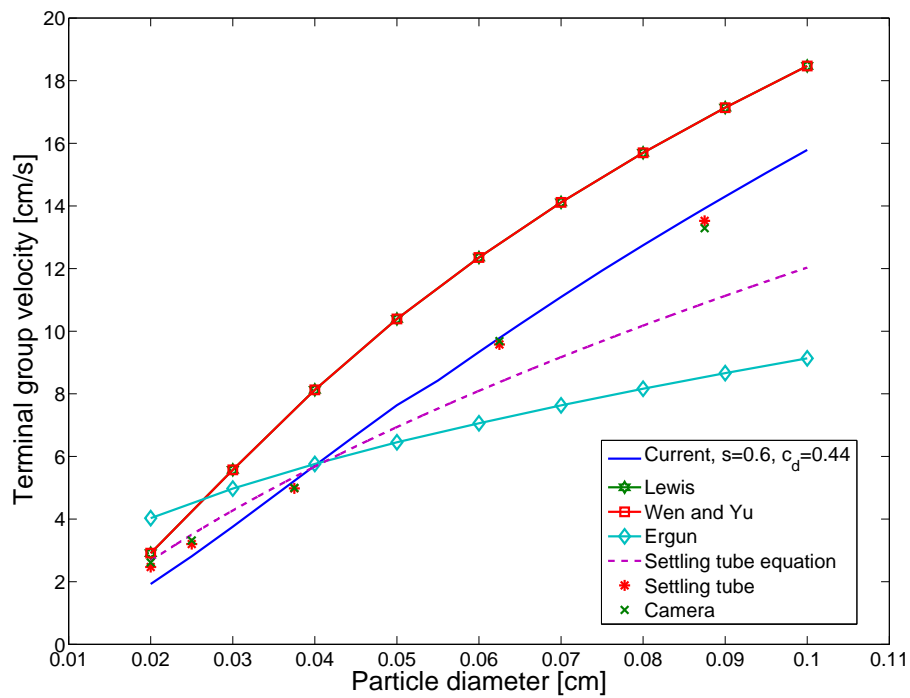
**Figure 10.2:** Comparison of the model developed in this work to empirical models proposed by Ergun, Lewis, and Wen and Yu and experimental data.

# Chapter 11

# Concluding Remarks

The main objective of this work was to address the problem of modelling two-phase flow. In doing so, a model has been developed to simulate the motion of discrete particles together with the motion of a Newtonian fluid which contains them. The fluid is modelled with microscopic Navier Stokes equations which are then averaged with the use of a Representative Unit Volume (REV). The particulate phase momentum conservation equation was obtained by examining the forces acting on a single spherical particle and using a summation method to deal with its discrete nature when determining averaged quantities.

Particle-particle collisions, due to increased volume fractions, were established by using the principle of momentum conservation and full elasticity in conjunction with a collision sphere model. The remaining point variables were expressed in terms of averages by adapting an existing version of the representative unit cell (RUC) model to include the motion of the particles.

The momentum transfer term was split into a Darcy and a Forchheimer regime. The viscous regime was then split into very high and very low particle volume fractions. Equations for the high particle volume fractions were obtained from the modified RUC model whereas the very low particle volume fractions were modelled with Stokes flow around a spherical particle. An asymptotic matching technique was then applied to match these extreme volume fractions in order to obtain an expression for the viscous regime that could also apply to intermediary particle volume fractions. The asymptotic matching technique was then again applied to match the Darcy and the Forchheimer regimes.

The above procedure yielded a momentum conservation and a mass conservation equation for each of the phases. A numerical code was developed in Fortran to solve these equations and was designated Two Phase Flow Simulator (2PMS). In order to demonstrate the prediction capabilities of 2PMS, experiments were performed at the Council for Scientific and Industrial Research (CSIR): A settling tube was used in conjunction with a camera to determine the settling velocity of five different sized ranges of spherical glass particles. The data obtained via the settling tube and that obtained with the camera, corresponded well with each other. These results were also accurately simulated with our theoretical model and since it was possible to simplify the momentum conservation equation for the particulate phase for instances where a terminal group velocity had been reached, it was possible to obtain solutions for such a limiting terminal case with either analytical or numerical integration methods. The reliability of 2PMS was demonstrated when it matched these results accurately as shown in Chapter 8. The accuracy of the model was again corroborated when it was tested against empirical data obtained by Richardson and Zaki (1954). Not only did the model perform well for the entire range of solid volume concentrations used in these experiments but it remained accurate through Reynolds number ranging between 0.02 and 7600.

The objective of modelling two-phase flow based purely on the physical traits of the constituent phases has however only been partially attained. It remains to specify how the fitting parameter used within the asymptotic matching technique is dependent on the physical properties of two-phase motion. In retrospect it was concluded that the Forchheimer regime should also be divided into its limiting concentrations and that the expressions derived for each should then be matched as was done with the Darcy part of the equation.

# Appendices

# Appendix A

# Forces acting on a sphere

## A.1  Introduction

The resultant force acting on a sphere, submerged in a continuum, is divided into a volume and a surface component. The volume forces consist of a weight, buoyancy and an added mass force which are denoted by $\underline{F}_W$, $\underline{F}_{Buoy}$ and $\underline{F}_{AM}$ respectively. The surface forces include a drag force, $\underline{F}_D$, a pressure force, $\underline{F}_P$, the Basset, Saffman and Magnus forces, respectively denoted by $\underline{F}_B$, $\underline{F}_S$ and $\underline{F}_M$, and a particle-particle collision force which is denoted by $\underline{F}_{pp}$. The Basset force is often referred to as the History force. A brief discussion is presented on each and an expression is given for the ratio of the velocity gradient related forces with the Stokes drag in order to quantify the relative importance of each.

## A.2  Volume forces

Weight and buoyancy are the two main volume forces acting on the particle. In addition, the notion of "added" mass has been introduced. The added mass force represents a fluid force exerted by the fluid particles around an accelerating body. The surrounding fluid is pulled along with the accelerating body and the body experiences a force as if its mass is increased by the amount of the "added" mass.

Added mass is dependent on the density of the fluid and it follows that it may be neglected for cases where the density of the body is far greater than that of the surrounding fluid. If the density of the fluid is, however, comparable or greater than that

of the body, the added mass may be greater than the mass of the body itself and will have a significant effect. However, for the current study, the concept of added mass will be neglected.

The volume of the carried mass generally depends on the particle geometry, and is given by

$$m_a = k m_p, \tag{A.2.1}$$

where $m_a$ and $m_p$ denote the added mass and the particle mass, respectively, and $k$ is a constant, which, for a sphere, equals 0.5 (Fan and Zhu (1998) and Kleinstreuer (2003)). The real mass, together with the added mass are referred to as the virtual mass of the body, and the virtual mass force, $\underline{F}_{VM}$ is given by

$$\underline{F}_{VM} = \frac{1}{2} \rho_c \nu_p \frac{d}{dt}(\underline{v}_c - \underline{v}_p), \tag{A.2.2}$$

where $\rho_c$ and $\nu_p$ denote the density of the continuum and volume of a particle, respectively, whereas the continuum- and particle velocities are, respectively, given by $\underline{v}_c$ and $\underline{v}_p$. The total volume force, experienced by the spherical body, is given by

$$
\begin{aligned}
\underline{F}_{Vol} &= \underline{F}_W + \underline{F}_{Buoy} + \underline{F}_{AM} \\
&= \nu_p \underline{g}(\rho_p - \rho_c) + \frac{\rho_c \nu_p}{2} \frac{d}{dt}(\underline{v}_c - \underline{v}_p),
\end{aligned} \tag{A.2.3}
$$

where $\rho_c$ is the continuum density.

This concludes the discussion on volume forces which act on the sphere as a result of inertia and the difference in densities between the sphere and its surrounding fluid matter.

## A.3 Surface forces

The surface of the body is exposed to the surrounding fluid and often moves with a velocity different to that of the fluid. The viscosity of the surrounding fluid, the relative velocity of the particle, and pressure gradients, induce forces on the surface of the body. The resultant surface force, $\underline{F}_{Surf}$, is divided into six components as

$$\underline{F}_{Surf} = \underline{F}_D + \underline{F}_P + \underline{F}_B + \underline{F}_S + \underline{F}_M + \underline{F}_{pp}, \tag{A.3.1}$$

where $\underline{F}_D$, $\underline{F}_P$, $\underline{F}_B$ denote the drag, pressure and Basset forces respectively. The Saffman and Magnus forces are given by, $\underline{F}_S$ and $\underline{F}_M$, while $\underline{F}_{pp}$ denotes the particle interaction force.

In the following sections a brief description will be given of each of the aforementioned surface forces.

### A.3.1 Pressure force

The definition of the pressure force is not consistent within literature: Crowe *et al.* (1998) and Fan and Zhu (1998) regard the pressure force to be due to the static pressure only, and argue that the pressure force is thus the cause of buoyancy. Buoyancy is, however, treated by many as a separate force to that induced by pressure in the surrounding fluid. Kleinstreuer (2003), for example, classifies buoyancy and pressure forces separately by introducing buoyancy as a surface force whilst the pressure force is classified as a volume force. The pressure force in this regard is given by

$$\underline{F}_P = -\nu_{p(i)}\left(\nabla p + \nabla \cdot \underline{\underline{\tau}}_c\right). \tag{A.3.2}$$

In this work, the approach followed by Crowe *et al.* (1998) and Fan and Zhu (1998) is applied and the pressure force will therefore be regarded as the force that arises due to static pressure differences within the continuum.

The local pressure gradient in a stationary fluid gives rise to a force in the direction of the pressure gradient. The net pressure force, $\underline{F}_P$, acting on the particle is given by (Crowe *et al.* (1998) and Fan and Zhu (1998)) as

$$\underline{F}_P = \int_{\partial \nu_{p(i)}} -p\,\underline{n}_p d\mathcal{S}, \tag{A.3.3}$$

where $\underline{n}_p$ is the outwardly directed normal unit vector on the particle wall and $\partial \nu_{p(i)}$ is the surface area of particle $i$. Following Crowe *et al.* (1998), the divergence theorem is applied to Equation (A.3.3), yielding

$$\underline{F}_P = \int_{\nu_{p(i)}} -\nabla p d\nu, \tag{A.3.4}$$

where $\nu_{p(i)}$ is the volume of the $i^{th}$ particle. Under the assumption that the pressure gradient remains constant over the volume of the particle, Equation (A.3.4) may be expressed as

$$\underline{F}_P \;\; = \;\; -\nabla p \nu_{p(i)}. \tag{A.3.5}$$

The pressure, $p$, in Equations (A.3.3)-(A.3.5) is the hydrostatic pressure which is given by Archimedes' principle, i.e. $p = \rho_c g \underline{y}$, where $\underline{y}$ is the diameter of the particle. It follows that the pressure gradient is given by

$$\nabla p \;\; = \;\; -\rho_c g \, \underline{k}, \tag{A.3.6}$$

where $\underline{k}$ is in the direction opposed to gravity (upward). The corresponding pressure force is given by

$$\underline{F}_P \;\; = \;\; \rho_c \, \underline{g} \nu_{p(i)}. \tag{A.3.7}$$

### A.3.1.1   Static and dynamic pressure components

Figure A.1 is a simplified depiction of fluid entering and exiting a cubically shaped control volume.
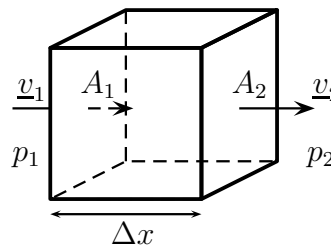


**Figure A.1:** Simplified conservation of mass.

The inflow and outflow fluid velocities are given by $\underline{v}_1$ and $\underline{v}_2$ respectively, $\Delta x$ is the width of the cube while $p_1$ and $p_2$ represent the pressures on the left- and right hand sides of the volume, respectively. The areas over which the fluid enters and exists the volume are given by $A_1$ and $A_2$. Conservation of momentum for an incompressible fluid, yields

$$\underline{F}_{res} \;\; = \;\; m_c \underline{a}_c, \tag{A.3.8}$$

where $\underline{F}_{res}$ is the resultant force acting on the fluid, whereas $m_c$ and $\underline{a}_c$ denote the mass and velocity of the cubic volume, respectively.

Pressure is defined as force per unit area, hence

$$p_2 A_2 - p_1 A_1 = m_c \frac{v_2 - v_1}{\Delta t},$$

$$\left( p_1 + \frac{\Delta p}{\Delta x} \Delta x \right) A_2 - p_1 A_1 = m_c \frac{v_1 + \frac{\Delta v}{\Delta x} \Delta x - v_1}{\Delta t},$$

where $\Delta v = v_2 - v_1$. If the inflow and outflow areas are equal in size (i.e. $A_1 = A_2$) it follows that

$$\frac{\Delta p}{\Delta x} V_c = m_c \frac{\Delta x}{\Delta t} \frac{\Delta v}{\Delta x}. \tag{A.3.9}$$

$$\tag{A.3.10}$$

Dividing the right-hand side of Equation (A.3.9) by the cube volume, $V_c$, and noting that $\Delta x / \Delta t = v$, yield the following expression for the pressure gradient

$$\frac{\Delta p}{\Delta x} = \rho_c v \frac{\Delta v}{\Delta x}. \tag{A.3.11}$$

In order to approximate an infinitesimally small volume, $\Delta x$, is assumed to approach zero, and Equation (A.3.11) may be expressed in differential form and generalised to vector form as

$$\frac{dp}{dx} = \rho_c \underline{v} \cdot \frac{d\underline{v}}{dx}. \tag{A.3.12}$$

Integration of the left- and right-hand sides of Equation (A.3.12) with regard to pressure and velocity, respectively, yields

$$\int_{p_o}^{p_{tot}} dp = \rho_c \int_{v_1}^{v_2} \underline{v} \cdot d\underline{v}$$

$$p_{tot} - p_o = \rho_c \frac{1}{2} \left( v_2^2 - v_1^2 \right). \tag{A.3.13}$$

It follows that

$$p_o + \frac{1}{2} \rho_c \left( v_2^2 - v_1^2 \right) = p_{tot}. \tag{A.3.14}$$

If $v_1 = 0$ then

$$p_o + \frac{1}{2} \rho_c v^2 = p_{tot}, \tag{A.3.15}$$

where $p_o$ denotes the static pressure, $p_{tot}$ denotes the total pressure and the dynamic pressure is denoted by $\frac{1}{2}\rho_c v^2$. This is identical to Bernoulli's equation which was derived using energy conservation. The total pressure is therefore made up out of two types of pressures: The first is the hydrostatic pressure which is present when the continuum is stationary, the second is the pressure due to the motion of the continuum. The orientation of the static pressure force is shown in Figure A.2.

Low static pressure
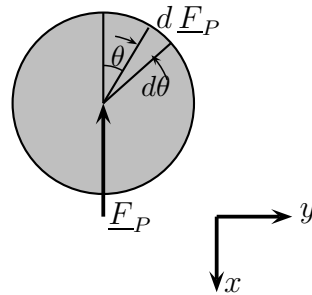


High static pressure

**Figure A.2:** Direction of the pressure force on a particle.

## A.3.2   Basset or History force

Whereas the added mass force accounted for the effect that relative acceleration had on the *volume* of the body, the Basset force arises from the effect that the accelerating fluid has upon the *surface* of the particle. The added mass force accounts for the form drag during acceleration. In turn, the Basset force accounts for the viscous drag effect due to acceleration. The Basset force accounts for the effect of past acceleration on the resistance and is often referred to as the *history force* and denoted by $\underline{F}_{HI}$ (Crowe *et al.* (1998)). The Basset force, $\underline{F}_B$, is given by (Fan and Zhu (1998))

$$\underline{F}_B \;=\; 6\left(\frac{d_p}{2}\right)^2 \sqrt{\pi \rho_c \mu_c} \int_0^t \frac{d/d\tau\left(\underline{v}_c - \underline{v}_p\right)}{\sqrt{t - \tau}} d\tau, \tag{A.3.16}$$

here $(t - \tau)$ is the time elapsed since the previous instance of acceleration from 0 to $t$. The particle diameter is given by $d_p$ whereas $\mu_c$ and $\rho_c$ are the dynamic viscosity and the density of the surrounding continuum, respectively. The particle- and continuum velocities are denoted by $\underline{v}_c$ and $\underline{v}_p$, respectively.

The Basset force becomes substantial at high acceleration rates. For constant acceleration the ratio of the Basset to the Stokes drag, $R_{BS}$, is given by Wallis (1969) as,

$$R_{BS} \;=\; \sqrt{\frac{18}{\pi} \frac{\rho_c}{\rho_p} \frac{\tau_S}{t}}, \tag{A.3.17}$$

where $\tau_S$ is the Stokes relaxation time defined as,

$$\tau_S \;=\; \frac{\rho_p d_p^2}{18 \mu_c}. \tag{A.3.18}$$

It follows that the Basset force may be negligible when the fluid-particle density ratio is small and/or the time elapsed since the previous instance of acceleration is much longer than the Stokes relaxation time.

## A.3.3   Saffman force

In sections where a velocity gradient exists, e.g. near a wall or in a region of high shear, a sphere moving at a constant velocity is subjected to a lift force caused by the velocity gradient (Johnson (1998)). This lift force is termed the Saffman force and was

originally derived by Saffman (1965) for the motion of a sphere at a constant velocity in a simple shear flow at low Reynolds numbers as

$$F_S \;=\; \frac{K\mu_c}{4}||\,\underline{v}_c - \underline{v}_p||d_p^2\sqrt{\frac{1}{\nu_c}}\gamma. \tag{A.3.19}$$

The constant $K$ was determined by Fan and Zhu (1998) as $K = 6.46$. The dynamic- and kinematic fluid viscosities are given by $\mu_c$ and $\nu_c$, respectively. The particle diameter is denoted by $d_p$ and $||\,\underline{v}_c - \underline{v}_p||$ is the magnitude of the relative velocity whereas $\gamma$ is the magnitude of the shear rate. The Saffman force is orientated perpendicular to the direction of fluid motion and is directed away from the region of high shear towards the region of low shear as illustrated in Figure A.3.
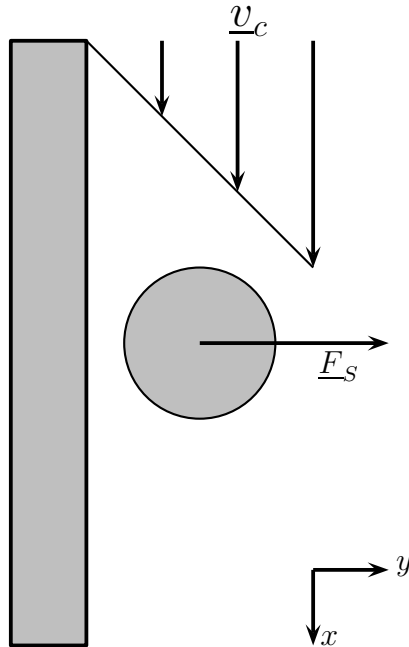


**Figure A.3:**  Direction of the Saffman force on a particle.

The ratio of the Saffman force to the Stokes drag, $R_{SS}$, is given by Fan and Zhu (1998) as

$$R_{SS} \;=\; \frac{Kd_p}{12\mu_c}\sqrt{\frac{1}{\mu_c}}\gamma. \tag{A.3.20}$$

In a shear flow, with a constant shear rate, $R_{SS}$ can be estimated by

$$R_{SS} = \frac{Kd_p}{12\mu_c}\sqrt{Re_p}, \tag{A.3.21}$$

which indicates that the Saffman force is negligible at small shear rates or small Reynolds numbers.

### A.3.4 Magnus force

Particle rotation may be caused by a) particles colliding with a rigid boundary, b) particles colliding with each other, or c) the presence of a strong shear fluid flow. In the low Reynolds number regime such a rotation will cause some of the surrounding fluid to rotate with the particle. Such a rotation will result in an increase of fluid velocity on the one side of the particle and a decrease on the opposite side as shown in Figure A.4. The particle will move towards the region of higher velocity. This is known as the Magnus effect and the force is known as the Magnus force.
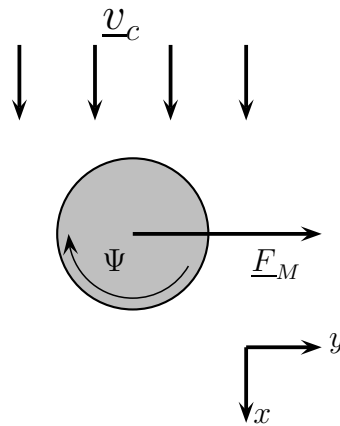


**Figure A.4:** Direction of the Magnus force on a particle.

The Magnus force for a spinning sphere in a uniform flow-field at low Reynolds numbers is given by Fan and Zhu (1998) as

$$\underline{F}_M = \frac{\pi}{8}d_p^3\rho_c\underline{\Psi} \times \underline{v}_p, \tag{A.3.22}$$

where $\underline{\Psi}$ denotes the angular velocity of the sphere. As seen from Equation (A.3.22), this force is independent of the viscosity of the fluid. The ratio, $R_{MS}$, of the Magnus

force to the Stokes drag is,

$$R_{MS} \;=\; \frac{d_p^2}{24}\frac{\rho_c}{\mu_c}\Psi. \tag{A.3.23}$$

From Equation (A.3.23), the Magnus force is negligibly small compared to the drag force when the particle size is small or the spin velocity is low.

## A.3.5 Drag force

Drag forces on a particle may originate from its motion relative to a surrounding continuum. For instances of high particle volume fractions, drag forces may also be a result of the relative motion of neighbouring particles.

### A.3.5.1 Drag due to particle-continuum interaction

The drag force due to the relative velocity between the particle and its surrounding fluid gives rise to a slip velocity. Such a slip velocity causes an unbalanced pressure distribution which brings about viscous stresses on the surface of the body. For a spherical particle in a uniform flow field the Stokes drag is given by

$$\underline{F}_D \;=\; C_D A_f \frac{\rho_c}{2}||\,\underline{v}_c - \underline{v}_p||(\,\underline{v}_c - \underline{v}_p), \tag{A.3.24}$$

where $A_f$ denotes the exposed frontal area of the particle to the direction of the incoming flow and $C_D$ is the drag coefficient, which is a function of the particle Reynolds number, $Re_p$:

$$Re_p \;=\; \frac{\rho_c d_p||\,\underline{v}_c - \underline{v}_p||}{\mu_c}. \tag{A.3.25}$$

Schlichting and Gersten (2000) combined a vast amount of experimental and analytical work on the value of $C_D$ by various authors into a single curve shown in Figure A.5.

Reynolds numbers that fall in the range $700 < Re_p < 10^5$ constitute the inertial regime for which the drag coefficient is given by $C_D = 0.44$. In this range, inertial effects dominate over viscous effects.

For Reynolds numbers lower than the aforementioned range, viscous effects prevail and it was shown by Stokes in 1850 that the drag coefficient is analytically given by $C_D = 24/Re_p$. The drag coefficient was obtained under uniform and undisturbed flow conditions. The sharp reduction in the drag coefficient at high $Re_p$ corresponds to the
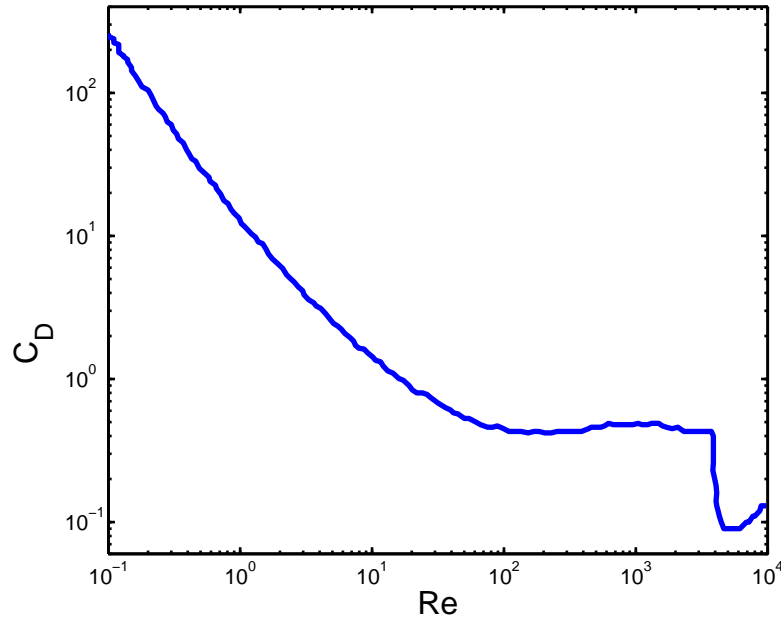
**Figure A.5:** Drag coefficient, $C_D$, for a smooth sphere.

transition from a laminar to a turbulent boundary layer over the particle (Fan and Zhu (1998)).

However, in practice the flow conditions are usually not uniform due to the fluid itself often being turbulent even when the relative velocity and resulting particle Reynolds numbers are small. Such turbulence brings about a change in the wake structure, which causes the body's surrounding surface pressure distribution to change. The turbulence causes $C_D$ to deviate from the Schlichting's curve in Figure A.5. Apart from turbulence, the drag coefficient can also be affected by the movement of neighbouring particles. Studies suggest (Fan and Zhu (1998)) that the drag coefficient of an individual particle under the influence of a neighbouring particle may be expressed by

$$\frac{C_D}{C_{D0}} = 1 - (1 - A) \exp\left(-B\frac{l}{d_p}\right), \tag{A.3.26}$$

where $C_{D0}$ is the drag coefficient from the standard curve, $l$ is the distance between the two interacting particles, and $A$ and $B$ are empirical coefficients which may be functions of $Re_p$ and the deflecting angle between the direction of the relative velocity and the line connecting the centres of the two interactive particles.

### A.3.5.2   Drag force due to particle-particle interaction

Interaction forces, $\underline{F}_{pp}$, are the result of collisions between particles, flow turbulence and/or Brownian motion effects. Shear flow causes particle interaction at high concentrations. An expression for the particle interaction force is derived in Chapter 5 under Section 5.5.

In summation the forces experienced by a single particle are given by,

$$
\begin{aligned}
m_p \frac{d\,\underline{v}_p}{dt} &= \underline{F}_{Vol} + \underline{F}_{Surf}. \\
&= \underline{F}_W + \underline{F}_{AM} + \underline{F}_D + \underline{F}_B + \underline{F}_S + \underline{F}_M + \underline{F}_P + \underline{F}_{pp}, \quad \text{(A.3.27)}
\end{aligned}
$$

where the buoyancy force is replaced by the pressure gradient force and the basset force, $\underline{F}_B$, is often referred to as the History force.

Under the assumption of a symmetric stress dyad, the Magnus and Saffman forces disappear. The virtual mass and Basset forces are regarded as negligible and the remaining forces are given by

$$
m_p \frac{d\,\underline{v}_p}{dt} \;=\; m_p\,\underline{g} + \int_{\partial \nu_p} \underline{n}_p \cdot \underline{\underline{\sigma}}_p \, d\mathcal{S}, \tag{A.3.28}
$$

where the first term on the right hand side denotes the weight force whilst the pressure gradient, drag and particle interaction forces are incorporated into a symmetric stress dyad, $\underline{\underline{\sigma}}_p$, which is integrated over the surface of the particle.

# Appendix B

# Averaging methods

## B.1   Introduction

The methods commonly used for the averaging of the conservation equations are discussed in this appendix. These include volume-, time-, and ensemble averages: Let $\Omega = \Omega(\underline{r}, t)$ be any parameter (e.g. scalar, vector or dyad). The property, $\Omega$, is examined at a fixed point in space, $\underline{r}$, and time, $t$. Either one of the phases may be present at this time. Volume averaging is performed around the stationary point $\underline{r}$ at a fixed time $t$, whereas time averaging is performed at the point $\underline{r}$ over a time interval including time $t$. The ensemble average is regarded as the statistical average of the parameter $\Omega$ at the point $\underline{r}$ and at time, $t$, over an abundant number of experiments exhibiting the same initial and boundary conditions (Enwald *et al.* (1997)).

## B.2   Volume averaging

Let the two phases under consideration be termed the $\alpha$- and $\beta$-phase, respectively. The volume average is taken over the whole volume $\mathcal{U}_o$ of a Representative Elementary Volume (REV) (Bachmat and Bear (1986)). If the parameter to be averaged exists only in the $\alpha$ volume and not in the $\beta$ volume, an appropriate toggle switch is needed when computing the integral over the entire volume. To this end a step function, $X(\underline{r}, t)$, is defined which has a value of unity in the $\alpha$-phase and is zero in the $\beta$-phase.

A building block in the construction of $X(\underline{r}, t)$ is the unit step function, which in one

dimension is given by

$$
H(x-a, t) \;=\; \begin{cases} 0, & \text{if } x \;<\; \alpha \\[2mm] 1, & \text{if } x \;\geq\; \alpha \end{cases} \tag{B.2.1}
$$

The derivative of the step function is defined as

$$
\frac{dH(x-a)}{dx} \;=\; \delta(x-a), \tag{B.2.2}
$$

where $\delta(x-a)$ is the Dirac delta function.

Consider the function $X^\alpha(x, t)$, shown in Figure B.1a. $X^\alpha(x, t)$ is a sum of step functions, i.e.

$$
X^\alpha(x, t) \;=\; H(x-a_0) + H(x-a_1) + H(x-a_2) + H(x-a_3). \tag{B.2.3}
$$

The derivative which is given by

$$
\frac{dX^\alpha(x, t)}{dx} \;=\; \delta(x-a_0) - \delta(x-a_1) + \delta(x-a_2) - \delta(x-a_3), \tag{B.2.4}
$$

and is shown in Figure B.1b.

A unit normal vector $\underline{n}_\alpha$ is defined which points outward from the $\alpha$-phase into the $\beta$-phase at the $\alpha\beta$-interface. Equation (B.2.4) may the be written as

$$
\frac{dX^\alpha(x, t)}{dx} \;=\; -\sum_{k=0}^{3} \underline{n}_\alpha \cdot \underline{i}\delta(x-a_k), \tag{B.2.5}
$$

where $\underline{i}$ is the unit vector in the positive $x$ direction. By analogy, Gray and Lee (1976) defined the gradient of a three-dimensional distribution, $X^\alpha(\underline{r}, t)$, where $\underline{r} = x\,\underline{i} + y\,\underline{j} + z\,\underline{k}$, as

$$
\nabla X^\alpha(\underline{r}, t) \;=\; \underline{n}_\alpha \delta(\underline{r} - \underline{r}_{\alpha\beta}), \tag{B.2.6}
$$

and $\underline{r}_{\alpha\beta}$ denotes the position vector of the $\alpha\beta$-interface.
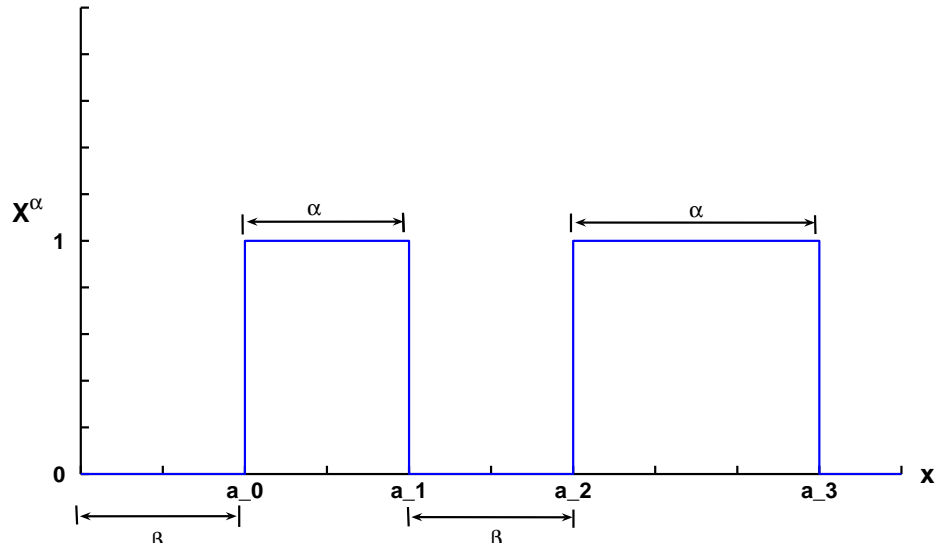
**(a)** Unit function.
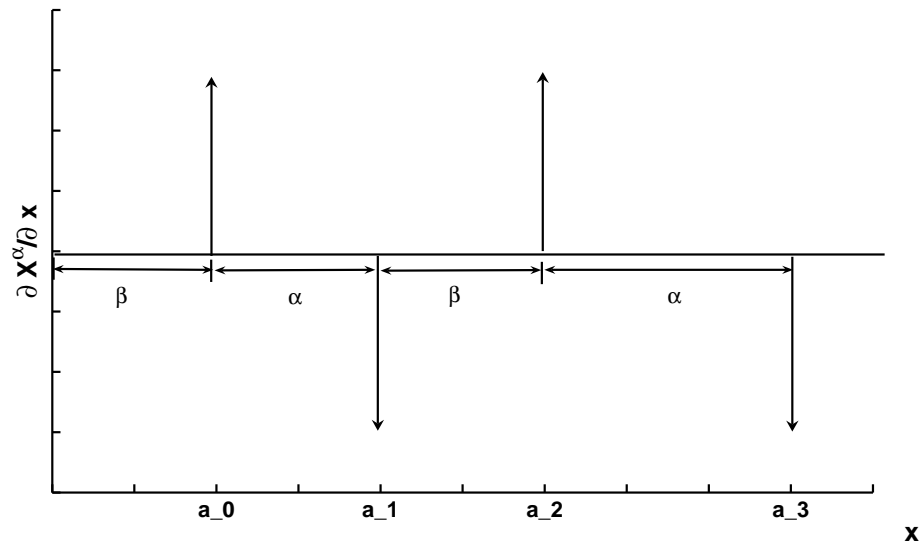


**(b)** Derivative of unit function

**Figure B.1:** One-dimensional distribution function $X^\alpha$ and its derivatives.

The volume average of a property, $\Omega$, is defined as

$$\langle\Omega\rangle_{\mathcal{U}_o} \;=\; \frac{1}{\mathcal{U}_o} \int\limits_{\mathcal{U}_o} \Omega X^\alpha(\underline{r},t)d\mathcal{U}, \qquad\qquad (\text{B.2.7})$$

where $\mathcal{U}_o$ is the averaging volume.

Let $D_p$, $D_V$ and $D_S$ denote the characteristic dimensions of the phases, the averaging volume and the physical system, respectively. Whitaker (1969) gives the conditions under which the volume averaging procedure may be applied as:

$$D_p \ll D_V \ll D_S. \tag{B.2.8}$$

## B.3 Time averaging

The time averaging operator is defined as

$$\langle \Omega \rangle_t \;\; = \;\; \frac{1}{T} \int_{t-T/2}^{t+T/2} \Omega X^\alpha (\underline{r}, t) d\tau. \tag{B.3.1}$$

According to Delhaye and Achard (1978)[1] and Munkejord and Papin (2005), the time interval, $T$, chosen for the averaging must satisfy the following conditions:

$$T_t \ll T \ll T_m, \tag{B.3.2}$$

where $T_t$ is the time scale of the turbulent fluctuations and $T_m$ is the time scale of the mean flow fluctuations.

## B.4 Ensemble averaging

The ensemble average is defined by

$$\langle \Omega \rangle_e \;\; = \;\; \int_\varrho \Omega X^\alpha (\underline{r}, t) dP(\zeta), \tag{B.4.1}$$

where $dP(\zeta)$ denotes the probability of observing process $\zeta$, whereas $\varrho$ is the set of all possible outcomes.

The averaging rules for volume averaging, which, due to its physical interpretability, is the preferred method of averaging in this work, are discussed in the next section.

## B.5 Averaging principles

The phase average, $\langle \Omega_\alpha \rangle$, of some property $\Omega$ is defined by

$$\langle \Omega_\alpha \rangle (\underline{r}, t) \;\; = \;\; \frac{1}{\mathcal{U}_o} \int_{\mathcal{U}_o} \Omega(\underline{r}, t) X^\alpha (\underline{r}, t) \, d\mathcal{U}, \tag{B.5.1}$$

---

[1] In Enwald *et al.* (1997)

where the volume of integration, $\mathcal{U}_o = \mathcal{U}_\alpha + \mathcal{U}_\beta$ is independent of space and time.

Physically, the $\alpha$-phase average is a property of the $\alpha$-phase only, although the average is taken over the entire averaging volume occupied by the $\alpha$- and $\beta$-phases. Because $X^\alpha$ is zero in the $\beta$-phase, Equation (B.5.1) may be written as

$$\langle \Omega_\alpha \rangle (\underline{r},t) \;\; = \;\; \frac{1}{\mathcal{U}_o} \int\limits_{\mathcal{U}_\alpha} \Omega(\underline{r},t)\,d\mathcal{U}. \tag{B.5.2}$$

The *intrinsic* phase average, $\langle \Omega_\alpha \rangle_\alpha$, of some property $\Omega_\alpha$ is given by

$$\langle \Omega_\alpha \rangle_\alpha \;\; = \;\; \frac{1}{\mathcal{U}_\alpha} \int\limits_{\mathcal{U}_\alpha} \Omega(\underline{r},t)d\mathcal{U}. \tag{B.5.3}$$

This type of average describes a property of the $\alpha$-phase, averaged over that phase only. The average is, however, assigned to the centre of the averaging volume, independent of whether or not the centre is located within the particular phase. Comparison of Equations (B.5.2) and (B.5.3) indicates that

$$\langle \Omega_\alpha(\underline{r},t) \rangle \;\; = \;\; \epsilon_\alpha(\underline{r},t) \langle \Omega_\alpha \rangle_\alpha (\underline{r},t), \tag{B.5.4}$$

where

$$\epsilon_\alpha(\underline{r},t) \;\; = \;\; \mathcal{U}_\alpha/\mathcal{U}_o \;\; = \;\; \frac{1}{\mathcal{U}_o} \int\limits_{\mathcal{U}_o} X^\alpha(\underline{r},t)d\mathcal{U}. \tag{B.5.5}$$

From the relation given by Equation (B.5.4) it follows that $\epsilon_\alpha$ is the fraction of the volume occupied by the $\alpha$-phase.

## B.6 Averaging theorems

The first theorem relates the average of a gradient to the gradient of an average and was developed by Slattery (1967) and Whitaker (1967), independently. If $\Omega$ is continuous within the $\alpha$-phase, this theorem states that

$$\langle \nabla \Omega_\alpha \rangle \;\; = \;\; \nabla \langle \Omega_\alpha \rangle + \frac{1}{\mathcal{U}_o} \int\limits_{\mathcal{S}_{\alpha\beta}} \Omega_\alpha \, \underline{n}_\alpha d\mathcal{S}, \tag{B.6.1}$$

where $\mathcal{S}_{\alpha\beta}$ is the $\alpha\beta$-interface and $\underline{n}_\alpha$ is the normal unit vector directed from the $\alpha$-phase into the $\beta$-phase. The relation may be proved using the function $X^\alpha$: From Equation (B.5.1) it follows that

$$\langle \nabla\Omega_\alpha \rangle \;=\; \frac{1}{\mathcal{U}_o} \int_{\mathcal{U}_o} [\nabla\Omega_\alpha(\underline{r},t)]\, X^\alpha(\underline{r},t)d\mathcal{U}. \tag{B.6.2}$$

The chain rule is applied to the integrand, yielding

$$\langle \nabla\Omega_\alpha \rangle \;=\; \frac{1}{\mathcal{U}_o} \int_{\mathcal{U}_o} [\nabla\Omega_\alpha(\underline{r},t)X^\alpha(\underline{r},t)]\, d\mathcal{U} - \frac{1}{\mathcal{U}_o} \int_{\mathcal{U}_o} \Omega_\alpha(\underline{r},t)\nabla X^\alpha(\underline{r},t)d\mathcal{U}. $$

$$\tag{B.6.3}$$

Substitution of Equation (5.5.30) into the second term of Equation (B.6.3) then yields

$$\langle \nabla\Omega_\alpha \rangle \;=\; \frac{1}{\mathcal{U}_o} \int_{\mathcal{U}_o} [\nabla\Omega_\alpha(\underline{r},t)X^\alpha(\underline{r},t)]\, d\mathcal{U} - \frac{1}{\mathcal{U}_o} \int_{\mathcal{U}_o} \Omega_\alpha(\underline{r},t)(-1)\underline{n}_\alpha\delta(\underline{r} - \underline{r}_{\alpha\beta})d\mathcal{U}. $$

$$\tag{B.6.4}$$

The last step of the proof follows from the fact that the last integral in Equation (B.6.4) involves the delta function which is zero everywhere except at the $\alpha\beta$-interface, $\mathcal{S}_{\alpha\beta}$. The value of an integral, of which the integrand is a $\delta$-function multiplied by some other quantity, is that quantity evaluated at the singular points of the $\delta$-function (Munkejord and Papin (2005)). It therefore follows that

$$\frac{1}{\mathcal{U}_o} \int_{\mathcal{U}_o} \Omega_\alpha(\underline{r},t)\,\underline{n}_\alpha\delta(\underline{r} - \underline{r}_{\alpha\beta})d\mathcal{U} \;=\; \frac{1}{\mathcal{U}_o} \int_{\mathcal{S}_{\alpha\beta}} \Omega_\alpha(\underline{r},t)\,\underline{n}_\alpha d\mathcal{S}, \tag{B.6.5}$$

and Equation (B.6.4) simplifies to

$$\langle \nabla\Omega_\alpha \rangle \;=\; \frac{1}{\mathcal{U}_o} \int_{\mathcal{U}_o} [\nabla\Omega_\alpha(\underline{r},t)X^\alpha(\underline{r},t)]\, d\mathcal{U} + \frac{1}{\mathcal{U}_o} \int_{\mathcal{S}_{\alpha\beta}} \Omega_\alpha(\underline{r},t)\,\underline{n}_\alpha d\mathcal{S}. \tag{B.6.6}$$

If $\nabla$, on the right-hand side of Equation (B.6.6), is considered to be $\nabla = \underline{i}\frac{\partial}{\partial x} + \underline{j}\frac{\partial}{\partial y} + \underline{k}\frac{\partial}{\partial z}$, then it may be removed from the integral since the volume of integration has been

specified to be independent of $\underline{r}$, hence Equation (B.6.6) may be expressed as

$$
\langle \nabla \Omega_\alpha \rangle = \nabla \left[ \frac{1}{\mathcal{U}_o} \int\limits_{\mathcal{U}_o} \Omega_\alpha(\underline{r}, t) X^\alpha(\underline{r}, t) d\mathcal{U} \right] + \frac{1}{\mathcal{U}_o} \int\limits_{\mathcal{S}_{\alpha\beta}} \Omega_\alpha(\underline{r}, t) \, \underline{n}_\alpha d\mathcal{S}, \quad \text{(B.6.7)}
$$

Application of Equation (B.5.1), yields

$$
\langle \nabla \Omega_\alpha \rangle = \nabla \langle \Omega_\alpha \rangle + \frac{1}{\mathcal{U}_o} \int\limits_{\mathcal{S}_{\alpha\beta}} \Omega_\alpha \, \underline{n}_\alpha d\mathcal{S}. \quad \text{(B.6.8)}
$$

Equation (B.6.8) concludes the derivation of an expression for the average of a spatial derivative.

The second rule relates the average of a time derivative to the time derivative of an average, and is given by

$$
\left\langle \frac{\partial \Omega_\alpha}{\partial t} \right\rangle = \frac{\partial}{\partial t} \langle \Omega_\alpha \rangle - \frac{1}{\mathcal{U}_o} \int\limits_{\mathcal{S}_{\alpha\beta}} \Omega_\alpha \, \underline{w} \cdot \underline{n}_\alpha d\mathcal{S}, \quad \text{(B.6.9)}
$$

where $\underline{w}$ is the velocity of a point on the $\alpha\beta$-interface. The proof of the relation given by Equation (B.6.9) commences with the application of the phase average, given by Equation (B.5.1). It follows that the average of the partial time derivative may be given as

$$
\left\langle \frac{\partial \Omega_\alpha}{\partial t} \right\rangle = \frac{1}{\mathcal{U}_o} \int\limits_{\mathcal{U}_o} \frac{\partial \Omega_\alpha}{\partial t}(\underline{r}, t) X^\alpha(\underline{r}, t) d\mathcal{U}. \quad \text{(B.6.10)}
$$

Subsequent application of the chain rule, yields

$$
\left\langle \frac{\partial \Omega_\alpha}{\partial t} \right\rangle = \frac{1}{\mathcal{U}_o} \int\limits_{\mathcal{U}_o} \frac{\partial}{\partial t} \left[ \Omega_\alpha(\underline{r}, t) X^\alpha(\underline{r}, t) \right] d\mathcal{U} - \frac{1}{\mathcal{U}_o} \int\limits_{\mathcal{U}_o} \frac{\partial X^\alpha(\underline{r}, t)}{\partial t} \Omega_\alpha(\underline{r}, t) d\mathcal{U}. \quad \text{(B.6.11)}
$$

In view of the assumption that $\mathcal{U}_o$ is independent of time, the order of differentiation and integration in the first term on the right side may be reversed and Equation (B.5.1)

invoked to obtain

$$
\left\langle \frac{\partial \Omega_\alpha}{\partial t} \right\rangle = \frac{\partial}{\partial t} \langle \Omega_\alpha \rangle - \frac{1}{\mathcal{U}_o} \int\limits_{\mathcal{U}} \frac{\partial X^\alpha(\underline{r},t)}{\partial t} \Omega_\alpha(\underline{r},t) d\mathcal{U}. \tag{B.6.12}
$$

If the $\alpha$-phase is deforming, $X^\alpha$ will be a function of time and the last term may be non-zero. The total derivative of $X^\alpha$ is

$$
\frac{dX^\alpha}{dt} = \frac{\partial X^\alpha}{\partial t} + \frac{dx}{dt}\frac{\partial X^\alpha}{\partial x} + \frac{dy}{dt}\frac{\partial X^\alpha}{\partial y} + \frac{dz}{dt}\frac{\partial X^\alpha}{\partial z}. \tag{B.6.13}
$$

The functions $\frac{\partial X^\alpha}{\partial x}$, $\frac{\partial X^\alpha}{\partial y}$ and $\frac{\partial X^\alpha}{\partial z}$ will only be non-zero on the $\mathcal{S}_{\beta\alpha}$ interface. If $\frac{dx}{dt}$, $\frac{dy}{dt}$, and $\frac{dz}{dt}$, are chosen to be the velocity components of the interface, the total derivative becomes a substantial derivative that moves with the interface. Because an observer moving with the interfacial boundary will see no change, this derivative is zero, i.e.

$$
\frac{dX^\alpha}{dt} = 0 = \frac{\partial X^\alpha}{\partial t} + \underline{w} \cdot \nabla X^\alpha, \tag{B.6.14}
$$

where $\underline{w}$ is the velocity of the phase interface[2]. It follows that

$$
\frac{\partial X^\alpha}{\partial t} = -\underline{w} \cdot \nabla X^\alpha. \tag{B.6.16}
$$

Substitution of Equation (B.6.16) into Equation (B.6.12), yields

$$
\left\langle \frac{\partial \Omega_\alpha}{\partial t} \right\rangle = \frac{\partial}{\partial t} \langle \Omega_\alpha \rangle + \frac{1}{\mathcal{U}_o} \int\limits_{\mathcal{U}_o} \underline{w}(\underline{r},t) \cdot \nabla X^\alpha(\underline{r},t) \Omega_\alpha(\underline{r},t) d\mathcal{U}. \tag{B.6.17}
$$

Equation (B.2.6) is applied and it follows that

$$
\left\langle \frac{\partial \Omega_\alpha}{\partial t} \right\rangle = \frac{\partial}{\partial t} \langle \Omega_\alpha \rangle + \frac{1}{\mathcal{U}_o} \int\limits_{\mathcal{U}_o} \underline{w}(\underline{r},t) \cdot (-1)\underline{n}_\alpha \delta(\underline{r} - \underline{r}_{\alpha\beta}) \Omega_\alpha(\underline{r},t) d\mathcal{U}. \tag{B.6.18}
$$

---

[2]In the summary of two-phase flow, given by Enwald *et al.* (1997), they cite Drew (1983) and presents the following relation

$$
\frac{dX^\alpha}{dt} = 0 = \frac{\partial X^\alpha}{\partial t} + \underline{v}_\alpha \cdot \nabla X^\alpha, \tag{B.6.15}
$$

where $\underline{v}_\alpha$ is the velocity of the $\alpha$-phase. Note that this applies specifically to $\underline{w} = \underline{v}_\alpha$, i.e. if there is no combustion or condensation.

As mentioned earlier, the integral involving the delta function is zero everywhere barring the interface $\mathcal{S}_{\alpha\beta}$. It therefore follows that

$$\left\langle \frac{\partial \Omega_\alpha}{\partial t} \right\rangle = \frac{\partial}{\partial t} \langle \Omega_\alpha \rangle - \frac{1}{\mathcal{U}_o} \int\limits_{\mathcal{S}_{\alpha\beta}} \Omega_\alpha \, \underline{w} \cdot \underline{n}_\alpha d\mathcal{U}. \tag{B.6.19}$$

Equation (B.6.19) concludes the derivation of an expression for the average of a time derivative.

The above two derivations exhibit the usefulness of the distribution function in proving theorems for local volume averaging. In earlier work by Whitaker, these theorems were proved using the general transport theorem (Whitaker (1967)).

The general averaging rules are given as (Enwald *et al.* (1997)):

$$\langle f + g \rangle = \langle f \rangle + \langle g \rangle \tag{B.6.20}$$

$$\langle \langle f \rangle g \rangle = \langle f \rangle \langle g \rangle \tag{B.6.21}$$

$$\langle \text{constant} \rangle = \text{constant} \tag{B.6.22}$$

$$\langle \nabla f \rangle = \nabla \langle f \rangle + \frac{1}{\mathcal{U}_o} \int\limits_{\mathcal{S}_{\alpha\beta}} f \, \underline{n}_\alpha d\mathcal{S} \tag{B.6.23}$$

$$\langle \nabla \cdot f \rangle = \nabla \cdot \langle f \rangle + \frac{1}{\mathcal{U}_o} \int\limits_{\mathcal{S}_{\alpha\beta}} f \cdot \underline{n}_\alpha d\mathcal{S} \tag{B.6.24}$$

$$\left\langle \frac{\partial f}{\partial t} \right\rangle = \frac{\partial \langle f \rangle}{\partial t} - \frac{1}{\mathcal{U}_o} \int\limits_{\mathcal{S}_{\alpha\beta}} f \, \underline{w} \cdot \underline{n}_\alpha d\mathcal{S}. \tag{B.6.25}$$

These averaging identities are applied to the instantaneous conservation Equations (2.6.1) and (2.6.2).

## B.7   Averaging of the conservation equations

The averaging procedures for the mass and momentum equations, by way of the application of identities given by Equations (B.6.20) to (B.6.25), are reviewed in Chapter 4.

# Appendix C

# Evaluation of the shear stress

## C.1 Introduction

The momentum conservation equations require the shear stress, $\underline{\underline{\tau}}_c$, due to continuum motion, to be evaluated inside the continuum as well as on the particle-continuum interface, $\mathcal{S}_{pc}$. In this appendix the assumptions made in calculating expressions for gradients and averages taken of shear stresses at these locations are discussed. The results of which are applied in Chapter 5 to the averaged momentum equations.

## C.2 Evaluation of the stress deviation term

Newtonian shear was given by Equation (5.2.5) in Section 5.2 as

$$\underline{\underline{\tau}}_c = \mu_c \left( \nabla \underline{v}_c + (\nabla \underline{v}_c)^T \right). \tag{C.2.1}$$

The average of the divergence of the shear stress is

$$\left\langle \nabla \cdot \underline{\underline{\tau}}_c \right\rangle = \left\langle \nabla \cdot \mu_c \nabla \underline{v}_c + \nabla \cdot \mu_c (\nabla \underline{v}_c)^T \right\rangle. \tag{C.2.2}$$

The viscosity, $\mu_c$, is assumed constant and Equation (C.2.2) may therefore be expressed as

$$\left\langle \nabla \cdot \underline{\underline{\tau}}_c \right\rangle = \mu_c \left\langle \nabla^2 \underline{v}_c + \nabla \cdot (\nabla \underline{v}_c)^T \right\rangle. \tag{C.2.3}$$

The divergence of the transpose of the velocity gradient, that appears on the right-hand side of Equation (C.2.3), is given by

$$\nabla \cdot (\nabla \underline{v}_c)^T = \nabla (\nabla \cdot \underline{v}_c), \tag{C.2.4}$$

**195**

and is zero due to the assumption of continuity (i.e. $\nabla \cdot \underline{v}_c = 0$). It follows that Equation (C.2.3) simplifies to

$$\left\langle \nabla \cdot \underline{\underline{\tau}}_c \right\rangle = \mu_c \left\langle \nabla^2 \underline{v}_c \right\rangle. \tag{C.2.5}$$

Equation (C.2.5) may be expressed as

$$\left\langle \nabla \cdot \underline{\underline{\tau}}_c \right\rangle = \mu_c \frac{1}{\mathcal{U}_o} \int_{\mathcal{U}_c} \nabla \cdot (\nabla \underline{v}_c) \, d\mathcal{U}. \tag{C.2.6}$$

The divergence theorem is applied to Equation (C.2.6) and it follows that

$$\left\langle \nabla \cdot \underline{\underline{\tau}}_c \right\rangle = \mu_c \frac{1}{\mathcal{U}_o} \int_{\mathcal{S}_{cc}} \underline{n}_c \cdot (\nabla \underline{v}_c) \, d\mathcal{S} + \mu_c \frac{1}{\mathcal{U}_o} \int_{\mathcal{S}_{pc}} \underline{n}_c \cdot (\nabla \underline{v}_c) \, d\mathcal{S}. \tag{C.2.7}$$

Subsequent application of Slattery's Averaging Theorem to Equation (C.2.7), yields

$$\left\langle \nabla \cdot \underline{\underline{\tau}}_c \right\rangle = \mu_c \frac{1}{\mathcal{U}_o} \nabla \cdot \int_{\mathcal{U}_o} (\nabla \underline{v}_c) \, d\mathcal{U} + \mu_c \frac{1}{\mathcal{U}_o} \int_{\mathcal{S}_{pc}} \underline{n}_c \cdot (\nabla \underline{v}_c) \, d\mathcal{S}, \tag{C.2.8}$$

and, finally, Equation (C.2.8) may be expressed as follows with the use of averaging notation

$$\left\langle \nabla \cdot \underline{\underline{\tau}}_c \right\rangle = \mu_c \nabla \cdot \left\langle \nabla \underline{v}_c \right\rangle + \mu_c \frac{1}{\mathcal{U}_o} \int_{\mathcal{S}_{pc}} \underline{n}_c \cdot (\nabla \underline{v}_c) \, d\mathcal{S}. \tag{C.2.9}$$

Alternatively, the average of the divergence of the shear stress may be expressed as

$$\left\langle \nabla \cdot \underline{\underline{\tau}}_c \right\rangle = \nabla \cdot \left\langle \underline{\underline{\tau}}_c \right\rangle + \frac{1}{\mathcal{U}_o} \int_{\mathcal{S}_{pc}} \underline{n}_c \cdot \underline{\underline{\tau}}_c \, d\mathcal{S}. \tag{C.2.10}$$

From Equations (C.2.9) and (C.2.10), it follows that

$$\nabla \cdot \left\langle \underline{\underline{\tau}}_c \right\rangle + \frac{1}{\mathcal{U}_o} \int_{\mathcal{S}_{pc}} \underline{n}_c \cdot \underline{\underline{\tau}}_c \, d\mathcal{S} = \mu_c \nabla \cdot \left\langle \nabla \underline{v}_c \right\rangle + \mu_c \frac{1}{\mathcal{U}_o} \int_{\mathcal{S}_{pc}} \underline{n}_c \cdot (\nabla \underline{v}_c) \, d\mathcal{S}.$$

$$\tag{C.2.11}$$

The continuum averaging rules are applied to the first term on the right-hand side of Equation (C.2.11). It follows that

$$
\nabla \cdot \left\langle \underline{\underline{\tau}}_c \right\rangle + \frac{1}{\mathcal{U}_o} \int_{\mathcal{S}_{pc}} \underline{n}_c \cdot \underline{\underline{\tau}}_c \, d\mathcal{S} = \mu_c \nabla \cdot [\epsilon_c \nabla \langle \underline{v}_c \rangle_c] + \mu_c \nabla \cdot \left[ \frac{1}{\mathcal{U}_o} \int_{\mathcal{S}_{pc}} \underline{n}_c \widetilde{\underline{v}}_c \, d\mathcal{S} \right] +
$$

$$
\mu_c \frac{1}{\mathcal{U}_o} \int_{\mathcal{S}_{pc}} \underline{n}_c \cdot (\nabla \underline{v}_c) \, d\mathcal{S}. \tag{C.2.12}
$$

The particle-continuum interface, $\mathcal{S}_{pc}$, is constant, and the integration and differentiation procedures may therefore interchange in Equation (C.2.12). It follows that

$$
\nabla \cdot \left\langle \underline{\underline{\tau}}_c \right\rangle + \frac{1}{\mathcal{U}_o} \int_{\mathcal{S}_{pc}} \underline{n}_c \cdot \underline{\underline{\tau}}_c \, d\mathcal{S} = \mu_c \nabla \cdot [\epsilon_c \nabla \langle \underline{v}_c \rangle_c] + \mu_c \frac{1}{\mathcal{U}_o} \int_{\mathcal{S}_{pc}} \nabla \cdot \underline{n}_c \widetilde{\underline{v}}_c + \underline{n}_c \cdot (\nabla \underline{v}_c) \, d\mathcal{S}
$$

$$
\tag{C.2.13}
$$

It is assumed that the gradient of the continuum velocity deviations, $\widetilde{\underline{v}}_c$, is negligibly small, allowing Equation (C.2.13) to be written as

$$
\nabla \cdot \left\langle \underline{\underline{\tau}}_c \right\rangle + \frac{1}{\mathcal{U}_o} \int_{\mathcal{S}_{pc}} \underline{n}_c \cdot \underline{\underline{\tau}}_c \, d\mathcal{S} = \mu_c \nabla \cdot [\epsilon_c \nabla \langle \underline{v}_c \rangle_c] + \mu_c \frac{1}{\mathcal{U}_o} \int_{\mathcal{S}_{pc}} \underline{n}_c \cdot (\nabla \underline{v}_c) \, d\mathcal{S}.
$$

$$
\tag{C.2.14}
$$

It follows that the left-hand side terms of Equation (C.2.14), which appear within the continuum momentum conservation equation, may be replaced by those on the right-hand side of Equation (C.2.14). In addition, the shear stress within the surface integral is equal to the gradient of the velocity on the $\mathcal{S}_{pc}$-interface. Following Enwald *et al.* (1997), Ishii (1977), Gidaspow (1986) and Mazzei and Lettieri (2007), the velocity on the $\mathcal{S}_{pc}$-interface is assumed to adhere to a slip assumption and is therefore a function of the relative velocity between the particle and the continuum. The aforementioned observations are applied in the averaging and closure procedures of Equations (5.4.6) and (6.4.2), respectively.

# Appendix D

# Momentum theorem

## D.1    Introduction

In the following appendix the momentum theorem is discussed. This discussion supplements the discussion given on the derivation for the particle-particle interaction force in Chapter 5.

## D.2    Derivation of the momentum theorem

According to the momentum theorem of mechanics the time rate of change of the momentum is equal to the sum of the acting external forces

$$\frac{d\underline{I}}{dt} = \sum \underline{F}_{ext}. \tag{D.2.1}$$

For a system with $n$ particles with masses $m_i$ and velocities $\underline{v}_i$ it follows that

$$\underline{I} = \sum_{i=1}^{n} m_i\, \underline{v}_i, \tag{D.2.2}$$

and thus

$$\frac{d}{dt} \sum m_i\, \underline{v}_i = \sum \underline{F}. \tag{D.2.3}$$

If the particles are assumed to form a continuum with density, $\rho(x,y,z,t)$, the sum changes into a volume integral. The rate of change of momentum is then

$$\frac{d\underline{I}}{dt} = \frac{d}{dt} \int_{\mathcal{V}(t)} \rho\, \underline{v}\, d\mathcal{V}. \tag{D.2.4}$$

198

The volume $\mathcal{V}$, which always contains the same particles, changes in a time interval from $\mathcal{V}(t)$ to $\mathcal{V}(t + \Delta t)$

$$
\frac{d}{dt} \int_{\mathcal{V}(t)} \rho\,\underline{v}\,d\mathcal{V} = \lim_{\Delta t \to 0} \frac{1}{\Delta t} \left[ \int_{\mathcal{V}(t + \Delta t)} \rho\,\underline{v}(t + \Delta t)d\mathcal{V} - \int_{\mathcal{V}(t)} \rho\,\underline{v}(t)d\mathcal{V} \right] \quad \text{(D.2.5)}
$$

A Taylor series expansion is applied to the first integrand

$$
\rho\,\underline{v}(t + \Delta t) = \rho\,\underline{v}(t) + \frac{\partial \rho\,\underline{v}}{\partial t}\Delta t + ..., \quad \text{(D.2.6)}
$$

and it follows that

$$
\frac{d\underline{I}}{dt} = \int_{\mathcal{V}(t)} \frac{\partial}{\partial t}(\rho\,\underline{v})d\mathcal{V} + \lim_{\Delta t \to 0} \left( \frac{1}{\Delta t} \int_{\Delta\mathcal{V}(t)} \rho\,\underline{v}d\mathcal{V} \right). \quad \text{(D.2.7)}
$$

The last integral can be changed into a surface integral over the surface $\mathcal{S}(t)$ by using the relation between the incremental volume element $d\mathcal{V}$ and the corresponding surface element $d\mathcal{S}$

$$
d\mathcal{V} = (\underline{v} \cdot \underline{n})\,d\mathcal{S}\Delta t. \quad \text{(D.2.8)}
$$

It follows that

$$
\frac{d\underline{I}}{dt} = \int_{\mathcal{V}(t)} \frac{\partial}{\partial t}(\rho\,\underline{v})d\mathcal{V} + \int_{\mathcal{S}(t)} \rho\,\underline{v}(\underline{v} \cdot \underline{n})d\mathcal{S}. \quad \text{(D.2.9)}
$$

For steady flows the time rate of change of momentum is given by the surface integral of the last equation (Krause (2005)). The surface, $\mathcal{S}$, of the volume, $\mathcal{V}$, considered is called a control surface.

# Appendix E

# Extension of collisional-kinetic force to two dimensions

## E.1   Introduction

In this appendix the particle-particle interaction force of Equation (5.5.51) is extended to two dimensions.

## E.2   Newton's law

The three dimensional form of the Newtonian law is given by

$$\underline{\tau} \;\; = \;\; 2\mu\underline{\underline{D}}, \tag{E.2.1}$$

where $\underline{\tau}$ is the stress tensor, $\mu$ is a constant of proportionality and $\underline{\underline{D}}$ is the *rate of deformation*- or *rate of strain* tensor which is related to the velocity gradient tensor, $\nabla\underline{v}$, but unlike $\nabla\underline{v}$, is symmetric.

The asymmetric velocity gradient tensor is divided into a symmetric *rate of strain tensor*, $\underline{\underline{D}}$, and an asymmetric *vorticity -or spin tensor*, $\underline{\underline{S}}$:

$$\nabla\underline{v} \;\; = \;\; \underline{\underline{D}} + \underline{\underline{S}}, \tag{E.2.2}$$

where

$$\underline{\underline{D}} \;\; = \;\; \frac{1}{2}(\nabla\underline{v} + \nabla\underline{v}^{T}), \tag{E.2.3}$$

**200**

and

$$\underline{\underline{S}} \;=\; \frac{1}{2}(\nabla \underline{v} - \nabla \underline{v}^T). \tag{E.2.4}$$

The symbol $T$, which appears in Equations (E.2.3) and (E.2.4), denotes the transpose operation and the symmetric tensor may be expressed in matrix form as

$$\frac{1}{2}(\nabla \underline{v} + \nabla \underline{v}^T) \;=\; \begin{pmatrix} \underline{i} & \underline{j} & \underline{k} \end{pmatrix} \begin{pmatrix} 2\frac{\partial u}{\partial x} & \frac{\partial v}{\partial x} + \frac{\partial u}{\partial y} & \frac{\partial w}{\partial x} + \frac{\partial u}{\partial z} \\ \frac{\partial u}{\partial y} + \frac{\partial v}{\partial x} & 2\frac{\partial v}{\partial y} & \frac{\partial w}{\partial y} + \frac{\partial v}{\partial z} \\ \frac{\partial u}{\partial z} + \frac{\partial w}{\partial x} & \frac{\partial v}{\partial z} + \frac{\partial w}{\partial y} & 2\frac{\partial w}{\partial z} \end{pmatrix} \begin{pmatrix} \underline{i} \\ \underline{j} \\ \underline{k} \end{pmatrix}. \tag{E.2.5}$$

The spin tensor given in Equation (E.2.4) does however not influence the viscosity and it follows that

$$\begin{aligned} \underline{\underline{\tau}} \;&=\; 2\mu \underline{\underline{D}} \\ &=\; \mu(\nabla \underline{v} + \nabla \underline{v}^T). \end{aligned} \tag{E.2.6}$$

To show that this is indeed the same as the law for one dimension: Let the velocity have an $x$-component only and let this component only be a function of the $y$-direction. It follows that

$$\frac{1}{2}(\nabla \underline{v} + \nabla \underline{v}^T) \;=\; \begin{pmatrix} \underline{i} & \underline{j} & \underline{k} \end{pmatrix} \begin{pmatrix} 0 & \frac{\partial u}{\partial y} & 0 \\ \frac{\partial u}{\partial y} & 0 & 0 \\ 0 & 0 & 0 \end{pmatrix} \begin{pmatrix} \underline{i} \\ \underline{j} \\ \underline{k} \end{pmatrix}. \tag{E.2.7}$$

This is equivalent to

$$\frac{1}{2}(\nabla \underline{v} + \nabla \underline{v}^T) \;=\; \frac{\partial u}{\partial y} \underline{i}\,\underline{j} + \frac{\partial u}{\partial y} \underline{j}\,\underline{i}. \tag{E.2.8}$$

Finally we have the original one dimensional form:

$$\underline{\underline{\tau}} \;=\; 2\mu \underline{\underline{D}}$$

$$\begin{pmatrix} 0 & \tau_{xy} & 0 \\ \tau_{yx} & 0 & 0 \\ 0 & 0 & 0 \end{pmatrix} \;=\; (2\mu)\left(\frac{1}{2}\right) \begin{pmatrix} 0 & \frac{\partial u}{\partial y} & 0 \\ \frac{\partial u}{\partial y} & 0 & 0 \\ 0 & 0 & 0 \end{pmatrix}, \tag{E.2.9}$$

and it follows that

$$\tau_{xy} = \tau_{yx} \quad = \quad \mu \frac{\partial u}{\partial y}. \tag{E.2.10}$$

The three dimensional force vector is thus given by

$$\underline{f}_{avg}^{rs} \quad = \quad -\underline{n}^{\perp} \cdot \frac{\epsilon_p \rho_p d_p}{4} |\nabla \underline{v} + \nabla \underline{v}^T| \left( \nabla \underline{v} + \nabla \underline{v}^T \right) \nu_i. \tag{E.2.11}$$

Let the shearrate tensor be denoted by

$$\dot{\gamma} \quad = \quad \nabla \underline{u} + \nabla \underline{u}^T,$$
$$= \quad \left( \frac{\partial u}{\partial y} + \frac{\partial v}{\partial x} \right) \underline{j}\,\underline{i} + \left( \frac{\partial u}{\partial y} + \frac{\partial v}{\partial x} \right) \underline{i}\,\underline{j}, \tag{E.2.12}$$

The magnitude of which is given by[1]

$$|\dot{\gamma}| \quad = \quad \sqrt{\frac{1}{2}Tr\left[ \begin{pmatrix} 0 & \frac{\partial u}{\partial y} + \frac{\partial v}{\partial x} \\ \frac{\partial u}{\partial y} + \frac{\partial v}{\partial x} & 0 \end{pmatrix} \cdot \begin{pmatrix} 0 & \frac{\partial u}{\partial y} + \frac{\partial v}{\partial x} \\ \frac{\partial u}{\partial y} + \frac{\partial v}{\partial x} & 0 \end{pmatrix} \right]},$$
$$= \quad \frac{\partial u}{\partial y} + \frac{\partial v}{\partial x}. \tag{E.2.14}$$

The shear stress term is thus given by

$$\underline{\underline{\tau}}_p \quad = \quad \mu_p \left[ \left( \frac{\partial u}{\partial y} + \frac{\partial v}{\partial x} \right) \underline{j}\,\underline{i} + \left( \frac{\partial u}{\partial y} + \frac{\partial v}{\partial x} \right) \underline{i}\,\underline{j} \right], \tag{E.2.15}$$

where the particle viscosity is given by

$$\mu_p = \frac{\epsilon_p \rho_p d_p^2}{12} \left( \frac{\partial u}{\partial y} + \frac{\partial v}{\partial x} \right). \tag{E.2.16}$$

Equation (E.2.11) may therefore be expressed as

$$\underline{f}_{avg}^{rs} \quad = \quad \frac{\epsilon_p \rho_p d_p}{4} \left( \frac{\partial u}{\partial y} + \frac{\partial v}{\partial x} \right) \left[ \left( \frac{\partial u}{\partial y} + \frac{\partial v}{\partial x} \right) \underline{i} + \left( \frac{\partial u}{\partial y} + \frac{\partial v}{\partial x} \right) \underline{j} \right] \nu_i. \tag{E.2.17}$$

---

[1]The magnitude of any tensor $\underline{\underline{A}}$ is defined as

$$|\underline{\underline{A}}| \quad = \quad \sqrt{\frac{1}{2}(A : A^T)} = \sqrt{\frac{1}{2}Tr(A^T \cdot A)}. \tag{E.2.13}$$

# Appendix F

# Directional components of the momentum equations

## F.1   Introduction

The mass conservation expressions, given by Equations (4.4.6) and (4.7.18), and the momentum conservation expressions, given by Equations (6.6.2) and (6.6.3), are reformulated and divided into their component expressions in order to make them suitable for discretisation. The elaborate averaging notation will be dropped here.

## F.2   Decomposition of vector equations into component form

Equation (4.4.6) is multiplied by the continuum velocity, $\underline{v}_c$, and the result is subtracted from Equation (6.6.2). A similar operation is performed with Equations (4.7.18) and (6.6.3), yielding the following simplified forms for continuum- and discrete phases, respectively:

$$\rho_c \epsilon_c \frac{\partial \underline{v}_c}{\partial t} + \rho_c \epsilon_c \, \underline{v}_c \cdot \nabla \, \underline{v}_c \;=\; \rho_c \, \underline{g} \epsilon_c - \epsilon_c \nabla p_c + \mu_c \nabla \cdot [\epsilon_c \nabla \, \underline{v}_c] -$$

$$\left[ \left[ \frac{\mu \epsilon_p}{d_p^2} \left( \frac{36 \epsilon_c \epsilon_p^{1/3}}{\left(1 - \epsilon_p^{2/3}\right)\left(1 - \epsilon_p^{1/3}\right)} + 18 \right) \right]^s + \left[ \frac{1}{2} \frac{c_d \rho_c}{d_p} \frac{\epsilon_p \epsilon_c^2}{\left(1 - \epsilon_p^{2/3}\right)^2} || \, \underline{v}_c - \underline{v}_p || \right]^s \right]^{1/s} \left( \underline{v}_c - \underline{v}_p \right),$$

$$\text{(F.2.1)}$$

and

$$\rho_p \frac{\partial}{\partial t} \epsilon_p \, \underline{v}_p + \rho_p \nabla \cdot \epsilon_p \, \underline{v}_p \, \underline{v}_p \;\; = \;\; \epsilon_p \, \underline{g} \, (\rho_p - \rho_c) - \frac{\epsilon_p^2 \rho_p d_p}{4} \left( \frac{\partial \overline{u}^{\,p}}{\partial y} + \frac{\partial \overline{v}^{\,p}}{\partial x} \right)^2 \hat{\underline{n}} +$$

$$\left[ \left[ \frac{\mu \epsilon_p}{d_p^2} \left( \frac{36 \epsilon_c \epsilon_p^{1/3}}{\left(1 - \epsilon_p^{2/3}\right)\left(1 - \epsilon_p^{1/3}\right)} + 18 \right) \right]^s + \left[ \frac{1}{2} \frac{c_d \rho_c}{d_p} \frac{\epsilon_p \epsilon_c^2}{\left(1 - \epsilon_p^{2/3}\right)^2} || \, \underline{v}_c - \underline{v}_p || \right]^s \right]^{1/s} \left( \underline{v}_c - \underline{v}_p \right).$$

$$(\text{F.2.2})$$

The $x$- and $y$ - components for Equation (F.2.1) are respectively given by

$$\rho_c \epsilon_c \frac{\partial u_c}{\partial t} + \rho_c \epsilon_c u_c \frac{\partial u_c}{\partial x} + \rho_c \epsilon_c v_c \frac{\partial u_c}{\partial y} \;\; = \;\; -\epsilon_c \frac{\partial p_c}{\partial x} + \mu_c \frac{\partial}{\partial x} \left( \epsilon_c \frac{\partial u_c}{\partial x} \right) + \mu_c \frac{\partial}{\partial y} \left( \epsilon_c \frac{\partial u_c}{\partial y} \right) -$$

$$\left[ \left[ \frac{\mu \epsilon_p}{d_p^2} \left( \frac{36 \epsilon_c \epsilon_p^{1/3}}{\left(1 - \epsilon_p^{2/3}\right)\left(1 - \epsilon_p^{1/3}\right)} + 18 \right) \right]^s + \left[ \frac{1}{2} \frac{c_d \rho_c}{d_p} \frac{\epsilon_p \epsilon_c^2}{\left(1 - \epsilon_p^{2/3}\right)^2} || \, \underline{v}_c - \underline{v}_p || \right]^s \right]^{1/s} \left( u_c - u_p \right),$$

$$(\text{F.2.3})$$

and

$$\rho_c \epsilon_c \frac{\partial v_c}{\partial t} + \rho_c \epsilon_c u_c \frac{\partial v_c}{\partial x} + \rho_c \epsilon_c v_c \frac{\partial v_c}{\partial y} \;\; = \;\; \rho_c g \epsilon_c - \epsilon_c \frac{\partial p_c}{\partial y} + \mu_c \frac{\partial}{\partial x} \left( \epsilon_c \frac{\partial v_c}{\partial x} \right) + \mu_c \frac{\partial}{\partial y} \left( \epsilon_c \frac{\partial v_c}{\partial y} \right) -$$

$$\left[ \left[ \frac{\mu \epsilon_p}{d_p^2} \left( \frac{36 \epsilon_c \epsilon_p^{1/3}}{\left(1 - \epsilon_p^{2/3}\right)\left(1 - \epsilon_p^{1/3}\right)} + 18 \right) \right]^s + \left[ \frac{1}{2} \frac{c_d \rho_c}{d_p} \frac{\epsilon_p \epsilon_c^2}{\left(1 - \epsilon_p^{2/3}\right)^2} || \, \underline{v}_c - \underline{v}_p || \right]^s \right]^{1/s} \left( v_c - v_p \right).$$

$$(\text{F.2.4})$$

The corresponding components for the particulate phase are given as

$$\rho_p \epsilon_p \frac{\partial u_p}{\partial t} + \rho_c \epsilon_p u_p \frac{\partial u_p}{\partial x} + \rho_p \epsilon_p v_p \frac{\partial u_p}{\partial y} \;\; = \;\; -\frac{\epsilon_p^2 \rho_p d_p}{4} \left( \frac{\partial u}{\partial y} + \frac{\partial v}{\partial x} \right)^2 +$$

$$\left[ \left[ \frac{\mu \epsilon_p}{d_p^2} \left( \frac{36 \epsilon_c \epsilon_p^{1/3}}{\left(1 - \epsilon_p^{2/3}\right)\left(1 - \epsilon_p^{1/3}\right)} + 18 \right) \right]^s + \left[ \frac{1}{2} \frac{c_d \rho_c}{d_p} \frac{\epsilon_p \epsilon_c^2}{\left(1 - \epsilon_p^{2/3}\right)^2} || \, \underline{v}_c - \underline{v}_p || \right]^s \right]^{1/s} \left( u_c - u_p \right),$$

$$(\text{F.2.5})$$

and

$$\rho_p \epsilon_p \frac{\partial v_p}{\partial t} + \rho_p \epsilon_p u_p \frac{\partial u_p}{\partial x} + \rho_p \epsilon_p v_p \frac{\partial u_p}{\partial y} = \epsilon_p g \left( \rho_p - \rho_c \right) - \frac{\epsilon_p^2 \rho_p d_p}{4} \left( \frac{\partial u_p}{\partial y} + \frac{\partial v_p}{\partial x} \right)^2 +$$

$$\left[ \left[ \frac{\mu \epsilon_p}{d_p^2} \left( \frac{36 \epsilon_c \epsilon_p^{1/3}}{\left( 1 - \epsilon_p^{2/3} \right) \left( 1 - \epsilon_p^{1/3} \right)} + 18 \right) \right]^s + \left[ \frac{1}{2} \frac{c_d \rho_c}{d_p} \frac{\epsilon_p \epsilon_c^2}{\left( 1 - \epsilon_p^{2/3} \right)^2} || \, \underline{v}_c - \underline{v}_p || \right]^s \right]^{1/s} \left( v_c - v_p \right).$$

$$(\text{F.2.6})$$

Equations (F.2.3), (F.2.4), (F.2.5) and (F.2.6) may now be put into discrete form.

# Appendix G

# Experimental camera data

**Table G.1:** Experimental camera data.

| Min size [cm] | Max size [cm] | Average [cm] | Begin frame | End frame | Distance [cm] | Velocity [cm/s] | Average velocity [cm/s] |
|---|---|---|---|---|---|---|---|
| 0.02 | 0.03 | 0.025 | 979 | 989 | 1 | 3.00 | 3.47 |
| 0.02 | 0.03 | 0.025 | 993 | 1002 | 1 | 3.33 | 3.47 |
| 0.02 | 0.03 | 0.025 | 732 | 741 | 1 | 3.33 | 3.47 |
| 0.02 | 0.03 | 0.025 | 767 | 775 | 1 | 3.75 | 3.47 |
| 0.02 | 0.03 | 0.025 | 771 | 780 | 1 | 3.33 | 3.47 |
| 0.02 | 0.03 | 0.025 | 822 | 831 | 1 | 3.33 | 3.47 |
| 0.02 | 0.03 | 0.025 | 856 | 866 | 1 | 3.00 | 3.47 |
| 0.02 | 0.03 | 0.025 | 960 | 969 | 1 | 3.33 | 3.47 |
| 0.02 | 0.03 | 0.025 | 978 | 988 | 1 | 3.00 | 3.47 |
| 0.02 | 0.03 | 0.025 | 800 | 808 | 1 | 3.75 | 3.47 |
| 0.02 | 0.03 | 0.025 | 867 | 877 | 1 | 3.00 | 3.47 |
| 0.025 | 0.05 | 0.0375 | 895 | 907 | 2 | 5.00 | 5.41 |
| 0.025 | 0.05 | 0.0375 | 911 | 924 | 2 | 4.62 | 5.41 |
| 0.025 | 0.05 | 0.0375 | 723 | 734.5 | 2 | 5.22 | 5.41 |
| 0.025 | 0.05 | 0.0375 | 769 | 780 | 2 | 5.45 | 5.41 |
| 0.025 | 0.05 | 0.0375 | 780 | 792 | 2 | 5.00 | 5.41 |
| 0.025 | 0.05 | 0.0375 | 807 | 836 | 4 | 4.14 | 5.41 |
| 0.025 | 0.05 | 0.0375 | 762 | 775 | 2 | 4.62 | 5.41 |
| 0.025 | 0.05 | 0.0375 | 789 | 800 | 2 | 5.45 | 5.41 |

Table G.1 – continued from previous page

| Min size [cm] | Max size [cm] | Average [cm] | Begin frame | End frame | Distance [cm] | Velocity [cm/s] | Average velocity [cm/s] |
|---|---|---|---|---|---|---|---|
| 0.025 | 0.05 | 0.0375 | 684 | 695 | 2 | 5.45 | 5.41 |
| 0.025 | 0.05 | 0.0375 | 728 | 740 | 2 | 5.00 | 5.41 |
| 0.025 | 0.05 | 0.0375 | 683 | 695 | 2 | 5.00 | 5.41 |
| 0.025 | 0.05 | 0.0375 | 673 | 685 | 2 | 5.00 | 5.41 |
| 0.05 | 0.075 | 0.0625 | 453 | 468 | 5 | 10.00 | 7.26 |
| 0.05 | 0.075 | 0.0625 | 471 | 487 | 5 | 9.38 | 7.26 |
| 0.05 | 0.075 | 0.0625 | 388 | 403.5 | 5 | 9.68 | 7.26 |
| 0.015 | 0.025 | 0.02 | 2593 | 2604 | 1 | 2.73 | 3.33 |
| 0.015 | 0.025 | 0.02 | 1895 | 1906 | 1 | 2.73 | 3.33 |
| 0.015 | 0.025 | 0.02 | 2121 | 2134 | 1 | 2.31 | 3.33 |
| 0.015 | 0.025 | 0.02 | 2186 | 2198 | 1 | 2.50 | 3.33 |
| 0.015 | 0.025 | 0.02 | 1728 | 1741 | 1 | 2.31 | 3.33 |
| 0.015 | 0.025 | 0.02 | 1743 | 1755 | 1 | 2.50 | 3.33 |
| 0.015 | 0.025 | 0.02 | 1511 | 1523 | 1 | 2.50 | 3.33 |
| 0.015 | 0.025 | 0.02 | 1526 | 1538 | 1 | 2.50 | 3.33 |
| 0.015 | 0.025 | 0.02 | 2181 | 2194 | 1 | 2.31 | 3.33 |
| 0.015 | 0.025 | 0.02 | 1639 | 1650 | 1 | 2.73 | 3.33 |
| 0.015 | 0.025 | 0.02 | 1647 | 1658 | 1 | 2.73 | 3.33 |
| 0.015 | 0.025 | 0.02 | 1811 | 1822 | 1 | 2.73 | 3.33 |
| 0.015 | 0.025 | 0.02 | 1852 | 1862 | 1 | 3.00 | 3.33 |
| 0.075 | 0.1 | 0.0875 | 579 | 591 | 5 | 12.50 | 13.49 |
| 0.075 | 0.1 | 0.0875 | 588 | 599 | 5 | 13.64 | 13.49 |
| 0.075 | 0.1 | 0.0875 | 1317 | 1328.5 | 5 | 13.04 | 13.49 |
| 0.075 | 0.1 | 0.0875 | 1322 | 1333 | 5 | 13.64 | 13.49 |
| 0.075 | 0.1 | 0.0875 | 1269 | 1280 | 5 | 13.64 | 13.49 |

# Appendix H

# Comparison between experimental data and theoretical prediction

The following figures are representative of the data listed in Tables 10.2 and 10.3. The circular points indicate results yielded by the model developed in this work whereas the starred data points denote the experiments which were done by Richardson and Zaki (1954). Corresponding colours indicate corresponding conditions (i.e. similar viscosities and densities).
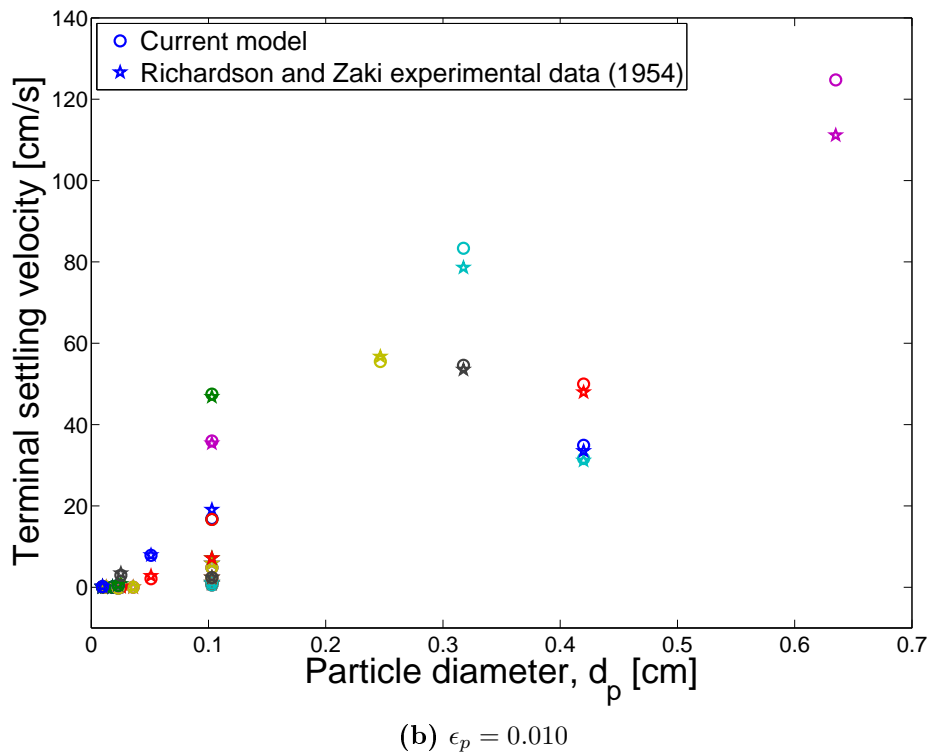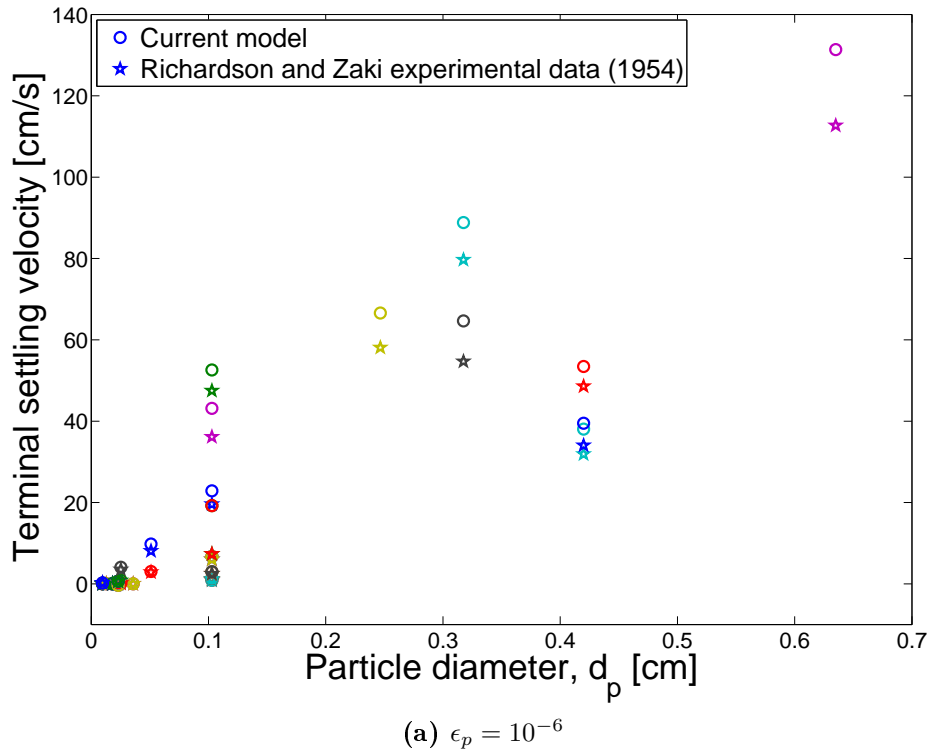
**(a)** $\epsilon_p = 10^{-6}$



**(b)** $\epsilon_p = 0.010$

**Figure H.1:** Comparison between values predicted for the group settling velocities from Equation (6.6.3) and experimental data from Richardson and Zaki (1954).

(c) $\epsilon_p = 0.050$



(d) $\epsilon_p = 0.100$
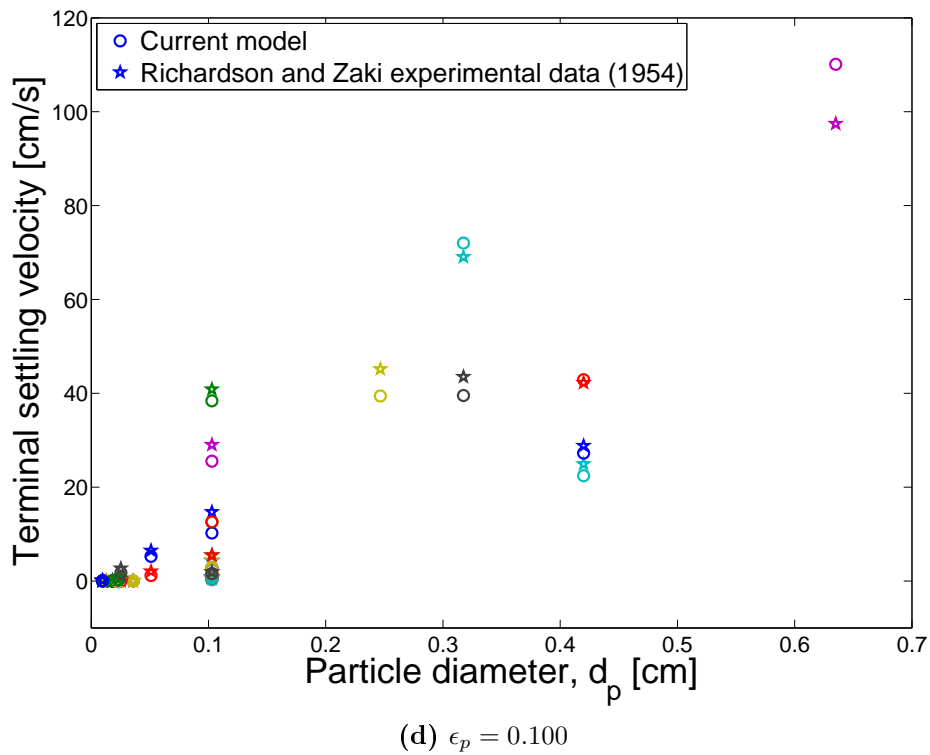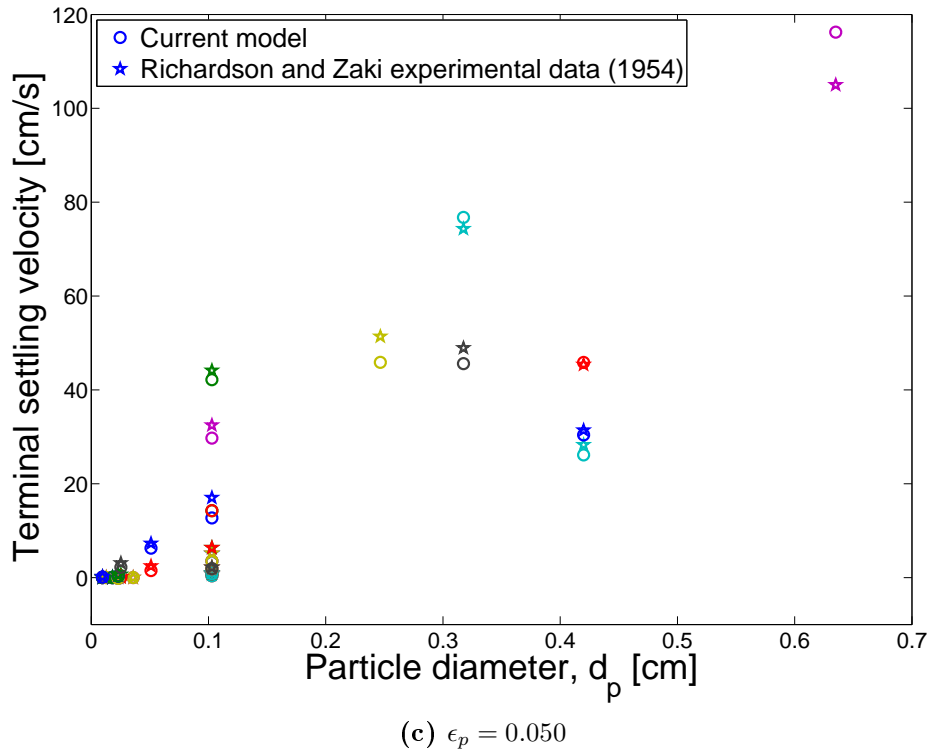
**Figure H.1:** Comparison between values predicted for the group settling velocities from Equation (6.6.3) and experimental data from Richardson and Zaki (1954).
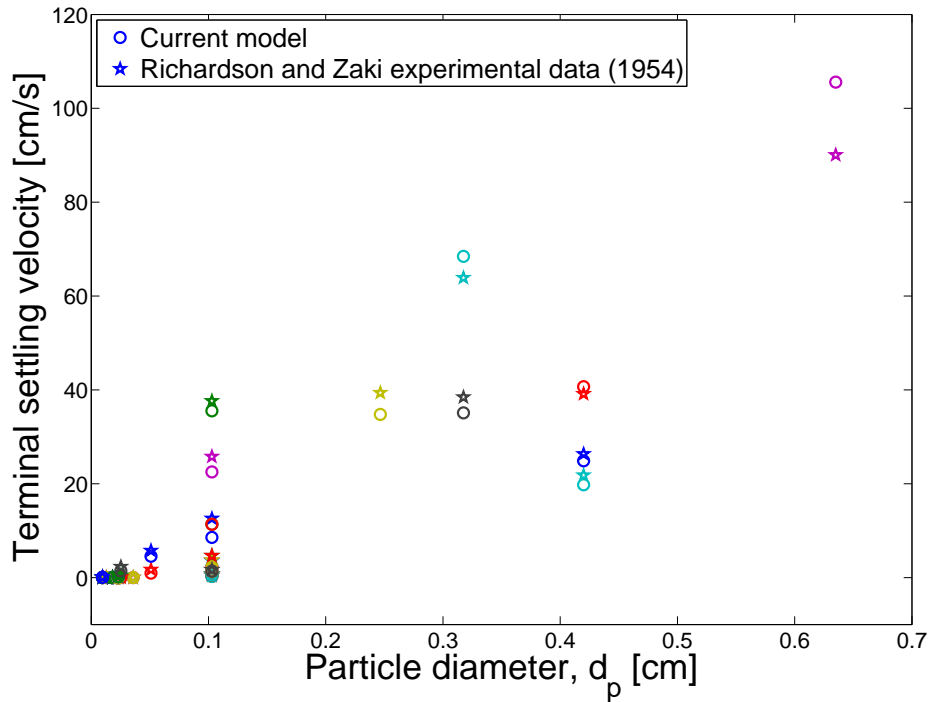
(e) $\epsilon_p = 0.150$
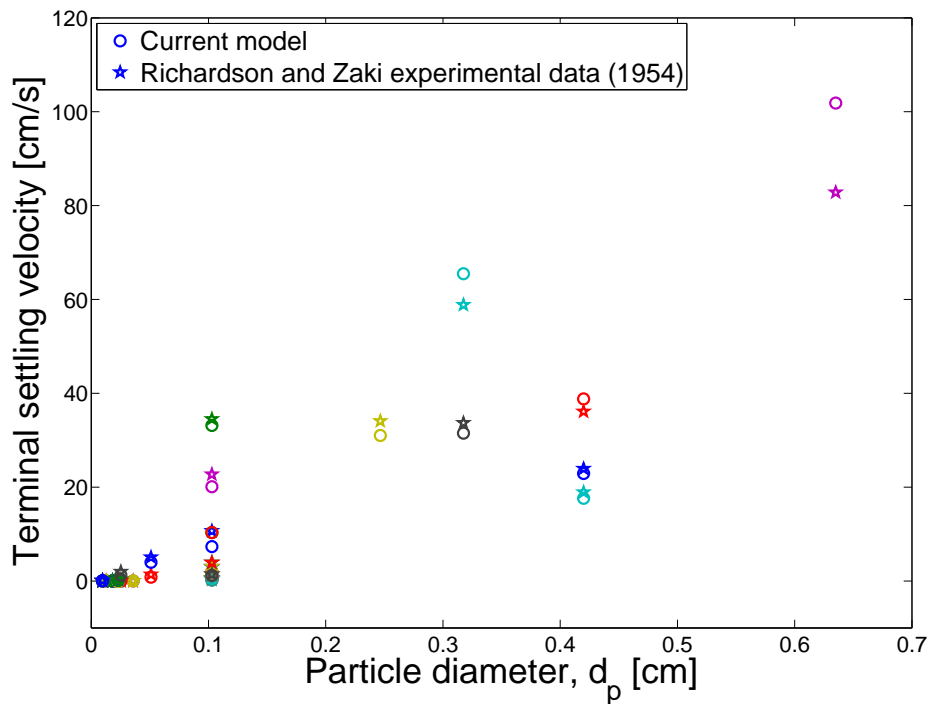


(f) $\epsilon_p = 0.200$

**Figure H.1:** Comparison between values predicted for the group settling velocities from Equation (6.6.3) and experimental data from Richardson and Zaki (1954).
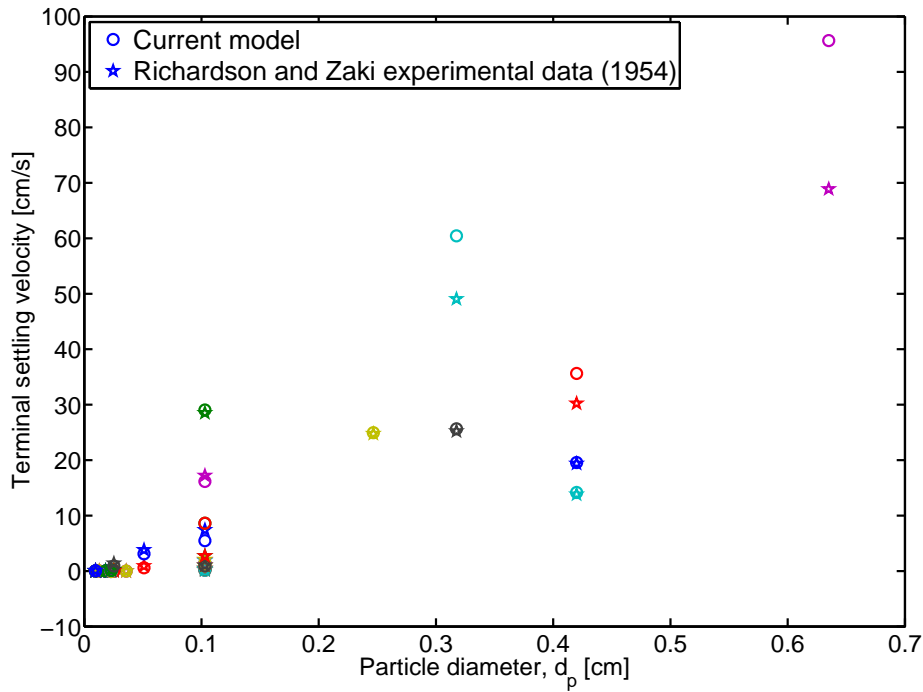
(g) $\epsilon_p = 0.300$
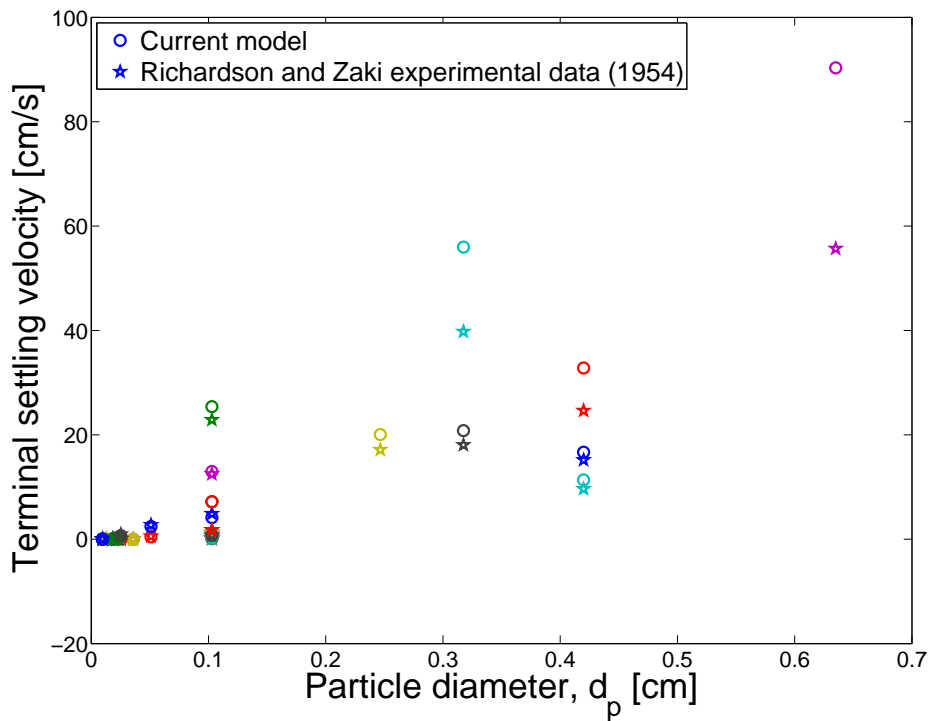


(h) $\epsilon_p = 0.400$

**Figure H.1:** Comparison between values predicted for the group settling velocities from Equation (6.6.3) and experimental data from Richardson and Zaki (1954).
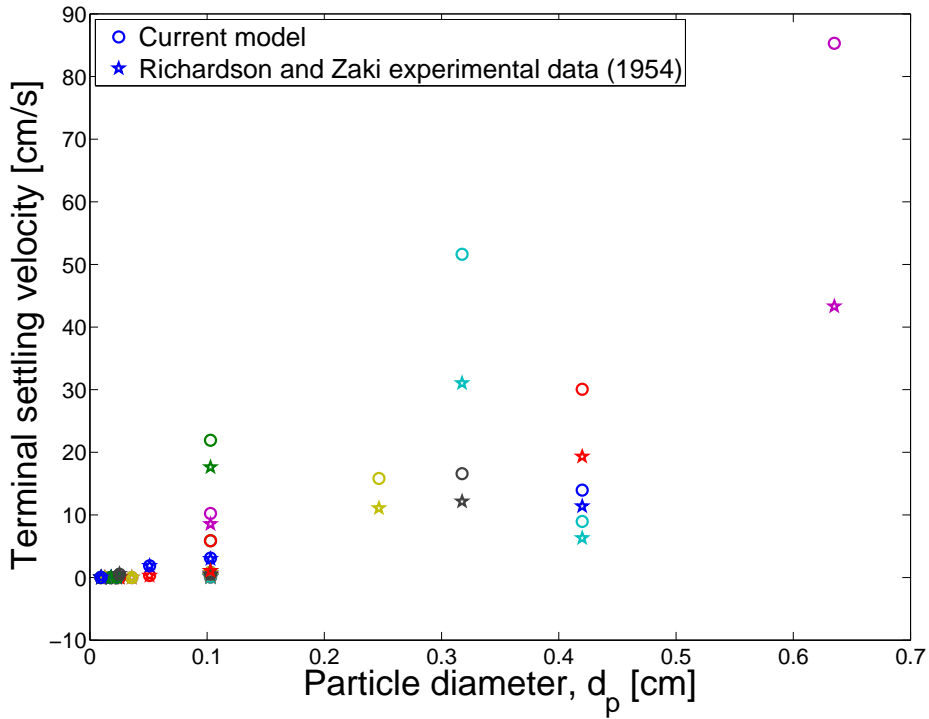
**(i)** $\epsilon_p = 0.500$
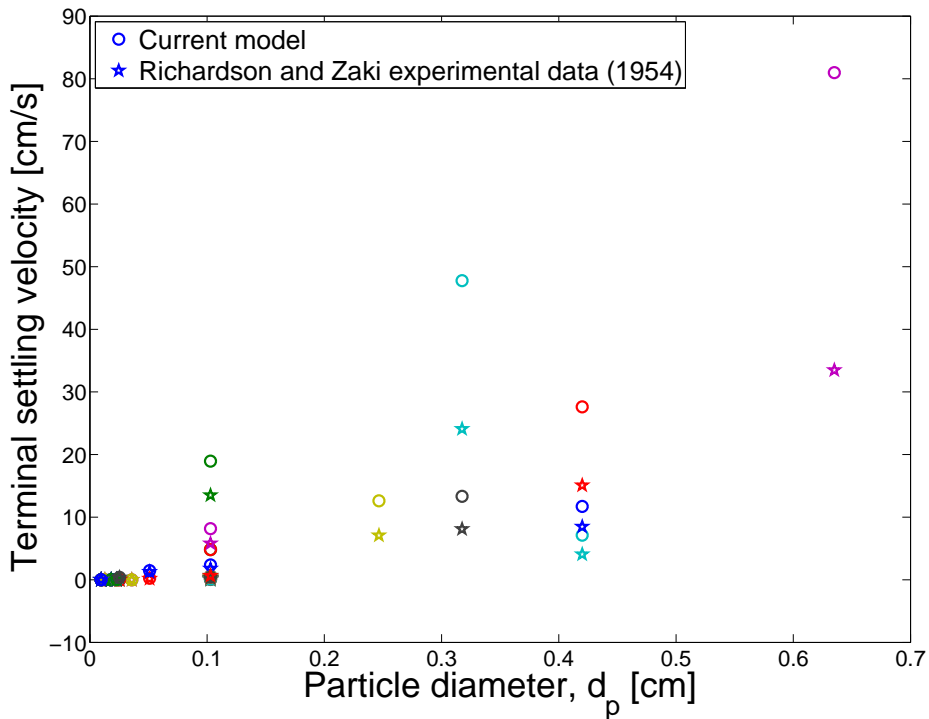


**(j)** $\epsilon_p = 0.585$

**Figure H.1:** Comparison between values predicted for the group settling velocities from Equation (6.6.3) and experimental data from Richardson and Zaki (1954).

# List of references

Ahmadi, G. and Ma, D. (1990). A thermodynamical formulation for dispersed multiphase turbulent flows. Basic theory. *Int. J. Multiphase flow.*

Allen, K.G. (2010). *Performance Characteristics of Packed Bed Thermal Energy Storage for Solar Thermal Power Plants.* Master's thesis, University of Stellenbosch, Department of Mechanical and Mechatronic Engineering.

Amsden, A.A., Daly, B.J., Dienes, J.K. and Travis, J. (1999). Detailed studies of reactor components. Los Alamos Science.

Anderson, T.B. and Jackson, R. (1967). A fluid mechanical description of fluidized beds. *I & EC Fundamentals*, vol. 6, no. 4, pp. 527–539.

Bachmat, Y. and Bear, J. (1986). Macroscopic modelling of transport phenomena in porous media: The continuum approach. *Transport in Porous Media*, vol. 1, pp. 213–240.

Barton, I.E. (1998). Comparison of SIMPLE- and PISO-type algorithms for transient flows. *International Journal for Numerical Methods in Fluids*, vol. 26, pp. 459–483.

Bird, R.B., Stewart, W.E. and Lightfoot, E.N. (2002). *Transport Phenomena.* 2nd edn. John wiley & Sons, Inc.

Bouillard, J.X., Lyczkowski, R.W. and Ding, J. (1992). Computer modeling of fluidized beds. In: *International Symposium on Energy, Environment and Information Management.*

Brennen, C.E. (2005). *Fundamentals of Multiphase Flows.* Cambridge University Press, California Institute of Technology Pasadena, California.

Brinkman, H.C. (1952). The viscosity of concentrated suspensions and solutions. *J. Chem. Phys*, vol. 20, pp. 571–573.

Campbell, C.S. and Wang, D.G. (1991). Particle pressure in gas-fluidized beds. *J. Fluid Mech*, vol. 227, pp. 495–598.

Chapman, S. and Cowling, T.G. (1970). The mathematical theory of non-uniform gases. Tech. Rep., Cambridge Mathematical Library.

Churchill, S.W. and Usagi, R. (1972). A general expression for the correlation of rates of transfer and other phenomena. *AIChe Journal*, vol. 18, pp. 1121–1128.

Clark, M.C. (2009). *Transport Modeling for Environmental Engineers and Scientists*. 2nd edn. John Wiley and Sons.

Clift, R., Grace, J.R. and Weber, M.E. (1978). *Bubbles, Drops, and Particles*. Academic Press. ISBN 9780121769505.
Available at: `http://books.google.co.za/books?id=n8gRAQAAIAAJ`

Concha, F. (2009). Settling velocities of particulate systems. *KONA Powder and Particle Journal*, , no. 27, pp. 18–37.

Conte, S.D. and de Boor, C. (1972). *Elementary Numerical Analysis*. McGraw-Hill, New York.

Croce, R., Griebel, M. and Schweitzer, M.A. (2006). A parallel level-set approach for two-phase flow problems with surface tension in three space dimensions. *AMS*.

Crowe, C., Sommerfeld, M. and Tsuji, Y. (1998). *Multiphase Flows With Droplets and Particles*. CRC Press.

Dartevelle, S. (2003 July). *Numerical and Granulometric Approaches to Geophysical Granular Flows*. Ph.D. thesis, Michigan Technological University.

Delhaye, J.M. and Achard, J.L. (1978). On the averaging operators introduced in two-phase flow. In: Banerjee, W. and Weaver, J. (eds.), *Transient Two-phase Flow*. CSNI Specialists Meeting.

Ding, J. and Gidaspow, D. (1990). A bubbling fluidization model using kinetic theory of granular flow. *AIChe Journal*, vol. 36, no. 4, pp. 523–538.

Ding, J., Lyczkowski, R.W. and W.Burge, S. (1993). Force2: A state-of-the-art two-phase code for hydrodynamic calculations. *NASA STI/Recon Technical Report N*, vol. 94, p. 11072.

Drew, D.A. (1983). Mathematical modeling of two-phase flow. *Annual Review of Fluid Mechanics*, vol. 15, pp. 261–291.

Drew, D.A. and Passman, S.L. (1999). *Theory of Multicomponent Fluids*. Springer Verlag.

Du Plessis, J.P. (1992). High reynolds number flow through granular porous media. *Computational Methods in Water Resources*, vol. 9, pp. 179–186.

Du Plessis, J.P. (1993). Laminar crossflow through prismatic porous domains. *R&D Journal*, vol. 9, pp. 18–24.

Du Plessis, J.P. (2003). *Porous Media Modelling*. University of Stellenbosch.

Du Plessis, J.P. and Diedericks, G.P.J. (1997). *Fluid Transport in Porous Media*, vol. 13 of *Advances in Fluid Mechanics*, chap. 2, pp. 61–105. Computational Mechanics Publications.

Du Plessis, J.P. and Masliyah, J.H. (1988). Mathematical modelling of flow through consolidated isotropic porous media. *Transport in Porous Media*, vol. 3, pp. 145–161.

Du Plessis, J.P., Montillet, A., Comiti, J. and Legrand, J. (1994). Pressure drop prediction for flow through high porosity metallic foams. *Chemical Engineering Science*, vol. 49, no. 21, pp. 3545–3553.

Du Plessis, J.P. and Woudberg, S. (2008). Pore-scale derivation of the ergun equation to enhance its adaptability and generalisation. *Chemical Engineering Science*, vol. 63, pp. 2576–2586.

Ehrhardt, M., Fuhrmann, J. and Linke, A. (2010). A model of an electrochemical flow cell with porous layer. *Networks and Heterogeneous Media*.

Eilers, H. (1943). Die viskositats-koncentrationsabhangigheit kolloider systeme in organischen losungsmitteln. *Kolloid Zeitschrift*, vol. 102, pp. 154–169.

Einstein, A. (1906). Eine neue bestimmung der moleküldimensionen. In: *Ann. Phys.* British Library.

Einstein, A. (1911). Berichtigung zu meiner arbeit: Eine neue bestimmung der moleküldimensionen. In: *Ann. Phys.* British Library.

Enwald, H., Peirano, E. and Almstedt, A.E. (1997). Eulerian two-phase flow theory applied to fluidization. *Int. J. Multiphase Flow*, vol. 22.

Ergun, S. (1952). Fluid flow through packed columns. *Chem. Eng. Prog.*, vol. 48, no. 89.

Fan, L.S. and Zhu, C. (1998). *Principles of Gas-Solid Flows*. Cambridge University Press.

Frankel, N.A. and Acrivos, A. (1967). On the viscosity of a concentrated suspension of solid spheres. *Chem. Engng Sci.*, vol. 22, pp. 847–853.

Gatignol, R. (1983). The faxen formulae for a rigid particle in an unsteady non-uniform stokes flow. *Journal de Mecanique Theorique et Appliquee*, vol. 1, pp. 143–160.

Gidaspow, D. (1986). Hydrodynamics of fluidization and heat transfer: Supercomputer modeling. *Appl Mech Rev*, vol. 39, no. 1, pp. 1–23.

Gidaspow, D. (1994). *Continuum and Kinetic Theory Descriptions*. Academic Press Inc.

Gomez, L.C. and Milioli, F.E. (2004). A numerical simulation analysis of the effect of the interface drag function on cluster evolution in a cfb riser gas-solid flow. *Brazilian Journal of Chemical Engineering*, vol. 21, no. 4, pp. 569–583.

Grad, H. (1949). On the kinetic theory of rarefied gases. *Comm. on Pure and Applied Mathematics*, vol. 2, pp. 331–407.

Graham, A.L. (1981). On the viscosity of suspensions of solid spheres. *Applied Scientific Research*, vol. 37, pp. 275–286.

Gray, W.G. and Lee, P.C.Y. (1976). On the theorems for local volume averaging of multiphase systems. *Int, J. Multiphase Flow*, pp. 333–340.

Haff, P.K. (1983). Grain flow as a fluid mechanical phenomenon. *Journal of Fluid Mechanics*, vol. 134, pp. 401–433.

Hamdan, M.H. and Savalha, K.D. (1996). Dusty gas flow through porous media. *Applied Mathematics and Computation*, vol. 75, pp. 59–73.

Hassanizadeh, M. and Gray, W.G. (1979). General conservation equations for multi-phase systems: 1. averaging procedure. *Advances in Water Resources*, vol. 2, pp. 131–142.

Hill, A.A. and Straughan, B. (2008). Poiseuille flow in a fluid overlying a porous medium. *J. Fluid Mech*, vol. 603, pp. 137–149.

Hjelmfelt, A.T. and Mockros, L.F. (1966). Motion of discrete particles in a turbulent fluid. *App. Sci. Res.*, vol. 16, no. 149.

Howes, A. and Whitaker, S. (1985). The spatial averaging theorem revisited. *Chemical Engineering Science*, vol. 40, no. 8, pp. 1387–1392.

Ishii, M. (1975). *Thermo-Fluid Dynamic Theory of Two-Phase Flow*. Paris, Eyrolles, Editeur (Collection de la Direction des Etudes et Recherches d'Electricite de France, No. 22).

Ishii, M. (1977). One-dimensional drift-flux model and constitutive equations for relative motion between phases in various two-phase flow regimes. Tech. Rep., Argonne National Laboratory.

Jackson, R. (1997). Locally averaged equations of motion for a mixture of identical spherical particles and a newtonian fluid. *Chemical Engineering Science*, vol. 52, no. 15, pp. 2457–2469.

Jenkins, J.T. and Richman, M.W. (1985). Grad's 13 moment system for a dense gas of inelastic spheres. *Arch. Ratio. Mech. Anal*, vol. 87, pp. 355–377.

Johnson, R.W. (1998). *The Handbook of Fluid Dynamics*. B. Stern.

Kashiwa, B.A. (1987). Statistical theory of turbulent incompressible multimaterial flow. Los alamos national laboratory report, University of Washington Doctoral Thesis.

Kleinstreuer, C. (2003). *Two-Phase Flow Theory and Applications*. Taylor and Francis.

Kmiec, A. (1982). Equilibrium of forces in a fluidized bed: Experimental verification. *Journal of Chemical Engineering*, vol. 23, p. 133.

Krause, E. (2005). *Fluid Mechanics: With Problems and Solutions, and An Aerodynamic Laboratory.* Springer-Verlag Berlin Heidelberg.

Landau, L. and Lifshitz, E. (1959). *Fluid Mechanics.* Pergamon Press.

Lewin, W. (2007). Mit physics lecture: Classical mechanics and momentum center of mass. MIT World web video.

Lewis, W.K., Billiland, W.C. and Bauer, W.C. (1949). Characteristics of fluidized particles. *Industrial and Engineering Chemistry*, vol. 41, p. 1104.

Liang, L. and Michaelides, E.E. (1992). The magnitude of Basset forces in unsteady multiphase flow computations. *J. Fluid Eng.*, vol. 114, pp. 417–419.

Lloyd, C.A., Du Plessis, J.P. and Halvorsen, B.M. (2004). On closure modelling of volume averaged equations for flow through two-dimensional arrays of squares. In: Rahman, M., Mendes, A. and Brebbia, C.A. (eds.), *Proceedings of the Fifth International Conference on Advances in Fluid Mechanics AFM2004.*

Loth, E. (2006). *Multiphase Flow Handbook*, chap. 13, pp. 1–20. Taylor and Francis.

Lu, H., Wang, S., Zhao, Y., Yang, L., Gidaspow, D. and Ding, J. (2005). Prediction of particle motion in a two-dimensional hard-sphere model. *Chemical Engineering Science*, vol. 60, pp. 3217–3231.

Lun, C.K.K. and Savage, S.B. (1986). The effects of an impact velocity dependent coefficient of restitution on stresses developed by sheared granular materials. *Acta Mechanica*, vol. 63, pp. 15–44.

Lyckowski, R.W. (2010). The history of multiphase computational fluid dynamics. *Ind. Eng. Chem. Res*, vol. 49, pp. 5029–5036.

Maxey, M.R. and Riley, J.J. (1983). Equation of motion for a small rigid sphere in a nonuniform flow. *Phys. Fluids*, vol. 26, pp. 883–889.

Maxwell, J.C. (1877). *Matter and Motion.* Cambridge University Press.

Mazzei, L. and Lettieri, P. (2007). A drag force closure for uniformly dispersed fluidized suspensions. *Chemical Engineering Science*, vol. 62, pp. 6129–6142.

Munkejord, S.T. and Papin, M. (2005). The effect of interfacial pressure in the discrete-equation multiphase model. *Elsevier Science*.

Neale, G. and Nader, W. (1974). Practical significance of brinkman's extension of darcy's law: Coupled parallel flows within a channel and a bounding porous medium. *The Canadian Journal of Chemical Engineering*, vol. 52, no. 4, pp. 475–478. ISSN 1939-019X.
Available at: http://dx.doi.org/10.1002/cjce.5450520407

Ngo, C.C. and Gramoll, K. (2006). *Multimedia Engineering Fluids*, chap. 4. www.ecourses.ou.edu.

Oesterle, B. and Petitjean, A. (1993). Simulation of particle-to-particle interactions in gas-solid flows. *Int. J. Multiphase Flow*, vol. 19, no. I, pp. 199–211.

P. de Wet, J. P. du Plessis, S.W. (2011). Application of power addition as modelling technique for flow processes: Two case studies. *Chemical Engineering Science*.

Panton, R.L. (1984). *Incompressible Flow*. Wiley, New York.

Patankar, S.V. (1980). *Numerical Heat Transfer and Fluid Flow*. Hemisphere Publishing Corporation. ISBN 0-07-048740-5.

Peirano, E. and Leckner, B. (1998). Fundamentals of trubulent gas-solid flows applied to circulating fluidized bed combustion. *Prog. Energy Combust. Sci*, vol. 24, pp. 259–296.

Post, S. (2011). *Applied and Computational Fluid Mechanics*, p. 483. Jones and Bartlett.

Pritchett, J.W., Blake, T.R. and Garg, S.K. (1978). A numerical model of gas fluidized beds. *AIChE Symp. Ser*, vol. 74, pp. 137–148.

Rafael, M. and Mahaffy, J.H. (1998). Numerical diffusion and the tracking of solute fields in system codes part i. one-dimensional flows. *Nuclear Engineering and Design*, vol. 179, pp. 297–319.

Richardson, J.F. and Zaki, W.N. (1954). Sedimentation and fluidisation: Part i. *Trans. Instn Chem. Engrs*, vol. 32, pp. 82–100.

Roscoe, R. (1952). The viscosity of suspensions of rigid spheres. *Brit. J. Appl. Phys.*, vol. 3, pp. 267–269.

Runshal, A.K. (2009). Brian spalding: Cfd and reality - a personal recollection. *International Journal of Heat and Mass Transfer*, vol. 52, pp. 4063–4073.

Saffman, P.G. (1965). The lift on a small sphere in a slow shear flow. *Journal of Fluid Mechanics*, vol. 22, pp. 385–400.

Schlichting, H. and Gersten, K. (2000). *Boundary-Layer Theory.* 8th edn. Springer, Heidelberg.

Simonin, O. (1995). Two-fluid model approach for turbulent reactive two-phase flows. Summer school on numerical modelling and prediction of dispersed two-phase flows. IMVU, Meserburg, Germany.

Simonin, O. and Viollet, P.L. (1989). Numerical study on phase dispersion mechanisms in turbulent bubbly flows. In: Erlangen, F. (ed.), *Proc. 5th Workshop On Two-Phase Flow Predictions*, pp. 156–166.

Slattery, J.C. (1967). Flow of viscoelastic fluids through porous media. *AIChE Journal*, vol. 13, no. 5, pp. 1066–1071.

Smit, G.J.F., Wilms, J.M. and Diedericks, G.P.J. (2010). Two-phase flow modeling for low concentration spherical particle motion through a newtonian fluid. *Applied Mathematics and Computation.* ISSN 0096-3003.
Available at: `http://www.sciencedirect.com/science/article/` `B6TY8-50KWFSP-7/2/4750b5389d8d7837921af2bef5e838e7`

Solbrig, C.W. and Hughes, E.D. (1971). Two phase flow equations which account for unequal phase velocities and unequal phase temperatures. Aerojet Nuclear Company manuscript.

Solbrig, C.W., Mortensen, G.A. and Lyckowski, R.W. (1976). An unequal phase velocitym unequal phase temperature theory applied to two-phase blowdown from a horizontal pipe. In: *In Proceedings of the 1976 Heat Transfer and Fluid Mechanics Institute*, pp. 60–76.

Soltau, C. (2009). *The Cross-Shore Distribution of Grain Size in The Longshore Transport Zone.* Master's thesis, Department of civil engineering, University of Stellenbosch.

Soo, S. (1990). *Multiphase fluid dynamics.* Science Press. ISBN 9787030001023. Available at: `http://books.google.co.za/books?id=lg-NQgAACAAJ`

Soo, S.L. (1962). Boundary layer motion of a gas-solid suspension. In: Shepherd, N.T. (ed.), *Proceedings of the Symposium on the Interaction between Fluids and Particles*, no. 9 in Institution of Chemical Engineers (Great Britain) Symposium Series, p. 50.

Spalding, D.B. (1976). The calculation of free-convection phenomena in gas-liquid mixtures. In: *ICHMT Seminar, Dubrovnik.* Hemisphere Publishing Corporation.

Spalding, D.B. (1980). *Numerical Computation of Multi-Phase Fluid Flow and Heat Transfer*, vol. 1 of *Recent Advances in Numerical Methods in Fluids*, pp. 139–167.

Spalding, D.B. (1983). Developments in the ipsa procedure for numerical computations of multiphase-flow phenomena with interphase slip, unequal temperatures, etc. *Numerical properties and methodologies in heat transfer*, vol. 1, pp. 421–436.

Succi, S., Karlin, I.V. and Chen, H. (2002). Colloquium: Role of the h theorem in lattice boltzmann hydrodynamic simulations. *Reviews of Modern Physics*, vol. 74, pp. 1203–1220.

Tadmor, Z. and Gogos, C.G. (2006). *Principles of Polymer Processing*, chap. 2, pp. 26–27. 2nd edn. Wiley & Sons.

Tanaka, T. and Tsuji, Y. (1991). Numerical simulation of gas-solid two-phase flow in a vertical pipe: On the effect of inter-particle collision. *ASME FED*, vol. 121.

van der Hoef, M.A., van Sint Annaland, M. and Kuipers, J.A.M. (2005). Computational fluid dynamics for dense gas-solid fluidized beds: A multi-scale modeling strategy. *China Particuology*, vol. 3, no. 1-2, pp. 69–77.

Van Doormaal, J.P. and Raithby, G.D. (1984). Enhancements of the SIMPLE method for predicting incompressible fluid flows. *Numerical Heat Transfer*, vol. 7, no. 2, pp. 147–163.

van Rijn, L.C. (2002). Principles of sediment transport in rivers estuaries and coastal seas. *Aqua Publications*.

van Wachem, B.G.M., Schouten, J.C., van den Bleek, C.M., Krishna, R. and Sinclair, J.L. (2004). Comparative analysis of cfd models of dense gas-solid systems. *AIChE Journal*, vol. 47, no. 5, pp. 1035–1051.

Vand, V. (1948). Viscosity of solutions and suspensions. *J. Phy. Colloid Chem*, vol. 52, pp. 277–321.

Versteeg, H.K. and Malalasekera, W. (1995). *An introduction to Computational Fluid Dynamics*. Pearson Education Limited.

Vojir, D.J. and Michaelides, E.E. (1994). Effect of the history term on the motion of rigid spheres in a viscous fluid. *Int. J. Multiphase Flow*, vol. 20, pp. 547–556.

Wallis, G.B. (1969). *One-Dimensional Two-Phase Flow*. New York McGraw-Hill.

Wassen, E. and Frank, T.H. (2000). Simulation of cluster formation in gas-solid flow induced by particle-particle collisions. *Journal of Multiphase flow*.

Wen, C.Y. and Yu, Y.H. (1966). Mechanics of fluidization. In: *Chemical Engineering Progress Symposium*, 62, p. 100.

Whitaker, S. (1967). Diffusion and dispersion in porous media. *AIChE Journal*, vol. 13, no. 5, pp. 420–427.

Whitaker, S. (1969). Fluid motion in porous media. In: *Flow Through Porous Media Symposium*, vol. 61, pp. 15–28.

Whitaker, S. (1980). *Advances in Drying*, vol. 1, chap. Heat and Mass Transfer in Granular Porous Media, pp. 23–61. Hemisphere Pub. Corp.

Wilms, J.M., Smit, G.J.F. and Diedericks, G.P.J. (2009). Two phase flow modelling for low concentration spherical particle motion through a newtonian fluid. *AIP Conference Proceedings*, vol. 1168, no. 1, pp. 673–676.
Available at: `http://link.aip.org/link/?APC/1168/673/1`

Wilms, J.M., Smit, G.J.F. and Diedericks, G.P.J. (2010). On particle-particle interaction forces for dilute systems. *AIP Conference Proceedings*, vol. 1281, no. 1, pp. 187–190.
Available at: `http://link.aip.org/link/?APC/1281/187/1`

Woudberg, S., Du Plessis, J.P. and Smit, G.J.F. (2006). Non-newtonian purely viscous flow through isotropic granular porous media. *Chemical Engineering Science*, vol. 61, pp. 4299–4308.

Yu, K.F. and Lee, E.W.M. (2009). Evaluation and modification of gas-particle co-variance models by large eddy simulation of a particle-laden turbulent flows over a backward-facing step. *International Journal of Heat and Mass Transfer*, vol. 52, pp. 5652–5656.